Novel therapeutic strategies for targeting EGFR mutated non-small cell lung cancer



CRUK/MRC Oxford Institute for Radiation Oncology
Department of Oncology
University of Oxford

Neele Drobnitzky

Trinity College, University of Oxford

Thesis submitted for the degree of Doctor of Philosophy in Radiobiology

Trinity Term, 2017

Novel therapeutic strategies for targeting EGFR mutated non-small cell lung cancer

Neele Drobnitzky

Trinity College, University of Oxford
Thesis submitted for the degree of Doctor of Philosophy in Radiobiology - Trinity Term, 2017

Background: NSCLC patients with EGFR M+ tumours have marked clinical responses to EGFR-TKIs. Most patients experience tumour regrowth, as drug resistance emerges through on-target secondary EGFR-mutations or other activating mutations that reactivate the downstream signalling. However, a significant number of patients become drug resistant through unknown mechanisms of resistance and these currently represent an area of high unmet clinical need. In this work, we aim to understand biological responses to sustained EGFR inhibition in EGFR mutated NSCLC cells, to generate EGFR-TKI resistant cell lines, and to utilise these resistant cell lines to identify novel treatment strategies to overcome or prevent EGFR-TKI resistance. **Methods:** We used human NSCLC cell lines with activating EGFR mutations commonly found in the clinic and treated them with both 1st and 3rd generation EGFR-TKIs (gefitinib and AZD9291, respectively). We also utilised 3D spheroids and *in vivo* tumour xenograft growth in both subcutaneous and orthotopic settings. Cell lines were analysed by western blotting, RPPA and RNAseq and a bioactive small molecule library was used to identify combination targets. **Key findings:** Our data demonstrate that EGFR mutant cells respond to EGFR-TKI treatment by acute changes in intracellular signalling, reduction in cell migration and proliferation, and the induction of apoptosis. Thereafter, surviving cells re-engage signalling and a resistant cell population resumes growth even in the presence of high concentrations of the drug. Broadly equivalent responses are seen in 2D, 3D and in *in vivo* models. Resistant cell lines included those both with (PC9^{GS} and PC9^{9291S}) and without (HCC827^{GS} and H1975^{9291S}) known resistance-conferring mutations (EGFR T790M, NRAS Q61R). Our screening approach using a bioactive small molecule library identified IGF-1R as a promising target for preventing and overcoming resistance to EGFR-TKIs in EGFR-TKI sensitive H1975 and EGFR-TKI resistant H1975^{9291S} cell lines, respectively. The effects on prevention of emergence of resistance were apparent in 2D and 3D, though these findings need to be confirmed in *in vivo* models. Of particular interest was the identification of AURK via our screen for targets for overcoming resistance and inhibitors of AURK selectively inhibited the growth of EGFR-TKI resistant cells in the presence but also absence of EGFR-TKIs. The underlying mechanisms for these newly arisen sensitivities remain to be determined. **Conclusions:** Sustained exposure of EGFR M+ NSCLC cells *in vitro* to EGFR-TKIs identifies three phases of drug response; sensitive, tolerant and resistant, associated with distinct phenotypic responses, culminating in the emergence of a highly resistant population of cells. Combination treatment of EGFR-TKIs with IGF-1R inhibitors appears to be an attractive approach for overcoming and preventing resistance if suitable biomarkers were available for patient selection. AURK-inhibition is a novel and potentially more broadly applicable approach to overcoming and potentially preventing EGFR-TKI resistance. Further validation work is required to demonstrate the *in vivo* activity and therapeutic potential of these combinations.

Acknowledgements

First, I would like to thank my supervisor Andy Ryan for all his support over the past 6 years. I could not have wished for a better supervisor and mentor and I am really grateful not only for all the advice, time and support on experiments and this thesis but also chats about career and life – thank you!

I would also like to thank all the staff of the Department of Oncology who helped me throughout this time, especially the BMS, Sean Smart and the rest of the imaging core, the bioinformatics core and Graham Brown for invaluable help with microscopy. I am particularly grateful to Sarah Norman and Katy Higgins for all their help throughout my time in the department.

A special thank you goes to current and previous members of the Ryan Lab: Agata, Agnes, Amalina, Anika, Aoife, John, Sam, Yanyan, Yasmin and especially Sivan for all her help on this thesis.

I am grateful to the Medical Research Council, as their funding allowed me to do this PhD.

My time in Oxford would not have been the same without all the great time with and support from friends from home and those I was lucky enough to meet here. Thank you so much Anni, Kim, Juliane, Lisa, Sophie, Jen, Debs, Greg and Anna.

Life over the past four years would have definitely not been the same without my dearest friend Luiza – thank you for your company, support, help and friendship - always!

An enormous thank you to Chris, not only for all the great time together, love and friendship over the past years but also for the incredible support and care over the last weeks.

Finally, I would like to thank my family. I would not be who I am and where I am without the support from my sisters, Oma, Gilla and Tina and most importantly Heike and Matthias!

Table of contents:

Abstract 1
Abbreviations 9
1 Introduction 14
1.1 Lung cancer and driver mutations 14
1.2 EGFR protein structure and function 20
1.3 EGFR signalling 24
1.4 EGFR mutations in NSCLC 27
1.5 EGFR inhibitors for the treatment of EGFR M+ NSCLC 30
1.6 Resistance mechanisms 37
1.7 Treatment options upon resistance 40
2 Material and Methods 44
2.1 Buffers, solutions and chemicals 44
2.2 Compounds 45
2.3 Cell culture 47
2.4 Mutagenesis of cells using benzo[a]pyrene 49
2.5 Spheroid growth 50
2.6 Viability assay for IC_{50} determination 50
2.7 384-well compound screen 51
2.8 Imaging-based detection of apoptosis 53
2.9 DNA extraction, polymerase chain reaction and DNA sequencing 56
2.10 RNA isolation and mRNA sequencing 58
2.11 Protein extraction, SDS-PAGE and western blotting 60
2.12 Reverse Phase Protein Array (RPPA) 63
2.13 Formalin fixation and paraffin embedding (FFPE) 64
2.14 H&E staining, immunohistochemistry and immunofluorescent staining of FFPE material 65
2.15 Cell cycle analysis 69
2.16 Generation of TKI resistant cells 70
2.17 *In vivo* studies 70
2.18 Analysis 72
3 Characterisation of cellular response to exposure to EGFR-TKIs 74
3.1 Effect of EGFR mutations on cellular response to exposure to EGFR-TKIs 75
3.2 Cellular response to EGFR-inhibition under 2D culture conditions 80
3.3 Discussion response to EGFR-inhibition under 2D culture conditions 91
3.4 Cellular response to EGFR-TKIs in 3D spheroids 93
3.5 Effects of EGFR-inhibition in *in vivo* models 105
3.6 Discussion response to EGFR-TKIs 3D/*in vivo* 111
4 Generation and characterisation of EGFR-TKI resistant EGFR M+ NSCLC cells 114
4.1 Generation of EGFR-TKI resistant cell lines *in vitro* 115
4.2 Characterisation of generated resistant cell lines: degree of resistance and known resistance-conferring mutations 117
4.3 Discussion on generation of EGFR-TKI resistant cell lines 123
4.4 Signalling in EGFR-TKI resistant cell line ($HCC827^{GS}$ and $H1975^{9291S}$) 126
4.5 RNA expression changes EGFR-TKI resistant cell lines ($HCC827^{GS}$ and $H1975^{9291S}$) 129
4.6 Compound screen for overcoming resistance to AZD9291 treatment in $H1975^{9291R}$ cells 131
4.7 Summary of characterisation and overcoming of population-based resistance to EGFR-TKIs 146
5 Prevention of emergence of resistance to EGFR-TKIs 149

5.1 Compound screen for increased effectiveness of AZD9291 treatment in EGFR-TKI sensitive cells 150
5.2 Summary prevention of emergence of resistance 160
6 General discussion and conclusion 163
Bibliography 178
Supplementary figures 204
Appendix 208

List of figures:

Figure 1-1: EGFR is the second most commonly mutated oncogene in lung adenocarcinoma. 17

Figure 1-2: Schematic view of EGFR protein structure and conformation of the EGFR monomer 22

Figure 1-3: Oligomerisation and activation states of the EGFR 24

Figure 1-4: EGFR phosphorylation sites and activated pathways 25

Figure 1-5: Signalling of EGFR through the PI3K/AKT and the MAPK pathways 27

Figure 1-6: Types and effects of mutations commonly found in in the EGFR kinase domain in NSCLC. 29

Figure 1-7: Mechanisms of resistance to targeted therapy 37

Figure 1-8: Mechanisms of Acquired Resistance in EGFR-mutant NSCLC patients 39

Figure 3-1: EGFR M+ cell lines are hypersensitive to gefitinib. 77

Figure 3-2: EGFR T790M gatekeeper mutation confers resistance to 1st but not 3rd generation EGFR-TKIs 78

Figure 3-3: Definition of treatment times, response time scales and resistance phases during EGFR-TKI treatment 79

Figure 3-4: Rapid and potent reduction in EGFR signalling after gefitinib and AZD9291 treatment in PC9 NSCLC cells. 81

Figure 3-5: RPPA analysis of AZD9291 treated PC9 and H1975 cells identifies reduced EGFR downstream signalling and induced stress response signalling 83

Figure 3-6: AZD9291 induced reduction in cell migration, proliferation and increased induction of apoptosis 85

Figure 3-7: Mid-term response of EGFR M+ cells show evidence of re-engagement of pAKT and pERK signalling after 96 h of AZD9291 treatment 87

Figure 3-8: HCC827 and H1975 cells reengage signalling and proliferation during AZD9291 treatment and become resistant. 90

Figure 3-9: Spheroid formation in EGFR M+ NSCLC cell lines 95

Figure 3-10: AZD9291 treatment leads to a dose- and time-dependent reduction in EGFR signalling in H1975 cells grown as 3D spheroids 97

Figure 3-11: Effects of AZD9291 treatment of H1975 3D spheroids assessed in FFPE sections – size and signalling 99

Figure 3-12 Effects of AZD9291 treatment of H1975 3D spheroids assessed in FFPE sections – mitosis and apoptosis 100

Figure 3-13: H1975 but not HCC827 spheroids regrow after initial shrinkage under AZD9291 treatment. 101

Figure 3-14: Re-engagement of signalling and regrowth of H1975 spheroids under long-term AZD9291 treatment 102

Figure 3-15: EGFR signalling and proliferation is reduced in H1975 spheroids under AZD9291 treatment but a subset of spheroids reengages signalling and grows under long-term treatment 104

Figure 3-16: AZD9291 treatment reduces of pEGFR levels *in vivo* and shrinks orthotopic lung tumours 106

Figure 3-17: Long-term treatment with EGFR-TKIs shrinks but does not eradicate established subcutaneous PC9 and HCC827 tumours. 107

Figure 3-18: Subcutaneous tumours of PC9 and HCC827 cells are viable after long-term treatment with gefitinib and AZD9291 and might be enriched for EGFR-TKI resistant cells. 109

Figure 3-19: Orthotopic H1975 lung tumours can regrow under long-term treatment with AZD9291 110

Figure 3-20: Comparison of findings on response and resistance to EGFR-TKIs in 2D, 3D and *in vivo* 113

Figure 4-1: EGFR M+ NSCLC cell lines resistant to gefitinib and AZD9291 can be isolated and show a > 100x increase in IC_{50} for selection drugs. 118

Figure 4-2: Resistance to EGFR-TKIs is maintained even after long-term culturing of cells in the absence of EGFR-TKIs 119

Figure 4-3: EGFR-TKI-resistant PC9 clones harbour resistance-conferring mutations in EGFR or NRAS, sustaining EGFR-signalling even in the presence of EGFR-TKI. 121

Figure 4-4: AZD9291 resistant PC9 and H1975 but not HCC827 form spheroids and are resistant to AZD9291 in 3D. 123

Figure 4-5: EGFR-TKI treatment does not reduce canonical EGFR-signalling in resistant cells 128

Figure 4-6: RNA sequencing analysis of $HCC827^{GS}$ and $H1975^{9291S}$ 130

Figure 4-7: Proliferation based compound screen for L1700 library was performed in 384-well plates and covered 190 targets 132

Figure 4-8: Effects of screen compounds were reproducible over two repeats and plates showed a similar range of effect sizes. 133

Figure 4-9: Distribution of hit compounds, other compounds and DMSO based on their anti-proliferative effect in AZD9291 treated $H1975^{9291S}$ compared to H1975. 134

Figure 4-10: Aurora Kinase, IGF-1R and mTOR inhibitors are enriched among the compounds most active against $H1975^{9291S}$ 137

Figure 4-11: Some, but not all, AURK inhibitors selectively inhibit proliferation of $H1975^{9291S}$ cells 138

Figure 4-12: AZD9291 sensitises $H1975^{9291S}$ cells to IGF-1R inhibitors. 140

Figure 4-13: Combination treatment of $H1975^{9291S}$ with AZD9291 and AZD1152 or OSI906 leads to induction of apoptosis and inhibition of signalling via AKT and ERK but not every AZD9291 selected cell line is sensitive to IGF-1R inhibitors. 141

Figure 4-14: Different EGFR-TKI resistant cell lines are differentially sensitive to co-treatment with inhibitors of AURK, IGF-1R, AKT and MEK 143

Figure 4-15: Growth of H1975^{9291S} spheroids is inhibited by AURK and IGF-1R inhibitors. 145

Figure 5-1: Combination treatments might prevent or delay the emergence of resistance by increasing the acute response and by delaying the entry of cells into tolerant and resistant phases. 150

Figure 5-2: Compound ranking for screen for prevention of emergence of resistance. 151

Figure 5-3: IGF-1R, AKT and mTOR inhibitors are positively enriched, as opposed to negatively enriched EGFR inhibitors. 152

Figure 5-4: H1975 cells are sensitised to IGF-1R inhibitors by AZD9291. 154

Figure 5-5: The sensitising effect of inhibitors of IGF-1R is cell line specific. 154

Figure 5-6: IGF-1R inhibitors prevent the emergence of resistance to AZD9291 in H1975 spheroids. 156

Figure 5-7: Inhibitors of AKT, Aurora Kinase, Bcl-2, FAK and PI3K but not MEK increase the extend and speed of induction of apoptosis under AZD9291 treatment in H1975 cells. 158

Figure 5-8: Inhibitors of Aurora Kinase, FAK and MEK increase both the extent and speed of induction of apoptosis under AZD9291 treatment in PC9 cells. ... 159

Figure 5-9: Combination effects of AURK and EGFR inhibitors are moderate in EGFR-TKI sensitive cells. 160

Figure 6-1: Response phases in cell culture models resemble treatment responses in patients under EGFR-TKI treatment 164

Figure 6-2: The extent of oncogenic shock upon inhibition of pro-survival signalling by EGFR-TKI treatment might influence the emergence of resistance. 166

Figure S 1: Changes in apoptotic cell number, total cell number and migration speed of PC9 under AZD9291 or gefitinib treatment 204

Figure S 2: HCC827 spheroids form hollow spheroids and are hypersensitive to AZD9291 treatment 205

Figure S 3: AZD9291 treatment leads to transient reduction of pAKT and pERK as well as increase in cleaved caspase in H1975 spheroids 206

Figure S 4: H1975^{9291S} cells are resistant to the AZD9291 active metabolite AZ5104 207

List of tables:

Table 1-1: Lung cancer stage at diagnosis and associated 5-year survival rates. 15

Table 1-2: Outline of main treatment options by stage of disease for patients with NSCLC 16

Table 1-3: Compounds targeting mutated oncogenes in patients with advanced lung adenocarcinoma 19

Table 1-4: EGFR-TKIs approved for use in NSCLC in USA and European Union (Sept 2017) 32

Table 2-1: Buffers and solutions used throughout this work 44

Table 2-2: Compounds used in this study 45

Table 2-3: Cell lines used in this study 47

Table 2-4: Primers for amplification of EGFR and NRAS 56

Table 2-5: Samples analysed using RNA sequencing 58

Table 2-6: Antibodies used for immunoblotting 62

Table 2-7: Antibodies for immunohistochemistry and immunofluorescence 67

Table 2-8: Secondary antibodies for immunofluorescence 68

Table 3-1: Cell lines used in this study, EGFR mutation status and determined IC_{50} values for gefitinib and AZD9291 76

Table 4-1: Selection conditions for resistant cell lines generated in this study 116

Table 4-2: Characterisation of resistant cell lines. 120

Table 4-3: Compounds that preferentially inhibit proliferation of $H1975^{9291S}$ in compared to H1975 target proteins including AKT, Aurora Kinase and IGF-1R. 135

Table 4-4: Significantly enriched targets within the 50 most selective compounds. 136

Table 4-5: Some but not all tested Aurora Kinase inhibitors show selectivity for $H1975^{9291S}$ cells over H1975. 139

Table 4-6: IGF-1R inhibitors showed increased inhibition of proliferation in AZD9291 treated $H1975^{9291S}$ compared to untreated H1975 cells. 140

Table 5-1: Significantly enriched targets within the 50 most selective compounds. 152

Table 5-2: All tested IGF-1R inhibitors showed increased inhibition of proliferation in AZD9291 treated compared to untreated H1975 cells. 153

Abbreviations

2D	Two-dimentional
3D	Three-dimentional
A549	A NSCLC cell line
ABL1	Abelson murine leukaemia viral oncogene homolog 1
AKT	AK mouse strain Transformed
ALK	Anaplastic lymphoma kinase receptor
ATCC	American Type Culture Collection
ATP	Adenosine triphosphate
AURK	Aurora Kinase
AXL	AXL receptor tyrosine kinase
AZD9291	osimertinib/TAGRISSO
BCL2	B-cell lymphoma 2
BIM	Bcl-2-like protein 11
bp	Base-pair(s)
BRAF	Rapidly Accelerated Fibrosarcoma kinase B
BrdU	Bromodeoxyuridine
C797S	EGFR mutation
CAIX	Carbonic anhydrase 9
Calu3	A NSCLC cell line
CDK	Cyclin-dependent Kinase
cDNA	complementary DNA
cfDNA	Circulating free tumour DNA
CHARM	Compound hierarchy of algorithms representing morphology
CO-1686	3rd generation EGFR-TKI
CO_2	Carbon dioxide
CST	Cell Signalling Technology
CT/PET	Computed tomography/positron emission tomography
CTX	Chemotherapy
DAPI	4',6-diamidino-2-phenylindole
DFG	Aspartate-phenylalanine-glycine
dH_2O	Distilled water
DMEM/F-12	Dulbecco's Modified Eagle's Medium/Nutrient F-12 Ham
DMSO	Dimethyl Sulfoxide
DNA	Deoxyribonucleic Acid

DoR	Duration of response
DPX	Distyrene, plasticiser, xylene
ds	Double-stranded
DUSP6	Dual-specificity phosphatase 6
ECM	Extra-cellular matrix
EDTA	Ethylenediaminetetraacetic Acid
EGFR	Epidermal Growth Factor Receptor
EMA	European Medicines Agency
EMT	Epithelial-to-mesenchymal transition
ERK1/2	Extracellular signal-regulated kinase 1 and 2
ESMO	European Society for Medical Oncology
ETS1	E26 transformation-specific 1
FACS	Fluorescence-activated cell sorting
FAK	Focal adhesion kinase
FBS	Foetal Bovine Serum
FDA	US Food and Drug Administration
FDR	False discovery rate
FFPE	Formalin fixation and paraffin embedding
FITC	Fluorescein isothiocyanate
FOXO	Forkhead box O
FRET	Förster resonance energy transfer
g	Gravitational Force
GF	Growth Factor
GFP	Green Fluorescent Protein
GRB2	growth factor receptor–bound protein 2
h	Hour(s)
H&E	Haematoxylin and Eosin
H1648	A NSCLC cell line
H1650	A NSCLC cell line
H1975	A NSCLC cell line
$H1975^{9291S}$	AZD9291-selected H1975 cells
HCC2935	A NSCLC cell line
HCC4006	A NSCLC cell line
HCC827	A NSCLC cell line
$HCC827^{GS}$	Gefitinib-selected HCC827 cells
HCl	Hydrochloric acid
HDAC	Histone Deacetylase

HER2 (ERBB2)	Human epiderman growth factor receptor 2
HER3	Human epiderman growth factor receptor 3
HGF	Hepatocyte growth factor
HH3	Histone H3
HPMC	Hydroxypropyl methylcellulose
HRP	Horseradix peroxidase
HSP	Heat Shock Protein
IC_{50}	Half-inhibitory concentration
IF	Immunofluorescence
IGF-1R	Insulin-like growth factor-1 receptor
IHC	Imunohistochemistry
JAK	Janus kinase
JNK	cJun N-terminal kinase
KRAS	Kisten Rat Sarcoma
L	Litre
L718Q	EGFR mutation
LC	Lung Cancer
m	Metre
M	Molar, mol/liter
M+	Mutation-positive
mAb	Monoclonal antibody
MEK1/2	Mitogen-activated protein kinase/ERK kinase 1 and 2
MET	Tyrosine-protein kinase Met
mg	Milligram
min	Minute(s)
mL	Millilitre
mM	Millimolar
mRNA	Messenger RNA
msec	Milliseconds
mTOR	Mechanistic Target of Rapamycin
NaCl	Sodium Chloride
NADP	Nicotinamide adenine dinucleotide phosphate
NaOH	Sodium hydroxide
NBF	Neutral buffered formalin
NCCN	National Comprehensive Cancer Network
NF-κB	Nuclear factor-kappa B

nM	Nanomolar
NRAS	Neuroblastoma Rat Sarcoma
NSCLC	Non-Small Cell Lung Cancer
ORR	Objective response rate
OS	Overall survival
pAb	polyclonal antibody
PARP	Poly (ADP-ribose) polymerase
PBS	Phosphate Buffered Saline
PBS-T	PBS with 0.5% Tween
PC9	A NSCLC cell line
$PC9^{9291S}$	AZD9291-selected PC9 cells
$PC9^{GS}$	gefitinib-selected PC9 cells
PCR	Polymerase chain reaction
PDK1	Phosphoinositide-dependent kinase 1
PFA	Paraformaldehyde
PFS	Progression-free survival
phospho or p	phosphorylated
PI	Propidium iodide
PI3K	Phosphatidylinositol 3-kinase
PI3KCA	Phosphatidylinositol 4,5-bisphosphate 3-kinase catalytic subunit alpha
PIP_2	phosphatidylinositol 4,5-bisphosphate
PIP_3	phosphatidylinositol 3,4,5-trisphosphate
PLK	Polo-like kinase
pM	Picomolar
PPIB	Peptidyl-prolyl cis-trans isomerase B
pS	Phophorylated Serine residue
pT	Phophorylated Threonine residue
PTB	Phosphortyrosine binding
PTEN	phosphatase and tensin homolog
pY	Phophorylated Tyrosine residue
Q61R	NRAS mutation
RAF	Rapidly accelerated fibrosarcoma
RAS	Rat sarcoma
RET	Rearranged during transfection proto-oncogene
RFP	Red fluorescent protein
RIN	RNA integrity number
RNA	Ribonucleoic Acid

RNAseq	RNA-sequencing
ROS1	Proto-oncogene tyrosine-protein kinase ROS
RPPA	Reverse phase protein array
RT	Room Temperature
RTK	Receptor Tyrosine Kinase
S6 kinase	p70 S6 kinase
S6 rp	S6 ribosomal protein
SCLC	Small Cell Lung Cancer
SD	Standard deviation
SDS	Sodium Dodecyl Sulfate
SDS-PAGE	SDS-Polyacrylamide Gel Electrophoresis
SEM	Standard Error of the Mean
SH2	Src homology 2
SH3	Src homology 3
SHC	SHC-transforming protein, adapter protein
SHP-1/2	SHP-1/2, non-receptor protein tyrosine phosphatases
SMA	Spheroid microarray
SOS	son of sevenless
SRC	Proto-oncogene tyrosine-protein kinase Src
STAT	Signal transducer and activator of transcription
STR DNA	Short Tandem Repeat DNA
T790M	EGFR mutation
TBE	Tris borate-EDTA
TBS	Tris-Buffered Saline
TBS-T	TBS with 0.5% Tween
TCGA	The Cancer Genome Atlas
TFS	ThermoFisher Scientific
TGFα	Transforming growth factor alpha
TKI	Tyrosine Kinase Inhibitor
TP53	Tumour suppressor p53
WT	Wild-type
ZD1839	gefitinib/IRESSA
γH2A.X	Phophorylated Histone H2AX
µg	Microgram
µL	Microlitre
µm	Micrometre

1 Introduction

1.1 Lung cancer and driver mutations

Lung cancer has been the most common cancer type world-wide for decades. With an estimated total of 1.8 million cases in 2012, it made up for 13% of all diagnosed cancers. Regions with the highest estimated age-standardised incidence rates are North America, Central and Eastern Europe and Eastern Asia, with incidence rates in women being lower than found in men (Ferlay, Soerjomataram et al. 2013).

Several risk factors are associated with lung cancer, including exposure to asbestos, a number of metals, organic chemicals, radiation and air pollution as well as genetic and viral factors (Sun, Schiller et al. 2007, Cogliano, Baan et al. 2011). The most important risk factor however is smoking, and European incidence rates of lung cancer show a link with smoking, with highest rates in Hungary and one of the lowest rates in Sweden (Ferlay, Soerjomataram et al. 2013, Dingemans, Reck et al. 2015). Of note, a significant proportion (15 % in men, 53 % in women, 25 % of total) of lung cancers are not attributed to smoking (Parkin, Bray et al. 2005). The major cause for lung cancer in never-smokers (< 100 cigarettes in life time), which are predominantly female and in the south-east Asian population, remains to be identified (Sun, Schiller et al. 2007).

Unfortunately, lung cancer is also the leading cause of cancer-related deaths world-wide. It is estimated to cause nearly one in five cancer deaths (1.59 million deaths, 19.4 % of all) in 2012 (Ferlay, Soerjomataram et al. 2013). Only one third of patients survive the first year after diagnosis and the 5-year survival rate is at 18 % in the US

and is even lower in the UK (Abdel-Rahman, Stockton et al. 2009, American Cancer Society 2017).

One of the main determinants of prognosis is the stage of the disease at the time of diagnosis. Nearly half of patients diagnosed with stage I lung cancer are still alive 5 years after diagnosis, whereas stage IV cancer remains practically incurable (Table 1-1). In the UK, only 1 in 5 patients present with localised tumours (stage I and II) with the majority presenting with mostly unresectable tumours (stage III and IV) (Table 1-1). This can be attributed to the non-specific symptoms. Early symptoms include cough, weight loss and dyspnea, followed by chest and bone pain, haemoptysis finger clubbing and hoarseness (Hamilton, Peters et al. 2005).

Table 1-1: Lung cancer stage at diagnosis and associated 5-year survival rates.

Cancer stage	Brief description	Stage at first diagnosis in UK (%) [1]	5-year survival rate (stage A/B in %)[2]
IA/IB	Tumour localised in lung - no spread to lymph nodes	14.5	49/45
IIA/IIB	Tumour localised in lung – spread to lymph nodes	7.3	30/31
IIIA/IIIB	Tumour spread locally in the lung and to lymph nodes	19.2	14/5
IV	Cancer has metastasised to the other lung or distant organs	47.9	1

A further determinant of prognosis is the availability of effective treatments. Treatment options include surgery, radiotherapy, chemotherapy, immunotherapy and targeted therapy. The choice of therapy depends on the performance status of the

[1] Data from National Cancer Registration and Analysis Service (NCRAS), data from 2012-2015

[2] Data from American Cancer Society (2017). "Cancer Facts & Figures 2017.".

patient, stage and histology, which in turn is associated with certain molecular characteristics of the tumour (NCCN 2016, Postmus, Kerr et al. 2017). Recommended treatment options are listed in Table 1-2 based on stage of disease.

Table 1-2: Outline of main treatment options by stage of disease for patients with NSCLC

From https://www.cancer.gov/types/lung/hp/non-small-cell-lung-treatment-pdq#link/_48414_toc (accessed Sept 2017). Pts: patients

NSCLC Stage	Primary Treatment Option(s)	Other treatment options
IA/IB	Surgery	Radiation therapy for pts who cannot have surgery or choose not to have surgery
IIA/IIB	Surgery Pts with completely resected stage II lung cancer may benefit from postoperative (adjuvant) cisplatin-based chemotherapy	Radiation therapy for pts who cannot have surgery or choose not to have surgery
IIIA	Chemotherapy followed by surgery Surgery followed by chemotherapy and/or radiation therapy	For pts with unresectable disease, radiation therapy alone, or administered sequentially with chemotherapy, or concurrently with chemotherapy
IIIB	Sequential or concurrent chemotherapy combined with radiation	Radiotherapy alone for pts unsuitable for chemotherapy
IV	Platinum-based doublet chemotherapy as 1st line treatment Single agent chemotherapy as 2nd line treatment Immune checkpoint inhibitors as 2nd line treatment	Targeted therapies as 1st line for patients with oncogenic mutations (EGFR, ALK) Pemetrexed maintenance therapy for pts with non-squamous NSCLC who have a response or stable disease after platinum-based combination chemotherapy

In general, carcinomas originating from the respiratory epithelium of the lung are referred to as lung cancers but there are two major subtypes based on histological features of the tumours. These are small cell lung cancer (SCLC, 10-15 % of cases) and non-small cell lung cancer (NSCLC, ~ 85 % of cases). NSCLC is further divided into adenocarcinoma, squamous cell carcinoma, large cell carcinoma and non-small cell carcinoma (Figure 1-1 A) (Howlader N 2015).

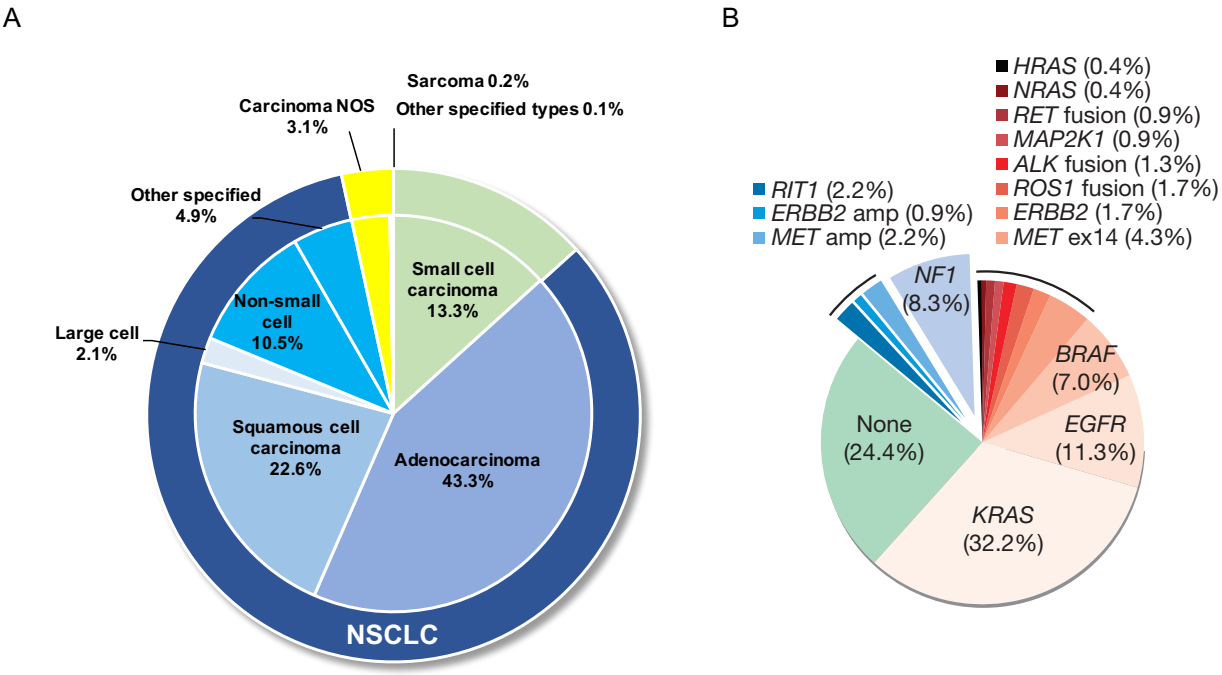


Figure 1-1: EGFR is the second most commonly mutated oncogene in lung adenocarcinoma.

A: Lung cancer histological subtypes based on Cancer of the Lung and Bronchus (Invasive). Data collected between 2008-2012 in USA and includes all race and gender, from (Howlader N 2015). B: Candidate driver oncogenes identified in adenocarcinoma samples by TCGA project (Cancer Genome Atlas Research 2014).

Within NSCLC, adenocarcinomas are the most common cancers (43.3 %) and they are more common in female than in male patients, and represent the dominant histology in non-smoking related lung cancer (Devesa, Bray et al. 2005, Sun, Schiller et al. 2007, Rudin, Avila-Tang et al. 2009, Howlader N 2015).

The most commonly mutated oncogenes in adenocarcinomas are Kirsten Rat Sarcoma (*KRAS)* and Epidermal Growth Factor Receptor (*EGFR)*, in smoking-

related and non-smoking related cancers, respectively (Figure 1-1 B) (Cancer Genome Atlas Research 2014). EGFR mutations are typically non-overlapping with other oncogenic drivers found in NSCLC (e.g. KRAS, ALK, ROS1, BRAF, RET and HER2 [1]) which make EGFR-mutant NSCLC a distinct disease entity (Gainor, Varghese et al. 2013, Garrido-Castro and Felip 2013, Stella, Scabini et al. 2013, Dong, Ren et al. 2016). Table 1-3 summarises compounds that are approved or under development for lung adenocarcinomas patients with different mutated oncogenes.

[1] mutations: KRAS, BRAF, HER2: human epidermal growth factor receptor 2; rearrangements/fusions: ALK: Anaplastic lymphoma kinase, ROS1, RET: rearranged during transfection and ERBB2

Table 1-3: Compounds targeting mutated oncogenes in patients with advanced lung adenocarcinoma

Mutated Oncogene	Approved compounds	Compounds in development[1]
KRAS, NRAS, HRAS[2]	None	trametinib, GDC-0623
EGFR	gefitinib, erlotinib, afatinib, osimertinib	(3rd generation only) HM61713, ASP8237, EGF816, PF-06747775[3]
BRAF	dabrafenib plus trametinib	
MET exon14[4]	None	crizotinib, cabozantinib
ERBB2[5]	None	afatinib, neratinib, dacomitinib, pyrotinib[6]
ROS1-fusion	crizotinib	PF-06463922, cabozantinib, lorlatinib
ALK-fusion	crizotinib, ceritinib, alectinib, brigatinib	
MAP2K1 (MEK1)	None	None
RET-fusion	None	alectinib, sunitinib, sorafenib, vandetanib, cabozantinib, apatinib, ponatinib, LOXO-292, lenvatinib[7]

[1] From https://clinicaltrials.gov/ (accessed Sept 2017)

[2] see: Kaufman, J. and T. E. Stinchcombe (2017). "Treatment of KRAS-Mutant Non-Small Cell Lung Cancer: The End of the Beginning for Targeted Therapies." JAMA **317**(18): 1835-1837.

[3] see: Wang, S., S. Cang and D. Liu (2016). "Third-generation inhibitors targeting EGFR T790M mutation in advanced non-small cell lung cancer." J Hematol Oncol **9**: 34.

[4] see: Awad, M. M., G. R. Oxnard, D. M. Jackman, D. O. Savukoski, D. Hall, P. Shivdasani, J. C. Heng, S. E. Dahlberg, P. A. Janne, S. Verma, J. Christensen, P. S. Hammerman and L. M. Sholl (2016). "MET Exon 14 Mutations in Non-Small-Cell Lung Cancer Are Associated With Advanced Age and Stage-Dependent MET Genomic Amplification and c-Met Overexpression." J Clin Oncol **34**(7): 721-730.

[5] see: Chuang, J. C., H. Stehr, Y. Liang, M. Das, J. Huang, M. Diehn, H. A. Wakelee and J. W. Neal (2017). "ERBB2-Mutated Metastatic Non-Small Cell Lung Cancer: Response and Resistance to Targeted Therapies." J Thorac Oncol **12**(5): 833-842.

[6] see: Peters, S. and S. Zimmermann (2014). "Targeted therapy in NSCLC driven by HER2 insertions." Transl Lung Cancer Res **3**(2): 84-88.

[7] see: Pirker, R. and M. Filipits (2015). "Alectinib in RET-rearranged non-small cell lung cancer-Another progress in precision medicine?" Ibid. **4**(6): 797-800.

1.2 EGFR protein structure and function

The epidermal growth factor receptor (EGFR, also known as ERBB1 or HER1) is one of four members of the ERBB lineage of proteins, and is among the most studied receptor protein-tyrosine kinases (Roskoski 2014). It was first described by Carpenter et al. in 1978 and research interest in EGFR increased in the early 1980s, after Cohen discovered that EGFR was a protein-tyrosine kinase and bound the epidermal growth factor (EGF) (Carpenter, King et al. 1978, Cohen, Ushiro et al. 1982, Cohen 1983).

The *EGFR* (*ERBB1/HER1*) gene is located on chromosome 7p11.2 and null mutations of the corresponding *Erbb1* gene in mice result in gastrointestinal, skin, and lung defects as well as perinatal lethality (Davies, Grosse et al. 1980, Shimizu, Behzadian et al. 1980, Kondo and Shimizu 1983, Miettinen, Berger et al. 1995). The gene contains 28 exons and spans approximately 200 kb. Multiple naturally occurring transcripts have been described, including the one coding for the full-length 170 kDa EGFR of 1210 amino acids (aa) (Reiter, Threadgill et al. 2001). Of note, numbering in the literature differs, depending on whether the 24-residue-long signal peptide is counted. Numbers in this work take the signalling peptide into account.

EGFR exists as a monomer, dimer or oligomer in the cell membrane, which can be induced by ligand binding. Dimerisation and oligomerisation occurs between EGFR molecules - as well as with other members of the ErbB family as HER2 and HER3 and IGF-1R (Morgillo, Woo et al. 2006) and MET (Ortiz-Zapater, Lee et al. 2017) - and enables kinase activation. Work from multiple groups indicates that tetramer formation occurs and might be important for efficient autophosphorylation and

signalling (Clayton, Walker et al. 2005, Clayton, Orchard et al. 2008, Kozer, Barua et al. 2014, Needham, Roberts et al. 2016).

The transmembrane receptor tyrosine kinase (RTK) EGFR consists of 3 distinct domains: the N-terminal extracellular (621 aa), the transmembrane (23 aa) and the intracellular domains (542 aa). The extracellular (ECM in Figure 1-2) domain is divided into four parts. Domains I and III are leucine-rich segments, involved in ligand binding and domains II and IV are involved in disulphide bond formation with their high number of cysteine residues. (Kondo and Shimizu 1983, Ullrich, Coussens et al. 1984, Arkhipov, Shan et al. 2013). The transmembrane domain is a 23-residue long α-helix, anchoring the receptor in the plasma membrane. It is thought to contain an N-terminal and a C-terminal dimerisation motif, allowing association of two neighbouring receptors in both the active and inactive state, respectively (Arkhipov, Shan et al. 2013, Endres, Das et al. 2013). The adjacent intracellular juxtamembrane (JM) segment consists of two segments (JM-A and JM-B) and plays a crucial role in the activation of the kinase (Jura, Endres et al. 2009, He and Hristova 2012). The kinase domain of nearly 300 amino acid residues consists of two lobes (N and C lobe). The smaller N lobe contains the adenosine triphosphate (ATP) binding loop and the regulatory helix α-C (Figure 1-3 B). The large C lobe contains two further regulatory elements. The kinase-typical Asp–Phe–Gly (DFG) activation segment coordinates ATP by Mg^{2+} binding and the so-called activation loop controls peptide binding depending on its conformation (Figure 1-3 A). (Roskoski 2014, Kovacs, Zorn et al. 2015). The C-terminal tail of the protein consists of 230 residues, contains a number of phosphorylation sites and is reported to have a non-globular, extended structure. It is thought to have an auto-inhibitory function and is important in binding of downstream signalling proteins (Gajiwala 2013, Keppel, Sarpong et al. 2017).

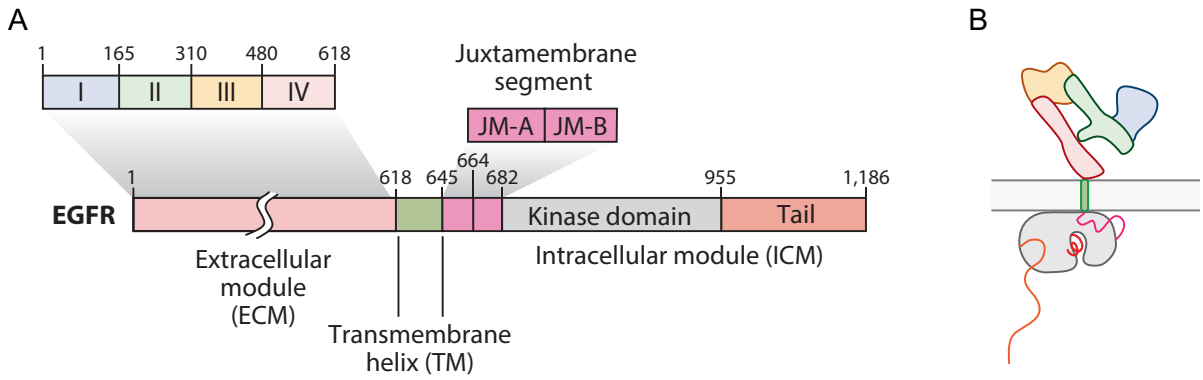


Figure 1-2: Schematic view of EGFR protein structure and conformation of the EGFR monomer
Cartoon of the domain architecture (A) and structure of the membrane bound EGFR monomer (B) from (Arkhipov, Shan et al. 2013, Kovacs, Zorn et al. 2015).

EGFR activation has been the subject of intense research focus and is now relatively well characterised. However, when considering structural-functional characterisation, it is important to keep in mind that the crystallisation of single-pass transmembrane proteins like EGFR is challenging. Knowledge about structure and function of EGFR has largely been gained from studies where parts but not the entire protein have been crystallised on their own or in conjunction with a number of different ligands or compounds. While such studies provide valuable mechanistic insights into the function of individual domains, there may be important aspects of EGFR's structure-function relationship that remain undiscovered. Additionally, the nature of the receptor's host membrane is thought to have an impact on receptor conformation and the high number of neighbouring molecules during crystallisation might influence observed conformations (Zhang, Gureasko et al. 2006, Arkhipov, Shan et al. 2013, Kovacs, Zorn et al. 2015, Kaplan, Narasimhan et al. 2016).

EGFR is activated by binding of a number of peptide growth factors, including the epidermal growth factor (EGF) and transforming growth factor α (TGFα). A detailed overview of all ligands is given by Roskoski et al. (Roskoski 2014). Ligand binding to domains I and III of each receptor leads to a conformational change in the

extracellular domain from a tethered to an extended form. This reveals the dimerisation element in domain II, which is buried in domain IV in the folded conformation of the receptor. This “dimerisation arm” is now free to interact with the corresponding element of the other receptor. Notably, the dimer interface is formed by the receptors themselves, with the ligand is binding on the ‘outside’ of a back-to-back dimer (Leahy 2004, Kovacs, Zorn et al. 2015). Following ligand binding, a rotation of ~130 ° takes place which alters the conformation of the transmembrane domain, favouring dimerisation at the N-terminal dimerisation motif over the C-terminal one in the transmembrane domain (Fleishman, Schlessinger et al. 2002, Arkhipov, Shan et al. 2013, Endres, Das et al. 2013). Changes in conformation also affect the juxtramembrane domain, where the JM-A domain packs against the JM-A domain of the dimer partner and the JM-B segment functions as a clamp, interacting with the kinase domain of the paired receptor (Figure 1-3 A). Structural coupling of these domains is crucial for receptor activation and potentiates receptor dimerisation (Jura, Endres et al. 2009, Red Brewer, Choi et al. 2009, Scheck, Lowder et al. 2012, Sinclair, Denton et al. 2014). The described changes lead to the formation of an asymmetric kinase dimer, with one activator/donor and one receiver/acceptor molecule. The activated acceptor kinase catalyses the phosphorylation of tyrosine residues in the donor kinase, which then serve as docking sites for downstream signalling molecules (e.g. GRB2, PI3K) containing phosphotyrosine binding (PTB) or Src homology 2 (SH2) domains (Roskoski 2014).

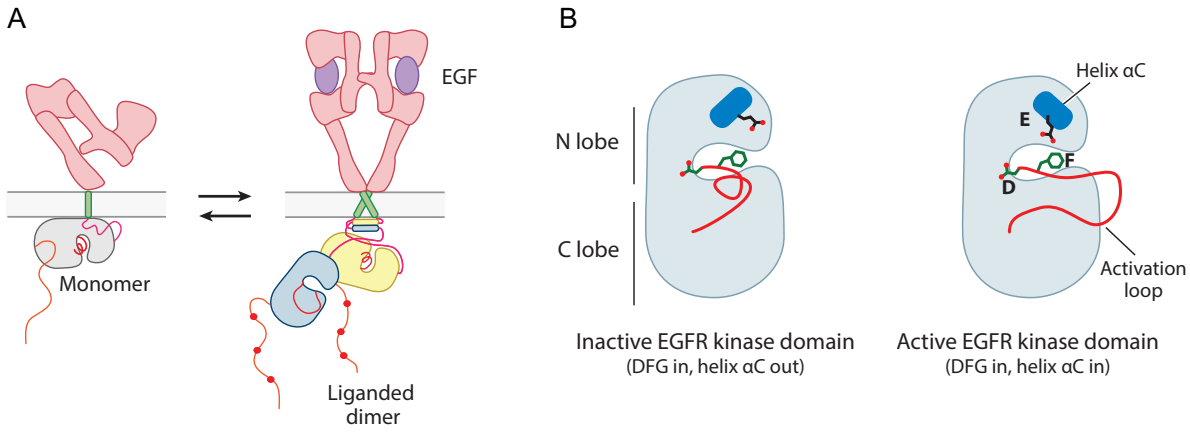


Figure 1-3: Oligomerisation and activation states of the EGFR

A: Schematic of the inactive monomeric and active dimeric states of the EGFR. B: Conformation of kinase domain in inactive and active form with changing orientation and conformation of the DFG and αC helix segments. DFG: activation segment. From (Kovacs, Zorn et al. 2015).

Details on the activation and control of the kinase function are reviewed by Jura et al. (Jura, Zhang et al. 2011). Of interest, it has been shown that that under certain conditions, EGFR activation is not dependent on ligand binding. Research from several groups suggests, that the intermolecular interaction that promotes kinase activation can occur under high concentrations of the receptor as well as in the presence of certain mutations (see chapter 1.4) (Zhang, Gureasko et al. 2006, Endres, Das et al. 2013, Needham, Roberts et al. 2016).

1.3 EGFR signalling

EGFR plays a major role in diverse cellular functions, including cell proliferation, differentiation, motility, and survival. It is also important in tissue development and is ubiquitously expressed in epithelial, mesenchymal, and neuronal cells and their cellular progenitors. Ligand binding leads to phosphorylation of a number of phospho-tyrosine (pY) residues in EGFR, as illustrated in Figure 1-4. Autophosphorylation sites include Y1068, Y1148 and Y1173 (Downward, Parker et al. 1984). Phosphorylation of EGFR leads to recruitment of adapter proteins, which activate a number of interconnected and overlapping pathways. These include the

phosphatidylinositol 3-kinase (PI3K)/AKT pathway and the RAS/RAF/MEK/ERK pathway.

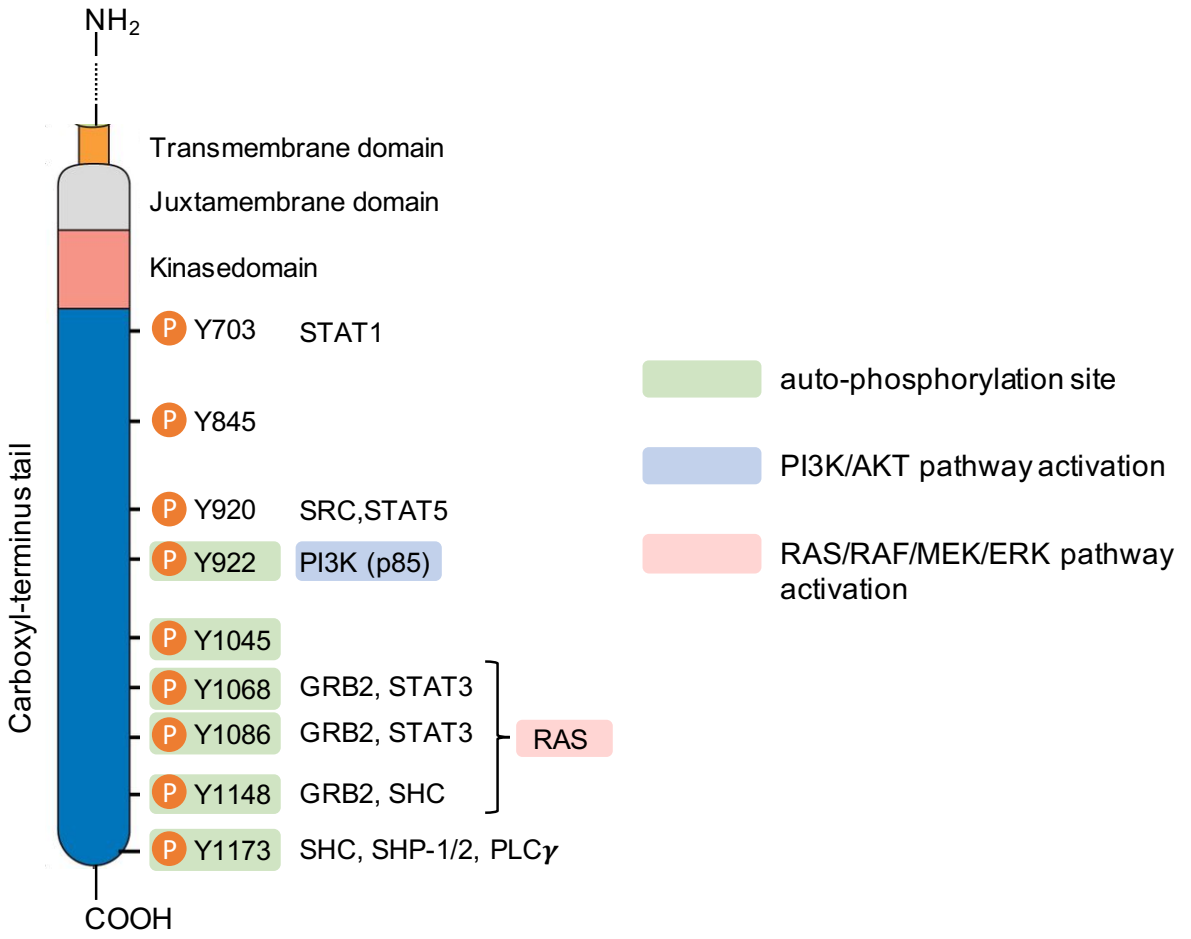


Figure 1-4: EGFR phosphorylation sites and activated pathways

Schematic of a number of phosphorylation sites of EGFR, corresponding adapter proteins and selected activated pathways. Adapted from (Chen, Zeng et al. 2016) and (Shostak and Chariot 2015)

The PI3K pathway has been reviewed extensively (Engelman, Luo et al. 2006). In short, activated receptors, importantly ERBB3 with its SH3 binding domains (Soltoff, Carraway et al. 1994, Hellyer, Cheng et al. 1998, Engelman, Janne et al. 2005), bind the regulatory p85 subunit of class I PI3K via their SH2 domain which allows the catalytic p110 subunit to catalyse the phosphorylation of phosphatidylinositol bisphosphate (PIP_2) to phosphatidylinositol triphosphate (PIP_3). This is counteracted by phosphatase and tensin homolog (PTEN). Increased PIP_3 levels at the plasma membrane lead to increased binding of a number of signalling proteins via their

pleckstrin homology domains, such as phosphoinositide-dependent kinase 1 (PDK1) and AKT. PDK1 as well as the mTOR-rictor kinase complex can then phosphorylate AKT, which allows AKT to dissociate from the membrane. It can then phosphorylate a number of cytoplasmic and nuclear targets and thereby regulate a range of cellular functions, including survival and cell growth. This is partly mediated via its ability to block FOXO-mediated transcription of cell-cycle inhibitors and pro-apoptotic proteins as well as promotion of protein synthesis via activation of MTOR (Engelman, Luo et al. 2006, Gadgeel and Wozniak 2013).

The RAS/RAF/MEK/ERK pathway is the most extensively studied MAPK-mediated pathway. MAPK signalling has been reviewed in detail, including a publication by Chang et al. (Chang and Karin 2001). In short, RAS activation via the adapter molecules GRB2 and SOS after EGFR activation leads to membrane recruitment and phosphorylation of RAF. Activated RAF can then phosphorylate and activate MEK1/2 and ERK1/2. ERKs then translocate to the nucleus and regulate a number of transcription factors that control the expression of multiple genes involved in survival and proliferation (Robinson and Cobb 1997, Montagut and Settleman 2009).

Key parts of these signalling pathways as well as cross inhibition and cross activation between the two are illustrated in Figure 1-5 (Mendoza, Er et al. 2011).

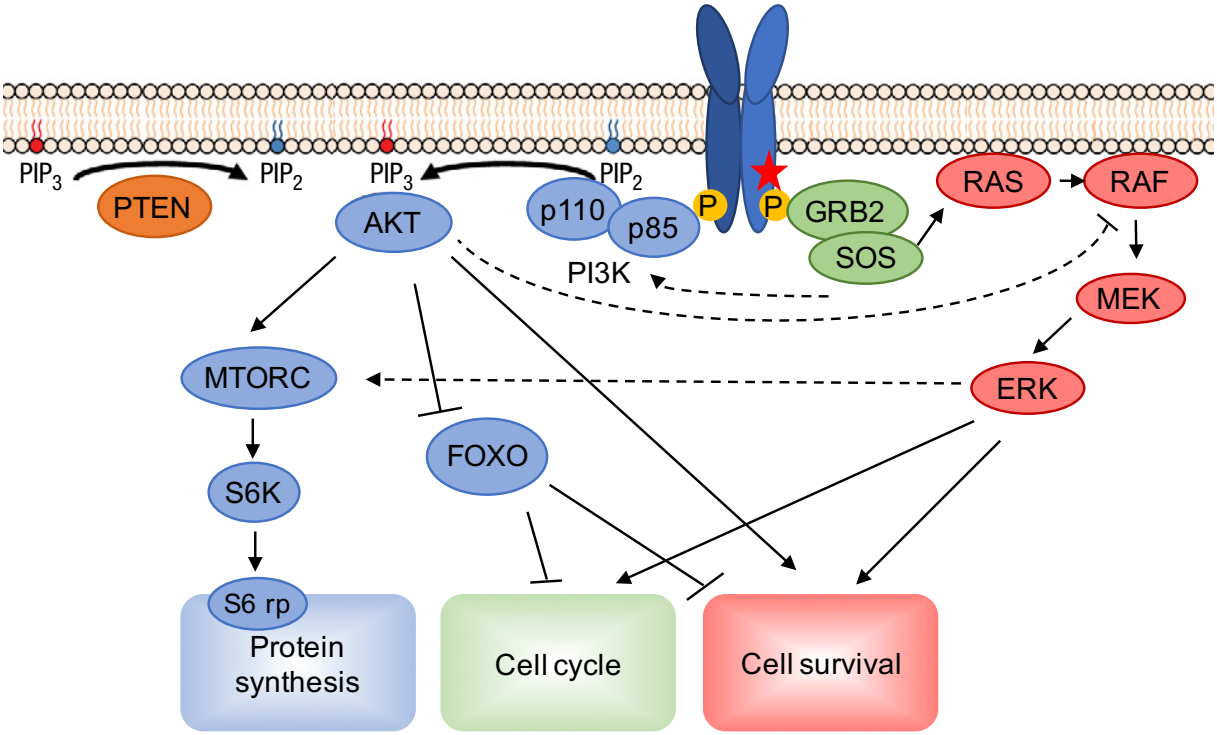


Figure 1-5: Signalling of EGFR through the PI3K/AKT and the MAPK pathways

Activated EGFR signals through the PI3K and MAPK pathway among others. Arrows indicate activation, terminated lines indicate inhibition. Cross talk between the two pathways is indicated with dashed lines. The red star represents an activating mutation in the EGFR (light blue). The dimer partner (dark blue) represents any of the possible dimerisation partners mentioned previously. Adapted from (Gadgeel and Wozniak 2013)

As mentioned above, activation of EGFR and downstream signalling is also possible in the absence of ligand binding, for example under high receptor density. Another mechanism of ligand-independent EGFR activation is through the presence of activating mutations in EGFR (illustrated in Figure 1-5), which are found in 11.3 % of lung adenocarcinomas (Cancer Genome Atlas Research 2014).

1.4 EGFR mutations in NSCLC

De novo somatic mutation in *EGFR* were first described in tumours from lung cancer patients in 2004 (Lynch, Bell et al. 2004, Paez, Janne et al. 2004, Pao, Miller et al. 2004). Further investigations identified these as activating mutations, found in exons 18-20 of *EGFR* (Chan, Gullick et al. 2006). Activating mutations were able to promote cellular transformation, allowing ligand-independent EGFR activation

(Greulich, Chen et al. 2005, Jiang, Greulich et al. 2005) and could be grouped into three types. Point mutations were identified within the nucleotide-binding loop in exon 18 and activation loop in exon 21, small in frame deletions in exon 19 and insertions in exon 20, summarised in Figure 1-6 A and in a review by Sharma et al. (Sharma, Bell et al. 2007). All activating mutations cluster around the ATP binding cleft between the N lobe and C lobe, as illustrated in Figure 1-6 B and increase kinase activity. The two most common mutations are an in frame exon 19 LREA deletion (45 %) and an exon 21 L858R point mutation (40-45 %) (Sharma, Bell et al. 2007). The LREA in-frame deletion brings the αC helix close to the active site and stabilises the active conformation of EGFR, leading to sustained EGFR signalling. Sustained activation of the EGFR with a L858R mutation is likely to be due to stabilisation of the activation loop as well as increased dimerisation (Gazdar, Shigematsu et al. 2004, Yun, Boggon et al. 2007, Shan, Eastwood et al. 2012, Sutto and Gervasio 2013). Of interest is that the affinity of the L858R mutant for ATP is increased dramatically by the T790M mutation in exon 20 (<1 % in treatment naïve patients) (Yun, Mengwasser et al. 2008, Yu, Arcila et al. 2014). Hereditary T790M mutations have been observed but data suggests, that this only leads to a weak activation of the EGFR and a somatically acquired second activating EGFR mutation as L858R is found in the majority of lung cancers of germline *EGFR* T790M carriers (Gazdar, Robinson et al. 2014). The L858R/T790M double mutant also shows a stronger interaction with the dimerization partners ERBB2, IGF-1R and MET, compared to mutant L858R (Wang, Ma et al. 2015, Ortiz-Zapater, Lee et al. 2017). Notably, it has been shown, that the conformational changes and increased activity resulting from a number of these mutations allow mutant proteins to activate other receptors – mutant EGFR but

importantly also other WT ERBB family members - more frequently (Red Brewer, Choi et al. 2009).

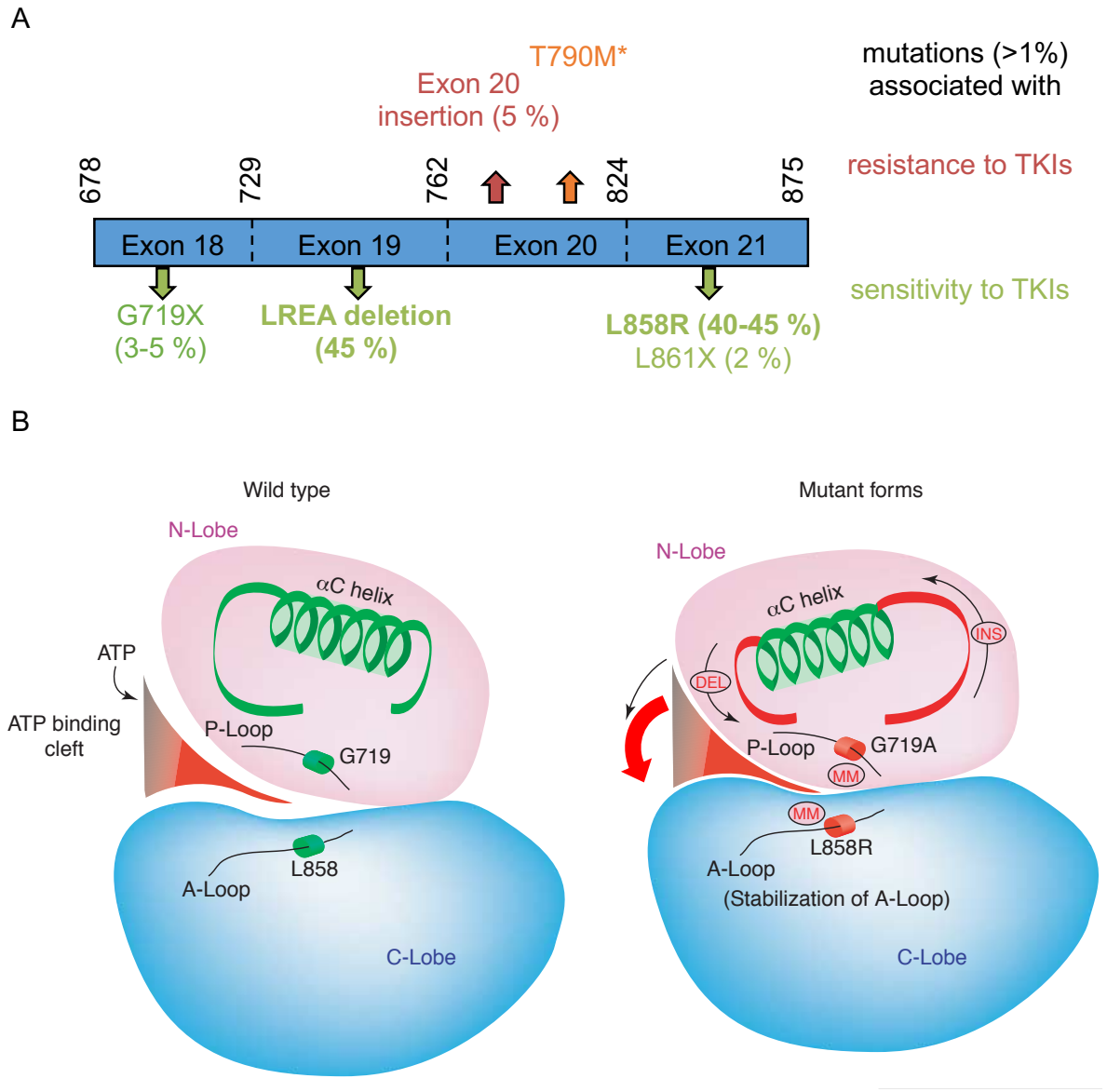


Figure 1-6: Types and effects of mutations commonly found in in the EGFR kinase domain in NSCLC.

A: Schematic of somatic EGFR TK domain mutations in lung cancer with a frequency of >1 % (incidence of mutations in brackets; green: EGFR-inhibitor sensitive, red: EGFR-inhibitor resistant, orange differentially sensitive to different generations of EGFR-inhibitors). A missense mutation is represented by the reference amino acid, followed by the residue number, followed by the mutant residue. X indicates that this position has been shown to be replaced by multiple different amino acids. * T790M mutation frequency is < 1 % in treatment naïve patients. Adapted from (Sharma, Bell et al. 2007), B: Conformation of the wild type and mutant EGFR kinase domain. Mutations, including missense mutations (MM), insertions (INS) and deletions (DEL) lead to a narrowing of the ATP binding cleft. From (Gazdar, Shigematsu et al. 2004).

Recent developments in the detection of circulating free tumour DNA (cfDNA) allow for detection of EGFR mutations in blood of patients for whom a biopsy could not be taken or is not sufficient for genetic analysis. Furthermore this technique allows

assessment of cfDNA over the course of the treatment, e.g. for monitoring of potential resistance-conferring mutations (Taniguchi, Uchida et al. 2011, Chabon, Simmons et al. 2016, Vallee, Audigier-Valette et al. 2016, Mayo-de-Las-Casas, Jordana-Ariza et al. 2017).

1.5 EGFR inhibitors for the treatment of EGFR M+ NSCLC

Following the ESMO Clinical Practice Guidelines for NSCLC, the treatment of choice for resectable NSCLC is surgery, independent of mutational status of known oncogenes. Inoperable patients should be treated with stereotactic radiotherapy (Postmus, Kerr et al. 2017). Patients with regional lymph node involvement benefit from adjuvant chemotherapy after surgery (Artal Cortes, Calera Urquizu et al. 2015) and ongoing research suggests that EGFR-mutation positive patients might benefit from adjuvant treatment with EGFR-inhibitors but there is no recommendation for adjuvant therapy at this point (Greig 2016, Huang, Li et al. 2016, Postmus, Kerr et al. 2017). Inoperable EGFR-mutation positive patients (IIIb and IV) should receive EGFR-targeted therapy (Postmus, Kerr et al. 2017).

Before the discovery of EGFR activating mutations, ATP-competitive EGFR TK-inhibitors (EGFR-TKIs) were developed and gained FDA approval (Pollack, Savage et al. 1999, Barker, Gibson et al. 2001, Rusnak, Lackey et al. 2001, FDA 2003). Observations of increased EGFR protein levels in cancers compared to normal tissues formed the original rationale for the use of EGFR-TKIs (Rusch, Baselga et al. 1993). However, studies showed that EGFR expression as detected via IHC was not a predictor of response to the compound (Bailey, Kris et al. 2003). It was only through observations in clinical trials, in which a subset of NSCLC patients showed dramatic tumour responses to gefitinib (EGFR-TKI) (Fukuoka, Yano et al. 2003,

Janne, Gurubhagavatula et al. 2004), that EGFR mutations were identified as predictors of sensitivity (Chou, Chiu et al. 2005, Janne, Engelman et al. 2005).

There are currently four EGFR-TKIs approved for use in EGFR-mutant NSCLC which can be grouped into 3 generations, based on their binding mode and selectivity for mutant over WT EGFR (Table 1-4).

Table 1-4: EGFR-TKIs approved for use in NSCLC in USA and European Union (Sept 2017)

Drug Name (generic INN)	EGFR-TKI generation [1]	Indication USA (FDA)[2]	Indication Europe (EMA)[3]
IRESSA (gefitinib)	1st	1st line treatment of patients with metastatic NSCLC whose tumours have EGFR exon 19 deletions or exon 21 (L858R) substitution mutations	Indicated as monotherapy for the treatment of adult patients with locally advanced or metastatic NSCLC with activating mutations of EGFR-TK
TARCEVA (erlotinib)	1st	The treatment of patients with metastatic NSCLC whose tumours that have EGFR exon 19 deletions or exon 21 (L858R) substitution mutations receiving first-line, maintenance, or 2nd or greater line treatment after progression following at least one prior chemotherapy regimen	Indicated for 1st line treatment of patients with locally advanced or metastatic NSCLC with EGFR activating mutations Also indicated for maintenance treatment in patients with locally advanced or metastatic NSCLC with EGFR activating mutations and stable disease after first-line chemotherapy Also indicated for the treatment of patients with locally advanced or metastatic NSCLC after failure of at least one prior chemotherapy regimen
GIOTRIF (afatinib)	2nd	Indicated for 1st line treatment of patients with metastatic NSCLC whose tumours have EGFR exon 19 deletions or exon 21 (L858R) substitution mutations Also indicated for treatment of patients with metastatic squamous NSCLC progressing after platinum-based chemotherapy	Indicated as monotherapy for the treatment of EGFR-TKI-naïve adult patients with locally advanced or metastatic NSCLC with activating EGFR mutation(s) Also indicated for locally advanced or metastatic NSCLC of squamous histology progressing on or after platinum-based chemotherapy
TAGRISSO (osimertinib)[4]	3rd	Indicated for the treatment of patients with metastatic EGFR T790M mutation-positive NSCLC whose disease has progressed on or after EGFR-TKI therapy	Indicated for the treatment of adult patients with locally advanced or metastatic EGFR T790M mutation-positive NSCLC

[1] 1st: ATP-competitive, inhibits both wild type and common mutant forms of EGFR, but not EGFR T790M; 2nd: Irreversible, inhibits both wild-type and common mutant forms of EGFR and also EGFR T790M; 3rd: Irreversible, selectively inhibits common mutant forms of EGFR and also EGFR T790M, but not wild-type EGFR

[2] Data from https://www.accessdata.fda.gov/scripts/cder/daf/index.cfm (accessed Sept 2017)

[3] Data from http://www.ema.europa.eu/ema/index.jsp?curl=pages/includes/medicines/medicines_landing_page.jsp&mid= (accessed Sept 2017)

[4] osimertinib is referred to as AZD9291 in this work

1st generation EGFR-TKIs were first used more than 15 years ago. They compete with ATP for the binding to the ATP-binding cleft between the N lobe and the C lobe of the EGFR kinase domain and show selectivity for EGFR over other RTKs (Pollack, Savage et al. 1999, Barker, Gibson et al. 2001, Wakeling, Guy et al. 2002).

Of great importance for the treatment of EGFR-mutant patients was the discovery that different EGFR mutants show different degrees of sensitivity to gefitinib or erlotinib binding. EGFR-activating mutations can therefore be grouped into EGFR-TKI-sensitive and -resistant mutations (Figure 1-6). The L858R mutant for example is highly sensitive, 10-100 fold more than the WT kinase (Pao, Miller et al. 2004, Mukohara, Engelman et al. 2005, Yun, Boggon et al. 2007) and the exon 20 insertion mutants are highly resistant (Greulich, Chen et al. 2005). Within the group of EGFR-TKI-sensitising mutations, there are different degrees of sensitivity (Jiang, Greulich et al. 2005, Yun, Boggon et al. 2007). As mentioned earlier, the ATP affinity of L858R/T790M double mutants is dramatically higher than in the L858R single mutant. The T790M mutation leads to increased binding of ATP compared to the EGFR-TKI, which is outcompeted and the receptor is drug resistant (Yun, Mengwasser et al. 2008).

The high degree of sensitivity of mutant EGFR to EGFR-TKIs was reflected in clinical trials. Several studies showed a significantly longer PFS in EGFR mutation-positive patients treated with gefitinib compared to carboplatin–paclitaxel treatment and no benefit of EGFR-TKI treatment in the EGFR-mutation negative population (Mok, Wu et al. 2009, Maemondo, Inoue et al. 2010, Mitsudomi, Morita et al. 2010). Overall survival (OS) however has repeatedly been reported to not be statistically different between EGFR-TKI and chemotherapy groups (Inoue, Kobayashi et al. 2013, Yoshioka, Mitsudomi et al. 2014), as summarised in a meta-analysis by Lee et al.

(Lee, Brown et al. 2013). This might be due to the high crossover of treatments on a number of the analysed studies although one recently published study on retrospective analysis of outcomes of EGFR mutation-positive patients identified a significant improvement in OS in patients treated with EGFR-TKIs compared to other treatments (24.3 vs 10.8 months) (Zhao, Chen et al. 2017). Importantly, quality of life has been assessed in four different randomised trials and confirmed superiority of first line EGFR-TKI over chemotherapy (Maemondo, Inoue et al. 2010, Mitsudomi, Morita et al. 2010, Thongprasert, Duffield et al. 2011, Zhou, Wu et al. 2011).

With the aim of prolonging progression-free survival (PFS) and improving OS further, the covalently-binding 2nd generation of EGFR-TKIs was developed (Solca, Dahl et al. 2012). Afatinib was designed to covalently bind to cysteine at position 797 (C797) and irreversibly block enzymatically active ERBB receptor family members (Rusnak, Lackey et al. 2001, Solca, Dahl et al. 2012). This irreversible binding enables them to overcome the enhanced ATP affinity conferred by the T790M mutation - which had been identified as a major cause of resistance (see chapter 1.6) - leading to successful inhibition of kinase activity. A detailed review of covalent EGFR-TKIs is given by Hossam et al. (Hossam, Lasheen et al. 2016).

In short, the benefit of the covalently-binding 2nd generation inhibitors (e.g. afatinib) is detectable but limited (Yang, Wu et al. 2015). Doses sufficient to inhibit T790M EGFR could not be achieved or maintained in patients, due to severe side effects (including skin rash and diarrhoea), mainly caused by inhibition of the WT EGFR molecule, as C797 is not a feature unique to mutant EGFR (Sequist, Besse et al. 2010, Miller, Hirsh et al. 2012, Katakami, Atagi et al. 2013).

The need for more potent and most importantly mutant-specific inhibitors led to the development of a 3rd generation of inhibitors, that could target T790M and EGFR-TKI-sensitizing mutations while sparing WT EGFR (Cross, Ashton et al. 2014).

3rd generation EGFR-TKIs include CO-1686, WZ4002 and AZD9291. Encouraging efficacy of these inhibitors *in vitro* and in preclinical models as well as clinical benefit in T790M mutation positive patients has led to accelerated approval of AZD9291 by the FDA in November 2015 (Janne, Ramalingam et al. 2014, Sequist, Soria et al. 2015, Greig 2016). Regular approval for the treatment of metastatic EGFR T790M mutation-positive NSCLC, which has progressed on or after EGFR-TKI therapy was granted in March 2017 (FDA 2017).

As described for the 2nd generation, 3rd generation inhibitors also bind covalently to the cysteine at position 797 and therefore reduce ATP binding to the kinase domain even in the presence of the T790M mutation (Cross, Ashton et al. 2014). In contrast to 2nd generation inhibitors, AZD9291 is mutant-specific; it was selected based on its selectivity for the L858R/T790M double mutant over the EGFR WT (Ward, Anderton et al. 2013). AZD9291 shows 200-fold and 20-fold higher potency for the L858R/T790M and L858R mutants over WT EGFR, respectively (Cross, Ashton et al. 2014).

Marked responses in clinical trials with EGFR T790M mutation positive patients led to the approval of AZD9291 by the FDA in 2015. Results showed a higher response rate in T790M mutation positive compared to mutation negative patients (61 % compared to 21 %) and longer PFS (9.8 vs. 2.8 months) (Janne, Yang et al. 2015), similar to that achieved by 1st line treatment with EGFR-inhibitors (Yoshioka, Mitsudomi et al. 2014).

Another study with 419 patients who had progressed under previous EGFR-TKI treatment and were EGFR T790M mutation-positive showed an objective response rate of 71 % under AZD9291 treatment. Furthermore, patients under AZD9291 treatment had a significantly longer PFS than patients treated with platinum therapy plus pemetrexed and importantly, the proportion of patients with grade 3 or higher adverse events was lower under AZD9291 (Mok, Wu et al. 2017).

Recently announced results from the phase III FLAURA study show superior objective response rates (ORR) and duration of response (DoR) to AZD9291 compared to gefitinib/erlotinib (ORR: 80 % vs 76 %; DoR: 12.7 vs 8.5 months). This was reflected in the significantly longer PFS (18.9 vs 10.2 months) as well as a clinically meaningful trend in overall survival benefit in patients treated with AZD9291 compared to gefitinib or erlotinib as 1st line therapy (Astra Zeneca 2017). A review by Greig gives an overview of completed and ongoing clinical trials as well as their reported outcomes, including the ADAURA trial on the adjuvant use of AZD9291 (Greig 2016).

Unfortunately, patients progress even under treatment with 3rd generation inhibitors. This is due to the emergence of resistance, commonly via mutations of cysteine at position 797 to serine (C797S), which prevents covalent drug binding (see chapter 1.6). Research is on-going to identify compounds that inhibit EGFR even in the presence of the C797S mutation, including approaches using allosteric mutant specific inhibitors or combination therapies of small molecule EGFR inhibitors and EGFR-targeting antibodies (Jia, Yun et al. 2016, Uchibori, Inase et al. 2017).

Importantly, acquired mutations in EGFR are not the only mechanism of resistance and the following chapter will summarise current knowledge about a number of different mechanisms of resistance to EGFR-TKIs.

1.6 Resistance mechanisms

Resistance to targeted therapies is not unique to EGFR-TKIs in lung cancer treatment. A review by Neel and Bivona gives an overview of mechanisms of resistance observed in lung cancer (Neel and Bivona 2017), which are also illustrated in Figure 1-7. Targeted therapies lose their ability to inhibit downstream signalling either by on-target mutations that prevent the inhibition of the kinase activity or by a number of different mechanisms that activate downstream signalling in a manner that is independent of phosphorylation of the target kinase. These resistance mechanisms include activating mutations in downstream pathways and activation of downstream pathways by parallel RTKs among others.

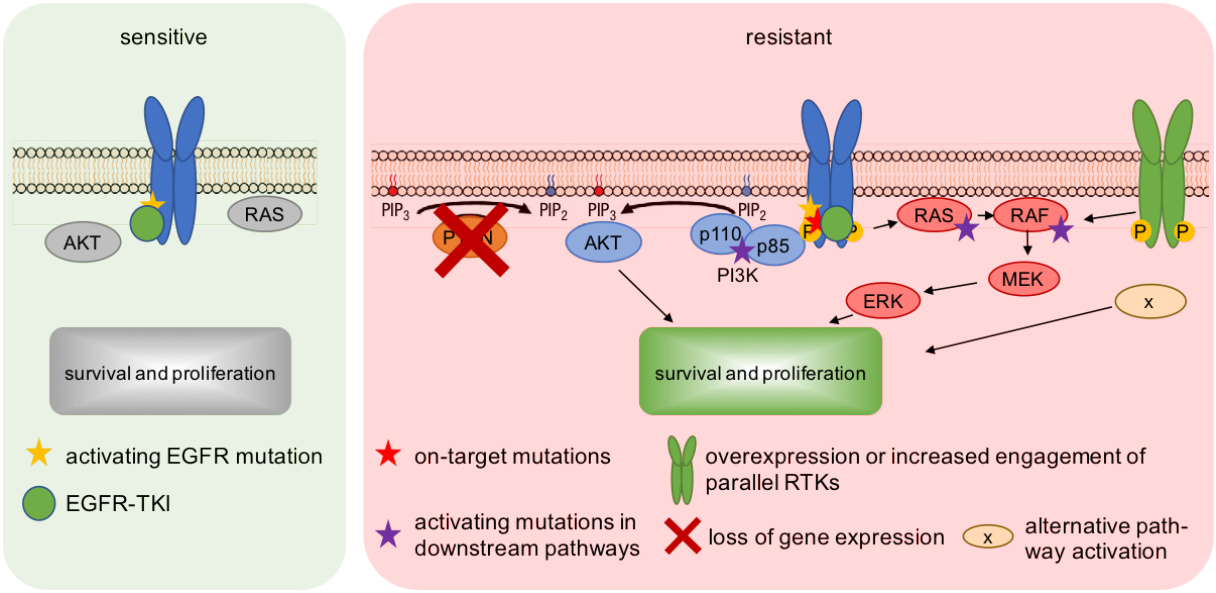


Figure 1-7: Mechanisms of resistance to targeted therapy

Treatment with EGFR-TKIs leads to decreased downstream signalling in an EGFR-TKI sensitive but not resistant cell. Resistance can be due to several mechanisms, illustrated above.

Studies analysing EGFR-mutated NSCLC tumours upon progression under EGFR-TKIs revealed a number of possible mechanisms of resistance and showed compound-specific effects between and within generations of EGFR-TKIs.

Mechanisms of acquired resistance to 1st generation EGFR-TKIs have been reviewed by a number of groups (Engelman and Janne 2008, Camidge, Pao et al. 2014, Morgillo, Della Corte et al. 2016) and an overview is given in Figure 1-8. They include *MET* and *ERBB2* amplification as well as overexpression of the MET ligand HGF, all of which can lead to activation of PI3K signalling via HER3 heterodimer formation (Engelman, Zejnullahu et al. 2007). Increased signalling has also been found to be due to IGF-1R or AXL pathway activation (Engelman, Zejnullahu et al. 2007, Neel and Bivona 2017). Furthermore, SCLC transformation, epithelial-to-mesenchymal transition (EMT) and activating mutations in PIK3CA and BRAF have been observed. The dominating mechanism of resistance however, is the EGFR T790M mutation, which occurs in nearly half of all patients (Sequist, Waltman et al. 2011, Yu, Arcila et al. 2013, Piotrowska, Niederst et al. 2014). The T790M mutation was first described as resistance mechanism in 2005, soon after the identification of activating EGFR mutations (Kobayashi, Boggon et al. 2005, Pao, Miller et al. 2005). The decreased binding of ATP-competitive EGFR-TKIs is likely to be due to the increased ATP affinity of the T790M mutant protein rather than steric hindrance by the bulky methionine, as commonly reported (Yun, Mengwasser et al. 2008). This can however be overcome with 3rd generation inhibitors, as described above.

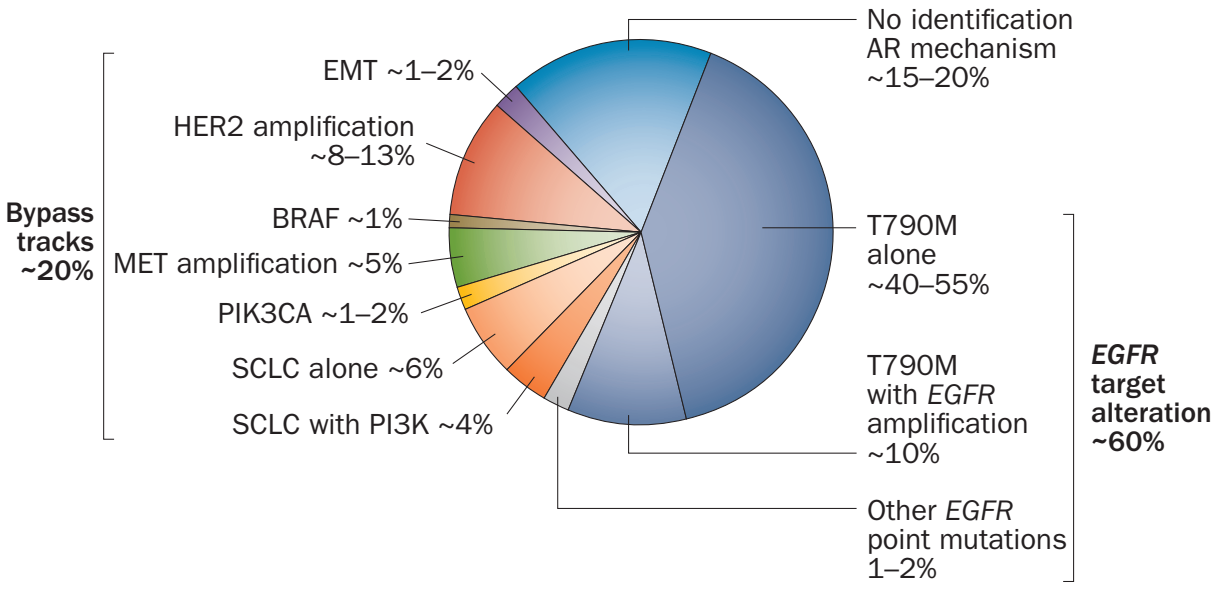


Figure 1-8: Mechanisms of Acquired Resistance in EGFR-mutant NSCLC patients
Mechanisms of acquired resistance to erlotinib and gefitinib. From (Camidge, Pao et al. 2014).

In vitro experiments recapitulate mechanism of resistance observed in patients, as T790M (Ogino, Kitao et al. 2007), MET amplification (Engelman, Zejnullahu et al. 2007), EMT (Yoshida, Song et al. 2016) among others but have also identified additional mechanisms not reported in patients. Among them are epigenetic changes that facilitate emergence of resistant cells, as discussed by Sharma et al. (Sharma, Lee et al. 2010). A recently published genetic screen has further identified chromatin modifiers as potential modifiers of EGFR-TKI sensitivity (Liao, Davoli et al. 2017).

Mechanisms of resistance to the 2nd generation inhibitor afatinib are reviewed by van der Wekken et al. and won't be discussed in this work (van der Wekken, Saber et al. 2016).

As with the 1st generation EGFR-TKIs, mechanisms of resistance to 3rd generation inhibitors are diverse but currently dominated by on-target mutations.

As shown in *in vitro* studies by Ercan et al., point mutations can confer resistance to 3rd generation EGFR-TKIs and mechanisms differ between inhibitors. Resistance to WZ4002, CO-1686 but not AZD9291 is conferred by EGFR L718Q and L844V mutations in addition to the C797S that is common to all three inhibitors (Ercan, Choi et al. 2015). This is in line with observations in patients, where the C797S mutation was detected in cell-free plasma DNA from nearly 40 % of AZD9291-resistant patients (Thress, Paweletz et al. 2015). Mutation of the cysteine in position 797 confers resistance, as it prevents the formation of the potency-conferring covalent bond. Patients without confirmed C797S mutation showed loss of T790M, which is in line with observations from studies where T790M becomes undetectable under treatment breaks (Sequist, Waltman et al. 2011, Hata, Katakami et al. 2013, Piotrowska, Niederst et al. 2015). However, this is unlikely to be the mechanism of resistance but rather mechanisms observed in resistance to 1st generation. Indeed, SCLC transformation, BRAF and other mutations in the EGFR kinase domain mutations as well as amplifications of MET, KRAS and HER2 and activation of other parallel pathways have been observed in patients (Walter, Sjin et al. 2013, Kim, Song et al. 2015, Planchard, Loriot et al. 2015, Chabon, Simmons et al. 2016, Ham, Kim et al. 2016, Ho, Liao et al. 2017, Ou, Wu et al. 2017).

1.7 Treatment options upon resistance

Response rates for patients on EGFR-TKIs are high but very few patients have complete responses (disappearance of visible tumours on CT/PET). The median tumour shrinkage relative to baseline has been reported to be 56 % for gefitinib

(Takeda, Okamoto et al. 2014) and is estimated to be similar for AZD9291 (Mok, Wu et al. 2017). The ESMO guidelines do not currently contain recommendations on continuation of treatment beyond progression on 3rd generation EGFR-TKIs (Postmus, Kerr et al. 2017) and conventional practice would be to change patients onto second/third-line treatments, such as chemotherapy. The role of EGFR-TKIs post-progression is however an important question. Results from a number of retrospective studies as well as the prospective ASPIRATION trial suggest a benefit in continuing EGFR-TKI treatment beyond radiological detection of progression (Maruyama, Wataya et al. 2009, Nishie, Kawaguchi et al. 2012, Park, Yu et al. 2016). This is in line with observations by a number of groups showing accelerated disease progression after EGFR-TKI treatment discontinuation, which is generally referred to as 'tumour flare'. Improvement of symptoms upon re-initiation of therapy suggests the presence of residual EGFR-TKI sensitive disease (Riely, Kris et al. 2007, Chaft, Oxnard et al. 2011). Studies on retreatment with EGFR-TKIs after a different line of therapy are ongoing and reported data to date indicates benefits from EGFR-TKI retreatment (ICARUS: NCT01530334 and IRENE: NCT02025218). Data on combination of EGFR-TKIs and chemotherapy is inconclusive in retrospective studies and the randomised phase III IMPRESS study does not show an advantage of double treatment overall (Faehling, Eckert et al. 2013, Goldberg, Oxnard et al. 2013, Halmos, Pennell et al. 2015, Soria, Kim et al. 2016). However, IMPRESS data indicates improved PFS with gefitinib + cisplatin-pemetrexed chemotherapy for T790M negative patients, while the opposite is shown for T790M positive patients (Soria, Kim et al. 2016). Data on corresponding studies with AZD9291 is not yet available. A review by van Assche et al. gives an overview of clinical trials on

combining EGFR-TKIs with other treatment modalities, as chemotherapy, surgery, radiotherapy and other targeted therapies (Van Assche, Ferdinande et al. 2014).

The combination of EGFR-TKIs with other targeted agents is of particular interest to this work. We hypothesise that there are changes in intracellular signalling upon sustained EGFR-TKI treatment that allow survival of a proportion of cells which eventually grow out to become a resistant cell population. We therefore hypothesise that identification and targeting of these new dependencies may be crucial in order to improve responses to EGFR-TKIs, to prevent emergence of resistance and to treat resistant disease. In order to address such a question, the availability of suitable model systems for studying emergence of resistance to EGFR-TKIs is critical. However, response and emergence of resistance to therapies differs between patients and patient material is highly variable and large sample numbers would be required to identify crucial mechanisms. Over the years many efforts have been made to use patient-derived material in *in vivo* studies, using patient-derived xenograft models or more recently circulating tumour cells derived explants (CDXs) (Lallo, Schenk et al. 2017). These are however difficult to obtain and time and cost of using these models, particularly considering variability in response and mechanisms of resistance, limits their practicability.

Established NSCLC cell lines are therefore a valuable research tool and are reported to be representative of their parental tumours (Wistuba, Bryant et al. 1999). In the case of resistance to EGFR-TKIs in NSCLC, *in vitro* studies on established cell lines have been shown to recapitulate resistance mechanisms observed in the clinic (Engelman, Zejnullahu et al. 2007, Ogino, Kitao et al. 2007, Yoshida, Song et al. 2016).

The aim of this work is to understand the response and resistance of EGFR-TKI sensitive cells to EGFR-TKIs, in order to improve response to EGFR-TKIs, prevent the emergence of resistance, and overcome resistance.

In detail, we aim to:

1. characterise biochemical changes and changes in signalling after sustained EGFR-TKI treatment
2. generate and characterise EGFR-TKI resistant cells
3. identify ways to selectively target EGFR-TKI resistant cells
4. identify ways to prevent or delay the emergence of resistance to EGFR-TKIs

2 Material and Methods

2.1 Buffers, solutions and chemicals

Unless otherwise stated, all chemicals were purchased from Sigma-Aldrich (St. Louis, USA).

Table 2-1: Buffers and solutions used throughout this work

Application	Buffer	Composition
Cell culture	1x PBS	10x PBS (Lonza) diluted in dH_2O
Western blotting	Lysis buffer (for western blot)	50 mM Tris-HCl pH 7.6, 137 mM NaCl, 10 % (v/v) glycerol (VWR), 0.1 % (v/v) Igepal, 0.1 % (v/v) SDS (AppliChem GmbH, Darmstadt, Germany) 50 mM sodium fluoride, 1 mM sodium orthovanadate and cOmplete protease inhibitor cocktail (Roche, Basel, Switzerland) in dH_2O[1]
Western blotting	5x sample loading buffer	25 mM Tris-Base pH 6.8, 1% (v/v) sodium dodecyl sulfate (SDS), 1 mM ethylenediamine tetraacetic acid (EDTA), 2.5% (v/v) β-mercaptoethanol, 0.25 mg/mL Bromophenol blue (Acros organics)
Western blotting	1x Tris-buffered saline (TBS)	1x pack OmniPur® TBS 20x Ready Pack Powder (Calbiochem, Darmstadt, Germany) dissolved in 20 L of dH_2O
Western blotting	TBS-T	1x TBS, 0.1 % (v/v) Tween-20
Western blotting	Running buffer	10x Tris/Glycine/SDS running buffer (Bio-Rad) diluted in dH_2O
Western blotting	Transfer buffer	10x Tris/Glycine buffer (Bio Rad) diluted in dH_2O with 20 % (v/v) methanol
Western blotting	Blocking and antibody buffer LICOR	1:1 mixture of Odyssey® TBS Blocking Buffer (LI-COR) and TBS (blocking) or TBS-T (antibody incubation)
Cell viability assay	Resazurin stock solution	12.5 mg/mL resazurin in dH_2O
Apoptosis assay	Hoechst 33258	Stock: 10 mg/mL Hoechst in dH_2O
Tissue fixation for FFPE	4 % Paraformaldehyde (PFA)	4 % PFA (w/v; VWR) dissolved in 1x PBS, pH adjusted to 7.4 with 5 M NaOH
H&E staining	Acid alcohol	1% (v/v) HCl (Fisher Scientific) in 70% (v/v) ethanol (Fisher Scientific) in dH_2O
H&E staining	Scott's tap water	41.7 mM sodium bicarbonate, 81.2 mM of magnesium sulfate (Scientific Laboratory Supplies) in

[1] Sodium orthovanadate and protease inhibitors were freshly added before use. The lysis buffer containing the remaining components was aliquoted and stored at 4°C

		dH_2O
H&E staining	Lithium carbonate	0.5% (w/v) lithium carbonate in dH_2O
IHC/ IF	Citrate buffer for antigen retrieval	10 mM citric acid and 0.05 % Tween-20 in distilled water (dH_2O), pH adjusted to 6.0 with 1 M NaOH
IHC/ IF	1x Phosphate buffered saline (PBS)	5x PBS tablets dissolved in 1 litre dH_2O
IHC/ IF	PBS-T	1x PBS, 0.1 % (v/v) Tween-20
IHC/ IF	Tris-EDTA buffer (for antigen retrieval)	10 mM Tris, 1 mM EDTA (VWR), 0.05 % (v/v) Tween-20, in dH_2O; pH adjusted to 9 with 1M HCl
IF	Permeabilisation and blocking buffer immunofluorescence	0.1% (v/v) Triton X-100, 1% (v/v) normal goat serum (Millipore), and 1% (w/v) BSA (Acros organics) in 1x PBS
Cell mutagenesis	Solution 1	50 mM $MgCl_2$, 7.5 mM NADP, 120 mM Glucose-6-phosphate in PBS
Cell mutagenesis	S9 extract	S9 from liver, pooled
Cell fixation and staining	Crystal violet fixation and staining solution	0.5% (w/v) crystal violet (Merck), 75% methanol, in dH_2O

2.2 Compounds

Compounds used in this study were bought from Selleck Chemicals as part of the L1100 library or made up as 10 mM stock solution in 100 % dimethyl sulfoxide (DMSO, VWR) and stored at -20 °C. A list of used compounds is given in Table 2-2.

Table 2-2: Compounds used in this study
The main target and supplier are listed for compounds used in this study

Compound	Main target	Supplier
ABT-263	Bcl-2	Selleck Chemicals
Afatinib	EGFR	Selleck Chemicals
Alisertib	Aurora Kinase	Selleck Chemicals
AMG-900	Aurora Kinase	Selleck Chemicals
AT9283	Aurora Kinase	Selleck Chemicals
Aurora A Inhibitor I	Aurora Kinase	Selleck Chemicals
AZ5104	EGFR	Selleck Chemicals
AZD1152	Aurora Kinase	Selleck Chemicals
AZD6244	MEK	Selleck Chemicals
AZD9291	EGFR	AstraZeneca, Medchem express, ChemieTek
BEZ235	PI3K	Selleck Chemicals

BMS-536924	IGF-1R	Selleck Chemicals
BMS-754807	IGF-1R	Selleck Chemicals
CCT129202	Aurora Kinase	Selleck Chemicals
CCT137690	Aurora Kinase	Selleck Chemicals
CO-1686	EGFR	ChemieTek
Erlotinib	EGFR	Selleck Chemicals
Everolimus	mTOR	Selleck Chemicals
Gefitinib	EGFR	Selleck Chemicals
GSK1904529A	IGF-1R	Selleck Chemicals
Hesperadin	Aurora Kinase	Selleck Chemicals
MK-2206	AKT	Selleck Chemicals
MK-5108	Aurora Kinase	Selleck Chemicals
MK-8745	Aurora Kinase	Selleck Chemicals
NVP-ADW742	IGF-1R	Selleck Chemicals
OSI-906	IGF-1R	Selleck Chemicals
PHA-680632	Aurora Kinase	Selleck Chemicals
PQ 401	IGF-1R	Selleck Chemicals
SNS-314	Aurora Kinase	Selleck Chemicals
TAK-901	Aurora Kinase	Selleck Chemicals
Trametinib	MEK	Selleck Chemicals
VS-6063	FAK	Selleck Chemicals
VX-680	Aurora Kinase	Selleck Chemicals

The screening library L1700 (Table S 7) was purchased as 10 mM stocks in DMSO from Selleck Chemicals. DMSO was used as a treatment control for in vitro assays.

For *in vivo* studies, compounds were made up as 80 mM stocks in DMSO, diluted in 1 % Tween 80 in dH_2O and injected intraperitoneally (i.p.). Formulation for oral administration (per os, p.o.) was in 0.5 % w/v hydroxypropyl methylcellulose (HPMC) in dH_2O. Fresh treatment solutions were prepared every week and kept at 4◦C between administrations.

2.3 Cell culture

2.3.1 Cell lines

Authenticated, mycoplasma free cell lines were purchased from ATCC. Cell lines used in this study are listed in Table 2-3, including their mutation status for EGFR, KRAS and TP53.

Table 2-3: Cell lines used in this study

Cell line name, histological subtype, provider, catalogue number and mutation status for EGFR, KRAS and TP53 are listed. **Bold** part of cell line names indicates the name used in this work.

Cell line	Histological subtype	Provider	EGFR	KRAS	TP53
NCI-**H1650**	Lung adenocarcinoma	ATCC[1] # CRL-5883	ΔE746_A750	wt	V225_spl
NCI-**H1975**	Lung adenocarcinoma	ATCC # CRL-5908	L858R, T790M	wt	R273H
HCC2935	Lung adenocarcinoma	ATCC # CRL-2869	ΔE746_A750, T751A	wt	Y220C
HCC4006	Lung adenocarcinoma	ATCC # CRL-2871	ΔL747_E749, A750P	wt	unclear
HCC827	Lung adenocarcinoma	ATCC # CRL-2868	ΔE746_A750	wt	V218del (codon)
PC9	Lung adenocarcinoma	[2]	ΔE746_A750	wt	R248Q
Calu-3	Lung adenocarcinoma	ATCC # HTB-55	wt	wt	M237I
NCI-**H1648**	Lung adenocarcinoma	ATCC # CRL-5882	wt	wt	L35fs*8
A549	Lung carcinoma not specified (NSCLC)	ATCC # CRL-185	wt	G12S	wt

[1] ATCC = American type culture collection (Manassas, USA); cell lines from ATCC were purchased in 2010-2012

[2] Kindly provided by Dr. Kazuto Nishio, Kinki University, Osaka, Japan in 04/2010

Upon arrival, authentication of the cell lines was confirmed by mitochondrial DNA sequencing (Hutter, Nickenig et al. 2004), which was carried out by Joe Ryan. Cells were passaged for no more than 25 times post-authentication (approximately 3 months).

2.3.2 Mycoplasma testing

Cells were tested for mycoplasma upon arrival by a PCR-based method (Ishikawa, Kozakai et al. 2006) and retested in regular intervals using MycoAlert™ (Lonza).

2.3.3 Cell maintenance and cell seeding

All cells were regularly maintained and cultured in Advanced DMEM/F-12 (Life Technologies) supplemented with 5 % foetal bovine serum (FBS, Sigma-Aldrich), 2 mM GlutaMAX™ (Life Technologies) and 50 U penicillin / 50 µg/mL streptomycin (Life technologies), at 37 °C in a humidified environment containing 5 % CO_2.

The culture medium was changed every two to four days and cells were passaged at sub-confluence (70-80 %). Routine passaging of the cells was done by preparing a cell suspension by removal of the medium, washing with PBS and trypsinisation with 0.25 % or 0.025 % Trypsin/EDTA (Life technologies), depending on the cell line.

Cell density and viability for routine maintenance and seeding of cells for experiments were determined using a haemocytometer. For this, cell suspensions were mixed with an equal volume of 0.4 % trypan blue solution (Life Technologies) and added to a Fuchs-Rosenthal counting chamber. For seeding of cells, the determined cell number per mL was used to dilute cells corresponding to desired plating densities in complete culture medium unless otherwise stated.

2.3.4 Cryostorage and thawing of cells

For cryopreservation cells were grown to 80-90 % confluency and trypsinised as described in 2.3.3. Cells were pelleted by centrifugation (5 minutes (min) at 225 x g) and resuspended in freezing medium, 10 % (v/v) DMSO in complete cell culture medium. Aliquots of 500 µL were transferred to cryogenic tubes which were then frozen at -80 °C overnight in an isopropanol container, before being transferred into the vapour phase of a liquid nitrogen storage tank.

Cells from liquid nitrogen storage were thawed at 37 °C for 2 minutes (min) and the cell suspension was diluted in 5 mL pre-warmed complete culture medium and cells were pelleted by centrifugation at 225 x g for 5 min. The supernatant was aspirated and the cell pellet resuspended in 12 mL complete culture medium and transferred into a T75 flask. Culture medium was changed again the next day.

2.4 Mutagenesis of cells using benzo[a]pyrene

Mutagenesis of PC9 cell was performed as described previously (Lindblad and Jackim 1982). In short, 5 x 10^6 cells were mixed with the mutagenesis medium (see below) and plated in T150 flasks.

Mutagenesis medium (see also Table 2-1):

4 mL of solution 1

40 µL of 10 mg/mL benzo[a]pyrene

400 µL of S9 extract

ad 40 mL advanced DMEM/F12 medium

Medium was changed into fresh advanced DMEM/F12 72 h after treatment with mutagenesis medium.

2.5 Spheroid growth

Multicellular tumour spheroids were generated using 96-well round bottom ultra-low attachment microplates (Corning, USA, #7007). 0.5-1x 10^4 cells in 200 µL complete culture medium were seeded in each well, plates were centrifuged at 250 x g at room temperature (RT) for 10 min and incubated for 24 h at 37 °C and 5 % CO_2 to allow for spheroid formation. For medium changes (every 2-7 days) and drug treatments, 100 µL medium were removed and replaced with 100 µL of fresh medium or 100 µL of medium containing 2x concentrated compounds, respectively. Unless otherwise stated, treatment was started on day 10 after seeding. Spheroid area was assessed regularly using a GELCOUNT™ imager (Oxford Optronix, UK). Images were acquired at 1200 dpi and automated image analysis performed with CHARM settings optimised for each cell line. Data were exported to Microsoft Excel for further analysis.

2.6 Viability assay for IC_{50} determination

To compare sensitivity for compounds between different cell lines, we determined the half maximal inhibitory concentration (IC_{50}) using a viability based assessment of proliferation. 500-1000 cells/well were seeded in triplicate in a 96-well plate and treatment was started the next morning using a dilution series of the drugs of interest. Depending on cell density, cell growth was assessed 5-6 days after treatment using resazurin (12.5 µg/ml final concentration). In metabolically active cells, the weakly fluorescent dye resazurin is reduced to highly fluorescent resorufin, thus allowing assessment of cell viability.

Fluorescence intensity of resorufin was measured using a POLARstar Omega plate reader (BMG Labtech GmbH, Ortenberg, Germany), exciting at 544 nm and reading emission at the wavelengths between 585–595 nm.

2.6.1 Calculation of IC_{50}

Data was collected and exported to Microsoft Excel 2010 using the MARS Data Analysis Software (BMGLabtech GmbH, Ortenberg, Germany). Microsoft Excel 2010 was used for blank correction and further analysis.

IC_{50} values were calculated using Origin pro 8.5.1, using a non-linear curve fit (category: growth/ sigmoidal; function: dose response). This allows the calculation of the inflection point of the dose response curve, which is considered the IC_{50} value. The function uses the following formula: $y = \frac{A1+(A2-A1)}{1+10^{(log_x 0-x)p}}$ where A1 is the top asymptote, A2 is the bottom asymptote, p is slope factor and x is the inflection point/IC_{50}. For IC_{50} determination, the concentration values were log_{10} transformed and the top asymptote (100%) was forced at approximately 2 log_{10} values below the lowest concentration of compound used and the bottom asymptote was forced at the highest concentration/ lowest y-value. For dose response curve generation in Prism, the linear concentration values were used.

2.7 384-well compound screen

In order to assess the ability of compounds from the L1700 compound library (Selleck Chemicals) to inhibit proliferation of H1975 and $H1975^{9291R}$ cells in the presence and absence of AZD9291, a resazurin based viability assay was performed. The screen was performed by Dr. Agata Patel in collaboration with the Target Discovery Institute, Oxford. Cells were seeded at 300 cells/well in 384-well

plates and treated with the compound library (1902 compounds + DMSO controls) +/- AZD9291 the following day. The experiment was performed in duplicate plates, testing each compound twice under each condition. Viability was assessed on day 6 after seeding using resazurin as described above. Collected data were analysed using Excel.

2.7.1 Analysis of compound screen

To determine the efficacy of the inhibitors under single and combination treatment with DMSO/AZD9291 (-/+ AZD9291), the average fluorescence intensity of the two plates for each compound was calculated and the relative viability under compound treatment determined using the following formula:

$$\textbf{\textit{relative viability (+/- AZD9291)}} = \frac{resorufin\ fluorescence\ after\ treatment\ with\ test\ compound\ (-/+AZD9291)}{resorufin\ fluorescence\ after\ treatment\ with\ DMSO\ (-/+AZD9291)}$$

We expected the relative viability of cells treated with DMSO or AZD9291 only to be a value = 1 on plates for single or combination treatments, respectively.

To identify compounds which were more effective under combination treatment in either cell line or in the resistant cell line compared to the parental cell line, the following calculations were used:

Effectiveness between conditions: $log_{10}(\frac{relative\ viability\ condition\ 1}{relative\ viability\ condition\ 2})$

where condition 1/2 indicate either:

(i) 1: parental cell line (+/- AZD9291), 2: resistant cell line (+/- AZD9291)

(ii) 1: parental/resistant cell line - AZD9291, 2: parental/resistant cell line + AZD9291

A $\log_{10}$ value of 0 indicates no difference in effect of a compound as there was a similar response in both conditions ($\log_{10}(1)=0$). Potential positive (selective for condition 2) and negative (selective for condition 1) “hit” compounds were identified as having a ($\log_{10}$(condition1/condition2)) value ≥ ± 2x standard deviations (SD) from the mean of all compounds per screen plate.

In order to identify targets that were significantly enriched within the 50 most effective compounds, we performed a two-tailed Fisher’s exact test. Compounds were ranked based on their effectiveness for each comparison and the number of compounds with a listed target within the top 50 and remaining 1942 compounds (including DMSO) for each of the listed 187 targets were counted. The Fisher’s exact test was performed in Excel using the Real Statistics Resource Pack software (Version 5.0 Mac 2016) (Zaiontz 2015). Targets with more than 5 compounds were reported. Graphs for enrichment of targets were generated following the method described by Subramanian et al. for gene set enrichment analysis (Subramanian, Tamayo et al. 2005).

2.8 Imaging-based detection of apoptosis

Time and extent of induction of apoptosis under single and double treatments were assessed using either detection of an overexpressed apoptosis marker using long-term live cell imaging or the Hoechst binding apoptosis assay.

2.8.1 Live cell imaging for induction of apoptosis

PC9 cells stably expressing the CaspeR3-GR construct were generated. The CaspeR3-GR apoptosis sensor consists of a green fluorescent protein (GFP) and a red fluorescent protein (RFP) connected by a linker region containing the caspase-3

cleavage sequence DEVD (Shcherbo, Souslova et al. 2009). GFP emission and RFP excitation spectra overlap, resulting in highly effective Förster Resonance Energy Transfer (FRET) when the two fluorescent proteins are in close proximity. This allows detection of signal in the green and red wavelengths following excitation in the blue range. Upon activation of caspase-3 and cleavage of the sensor in the linker region, FRET becomes less likely and emission in the red range will be reduced, while emission in the green range is maintained. Quantification of the green/red ratio in imaging performed under the described setup allows for detection of induction of apoptosis in these cells, marked by an increase in the ratio.

Cells were seeded in a 96-well plate (2000 cells/well, in duplicate) and imaged for 48 h after treatment using a Nikon TE2000 wide field microscope with a pE300 light source from CoolLED and data acquired using NIS-Elements AR (version 3.22.15, Nikon Corporation). The following filter settings were used:

- modified FITC Nikon cube (Dichroic 505 nm long pass, emission filter removed)
- Excitation filter 465-495 nm
- Emission filter GFP 517/30
- Emission filter RFP 605/40

Quantification of number of apoptotic cells was done using the IMARIS software (Bitplane AG, Switzerland). Cells were detected using the surface detection algorithm and the total number and area of surfaces determined for each time point. Quantification of apoptotic cells was performed by generating an artificial channel 3 (channel 3 = GFP channel - RFP channel), intensity of which increases upon

induction of apoptosis and reporting the total intensity of channel 3 over time. The following formula was used to calculate a surrogate of degree of apoptosis:

relative number of apoptotic cells (at time x)= $\frac{total\ intensity\ channel\ 3\ (x)/total\ surface\ area\ (x)}{total\ intensity\ channel\ 3\ (y)/total\ surface\ area\ (y)}$

where y is the time point of maximum value for $\frac{total\ intensity\ channel\ 3\ (x)}{total\ surface\ area\ (x)}$ *within the first hour of the experiment.*

The tracking function of IMARIS was used to track cells and determine migration speed over time.

2.8.2 Hoechst binding apoptosis assay

Binding of Hoechst 33258 to DNA is more easily detectable in apoptotic cells compared to normal cells due to increased uptake and greater condensation of nuclei in apoptotic cells. This difference in Hoechst signal in images acquired using the INCell analyzer 1000 (GE Healthcare, ex360 nm and em460 nm) is used as a way of detecting apoptosis cells in the Hoechst binding assay described by Bokobza et al. (Bokobza, Jiang et al. 2014). Cells were seeded in 96-well plates and treated with DMSO or compounds the next day. Seeding number and treatment time were dependenr on the time course of interest. Thirty min before image acquisition on the INCell analyzer 1000, Hoechst 33258 was added to a final concentration of 15 µg/mL. Analysis was performed using the INCell analysis software. Hoechst staining intensity and compactness of the nuclei were measured and cells with intensely stained compact nuclei were scored as apoptotic. The fraction of apoptotic cells was determined for each well.

2.9 DNA extraction, polymerase chain reaction and DNA sequencing

In order to confirm the EGFR mutation status of cell lines used for this study and to check for newly acquired mutations in EGFR and NRAS in resistant cell lines, sequencing of exons of interest was performed.

2.9.1 DNA extraction

Cells were seeded in 10 cm tissue culture plates (3-8 x 10^5 depending on cell line), and harvested by trypsinisation and centrifugation (280x g, 5 min) then they reached ~70 % confluency. DNA was isolated using the MasterPure™ DNA Purification Kit (Epicentre Biotechnologies), according to the manufacturer's instructions. DNA concentration was measured using a NanoDrop 1000 spectrophotometer, and purified DNA was stored at - 20˚C.

2.9.2 Polymerase chain reaction and DNA Sequencing

Exon 19-21 of EGFR and 2-3 of NRAS was amplified using polymerase chain reaction (PCR). The primers (Sigma-Aldrich) used were as follows:

Table 2-4: Primers for amplification of EGFR and NRAS

Gene	Exon	Sequence
EGFR	19 - Forward	GCAATATCAGCTTAGGTGCGGC
	19 - Reverse	CATAGAAAGTGAACATTTAGGAT
	20 - Forward	CCATGAGTACGTATTTTGAAACTC
	20 - Reverse	CATATCCCCATGGCAAACTCTTGC
	21 - Forward	CTAACGTTCGCCAGCCATAAGTCC
	21 - Reverse	GCTGCGAGCTCCATAATGTCTGG
NRAS	2 - Forward	TGATCCGACAAGTGAGAGACAG
	2 - Reverse	TGTGGCTCGCCAATTAACC
	3 - Forward	ACCTCATTTCCCCATAAAGATTCAG
	3 - Reverse	CCACACCCCCAGGATTCTTAC

PCR reactions were prepared with the following components:

DNA: 50 ng
Forward primer: 0.4 µM
Reverse primer: 0.4 µM
MiFi DNA polymerase (Bioline Reagents, UK): 1 µL
5x MiFi buffer containing dNTPs (Bioline Reagents, UK): 5 µL
dH_2O: to 25 µL

The reactions were performed using a thermal cycler (Applied Biosystems) with the following conditions (EGFR/NRAS):

Hot start:	*95 °C,*	*3 min*	
Denaturation:	*94 °C,*	*30 sec*	*35 cycles*
Annealing:	*56/57 °C,*	*30 sec*	
Extension:	*72 °C,*	*30 sec*	
Final extension:	*72 °C,*	*7 min*	

Successful amplification of an appropriately-sized product was confirmed by gel electrophoresis. A fraction of each product was mixed with 6x DNA loading buffer (ThermoFisher Scientific) and loaded onto a 1.5 % agarose gel (Sigma-Aldrich) in 0.5x Tris Borate-EDTA (TBE) buffer (Table 2-1) alongside the GeneRuler 1 kb Plus DNA ladder (ThermoFisher Scientific). PCR products were then purified using the MinElute® PCR purification kit (Qiagen), according to the manufacturer's protocol. The purified products were sequenced externally, using Sanger DNA Sequencing (Source BioScience) and the sequences visualised with FinchTV (Geospiza) to identify mutations in the EGFR and NRAS genes.

2.10 RNA isolation and mRNA sequencing

Expression analysis in parental and resistant cell lines was performed using mRNA sequencing. Sequencing data was also used to identify newly acquired mutations in the transcriptome of resistant cell lines. Samples and conditions are listed in Table 2-5.

Table 2-5: Samples analysed using RNA sequencing

Sample	cell line	treatment
1	PC9	DMSO
2	PC9	DMSO
3	HCC827	DMSO
4	H1975	DMSO
5	$PC9^{GS}$	DMSO
6	$PC9^{GS}$	0.25 µM gefitinib for 48h
7	$PC9^{9291S}$	DMSO
8	$PC9^{9291S}$	0.25 µM AZD9291 for 48h
9	$HCC827^{GS}$	DMSO
10	$HCC827^{GS}$	0.25 µM AZD9291 for 48h

2.10.1 RNA isolation and purification

Cells were seeded in 10 cm cell culture dishes (3-8 x 10^5 depending on cell line) and allowed to attach over night before medium was changed to medium containing compounds. 24 h prior to RNA isolation, the medium was changed. RNA was isolated following the manufacturer's protocol (RNeasy® plus mini kit, Qiagen), using a volume of 600 µL of buffer RLT and breaking up cells using a syringe with needle.

The concentration and purity of the RNA was measured on a NanoDrop 1000 spectrophotometer. The concentration ranged from 387 ng/µL to 2844 ng/µL. The absorbance ratios 260 nm/280 nm and 260 nm/230 nm were between 1.99 – 2.09

and 1.84 - 2.23, respectively, indicating sufficiently pure RNA preparations. RNA integrity, as determined by Source Bioscience was appropriate (RIN between 8.2 and 10). Purified RNA was stored at -80 ºC until use.

2.10.2 RNA Sequencing and data analysis

Samples were analysed by Source Bioscience and gene expression quantified using a previously described analysis pipeline (Trapnell et al., 2012). The Stranded total RNA libraries were prepared in accordance to the Illumina TruSeq Stranded mRNA Sample Preparation (October 2013 Rev E.) for Illumina Paired-End (PE) Multiplexed Sequencing. In short, poly-A mRNA in the tRNA samples was purified using Illumina poly-T oligo-attached magnetic beads and mRNA was fragmented and primed with random hexamers for cDNA synthesis. This was followed by addition of a single 'A' nucleotide to the 3' end of the blunt fragments to prevent ligating to one another during adapter ligation reaction. The adapters and indexes were ligated to the end of the double-stranded cDNA to prepare the sample for hybridisation onto a flow cell. The samples were then amplified through 15 cycles of PCR to select samples that have the adapter molecules present on both ends of the DNA. The libraries were validated on the Agilent BioAnalyzer 2100 to check the size distribution of the libraries and on the Qubit High Sensitivity to check the concentration of the samples.

Two pools of six samples each were loaded at a concentration of 8 pM onto one lane each of an Illumina HiSeq2000 flow cell v3. Samples were sequenced using 100 bp PE runs.

Analysis of sequencing data was performed by Dr. Alexander Kanapin (Computational Genomics Lead, Department of Oncology, University of Oxford). In short, the raw fastq sequencing reads alignment and quantification of expression was

made with STAR (version 2.5.1) against human genome hg19 and RefSeq gene annotation.

Quality control resulted in good mapping quality: ~80% of reads have been mapped into genes. There was a good concordance between replicates on the level of read counts. The differential expression calling was performed with DESeq2 algorithm using FDR < 0.01.

Variant calling in the RNASeq data has been done with RNASeqmut (version 0.6 with STAR alignment support). The recommended protocol for variant calling (https://github.com/davidliwei/rnaseqmut), including raw variant calling, merging variants, genotyping and filtering was used with standard default parameters.

Analysis was performed in Excel and selected datasets were analysed for pathway enrichment, using MetaCore™ Key Pathway Advisor (Thomson Reuters; New York, NY, USA; http://ipscience.thomsonreuters.com/product/metacore, accessed July 2016).

2.11 Protein extraction, SDS-PAGE and western blotting

Whole cell protein was extracted using the lysis buffer as described in Table 2-1.

2.11.1 Protein extraction 2D culture

Cells were plated in 6-well plates (3-6 x 10^4 cells depending on cell line) or 6 cm tissue culture dishes (0.6-1.2 x 10^5 cells depending on cell line). When at ~70 % confluency, medium was replaced with fresh medium with or without drug for indicated times. In the case of resistant cell lines, selection drugs were not added to cells when seeded for experiments. All steps during protein extraction were performed on ice and cell lysates included cells collected from the supernatant and

wash steps. In short, cells were washed twice with ice cold PBS and lysis buffer was added onto the cells. The supernatant and PBS washes were centrifuged (3 min 250 x g) and pelleted cells washed twice with PBS. Cells from the plates were scraped off using a disposable rubber scraper and the cell lysate was transferred to a tube containing the corresponding washed cell pellet. Samples were homogenized by sonication (3 x 10 sec using Bioruptor® Plus, Diagenode) and cell debris was removed by centrifugation at 16,100 x g for 15 min at 4 ˚C. Protein concentration was determined using a NanoDrop 1000 spectrophotometer.

2.11.2 Protein extraction 3D spheroids

Spheroids were grown as described in chapter 2.5 and lysed at endpoints as defined in each experiment. The 96-well spheroid plates were placed on a pre-warmed tray and 6-12 spheroids per condition were collected in 1.5 mL reaction tubes using a 1 mL pipette tip with the end widened by cutting. Spheroids were allowed to settle and medium was removed. Spheroids were washed twice using 500 µL of ice-cold 1x PBS. 25 µL of protein lysis buffer were added and samples were vortexed twice for 5 sec each before freezing at -20 ˚C until further processing. Lysates were then homogenised by sonication (≥ 3 x 10 sec cycles), pipetting and vortexing, and cell debris was removed by centrifugation (16,100 x g, 15 min, 4 ˚C). Protein concentration was measured using the NanoDrop 1000 spectrophotometer.

2.11.3 SDS-polyacrylamide gel electrophoresis (PAGE) and immunoblotting (western blotting)

Protein lysates (7.5-25 µg per lane, diluted in 5x Laemmli sample loading buffer) were resolved by SDS-PAGE on 4-15 % gradient Mini-PROTEAN® TGX™ or

Criterion™ TGX™ precast gels (BioRad) and transferred to nitrocellulose membranes. Membranes were blocked (1 h at RT, LI-COR blocking buffer, described in Table 2-1) and incubated with primary antibodies (overnight, 4 °C, Table 2-6), followed by secondary antibodies (1 h at RT, Table 2-6). Detection was performed on an Odyssey Infrared Imager (LI-COR Biosciences).

PPIB and ß-ACTIN were used as loading controls. For simplicity, in the blots in this work, only one representative loading control is shown for in experiments for which antigens were detected on several identical membranes. Antigens detected on the same membrane are labelled in the same colour on the blot description. Western blots are representative of at least two independent experiments unless otherwise stated.

Table 2-6: Antibodies used for immunoblotting

Antibody name (clone)	Dilution	Source and catalogue number
β-actin (AC-15)	1:5000	Sigma-Aldrich[1] #A1978
AKT (40D4)	1:2000	CST #2920
pAKT S473 (193H12)[2]	1:1000	CST #4058
CA9 pAb[3]	1:1000	Abcam # ab15086
Cyclin D1 (EPR2241)	1:10000	Abcam # ab134175
DUSP6 (ERP129Y)	1:1000	Abcam #ab76310
EGFR pAb	1:1000	CST #2232
pEGFR Y1068 pAb	1:1000	Invitrogen #44788G
ERK (L34F12)	1:1000	CST #4696
pERK T202/Y204 pAb	1:1000	CST #4376
ETS-1 (D808A)	1:1000	CST #14069
pHistone H2A.X S139 (JBW3010)[1]	1:2000	Millipore #05-636

[1] Sigma-Aldrich: Sigma-Aldrich Company Ltd. (Gillingham, UK), CST: Cell Signaling Technology, Inc (Danvers, USA), Abcam: Abcam, plc (Cambridge, UK), Invitrogen: Invitrogen/Thermo Scientific (Waltham, MA, USA), Millipore: Merck Millipore (Billerica, MA, USA)

[2] pXXX: phosphorylated antigen, phosphorylation site(s) specified

[3] pAb: polyclonal antibody

pHistone H3 S10 pAb	1:5000	Millipore #06-570
pMEK1/2 S221 pAb	1:500	CST #2338
Mouse IgG (H + L) conjugated to IRDye® 680RD	1:5000	Odyssey®, LI-COR Biosciences, UK #926-68070
PARP pAb	1:2000	CST #9542
PPIB pAb	1:2000	Abcam #ab16045
Rabbit IgG (H + L) conjugated to IRDye® 800CW	1:5000	Odyssey®, LI-COR Biosciences, UK #926-32211
pS6 Ribosomal Protein (54D2)	1:1000	CST #2317
pS6 Ribosomal Protein S240/244 (D68F8)	1:1000	CST #5364

2.12 Reverse Phase Protein Array (RPPA)

The Reverse Phase Protein Array (RPPA) analysis was performed in collaboration with Dr. Neil Carragher and Alison Munro at the Protein and Antibody Microarray Facility at the Edinburgh Cancer Discovery Unit.

Protein lysates were prepared after indicated treatments using the CLB1 buffer supplied by the RPPA facility and sent off to Alison Munro for analysis on the ZEPTOSENS platform. Data normalisation by protein loading was performed by Alison Munro, using the normalisation process as described by Liu et al. (Liu, Ju et al. 2014). Raw data was converted from log2 values to linear values and the median for each antibody determined across the sample set. Each raw linear value was then divided by the median within each antibody to get the median centered ratio. Subsequently, the median from median centered ratios for each sample across the entire panel of antibodies was calculated and is considered the correction factor for protein loading adjustment. A sample was considered an outlier if the correction factor was above 2.5 or below 0.25. To calculate the normalised linear value, raw

[1] pHistone H2A.X S139: γH2A.X (S139)

data in linear value was divided by the correction factor. This normalisation showed no outliers in our study and further analysis was performed on all samples using a two-tailed t-test in Excel to test for difference of samples treated with doses of 100 nM, 300 nM or 1 µM at each time point compared to the untreated control. To assess changes between parental and resistant lines, t-tests were performed between samples of untreated parental cell lines compared to samples from resistant cell lines treated with 0 µM or 0.25 µM AZD9291 for 72 h. Antigens with a p-value of ≤ 0.05 were considered significantly changed.

2.13 Formalin fixation and paraffin embedding (FFPE)

Samples were fixed in 4 % PFA or 10 % neutral buffered formalin (NBF) (Sigma-Aldrich #HT501128-4L) and stored in 70 % ethanol (cell pellets and tissues) or 1x PBS (spheroids) until further processing. Overnight processing was performed in a LEICA TP 1050 tissue processor and samples were paraffin embedded the next day using a Thermo Fisher Scientific HistoStar embedding workstation. Samples were cut at a thickness of 4 µm using a Leica RM2125 microtome and mounted onto charged slides (ThermoFisher Scientific #J3800AMNZ). For spheroid staining, 3-5 sections from each block were collected on each slide for detection of antigens at different depths within the spheroid.

2.13.1 FFPE: 3D spheroids

At the time points of interest, spheroids were collected for formalin fixation as described in chapter 0. PBS-washed spheroids were fixed in 10 % NBF for 30 min at RT. Formalin was removed and spheroids were washed in 1x PBS and stored in PBS until further processing. For overnight processing, the spheroids were carefully placed on a glass slide and excess PBS was removed with a 10 µL tip. Agarose (1 %

(w/v), Sigma-Aldrich) dissolved in 1x PBS or Richard-Allan Scientific HistoGel Specimen Processing Gel (Histogel, Thermo Fisher Scientific) was liquefied by heating and gently placed over the spheroids on the glass slide and left to solidify. Processing of the agarose/histogel encapsulated spheroids was done in a biopsy insert (ThermoFisher Scientific #12618366) which was placed in a histosette® (Simport® #M490-3). For the preparation of spheroid microarrays (SMA), groups of fixed spheroids were immobilised on individual pillars of the custom-designed SMA mould (in collaboration with Sean Smart, Imaging core of the Department of Oncology, University of Oxford, modified from (Kang, Lee et al. 2016)) and embedded in Histogel for immediate overnight processing and paraffin embedding.

2.13.2 FFPE: mouse tissue

Mouse tissue was immediately placed in > 10 volumes of 4% PFA or 10 % NBF and stored at 4ºC overnight. On the following day, the PFA/NBF was removed and the tissue was placed in 70% ethanol at 4ºC until overnight processing and paraffin embedding.

2.14 H&E staining, immunohistochemistry and immunofluorescent staining of FFPE material

For deparaffinisation and rehydration, sections were heated (50 ˚C, 10 min), immersed twice (3 min each) in Citroclear (HD Supplies, UK), followed by a decreasing ethanol series and dH_2O.

2.14.1 Haematoxylin and Eosin staining (H&E)

For H&E staining, deparaffinised and rehydrated sections were immersed in filtered Harris's haematoxylin (VWR; #351945S) for 3-5 min, followed by running tap water

for 3 min to remove excess staining solution and then rinsed in dH_2O. Slides were differentiated by quick immersion (10 dips) in acid alcohol and blued in Scott's tap water and lithium carbonate (see Table 2-1). Samples were rinsed in dH_2O after each step. In preparation for staining with alcoholic Eosin, slides were sequentially dipped (10 times each solution) in 50 %, 70 %, 90 % and 90 % ethanol. Slides were then immersed in alcoholic Eosin (Sigma-Aldrich; #HT110132) for 2-3 min. Differentiation of the Eosin stain was done in four 90 % ethanol solutions (10 dips each). Slides were quickly immersed in 100 % ethanol (2x 10 dips) before immersing the slides in 2 containers of xylene (1 min each). Excess liquid was removed, cover slips (Thickness #1; VWR; #631-0137) were mounted using DPX mountant, and slides were left to air dry at RT overnight. Excess DPX mountant was removed from dried slides before scanning at 20x magnification (or 40x using a doubler) using the Aperio ScanScope CS digital slide scanner.

2.14.2 Immunohistochemistry

Deparaffinised and rehydrated sections were immerged in antigen retrieval buffer and heated in a Decloaking Chamber (Biocare Medical). For details on antigen retrieval conditions, dilutions and incubation times for each primary antibody, see Table 2-7. In brief, specimens were heated in antigen retrieval buffer and then allowed to slowly cool down at RT for 20 min. Slides were then washed in PBS-T for 3 min and, when necessary, a mouse on mouse blocking step was performed using Mouse on Mouse (M.O.M.™) Blocking Reagent (diluted 1:25 in PBS; Vector Laboratories, #MKB-2213). This step was only included if staining was performed on mouse tissue and the primary antibody was raised in a mouse. Subsequently, primary antibodies (diluted in antibody diluent (Abcam; #ab64211) as described in

Table 2-7) were applied and incubated overnight at 4 °C. Slides were washed twice with PBT-T (3 min each) and incubated with secondary antibody (mouse/rabbit Polymer/HRP solution - Dako EnVision^{TM} + Dual Link System-HRP (DAB^{+}) #K4065 or Dako EnVision+ System- HRP Labelled Polymer Anti-Rabbit #K4002 for antibodies raised in mouse or rabbit, respectively) for 20 min at RT. Slides were rinsed with 1x PBS-T and washed with 1x PBS-T (2x 3 min each) and incubated with diaminobenzidine (DAB+, Dako EnVision^{TM} + Dual Link System-HRP (DAB^{+}) #K4065) for 0.5-5 min at RT, depending on the desired staining intensity. For experiments with inter-sample comparisons, incubation times were kept the same. DAB+ solution was removed and slides were washed in tap water for 5 min, followed by counter staining with aqueous Gill's Haematoxylin solution for 20 seconds at RT. Excess Haematoxilin was removed by washing of slides in running tap water for 5 min. Dehydration and mounting was performed as previously described in 0. Images were exported using ScanScope software (Aperio).

Table 2-7: Antibodies for immunohistochemistry and immunofluorescence

Antibody name (clone)	Antigen retrieval conditions: buffer, heating temperature and time	Primary antibody dilution (IHC/IF) and incubation conditions	Source and catalogue number
pAKT S473 (D9E)	Citrate, 125 °C, 2 min	1:100	CST #4060
EGFR (EP38Y)	Citrate, 125 °C, 2 min	1:100/1:500, ON 4 °C	Thermo Scientific #RM-2111-S0
pEGFR Y1068 (D7A5)	Tris-EDTA, 125 °C, 2 min	1:100/1:1000, ON 4 °C	CST #3777
Cleaved caspase 3-D175 pAb	Citrate, 110 °C, 2 min	1:600, ON 4 °C	CST #9661
pERK T202/Y204	Citrate, 125 °C, 2 min	1:1000, ON 4 °C	CST #4376

pHistone H2A.X S139 (JBW3010)	Citrate, 110 °C, 2 min	1:3000/1:3000, ON 4 °C	Millipore # 05-636
pHistone H3 S10 pAb	Citrate, 125 °C, 2 min	1:2000/1:5000, ON 4 °C	Millipore #06-570
pS6 Ribosomal Protein S240/244 (D68F8)	Citrate, 125 °C, 2 min	1:1000, ON 4 °C	CST #5364

2.14.3 Immunofluorescence staining

For immunofluorescence staining, sections were deparaffinised, rehydrated and antigen retrieval performed as described in 0. Cell permeabilisation and blocking was performed using the corresponding buffer (see Table 2-1) for 1 h at RT. Primary antibodies were diluted in antibody diluent (Abcam) and specimens were incubated with the antibody solutions at 4 °C overnight (see Table 2-7 for dilutions). Excess primary antibody was removed by washing the slides 3 times with 1x PBS and specimens were then incubated with the corresponding secondary antibodies in antibody diluent (Table 2-8) for 1 h at RT. Excess secondary antibody was removed by washing 3 times with 1x PBS and mounting of coverslips (Thickness #1; VWR; #631-0137) was done using Fluoroshield™ mounting medium containing DAPI (Sigma #F6057). Images were acquired using a confocal microscope (Zeiss LSM 710) with a 20x objective. Analysis was performed using the IMARIS software and representative images exported using NIS Elements (Nikon).

Table 2-8: Secondary antibodies for immunofluorescence

Antibody name	Dilution	Source and catalogue number
Alexa Fluor® 488 goat anti-rabbit IgG	1:1200	Life Technologies #A11008
Alexa Fluor® 555 goat anti-mouse IgG	1:1200	Life Technologies #A 21422

2.15 Cell cycle analysis

Cells were seeded in 6 cm plates and allowed to adhere overnight. Treatment was started when cells reached 70 % confluency, for times indicated in the experiment. Twenty min before the end of treatment, cells were pulse labelled with 20 µM bromodeoxyuridine (BrdU) and protected from light for 20 min. Cells were collected for analysis by collection of the culture medium, trypsinisation of cells as described previously and the trypsinisation reaction stopped using the collected medium. Cells were pelleted by centrifugation (280 x g for 5 min) and supernatant discarded. The cell pellets were resuspended in 100 µl of PBS and fixed by drop-wise addition of 1 ml ice-cold 70 % ethanol while vortexing. Prior to further processing, cells were incubated on ice for at least 30 min or stored at -20 °C. Cell were pelleted by centrifugation (280 x g for 5 min) and resuspended in 2 M HCl (Fisher Scientific) containing 0.1 mg/ml pepsin (Sigma-Aldrich). After 20 min of incubation, cells were pelleted and washed twice with 1x PBS and once with 1x PBS containing 2 % FBS. Cells were then incubated with anti-BrdU antibody (BD Biosciences, #347580, 1:100 in 100 µl of PBS containing 2 % FBS) for 90 min at RT, vortexing every 30 min. Subsequently cells were washed once with PBS containing 2 % FBS and incubated with the secondary antibody (goat anti-mouse Alexa 488 secondary antibody (Life Technologies), 1:200 in 100 µL PBS containing 2 % FBS) for 1 h at RT in the dark. Finally, cells were washed once with PBS and resuspended in 0.5 ml propidium iodide (PI; 20 µg/ml in PBS, Calbiochem). Intensity of anti-BrdU and PI staining of 10 000 cells per sample were assessed using a FACScan Flow Cytometer (BD Biosciences) and BD CellQuest^{TM} Pro software. PI FACS data was analysed using automated analysis settings on ModFit LT (Verity Software House, USA), using

automatic compensation for debris and aggregates. Anaylsis of BrdU incorporation was performed using FlowJo software (Tree Star Inc, USA).

2.16 Generation of TKI resistant cells

0.5-1 x 10^6 parental cells/ 10 cm plate were seeded and EGFR-TKIs added the next day and medium changed at least once a week. After 1-2 weeks of treatment, resistant clones or resistant populations were isolated. If populations were morphologically heterogeneous, clones were isolated. Thereafter, resistant cells were maintained in 1 μM gefitinib/AZD9291 with the compounds being added the day after cell plating. The concentration of 1 μM was chose, as plasma levels in patients are 0.5-2 μM for gefitinib (Yamaguchi, Isogai et al. 2015) and 1 μM for AZD9291 (Planchard, Brown et al. 2016).

2.17 *In vivo* studies

Animal procedures were carried out after local ethical committee review under a project license issued by the UK Home Office under the UK Animals (Scientific Procedures) Act 1986, and performed according to national guidelines (Workman, Aboagye et al. 2010). For cell injection and imaging procedures, mice were anaesthetised using isoflurane in air/oxygen. Approximately 4% isoflurane was used for induction of anaesthesia and 2-3% for maintenance depending on the breathing rate and depth of anaesthesia. Oxygen was supplied at a rate of 1-2 L/min. Gefitinib and AZD9291 doses are based on doses used in (Cross, Ashton et al. 2014).

2.17.1 Subcutaneous tumour model

HCC827 and PC9 cells were resuspended in 50 % matrigel (Corning, #356234) in DMEM/F12 media to obtain a concentration of 5.0 x 10^6 per 0.1 mL. 100 μL of this

solution were subcutaneously (s.c.) injected into a single site on the back of anaesthetized Balb/C female nude mice (CAnN.Cg-Foxn1nu/Crl, 6-8 weeks old, 15-18 g, Charles River Laboratories International, Inc., n=12 or n=8 for HCC827 or PC9, respectively). When tumours reached an average size of 150 mm^3, mice were randomized to receive gefitinib (5 mg/kg/d i.p. in 1 % Tween-80, days 1-5 each week) or AZD9291 (1 mg/kg/d i.p. in 1 % Tween-80, days 1-5 each week) for 6 weeks. Control animals did not receive any treatment. Tumour sizes were measured using callipers and mice weighed three times per week. Tumour volume (V) was calculated using the following formula:

$$V(mm^3) = 0.5\ x\ [l\ (mm)\ x\ w\ (mm)\ x\ h\ (mm)]$$

with h being the height, w being the length of the shortest and l the length of the longest side, respectively. Mice were sacrificed when their tumour size reached 400 mm^3 or 42 days after treatment start, which ever occurred earlier. For isolation of cells for ex vivo culture, tumours were excised and a fraction of tissue was transferred into advanced DMEM/F12 cell culture medium. Mechanical dissociation was then performed in the tissue culture hood, cells were transferred into cell culture dishes. The remaining tumour tissue was fixed in > 10 volumes of 4% PFA at 4ºC overnight and then stored in 70% ethanol at 4ºC until further tissue processing and paraffin embedding (see chapter 0).

2.17.2 Orthotopic tumour model

Orthotopic injection of cells was performed following the method described by Onn et al. (Onn, Isobe et al. 2003). Luciferase labelled cells were generated by lentiviral transduction and selection of successfully transduced cell populations by antibiotic selection. Lentiviral particles for expression of firefly luciferase under the EF1A

promoter were purchased from Amsbio (LVP434, AMS Biotechnology, UK). Target cells were pre-treated with 6 µg/mL polybrene for 20 min and infected at a multiplicity of infection of 10. Antibiotic selection in 0.5 µg/mL puromycin (Calbiochem) was started 72 h after infection.

Firefly luciferase expressing H1975, H1975^{9291S}, HCC827 and HCC827^{9291S} cells (0.05 mL, 1.0x10^{6}) in 50 % matrigel were injected intrathoracically into a single site on the left side of anaesthetized Balb/C female nude mice (purchased from Envigo, UK). Treatment with 2.5 mg/kg/d AZD9291 or vehicle (0.5% w/v hydroxyl propyl methyl cellulose (HPMC) in deionised water) was administered p.o. once daily for times indicated in the experiments. Tumour burden was monitored using the IVIS Spectrum In Vivo Imaging System (PerkinElmer) at regular intervals from as early as 10 days after cell injection. For imaging, animals were injected i.p. with 10mL/kg of luciferin (15 mg/mL in PBS freshly prepared and filter sterilised before imaging, Xenolight, PerkinElmer) and anaesthetised with isofluorane 3 min post-injection. Animals were then transferred onto the imaging table of the imaging system and separated by shields to avoid signal flow over between animals. Using the IVIS Living Image 4.3.1 software, images were acquired every min until the maximum photon flux per animal was reached.

Image quantification was performed using the IVIS Living Image software, data was exported to Excel for further analysis.

2.18 Analysis

Values are expressed as average ± standard error of the mean (SEM), unless stated otherwise. Using Excel (V15.37, Microsoft Office), Student's t-tests were performed for analysis of statistical significance. Analyses for overlap between datasets were

done using InteractiVenn (Heberle, Meirelles et al. 2015). The Fisher's exact test for enrichment analysis of targets in the compound screens was performed in Excel using the Real Statistics Resource Pack software (Version 5.0 Mac 2016) (Zaiontz 2015).

The calculation of the running enrichment score for graphical representation of enrichment of compounds with selected targets is based on the genset enrichment analysis described by {Subramanian, 2005 #1931}. The running enrichment score for compound at position x (ES(x)) is calculated using the following formulas:

For compounds inhibiting the selected target:

$$\mathrm{ES(x)} = \mathrm{ES(x-1)} + \sqrt{\frac{n-t}{t}}$$

For compounds not inhibiting the selected target:

$$\mathrm{ES(x)} = \mathrm{ES(x-1)} - \sqrt{\frac{t}{n-t}}$$

Where n is the number of compounds in the screen and t is the number of compounds that inhibit the selected target.

No correction for multiple testing was made in the statistical tests.

3 Characterisation of cellular response to exposure to EGFR-TKIs

The aim of this part of this work is to characterise the extent and timing of changes during sustained EGFR-TKI treatment in different EGFR mutation-positive cell line models and in different preclinical models. Mutations in the EGFR gene are found in 11.3 % of patients with adenocarcinoma of the lung (Cancer Genome Atlas Research 2014). Activating mutations around the ATP binding pocket of EGFR lead to ligand-independent activation of the kinase domain and its dimerisation partners, followed by activation of downstream signalling pathways. Three generations of highly potent EGFR-TKIs have been developed which differ in their ability to selectively inhibit mutant EGFR and to overcome the resistance-conferring EGFR T790M mutation. The main compounds utilised in this work are the 1st generation EGFR-TKI, gefitinib (ZD1839, IRESSA) and the 3rd generation EGFR-TKI, AZD9291 (osimertinib, TAGRISSO), although data on erlotinib (1st generation EGFR-TKI), afatinib (2nd generation EGFR-TKI) and CO-1686 (3rd generation EGFR-TKI) are also included in some experiments. First generation inhibitors inhibit EGFR kinase activity by reversible, ATP-competitive binding whereas 2nd and 3rd generation inhibitors bind EGFR by irreversible, covalent binding. Treatment of EGFR mutation-positive patients with EGFR-TKIs has shown to lead to improved PFS as well as positive trends in OS (Lee, Brown et al. 2013, Astra Zeneca 2017, Zhao, Chen et al. 2017).

This chapter will examine the effect of EGFR-TKIs in different EGFR-mutant and EGFR WT NSCLC cell lines and then look at effects of EGFR-TKI exposure over the short-, mid- and long-term. We will use 2D cell culture models and expand findings into more complex 3D spheroid models. Furthermore, we will use established

subcutaneous xenograft models as well as orthotopic lung xenograft models, which are thought to represent a more relevant tumour microenvironment (Killion, Radinsky et al. 1998).

3.1 Effect of EGFR mutations on cellular response to exposure to EGFR-TKIs

NSCLC cells with activating EGFR mutations (EGFR M+) are known to be hypersensitive to EGFR-TKIs (Sharma, Bell et al. 2007). We used a viability based proliferation assay (Figure 3-1 A) and confirmed that most EGFR M+ cells within our NSCLC cell line panel were sensitive, with low nanomolar-range IC_{50}s for gefitinib and AZD9291 (Table 3-1 and Figure 3-1 B). H1975 cells have an EGFR T790M mutation, which confers resistance to gefitinib but not AZD9291 (Table 3-1). Compared with other EGFR M+ NSCLC cell lines, H1650 cell proliferation was less affected by EGFR-TKI treatment despite a reduction in pEGFR levels under EGFR-TKI treatment (Table 3-1 and Figure 3-1 B and C), which may be due to a PTEN mutation (Sos, Koker et al. 2009).

Table 3-1: Cell lines used in this study, EGFR mutation status and determined IC_{50} values for gefitinib and AZD9291

Cell lines are grouped as EGFR M+, gefitinib-sensitive cell lines (green), EGFR M+, gefitinib-resistant cell lines (red), EGFR M+, gefitinib and AZD9291 resistant cell lines (orange) and EGFR WT cell lines (blue). Values represent data from three independent experiments (* or one experiment), performed in technical triplicates. n.d. IC50 not determined.

Cell line	IC50 (μM) for gefitinib (mean ±SEM)	IC_{50} (μM) for AZD9291 (mean ±SEM)	EGFR mutational status
HCC827	0.004 (0.0007)	0.016 (0.009)	ΔE746_A750
HCC2935	0.005 (0.0007)	0.0013 (0.0004) *	ΔE746_A750, T751A
HCC4006	0.016 (0.003)	0.0002 (0.00003) *	ΔL747_E749, A750P
PC9	0.02 (0.001)	0.006 (0.0007)	ΔE746_A750
H1975	9.31 (0.29)	0.007 (0.0009)	L858R, T790M
H1650	2.43 (0.95)	0.24 (0.03)	ΔE746_A750
Calu3	0.19 (0.02)	0.1 (0.03)	wt
H1648	0.55 (0.11)	n.d.	wt
A549	8.39 (0.45)	1.49 (0.23) *	wt

We next investigated intracellular signalling changes by western blotting. As expected, EGFR M+ cell lines were sensitive to gefitinib. Treatment led to a time dependent reduction in EGFR-signalling, as measured by levels of pEGFR, pAKT and pERK and induction of apoptosis, measured by increased levels of cleaved PARP. EGFR WT cell lines as well as gefitinib-resistant H1975 cells showed no reduction in EGFR signalling and no induction of apoptosis after gefitinib treatment. DUSP6, a dual specificity phosphatase that negatively regulates ERK1/2 phosphorylation (Jeffrey, Camps et al. 2007) and is itself regulated by ERK (Plotnikov, Zehorai et al. 2011), was reduced upon drug treatment in sensitive cell lines (Figure 3-1C).

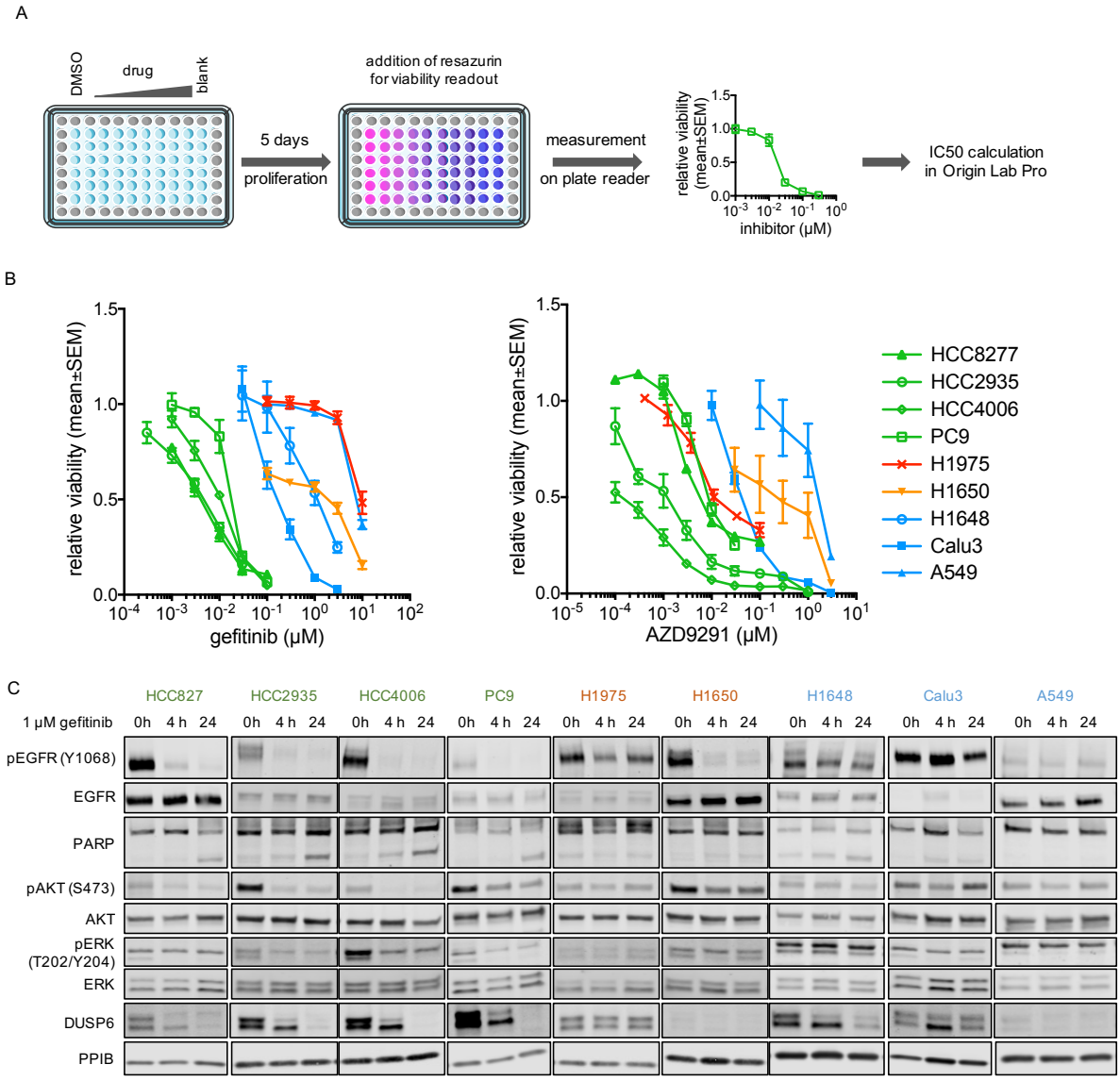


Figure 3-1: EGFR M+ cell lines are hypersensitive to gefitinib.

A: Setup for assessment of viability after 5-day drug treatment in 96-well assay. Cells were seeded at 500-1000 cells/well. Treatment with increasing doses of compounds was added the next day and viability assessed using resazurin at the end of the experiment. Data were collected using a plate reader and analysed with excel and Origin Lab Pro for normalisation and IC50 calculation, respectively. B: Representative dose response curves for NSCLC cell lines treated with gefitinib or AZD9291 for 5 days at the indicated doses. Proliferation of H1648 was not assessed with AZD9291. Data are from one experiment performed in technical triplicates, representative of at least 3 independent biological repeats. C: Western blot analysis of signalling after gefitinib treatment in cell line panel. Cells were treated with 1 μM gefitinib for the indicated times before preparation of cell lysates. PPIB was used as a loading control. Colour coding of cell lines as in Table 3.1.

To confirm inhibition of EGFR signalling by AZD9291 in gefitinib-sensitive (HCC827 and PC9) as well as the gefitinib-resistant L858R/T790M mutant H1975 cells, we performed western blotting. AZD9291 treatment led to reduction in EGFR signalling via pEGFR, pAKT and pERK and induction of apoptosis in all three cell lines (Figure 3-2).

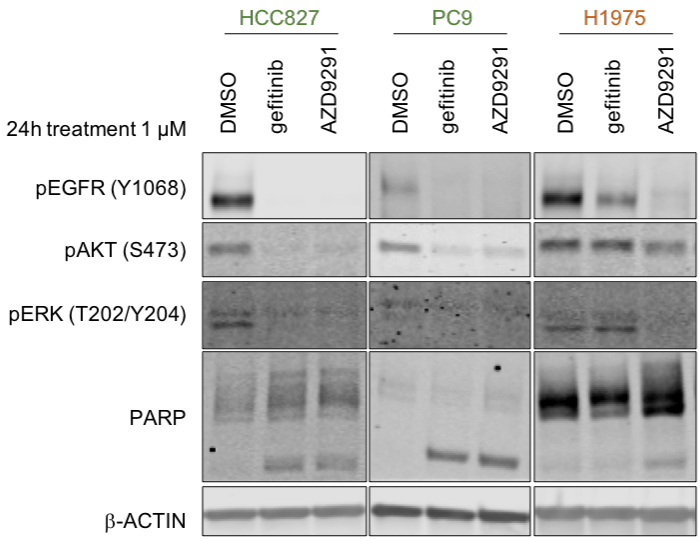


Figure 3-2: EGFR T790M gatekeeper mutation confers resistance to 1st but not 3rd generation EGFR-TKIs
Western blot analysis of EGFR M+ cells HCC827 and PC9 and EGFR M+/T790M cell line H1975 treated with DMSO, 1 µM gefitinib or 1 µM AZD9291 for 24 h before preparation of cell lysates. β-actin was used as a loading control.

In summary, we confirmed that NSCLC cell lines with activating EGFR mutations are sensitive to EGFR-TKIs of all generations with the exception of H1975. H1975 cells harbour the T790M mutation, which confers resistance to the ATP-competitive 1st generation inhibitor gefitinib but not the covalently binding 3rd generation inhibitor AZD9291. Both inhibitors led to reduced levels of EGFR autophosphorylation at Y1068 in EGFR-mutant cells, indicating inhibition of kinase activity. Inhibition of EGFR phosphorylation in EGFR-mutant cells - but not in cells with WT EGFR or existing mechanisms of resistance to EGFR-TKI treatment - led to reduction of phosphorylation levels of the downstream markers AKT and ERK and increased apoptosis assessed by levels of cleaved PARP. These data are in line with published work, showing dependency of EGFR M+ cells on EGFR signalling (Jiang, Greulich et al. 2005).

As PC9, HCC827 and H1975 are representative cell lines for the most commonly occurring EGFR mutations in NSCLC (see chapter 1.4), the rest of this study

focussed primarily on these three cell lines, although certain experiments were extended to include HCC4006 and HCC2935 cells.

Over the following chapters, we will describe the response of EGFR M+ cells to EGFR inhibition in greater depth. With increasing time of exposure to EGFR-TKIs, different processes dominate the cellular and phenotypic responses. We postulate that the response to EGFR-TKI treatment can be divided into (i) **drug sensitive**, (ii) **drug tolerant** and (iii) **drug resistant** phases (Figure 3-3).

EGFR-TKI treatment times are referred to as **short** (≤ 24 h) or **long** (> 24 h), and the phenotypic responses are considered **acute** or **prolonged** based on whether they occur shortly after treatment start, or are evident only after sustained drug treatment (Figure 3-3).

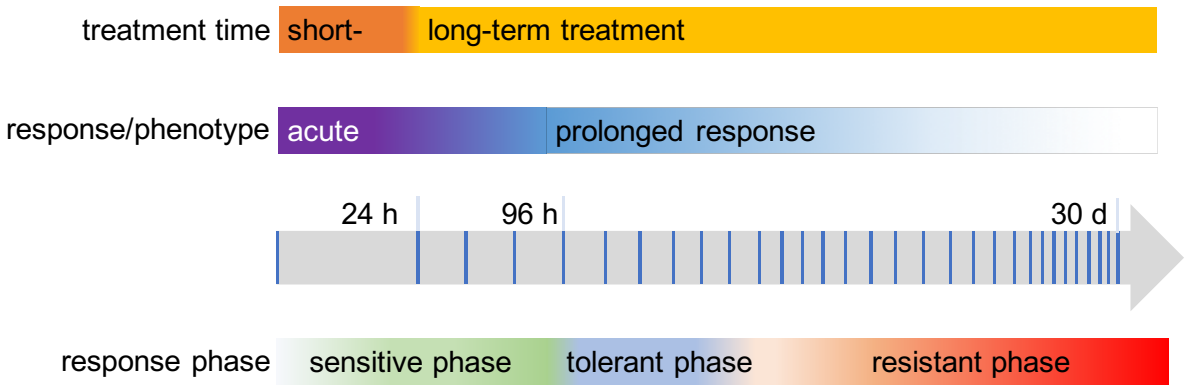


Figure 3-3: Definition of treatment times, response time scales and resistance phases during EGFR-TKI treatment

Treatment times up to 24 h are referred to as short-term treatments, whereas long-term treatments are greater than 24 h. Initial phenotypic changes, including reduction in signalling and induction of apoptosis after treatment start are referred to as acute responses, in contrast to prolonged responses, which include changes after the maximum induction of apoptosis. Furthermore, we divide the cellular response to EGFR-TKI treatment into drug sensitive, tolerant and resistant phases.

3.2 Cellular response to EGFR-inhibition under 2D culture conditions

3.2.1 Biochemical changes during short-term exposure to EGFR-TKIs

To characterise early signalling changes after short-term treatment with EGFR-TKIs, we performed western blot analyses on cells treated with a range of doses of either gefitinib or AZD9291 for up to 8 hours (Figure 3-4). Treatment with gefitinib at doses of ≥10 nM or more but not 3 nM led to a reduction of pEGFR levels even at the earliest time point measured (15 min) (Figure 3-4). In contrast, treatment with 3 nM AZD9291 for 8 hours was sufficient to reduce levels of pEGFR, although higher doses led to a more rapid reduction. Quantification of pEGFR/EGFR levels is shown in Figure 3-4. Quantification and interpretation of relative pEGFR/EGFR levels is however of limited quality due to the high background (including spots) of the EGFR antibody in this experiment. While similar effects could be observed for levels of pERK, levels of pAKT were only reduced at longer treatment times (Figure 3-4). The difference in dynamics between gefitinib and AZD9291 might reflect the differences in binding modes of the two inhibitors (Cross, Ashton et al. 2014).

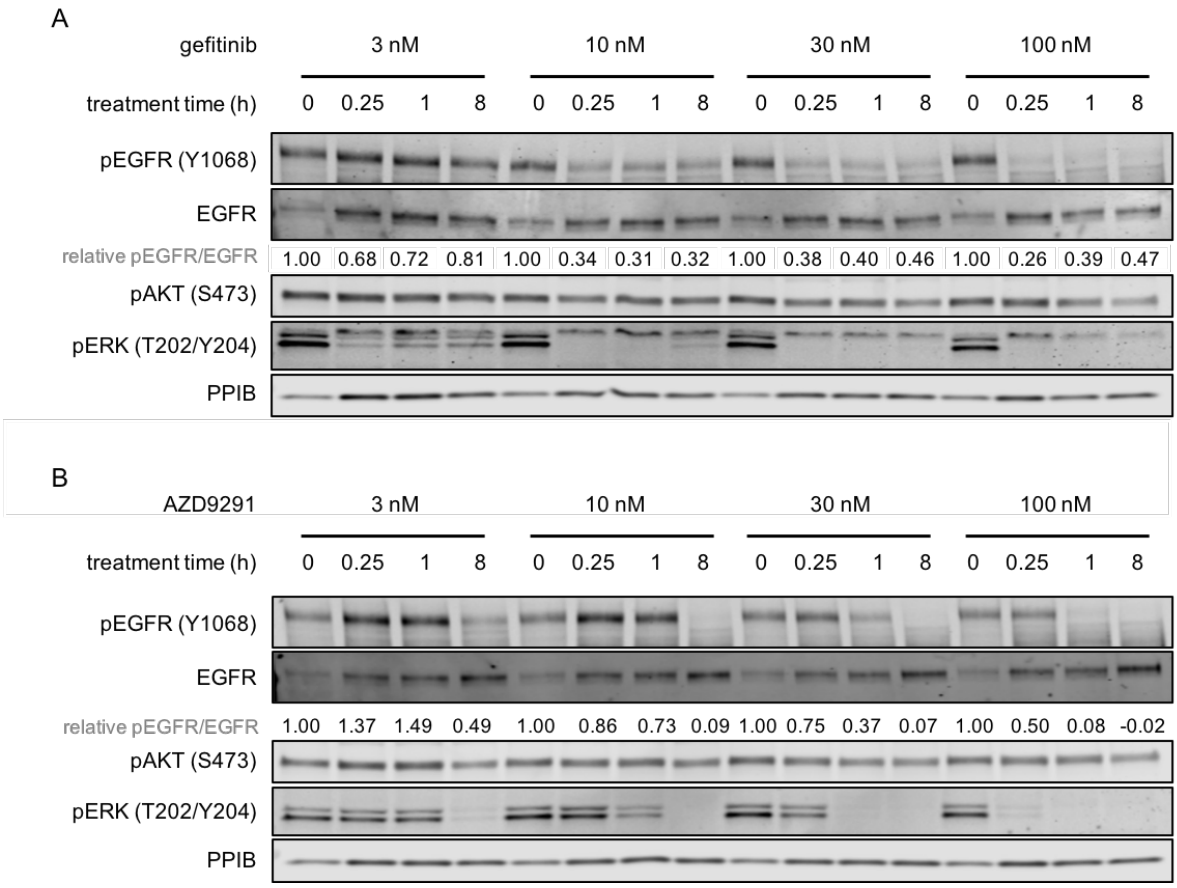
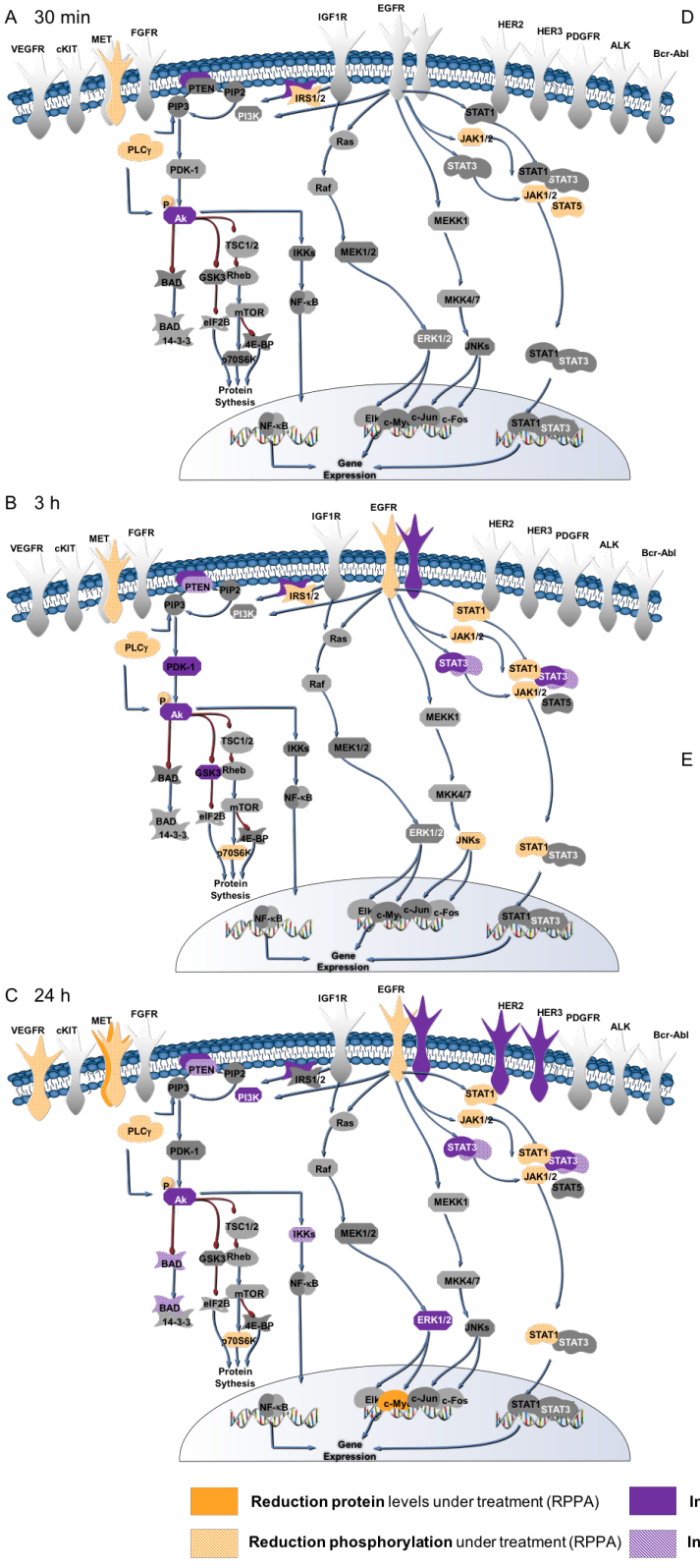


Figure 3-4: Rapid and potent reduction in EGFR signalling after gefitinib and AZD9291 treatment in PC9 NSCLC cells.

Western blot time course analysis of cells exposed to gefitinib (A) or AZD9291 (B). Cells were treated with indicated doses for indicated times before lysate preparation. Quantification of pEGFR signal relative to signal of corresponding EGFR was performed using the Image studio Lite software and is given for each sample. Data are normalised to each of the untreated samples of the dose group (value of 1.00). PPIB was used as a loading control.

To investigate signalling changes more broadly in response to EGFR-TKI treatment, we performed a reverse phase protein array (RPPA) analysis using a platform with 117 different antibodies (see full list in Table S 1) on PC9 and H1975 cells. To minimise cell-line-specific effects, we identified changes that were significant in both cell lines when comparing untreated cells to cells treated with 100 nM, 300 nM and 1 µM. Significance of changes was tested using a two-tailed student's t-test with a cut-off of $p \leq 0.05$. Results confirmed the down-regulation of phosphorylation levels of immediate targets tested previously (by western blotting), such as EGFR and AKT but also showed reduction in a number of interrelated pathways, including NF-κB and

STAT signalling. A time-dependent change in signalling was also apparent, for example, phospho-S6-kinase levels were only significantly reduced after 3 h or beyond. Of interest, several of the proteins with reduced phosphorylation levels also had increased total protein levels (Figure 3-5).



down	30 min	3 h	24 h
pStat5 Y694			
pIRS-1 S636/639			
pSrc Y416			
pAkt S473			
pPLC-gamma1 Y783			
pMet Y1349			
pJAK1 Y1022/T1023			
pStat1 Y701			
pSAPK/JNK T183/Y185			
pEGFR Y1173			
pp70 S6 Kinase T421/S424			
pS6 Ribosomal protein S240/244			
pRb S807/811			
pRb S780			
pVEGFR Y951			
pS6 Ribosomal protein S235/236			
pc-Jun S73			
pVEGFR Y1175			
pStat1 S727			

up	30 min	3 h	24 h
pStat3 Y705			
pPTEN P S380/T382/383			
pIKK alpha/beta S176/177			
pBad S136			

down	30 min	3 h	24 h
Met			
c-Myc			
Rb			

up	30 min	3 h	24 h
Src			
IRS-1			
Akt			
PTEN			
MAPKAPK-2			
p53			
PDK-1			
GSK-3-beta			
EGFR			
Stat3			
ERK1/2			
PI3 Kinase p110-alpha			
Tsc-2			
HER2			
Stat6			
Bcl-2			
HER3			
Prohibitin			

Reduction protein levels under treatment (RPPA)

Increased protein under treatment (RPPA)

Reduction phosphorylation under treatment (RPPA)

Increased phosphorylation under treatment (RPPA)

Figure 3-5: RPPA analysis of AZD9291 treated PC9 and H1975 cells identifies reduced EGFR downstream signalling and induced stress response signalling

RPPA analysis of changes common to both PC9 and H1975 cells after treatment with AZD9291 (0.1 – 1 μM). Selected significant changes (lysates from untreated cells compared to all lysates of cells treated with 0.1/0.3/1 μM) after treatment times of 30 min (A), 3 h (B) and 24 h (C) are highlighted in signalling diagrams. A list of all significant changes in phospho-proteins levels are given in (D) and for total proteins levels in (E). Colour and pattern coding indicates type and direction of change. Data are based on one biological repeat per condition.

3.2.2 Acute cellular response under short- and long-term treatment

To examine the phenotypic effects of EGFR-TKIs on cell migration, proliferation and viability, we performed live cell imaging using PC9 cells stably expressing the CaspeR3-GR sensor for detection of caspase 3 activation and tracking of cells. In this system, PC9 cells have been transfected with CaspeR3-GR and stably express a hybrid protein consisting of GFP and RFP separated by a peptide linker containing a caspase 3 cleavage site (Shcherbo, Souslova et al. 2009). Upon excitation of GFP (at 465-495 nm), FRET (Förster Resonance Energy Transfer) from the GFP to the RFP (dependent on close proximity of the two proteins) results in emission fluorescence that is detectable in both the green (max. 505 nm) and red emission channels (590 nm). Upon induction of apoptosis and activation of caspase 3, the peptide linker region is cleaved, GFP and RFP dissociate, and FRET is reduced, resulting in a loss of RFP emission (max. 584 nm) upon excitation of GFP (Figure 3-6 A). Overall, caspase 3 cleavage of the linker leads to increased green signal and decreased red signal.

Using live cell microscopy, we showed that AZD9291 treatment of PC9- CaspeR3-GR cells resulted in a rapid reduction in migration speed and cell proliferation, followed by the induction of apoptosis after 18-20 h, as measured by loss of RFP emission (Figure 3-6 B and C). These effects were dose-dependent and similar effects could be observed under gefitinib treatment (Figure S 1).

In order to confirm effects of EGFR-TKI treatment on the cell cycle, we performed PI FACS analysis on H1975 and HCC827 cells (Figure 3-6 D/E). 24 h treatment led to an accumulation of cells in G1 and an increase in cells in sub-G1, consistent with inhibition of proliferation and an increase in apoptosis.

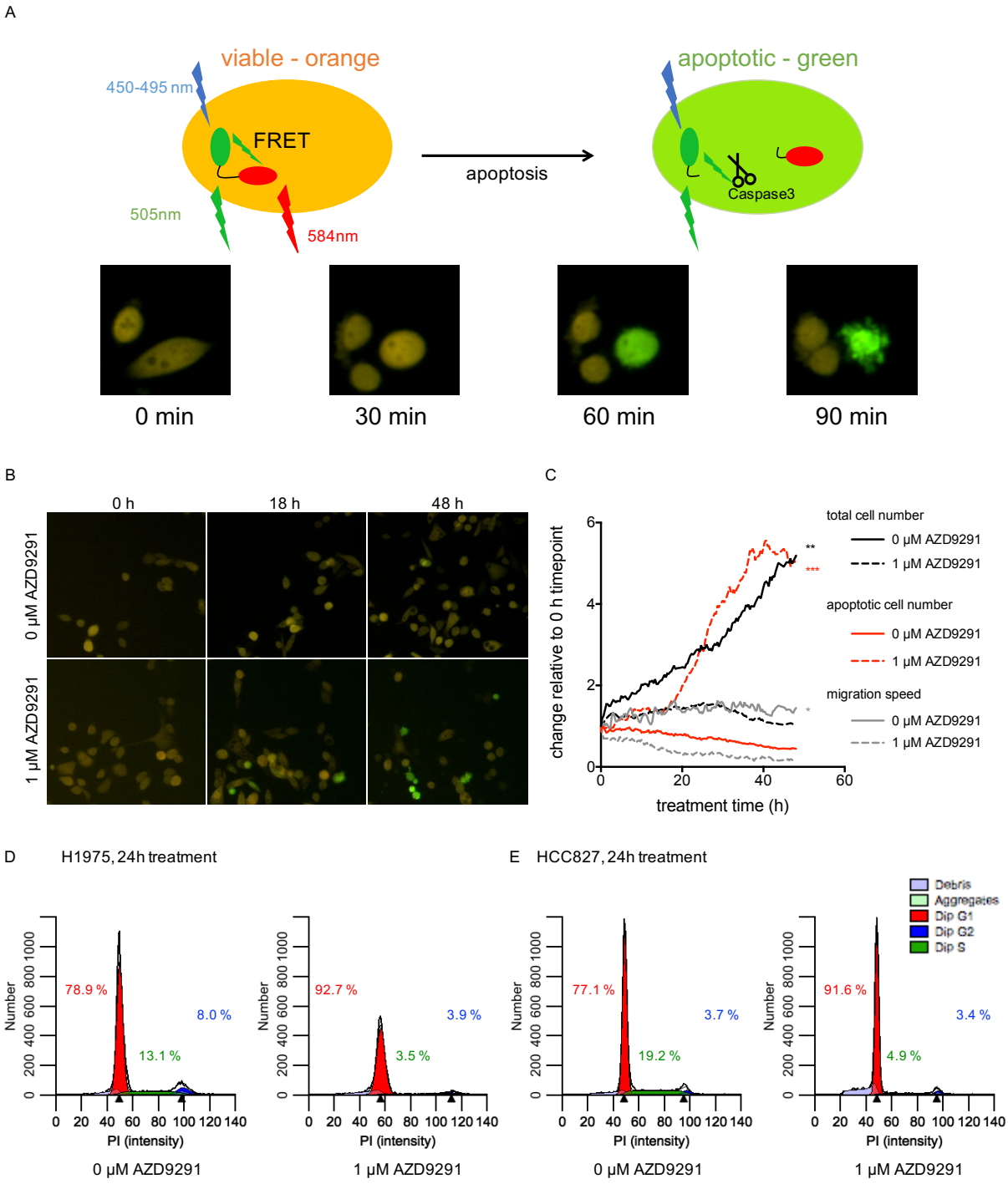


Figure 3-6: AZD9291 induced reduction in cell migration, proliferation and increased induction of apoptosis

A: Setup for live cell detection of caspase 3 activation using cells expressing CaspeR3-GR construct. GFP and RFP images are merged to generate an orange overlay image. Relative reduction in RFP signal leads to green appearance of apoptotic cells due to loss of FRET. Wavelengths indicate the excitation wavelength used and the maximum emission wavelengths of the GFP and RFP proteins. B: Representative images of PC9 CaspeR3-GR cells at indicated times after treatment start with 0 µM or 1 µM AZD9291, showing increased number of green (apoptotic) cells over time in AZD9291 treated cells. C: Quantification of live cell imaging over 48 h. Cell number, number of apoptotic cells and migration speed as calculated by IMARIS software are relative to the highest measurement within the first hour. Data represents the mean of 2 wells/condition of one experiment. Statistically significant differences between untreated and treated cells at the final time point are indicated for each measure. * p≤0.05, ** p≤0.01, *** p≤0.001. The SEM is omitted in the graph for clarity. D/E: PI FACS analysis of DNA content of H1975 (D) and HCC827 (E) cells 24h after treatment with 0 µM or 1 µM AZD9291 (n=1 per condition).

To better compare the time course and extent of induction of apoptosis in different cell lines, we used an INCell Analyzer-based Hoechst assay for detection of apoptotic cells (Figure 3-7 A) (Bokobza, Jiang et al. 2014). The time course and extent of induction of apoptosis differed between PC9 and H1975 cells. PC9 cells were rapidly apoptotic (Figure 3-7 B), whereas H1975 showed slower induction of apoptosis (Figure 3-7 C). Quantification of the total number of viable cells over time showed an initial increase up to 18 h followed by a decrease in cell number which was more marked in PC9 compared to H1975 cells (Figure 3-7 E for quantification of live cells and D for images of fixed plates of H1975 cells). Quantification of apoptosis in HCC827 cells using the Hoechst assay was unreliable, as these cells grow in tight clusters with overlapping nuclei.

During continuous EGFR-TKI treatment, this relatively lower extent of apoptosis in H1975 compared to PC9 cells was of particular interest. The previously described early reduction in EGFR signalling 24 h after EGFR-TKI treatment could be observed in both H1975 and HCC827 cells (Figure 3-7 F), as well as in HCC4006 cells (Figure 3-7 G). Nevertheless, sufficient cells survived treatment and re-engagement of EGFR downstream signalling (pAKT, pERK and pS6 ribosomal protein (pS6 rp)) could be observed as early as 48 h after treatment start, while pEGFR levels remained low. Due to the high degree of cell death in PC9 over this time course, corresponding western blot experiments in PC9 were not possible as sufficient protein extract could not be recovered.

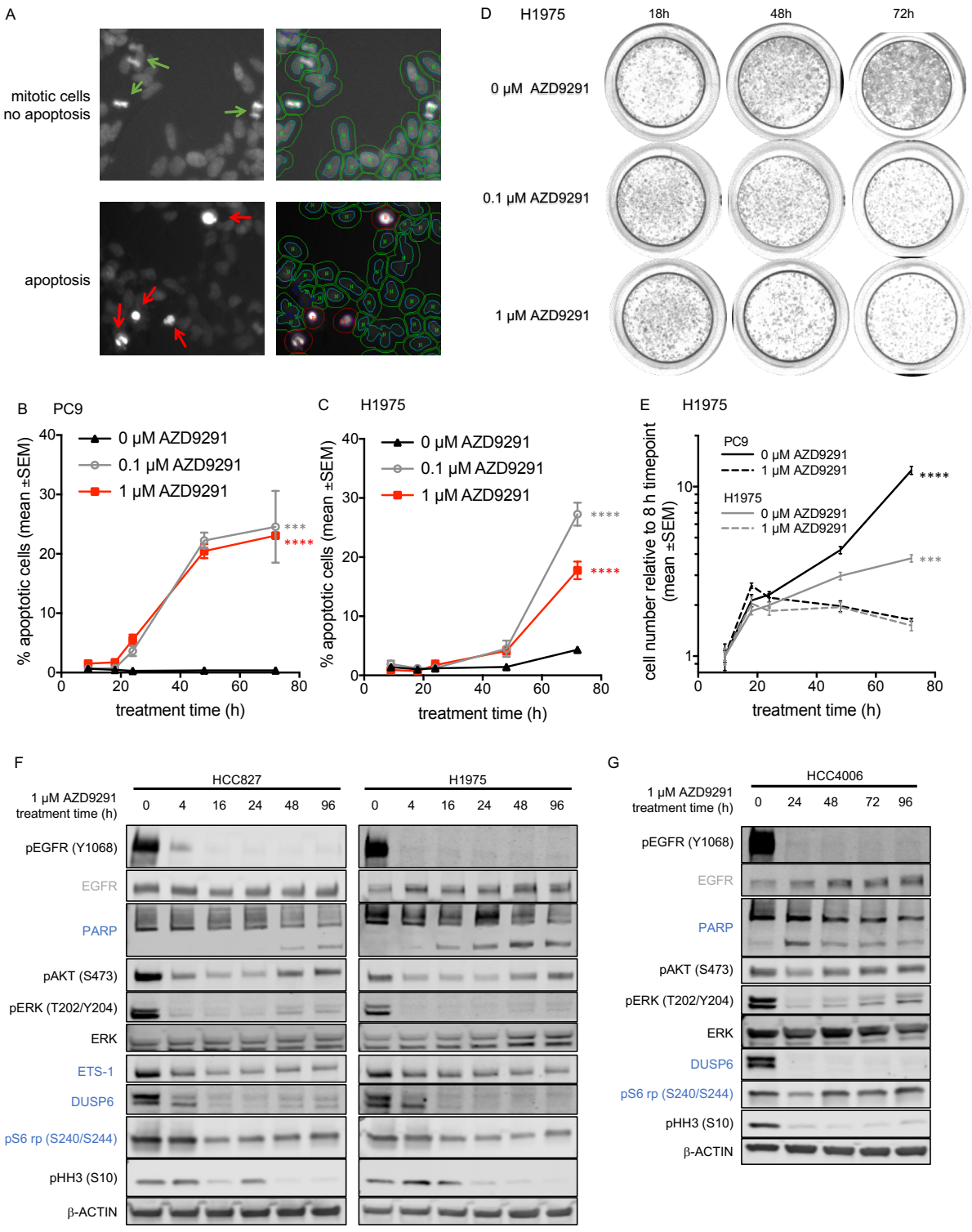


Figure 3-7: Mid-term response of EGFR M+ cells show evidence of re-engagement of pAKT and pERK signalling after 96 h of AZD9291 treatment

A: Automated image analysis in the INCell Analyzer Hoechst assay counts non-apoptotic cells (green outline on right), including mitotic cells (green arrow) and apoptotic cells (red arrow, red outline on right). Subsequently the percentage of apoptotic cells is calculated for each well. The mean apoptotic fraction over time for different treatments is shown for PC9 (B) and H1975 (C). Quantification of live cells is shown in (E). Data are from one representative experiment (total n=2) performed in technical triplicates. The mean number of quantified cells/well at the 8 h time point for untreated/0.1 µM/1 µM AZD9291 treated H1975 or PC9 is 179/172/169 or 269/303/298, respectively. B/C/E: Statistical significance of differences between treatments and untreated controls are indicated with *** for p≤0.001 and **** for p≤0.0001. D: Representative pictures of wells from (C), fixed at each time point.

F/G: Western blot analysis of time course of treatment of HCC827 and H1975 cells (F) and HCC4006 (G) with AZD9291. Cells were treated with 1 μM AZD9291 for indicated times (0-96 h) before lysate preparation. β-actin was used as a loading control and antigens of the same colour writing were detected on the same membrane.

3.2.3 Cellular response to long-term treatment with EGFR-TKIs

As described above, the abilities of HCC827, H1975, HCC4006 and PC9 cells to tolerate sustained high dose EGFR-TKI treatment appeared to differ significantly. To assess this, we seeded cells in 10 cm plates and once cells had reached 70 % confluence treatment with AZD9291 (H1975) or gefitinib (PC9 and HCC827) at doses of > 100x IC_{50} was initiated for up to 2 weeks. In the case of HCC827 and H1975, a high proportion of cells survived treatment with gefitinib or AZD9291 (Figure 3-8 A, left and middle). Some or all cells of the surviving HCC827 or H1975, respectively, showed morphological changes compared to the parental cells (see chapter 4). In contrast, PC9 cells did not survive as a population but individual colonies emerged under gefitinib treatment (3 colonies/10^8 cells plated, Figure 3-8 A, right). AZD9291 selection had a more potent effect in PC9 cells, whereby colonies did not grow out even with treatment periods of up to 3 weeks but a low number of cells remained on the plate and were able to grow after drug withdrawal (see chapter 4).

We consider this survival during the drug tolerant phase and subsequent ability to proliferate under treatment to be signs of the emergence of resistance. In order to determine when and which signalling changes occur during the process of emergence of resistance, HCC827 and H1975 cells were exposed to 1 μM AZD9291 and western blot analysis performed on different days over a period of up to 2 weeks (day 0 to day 14 samples). In addition, cells surviving 14 days were passaged in 1 μM AZD9291 for further 2-3 weeks (day 30+ samples). Confirming and extending previous results, EGFR signalling was reduced within 24 h (pEGFR, pAKT, pERK, pS6, DUSP6), followed by an increase in apoptosis (measured by cleaved PARP)

and a decrease in cell proliferation (measured by the mitosis marker, pHH3) over the next 1 to 3 days (Figure 3-8 B). These initial changes were followed by a re-engagement of AKT/ERK signalling, a reduction in apoptosis and, importantly, an increase in proliferation as measured by pHH3 over the following 4 to 30+ days (Figure 3-8 B). Re-engagement of AKT/ERK signalling and cell proliferation was observed earlier in HCC827 than in H1975 cells. Furthermore, recovery of pERK levels was less pronounced in H1975 compared to HCC827 cells (Figure 3-8 B). These changes in signalling were in line with the observations from BrdU-FACS analysis for H1975 (Figure 3-8 C) and HCC827 (data not shown). EGFR-TKI treatment led to a marked reduction in the proportion of BrdU positive (S-phase) cells after 1 day. A small increase in S-phase was evident between day 1 and day 14 in cells treated with AZD9291 (Figure 3-8C). Analysis of cells exposed to AZD9291 for 14 days followed by a 24 h drug withdrawal showed a marked increase in the S-phase cell population of nearly 10-fold, compared to cells without withdrawal (Figure 3-8C), indicating a substantial proportion of cells within the population were viable and had proliferative potential.

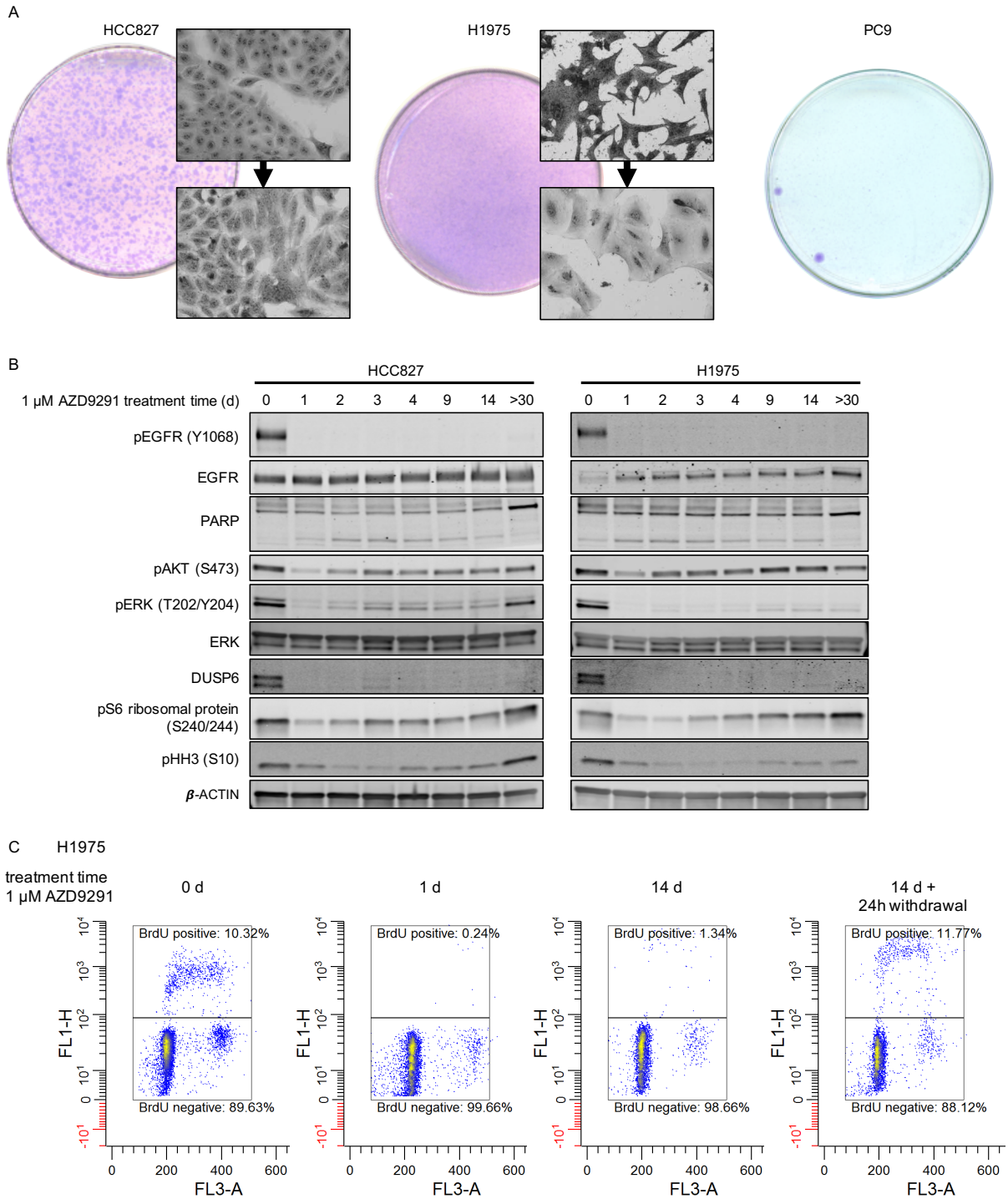


Figure 3-8: HCC827 and H1975 cells reengage signalling and proliferation during AZD9291 treatment and become resistant.

A: HCC827 and PC9 were treated with 1 µM gefitinib and H1975 with 1 µM AZD9291 for 2-3 weeks. Plates were fixed and stained with methanol/crystal violet. Microscopic bright field images show parental cells on the top and cells after long-term EGFR-TKI exposure on the bottom. B: Western blot analysis of HCC827 and H1975 cells treated with 1 µM AZD9291 for different durations. Medium was changed and AZD9291 replenished 24 h before lysate preparation for culture dishes of each time point and every 72 h for all other dishes. Surviving cells on day 14 were expanded in new culture vessels and maintained under AZD9291 treatment for further 2-3 weeks, with standard passaging every 3-5 days. Beta-actin was used as loading control. C: BrdU-PI-FACS analysis of H1975 cells on indicated days after treatment start. BrdU treatment was performed 20 min prior to sample collection and fixation to identify cells in S-phase. FL3-A: propidium iodide, FL1H: BrdU. A total of 10,000 ungated events were acquired for each condition.

3.3 Discussion response to EGFR-inhibition under 2D culture conditions

In summary, in standard 2D culture conditions, we showed that short-term treatment of EGFR M+, EGFR-dependent NSCLC cell lines led to a rapid initiation of an acute biochemical response. This was characterised by a reduction in autophosphorylation of EGFR and a reduction of activation of the key downstream pathways PI3K-AKT-mTOR and RAS-RAF-MEK-ERK, assessed by levels of pAKT and pERK. RPPA analysis additionally identified reduction of phosphorylation of other immediate targets of EGFR (e.g. JAK/STAT, PLCγ and JNK). Inhibition of these immediate targets was followed by reduced phosphorylation of downstream targets (e.g. p70S6K, S6 ribosomal protein). This is in line with results obtained by a number of groups using EGFR-mutated NSCLC cell lines or Ba/F3 cells expressing mutant EGFR forms (Jiang, Greulich et al. 2005, Sharma, Gajowniczek et al. 2006, Cross, Ashton et al. 2014, Hirano, Yasuda et al. 2015), thus validating our experimental approach. A number of recently published studies using phosphoproteomics to investigate changes under treatment with 1st generation EGFR-TKIs (Yoshida, Zhang et al. 2014, Zhang, Belkina et al. 2015, Zhang, Maity et al. 2017) are in line with observations made in this work and associate these changes with EGFR-TKI sensitivity. To our knowledge this is the first published study to perform time-resolved RPPA analysis of EGFR M+ NSCLC cells under treatment with a 3rd generation EGFR-TKI and we show that these changes are dynamic, as for example seen in STAT signalling. Signal transducers and activators of transcription (STAT) proteins function downstream of EGFR. We observed significant reduction of STAT5 pY694 levels at 30 min, which was followed by reduction in levels of STAT1 pY701 and pS727 at 3 h and 24 h, respectively. STAT signalling is known to mediate the transcription of several proteins involved in proliferation, cell cycle progression, and

inhibition of apoptosis (Quesnelle, Boehm et al. 2007) and has been reported to play a role in response and resistance to EGFR-TKIs (Alvarez, Greulich et al. 2006, Kim, Kwon et al. 2012). We subsequently showed that these changes are followed by phenotypic changes, such as reduction in migration and proliferation (G1-arrest) as well as induction of apoptosis, as previously reported in the literature (Cross, Ashton et al. 2014, Li, Song et al. 2016). We identified PC9 cells as highly apoptotic compared to H1975, HCC827 and HCC4006 cells under high dose EGFR-TKI treatment, although the reason for the observed differences in kinetics and extent of induction of apoptosis in PC9 is unclear but might be related to high BIM levels in PC9. BIM is a pro-apoptotic member of the family of Bcl-2 proteins and an important mediator of targeted therapy-induced apoptosis (Faber, Corcoran et al. 2011). Reported relative sensitivities to long-term EGFR-TKI exposure between these cell lines differ in the literature, showing higher sensitivity for HCC827 over PC9 (Tricker, Xu et al. 2015) or for PC9 over HCC827 or H1975 (Sharma, Lee et al. 2010, Eberlein, Stetson et al. 2015). The reason for this is unknown but medium conditions and source of these cells might have an impact on cellular response. Concluding, we define this phase of initial response to EGFR-TKIs as the drug sensitive phase.

Importantly, our work has shown that in H1975, HCC827 and HCC4006 cells, a significant number of cells survived the acute drug response phase and transitioned from the drug sensitive to a drug tolerant phase. The tolerant phase was characterised by re-engagement of EGFR-downstream signalling via AKT and subsequently ERK under sustained inhibition of EGFR autophosphorylation with long-term EGFR-TKI treatment. However, our data do not allow us to exclude the option that the apparent re-engagement of signalling is due to preferential killing of cells expressing low levels of pERK/pAKT. Irrespective of this, the consequence is

that after prolonged treatment with EGFR-TKI, a proportion of cells survive and enter the drug resistant phase, proliferating under high dose EGFR-TKI treatment. The process of re-engagement of EGFR downstream signalling and emergence of resistance has been observed in similar time scales in other published studies (Ercan, Xu et al. 2012, Eberlein, Stetson et al. 2015, Tricker, Xu et al. 2015, Ichihara, Westover et al. 2017), and although one other study describes a reactivation of ERK within hours (Phuchareon, McCormick et al. 2015), this has not been observed by other groups. To our knowledge, this is however the first published study documenting the re-engagement of signalling and subsequent proliferation under continued EGFR-TKI treatment to this extent and describing distinct phases of sensitivity, tolerance and resistance under 2D culture conditions.

3.4 Cellular response to EGFR-TKIs in 3D spheroids

The investigation of drug effects in 2D cell culture is straightforward and well established. Nonetheless, the 2D environment does not reflect the complexity observed in tumours *in situ*. However, *in vitro* 3D models can recapitulate at least some of the features of tumour growth *in situ*. 3D spheroid models possess a number of features of tumours, such as increased cell-cell interactions, zones of differential proliferation, and gradients in nutrients, drug penetration and oxygen (Sutherland, McCredie et al. 1971, Sutherland 1988). Compared with 2D culture, cells grown as spheroids show differences in a number of factors, including cell cycle duration, morphology, drug sensitivity, and metabolism as well as gene and protein expressions (Reviewed in (Hirschhaeuser, Menne et al. 2010, Amann, Gamerith et al. 2015, Nath and Devi 2016)).

To assess the ability of HCC827, H1975 and PC9 to form spheroids, cells were seeded in round bottom low-attachment 96-well plates, centrifuged to facilitate cell aggregation (Figure 3-9 A), and spheroid size was assessed regularly using the GelCount imager and corresponding analysis software. Representative spheroid images and quantification over time are shown in Figure 3-9 B and C. Spheroid formation in HCC827 cells was most variable, generally forming one dominant spheroid, surrounded by several smaller spheroids. HCC827 spheroids showed a high level of integrity, withstanding medium change without disaggregating. After an initial compaction period (~ 2 days) HCC827 spheroids showed constant growth, with a more than 4-fold increase in size at day 16 after seeding. H1975 cells formed a single tight spheroid, that compacted to its minimum size around day 7 after seeding. By day 16 it had increased in size by 1.8-fold compared to the maximal compaction on day 7. PC9 cells formed loose spheroids that could be disaggregated by pipetting. There was no initial period of compaction, and spheroid area increased steadily from day 1 after seeding, reaching a maximum on day 8 (approx. 2.7-fold increase) before spheroids showed less well-defined borders, suggesting increased amount of cell debris, and medium acidification was obvious within 1 day of all subsequent medium changes.

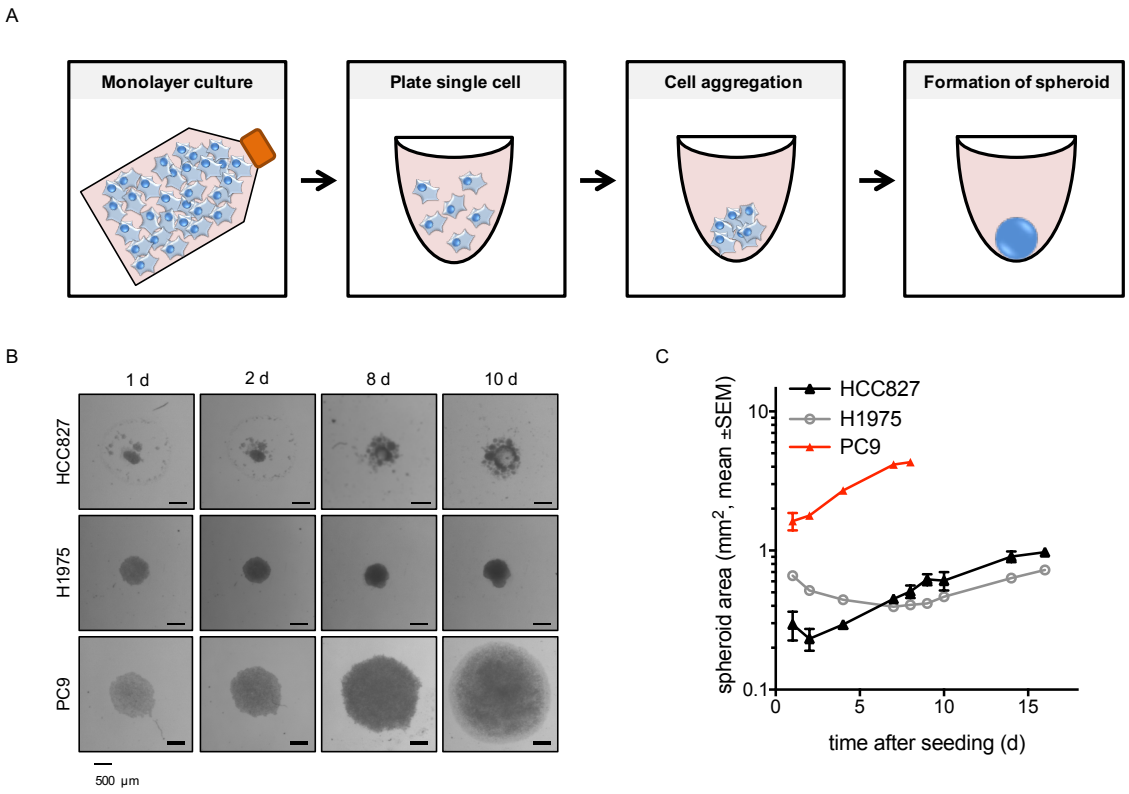


Figure 3-9: Spheroid formation in EGFR M+ NSCLC cell lines

A: Schematic of spheroid production. B: Representative images of spheroid formation of HCC827, H1975 and PC9 on different days after seeding of 10,000 cells/well. Images were acquired on GelCount scanner and used for quantification in (C). C: Spheroid growth over time represented as area quantified on the GelCount. Data represent mean and SEM of 3 spheroids per group. Quantification of spheroid size of PC9 was stopped at day 8, before spheroids showed signs of cellular debris (B, d10).

To assess the effects of AZD9291 exposure on spheroid growth, signalling and integrity, H1975 cells were seeded to form spheroids and treatment started on day 10 after seeding (as this was past the point of maximum compaction on day 7). Spheroids were treated with AZD9291 and at different time points after treatment start either collected for FFPE analysis or lysed for western blotting.

Comparison of cell lysates from 3D spheroids and cells cultured in 2D revealed differences in levels of a number of antigens (Figure 3-10). Untreated spheroids showed higher levels of pEGFR and pS6 rp but not pAKT or pERK compared to 2D cultured cells. Western blotting also revealed lower levels of cyclin D1 (a member of the family of G_1 cyclins, important for G_1 to S cell cycle transition) and ETS-1 (a

transcription factor and key effector of ERK signalling) (Plotnik, Budka et al. 2014) expression in 3D culture, although the significance of this is not known. PARP1 was expressed as a single, well-defined band in 3D compared to 2D, perhaps suggesting a lower level of post-translational modifications. Following treatment with 10 nM or 100 nM AZD9291, reduction in levels of pEGFR and some downstream targets was more marked in 3D compared to 2D, as assessed at the 24 h time point. Levels of cleaved PARP and γH2A.X, as markers of apoptosis and DNA damage, increased more in 3D spheroids treated with 100 nM compared to the corresponding 2D condition. In the 3D model, changes induced by AZD9291 at 10 or 100 nM were generally more apparent at treatment times longer than 4 h, although a low dose of 1 nM AZD9291 did not have any clear effects up to 96 h.

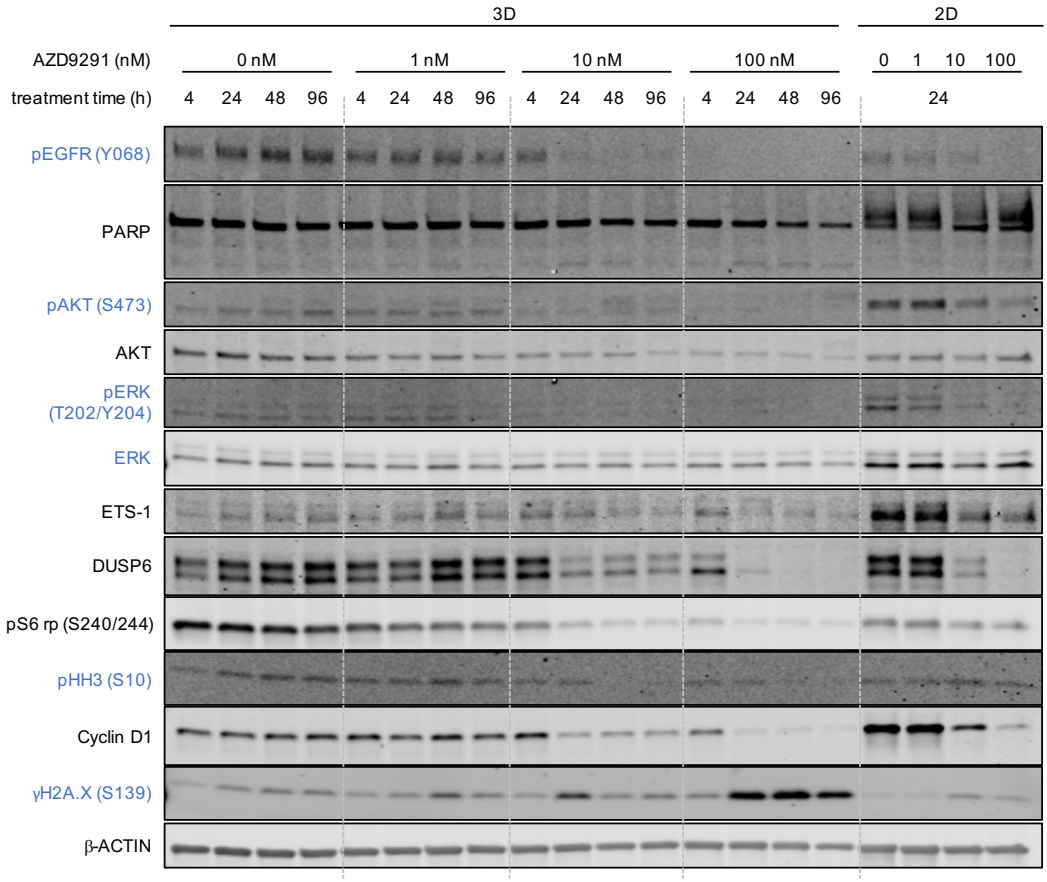


Figure 3-10: AZD9291 treatment leads to a dose- and time-dependent reduction in EGFR signalling in H1975 cells grown as 3D spheroids

Western blot analysis of a dose-dependent time course of H1975 cells grown as 3D spheroids (9 spheroids per condition) and in 2D culture. Treatment times (4-96 h) and doses (1-100 nM) are indicated above, treatment was started on day 10 or 2 after seeding for 3D and 2D conditions, respectively. β-actin was used as a loading control and antigens of the same colour writing were detected on the same membrane.

To examine spheroid size and integrity in more detail, H&E staining was performed on 4 µm sections of FFPE spheroids (Figure 3-11 A). AZD9291 treated spheroids appeared to have an increased number of lacunae after drug treatment. These lacunae (i.e unfilled spaces, gaps) suggest that cells might have died through apoptosis or other cell death mechanisms. Indeed, many of the lacunae showed evidence of cellular fragments. The decrease in spheroid size was dose and time dependent, as shown in (Figure 3-11 B). On average spheroids treated with 10 nM or 100 nM AZD9291 showed marked shrinkage compared to spheroids treated with

1 nM which did not show shrinkage compared to the untreated control over the time course studied.

Heterogeneity of signalling responses across the spheroid was assessed via staining for selected antigens on 4 μm sections using immunofluorescence (IF). Observed reductions in levels of pEGFR (Figure 3-11 C) and pS6 rp (Figure 3-11 D) were in line with results from western blotting experiments described above. Of interest is that the reduction in pEGFR signal was more complete and homogeneous than for pS6 rp. Even after 48 h treatment with 100 nM AZD9291, spheroids showed areas of positive staining for pS6 rp. Quantification of pHH3 and γH2A.X positive cells (Figure 3-12), confirmed a reduction in number of mitotic and increase in number of apoptotic cells (at 100 nM AZD9291) in a time and dose-dependent manner, in line with the changes observed via western blotting and in spheroid size described above.

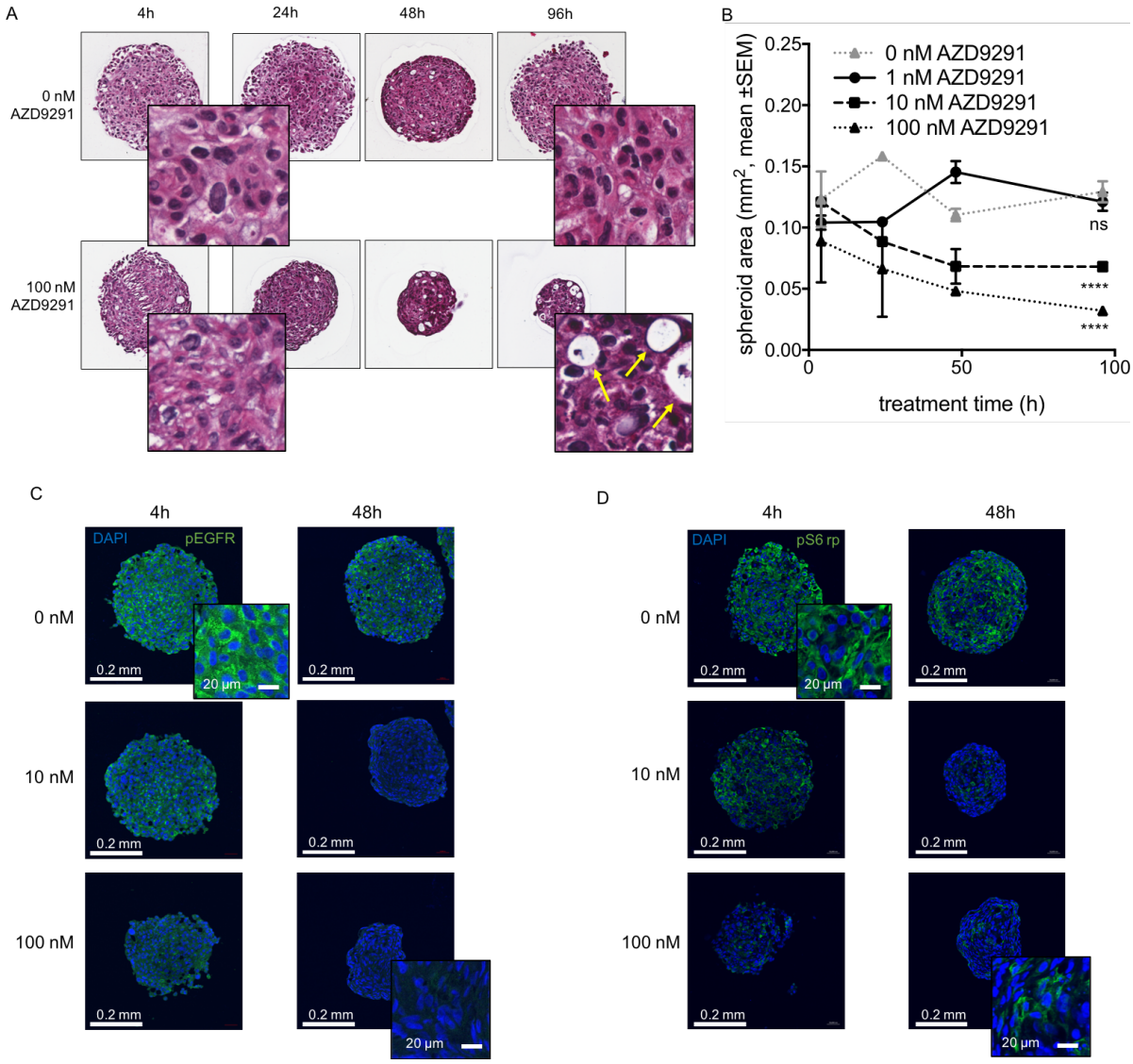


Figure 3-11: Effects of AZD9291 treatment of H1975 3D spheroids assessed in FFPE sections – size and signalling

A: Representative pictures of H&E staining of H1975 spheroids treated with DMSO or 100 nM AZD9291 for up to 96 h. Spheroid integrity is significantly compromised after 48h of treatment with AZD9291, showing increased number of gaps (lacunae, yellow arrows) usually with evident cellular fragments. B: Spheroid area measured on H&E stained spheroids. Data represent the mean and SEM of the maximum area of each of three spheroids per treatment group. Statistical significance of differences between treatments and untreated controls at the 96 h timepoint are indicated with **** for p≤0.0001 or ns for p>0.05. C/D: Representative images of spheroids stained for pEGFR (C) and pS6 rp (D) at 4 h and 48 h after treatment with AZD9291. Staining was performed on at least 3 independent spheroids and 3 sections per spheroid and DNA is stained with DAPI.

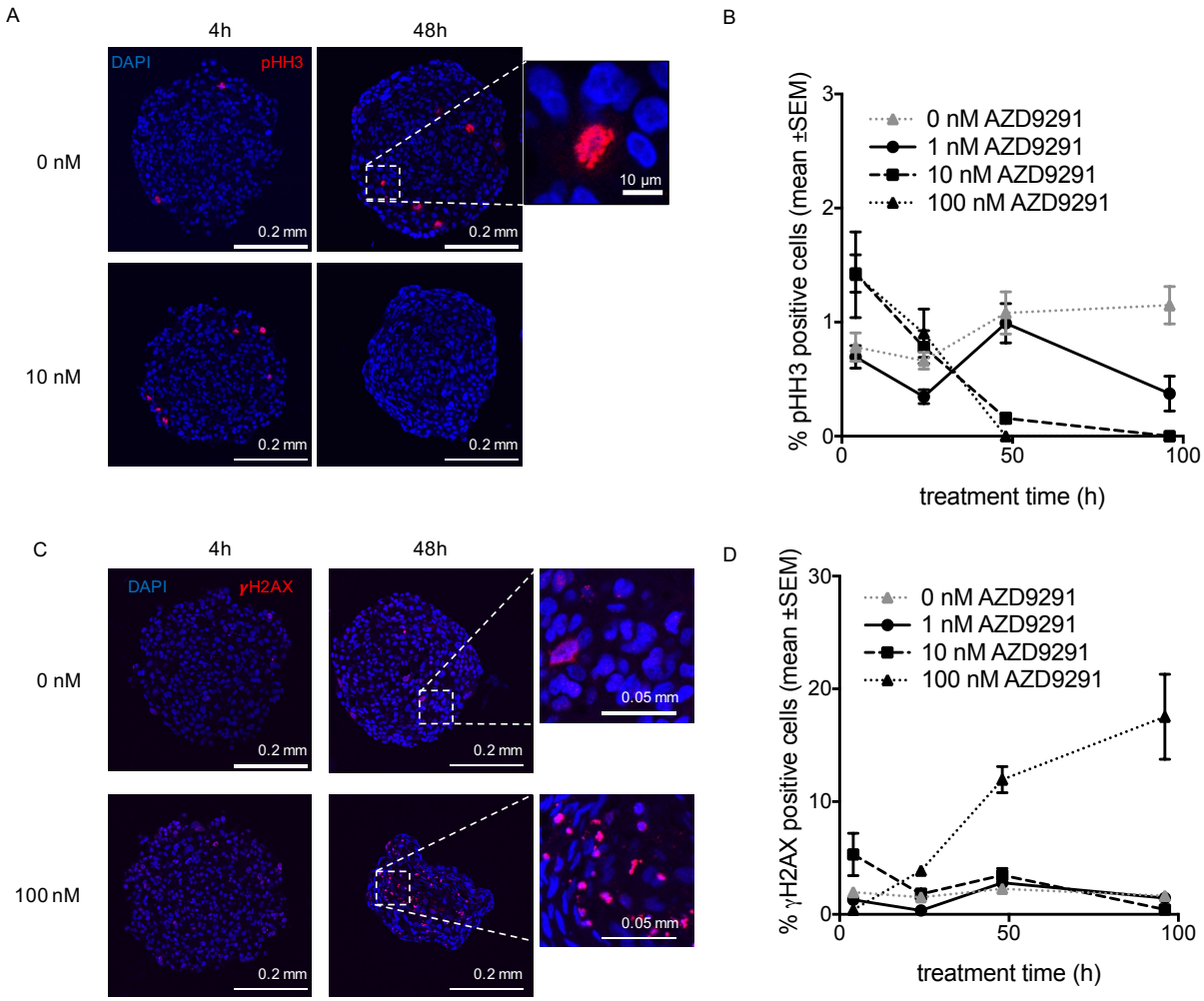


Figure 3-12 Effects of AZD9291 treatment of H1975 3D spheroids assessed in FFPE sections – mitosis and apoptosis

Representative spheroids stained for pHH3 and γH2A.X after AZD9291 treatment are shown in (A) and (C), respectively. Quantification of pHH3 staining is shown in (B) and in (D) for γH2A.X. Data represents the mean % of positive cells and SEM of all sections for three spheroids per treatment group. DNA is stained with DAPI.

To test the ability of HCC827 and H1975 spheroids to regrow under AZD9291 treatment, cells were seeded for spheroid formation as described previously and treated with different doses of AZD9291 for 28 days (Figure 3-13). For H1975, 10 nM AZD9291 was sufficient to initially reduce spheroid size but allow for the emergence of resistance under long-term treatment (Figure 3-13 B). HCC827 spheroids were very sensitive to AZD9291 treatment, and did not regrow over the duration of the experiment, even at doses as low as 1 nM (Figure 3-13 A). H1975 spheroid growth was still inhibited to some extent by EGFR-TKI treatment even at the point of

regrowth since spheroid growth was increased after AZD9291 withdrawal compared with continued AZD9291 treatment (Figure 3-13 C).

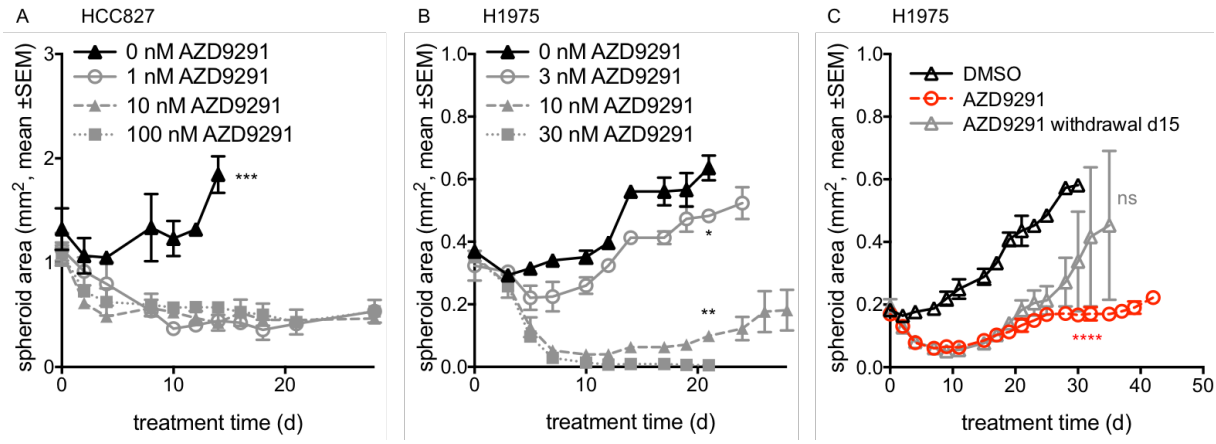


Figure 3-13: H1975 but not HCC827 spheroids regrow after initial shrinkage under AZD9291 treatment.
Spheroids of HCC827 (A) and H1975 (B/C) cells were seeded as described previously and treated with the indicated doses on day 10 after seeding. Medium was exchanged every 3-7 days. Spheroids were imaged with the GelCount and sizes determined using the Gelcount software. Statistical significance of the difference in spheroid growth on d14 (A), d21 (B) or d30 (C) between untreated spheroids and spheroids treated with 1 nM (A), 3 nM/10 nM (B) or continued/discontinued treatment (C) is indicated with **** p≤0.0001, *** p≤0.001, ** p≤0.01, * p≤0.05, ns p>0.05.

To examine changes in spheroid size and signalling under long-term AZD9291 treatment, H1975 spheroids were treated with 10 nM AZD9291 and collected as FFPE samples or for western blot analysis for up to 76 days (Figure 3-14).

Spheroid size was initially reduced during AZD9291 treatment but increased steadily after day 18 (Figure 3-14). With increasing treatment time, heterogeneity in spheroid size increased markedly. On retrospective examination of individual well data at day 76, it was apparent that there were two distinct categories of spheroid based on their growth patterns – (i) those with no evidence of regrowth, and (ii) those with clear regrowth (Figure 3-14 B/C). The mean size of 12 out of 20 spheroids ('regrowth' group) increased after day 8 of treatment whereas the mean size of the remaining 8 spheroids ('no regrowth' group) decreased further and did not show regrowth until the end of the experiment (Figure 3-14 B/C).

Western blotting analysis showed that in contrast to results from 2D experiments, levels of pEGFR were reduced initially but increased at day 8 of treatment. Comparison of lysates at the end of the experiments showed increased pEGFR levels in the 'regrowth' but not the 'no regrowth' group. Similar to experiments in 2D, levels of pAKT, pERK and pS6 rp showed an initial decrease followed by re-engagement of signalling and pHH3 levels increased after day 12 (Figure 3-14 A). Interestingly, levels of total EGFR increased with increasing spheroid size in both treatment groups and CAIX (carbonic anhydrase 9, a marker of hypoxia) protein levels were increased in larger spheroids (Figure 3-14).

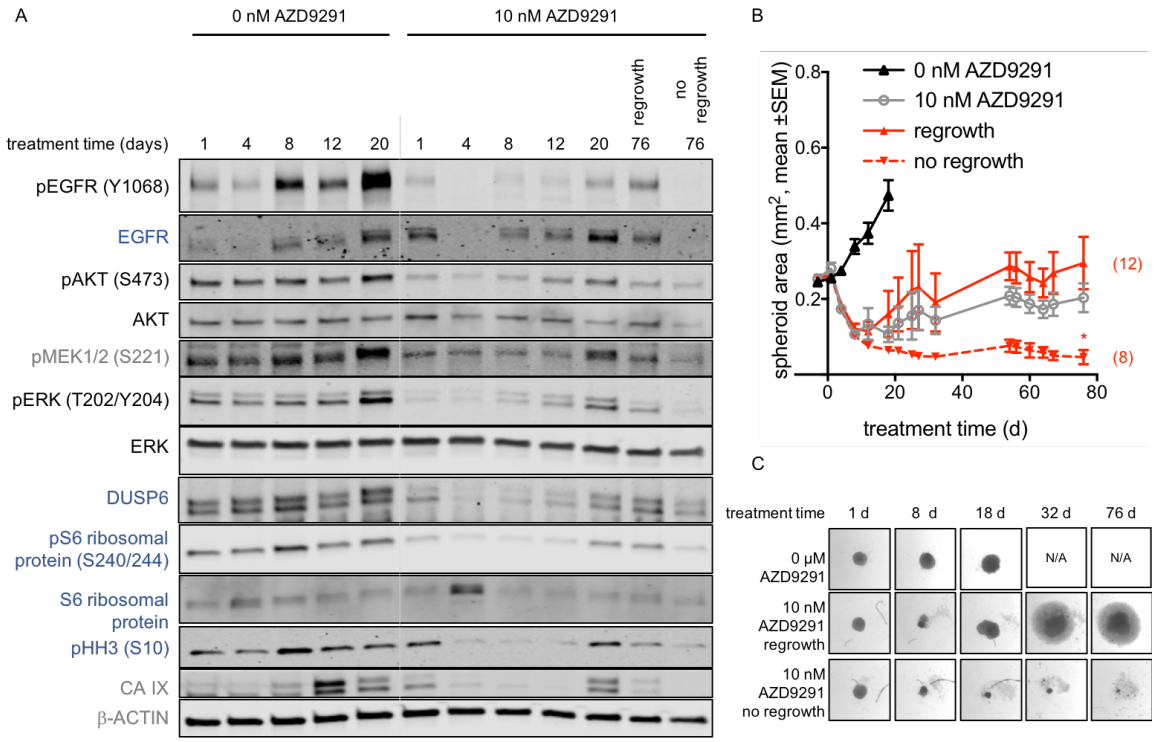


Figure 3-14: Re-engagement of signalling and regrowth of H1975 spheroids under long-term AZD9291 treatment

A: Western blot analysis of H1975 spheroids (DMSO/AZD9291 treatment: 8/14 spheroids per time point) under DMSO or AZD9291 treatment. Collection of spheroids for western blotting on day 76 was done in two groups, those that had regrown and those that had not regrown. Lysates from earlier time were for the whole group independent of spheroid growth. Untreated spheroids were not analysed after day 20. β-actin was used as a loading control and antigens of the same colour writing were detected on the same membrane. B: Quantification of spheroid size over time. Spheroids were imaged with the GelCount and sizes determined using the Gelcount software. Red lines represent spheroids of the AZD9291 treated group, that were retrospectively grouped as 'regrowth' or 'no regrowth' for additional analysis, the number in brackets indicates the number of spheroids per group. Statistical significance of the difference in spheroid size between the regrowth and no regrowth group on d76 is indicated with * p≤0.05. C: Pictures of one representative spheroid for each group over time. The size of the inner dark area only was determined in cases where cell debris (grey) accumulated around the spheroid.

Equivalent experiments in HCC827 confirmed that HCC827 spheroids were more sensitive to AZD9291 treatment than H1975 spheroids but it was not possible to analyse long-term treated samples because spheroid integrity was lost under treatment and there was insufficient material for western blotting analysis at late time points due to the marked spheroid shrinkage (Figure S 2).

To confirm changes observed in western blotting and further investigate the link between changes and spheroid fate, a spheroid microarray was created containing all the spheroid FFPE samples and sections were analysed using DAB based staining.

Staining for pEGFR, pAKT, pERK, pS6 rp, pHH3 and cleaved caspase 3 (CC3) (pEGFR, pS6 rp and pHH3 see Figure 3-15, data for pAKT, pERK, CC3, CAIX and EGFR see Figure S 3) was in line with the initial decrease and subsequent re-engagement of AKT/ERK signalling observed in western blotting experiments. This staining was also consistent with the induction of apoptosis after treatment, inferred from spheroid shrinkage. In addition, comparison of staining in small (‘no-regrowth’) and large (‘regrowth’) spheroids showed that re-engagement of AKT/MEK signalling was more pronounced in larger spheroids. Heterogeneity in spheroid size was particularly apparent after a treatment time of more than 8 days. This is in line with increased levels of pEGFR and downstream targets in ‘regrowth’ and ‘no regrowth’ samples on day 76 analysed by western blotting, as described above. IHC staining for EGFR and CAIX on serial sections did not show increased EGFR levels in hypoxic areas, although EGFR signal was very weak.

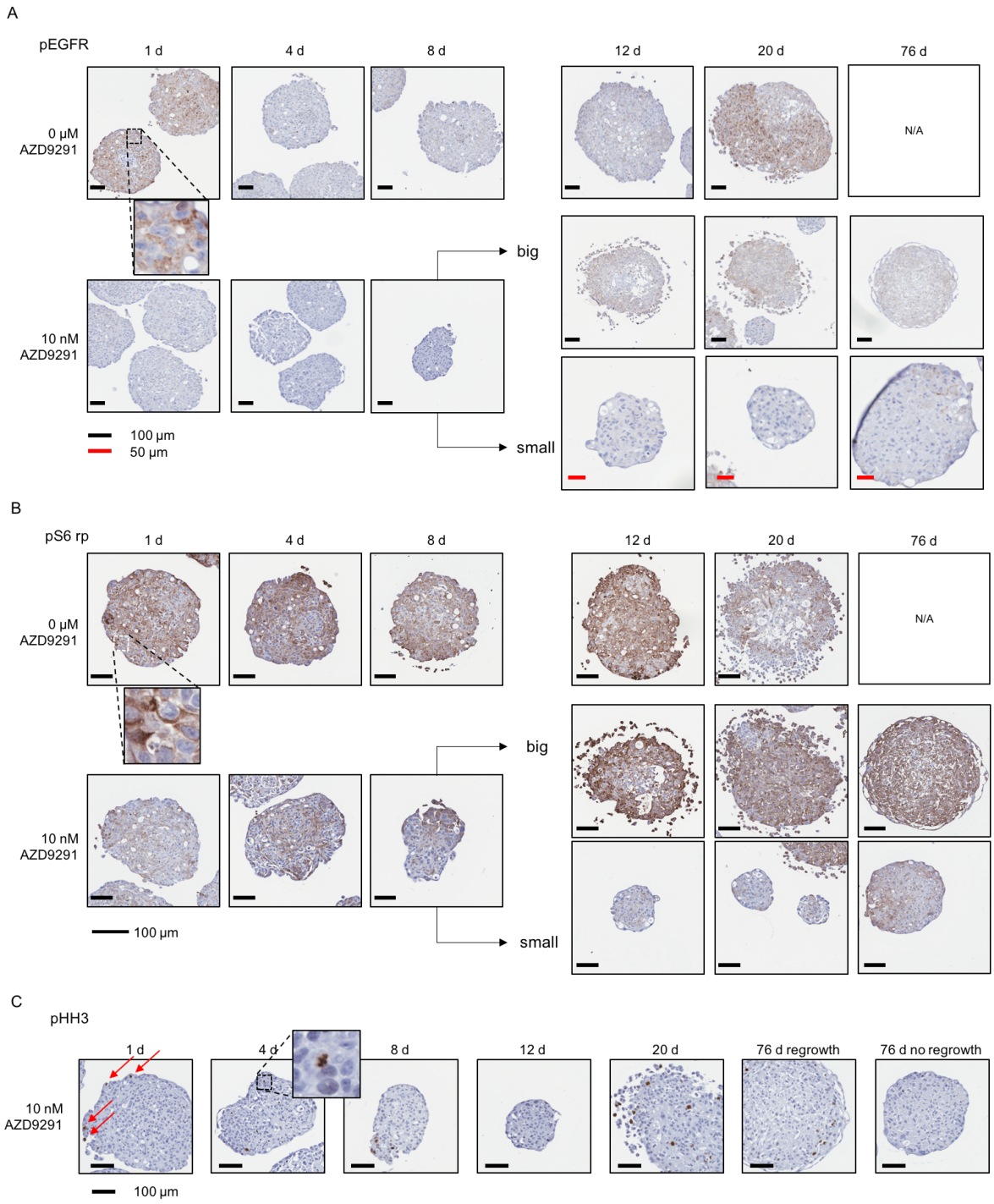


Figure 3-15: EGFR signalling and proliferation is reduced in H1975 spheroids under AZD9291 treatment but a subset of spheroids reengages signalling and grows under long-term treatment

DAB-based visualisation of pEGFR (A), pS6 rp (B) and pHH3 (C) in H1975 spheroids. Images show representative spheroids for each time point of 4/6 spheroids per time point for the untreated/treated group. Nuclei were counterstained with haematoxylin.

3.5 Effects of EGFR-inhibition in *in vivo* models

To extend our observations in 2D and 3D spheroids to more advanced models, we investigated the effect of short- and long-term AZD9291 treatment in subcutaneous and orthotopic xenografts. In these models, human tumour cells grow in the context of a stroma that includes fibroblasts, innate immune cells and blood vessels, either in a heterotopic tissue (subcutaneous) or tissue-of-origin (orthotopic) setting. The latter is considered to represent a more relevant microenvironment (Killion, Radinsky et al. 1998). Importantly, the drugs (EGFR-TKIs) are delivered through the blood supply, rather than directly applied to the tumour cells, which allows for dynamic changes in drug levels which is relevant to the clinical situation.

Treatment with AZD9291 at 1 mg/kg for as little as 1 h led to a decrease in levels of pEGFR and an increase of EGFR levels in an established subcutaneous HCC827 tumour (Figure 3-16 A). Sustained treatment with AZD9291 for up to 12 days led to a shrinkage of established tumours in an orthotopic H1975 xenograft model (Figure 3-16 B). These effects at clinically relevant doses of AZD9291 are consistent with the decreased signalling and reduced cell proliferation as well as increased cell death after AZD9291 treatment observed in 2D and 3D spheroids and results by other groups (Cross, Ashton et al. 2014).

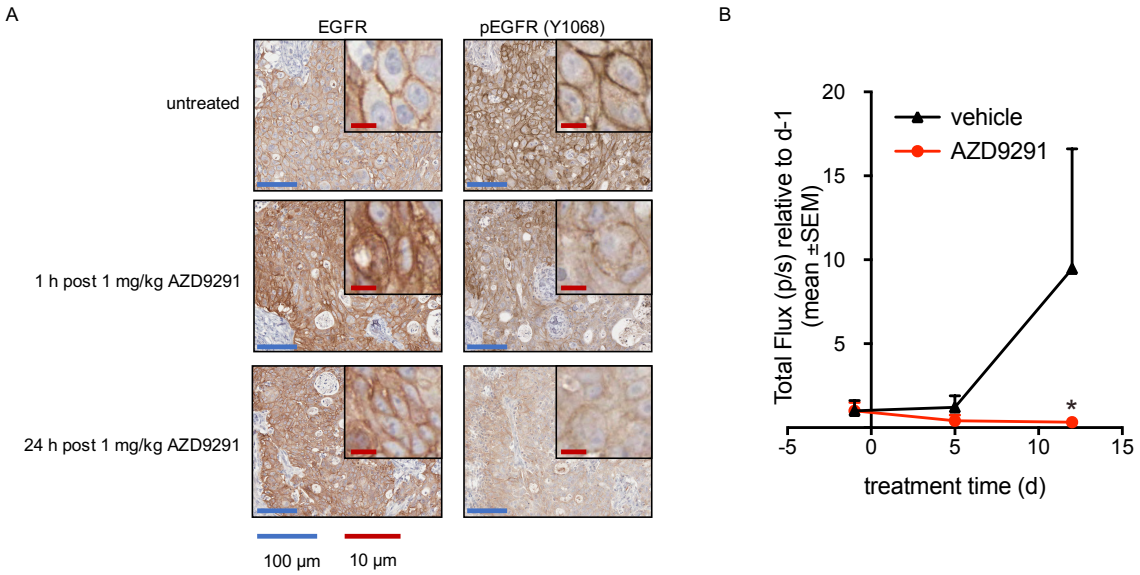


Figure 3-16: AZD9291 treatment reduces of pEGFR levels *in vivo* and shrinks orthotopic lung tumours

A: IHC staining for EGFR and pEGFR in tumours of mice at indicated times after treatment with 1 mg/kg AZD9291. Brown staining indicates the presence of the antigen, nuclei are counterstained in blue with haematoxylin. B: Luciferase activity of luciferase expressing H1975 cells in the orthotopic lung model was measured by IVIS and the maximum flux determined for each animal at indicated time points. Data represents the mean and SEM of 4 animals per group. Animals were treated daily for 12 days with 2.5 mg/kg/d p.o. AZD9291. Statistical significance of the difference in mean total flux between the vehicle and AZD9291 group on d12 is indicated with * p≤0.05.

To assess the effect of sustained EGFR-TKI treatment *in vivo*, mice bearing established (150 mm^3) subcutaneous xenograft tumours of PC9 or HCC827 cells were treated with gefitinib or AZD9291 over a period of 42 days (Figure 3-17 A). Tumours of both cell lines were sensitive to EGFR-TKI treatment, reflected by an initial reduction and then stabilisation of tumour size (neither growth nor further shrinkage). PC9 tumours showed greater regrowth after treatment breaks than HCC827 tumours and both tumour models showed regrowth during the final treatment break before sample collection (Figure 3-17 B and C).

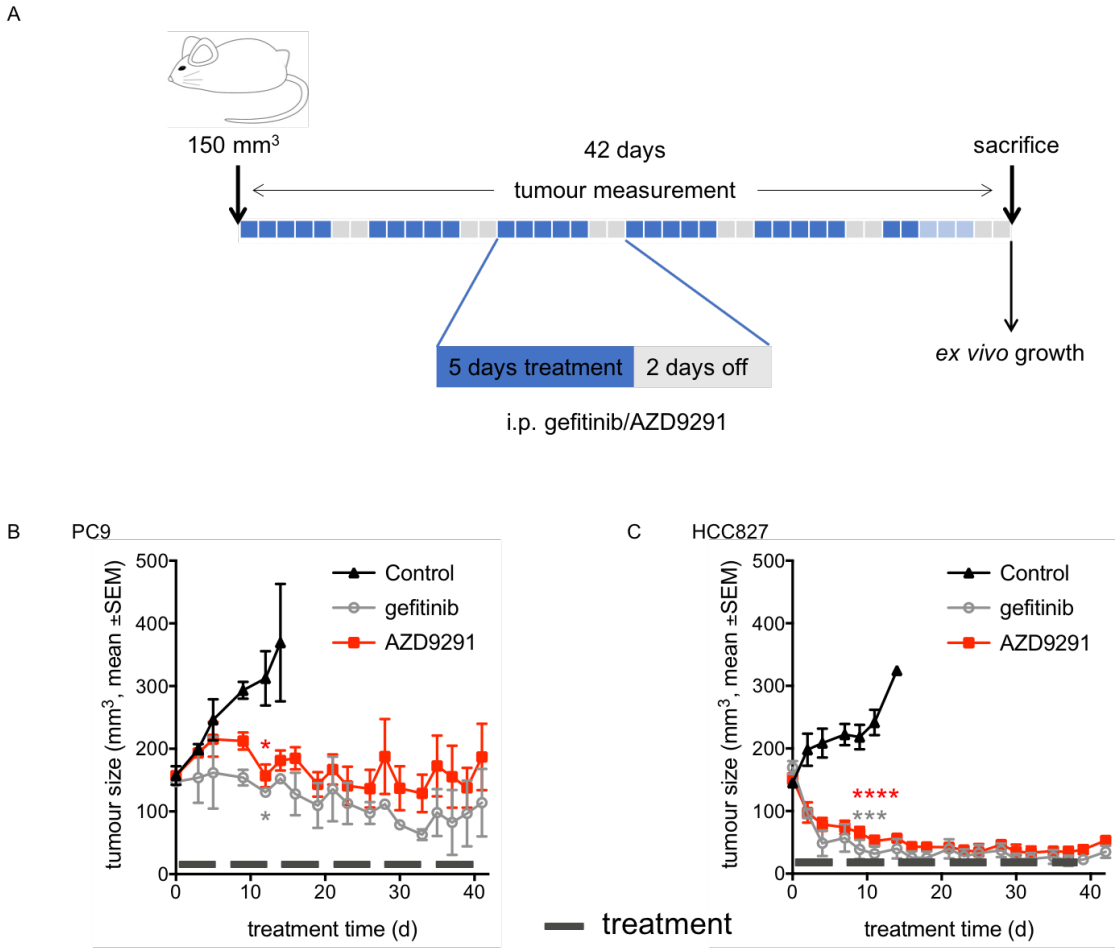


Figure 3-17: Long-term treatment with EGFR-TKIs shrinks but does not eradicate established subcutaneous PC9 and HCC827 tumours.

A: PC9 and HCC827 cells were grown as subcutaneous xenograft tumours in Balb/C nude mice. Tumour growth was assessed regularly before collection of the tumour 42 days after treatment start for cell isolation and FFPE processing. Then tumours reached 150 mm^3, treatment was given in 6 cycles of 5 days on/2 days off treatment (last treatment cycle in HCC827 was modified, 2 days on treatment, followed by no drug for 5 days). For PC9 tumours, during the first two weeks of dosing, EGFR-TKIs were dose-escalated (5-20 mg/kg/d (gefitinib) or 1-4 mg/kg/d (AZD9291)) until tumour shrinkage was apparent. Subsequently doses were maintained at 20 and 4 mg/kg/d for gefitinib (2 animals) and AZD9291 (3 animals), respectively. Mice bearing HCC827 tumours were treated with 5 mg/kg/d or 1 mg/kg/d of gefitinib (4 animals) or AZD9291 (4 animals), respectively. Tumour size is reported over time for each treatment group in PC9 (B) and HCC827 (C). Grey bars indicate days of treatment. Statistical significance of differences on day 12/11 (PC9/HCC827, before second treatment break) between treatments and untreated controls (2/3 animals for PC9/HCC827) are indicated with * for p≤0.05, *** for p≤0.001 and **** for p≤0.0001.

To confirm that tumours contained proliferating cells, we analysed FFPE samples by H&E staining and IHC for pHH3. Staining indicated the presence of proliferative (pHH3 positive) tumour cells in sections from all treatment groups in both cell lines (Figure 3-18 A and B). At the time of sacrifice, cells were also isolated from the tumours and cultured *ex vivo* (Figure 3-18 C). Experiments showed increased IC_{50}s for AZD9291 and/or gefitinib in 2D cell culture *ex vivo* for PC9 from EGFR-TKI

treated animals compared to cells from untreated animals (Figure 3-18 D), although we could not show this for *ex vivo* HCC827 cells (data not shown). However, long-term exposure of *ex vivo* cultured HCC827, suggested a greater potential for resistance to high doses of AZD9291 in cells from treated animals compared to untreated animals (Figure 3-18 E).

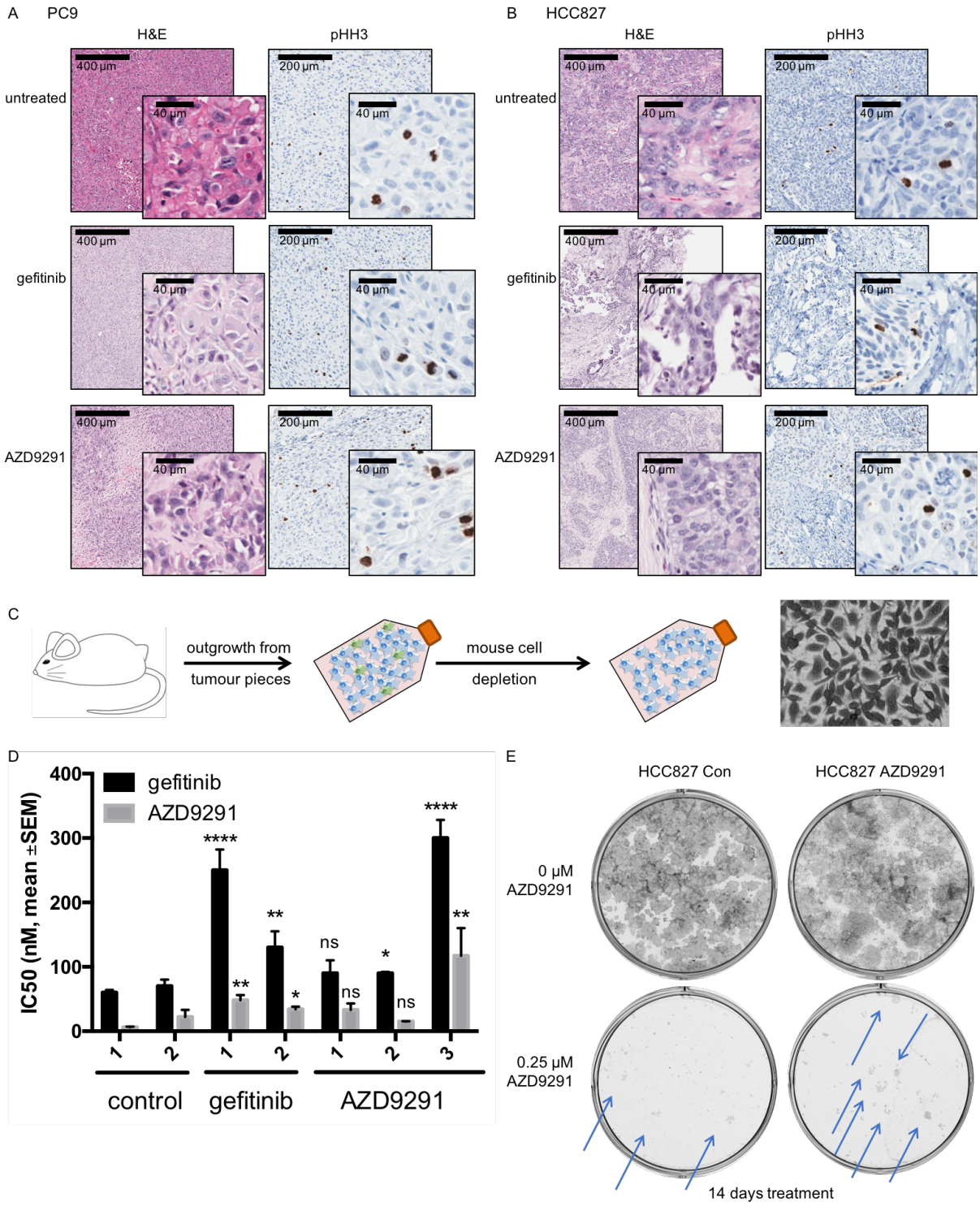


Figure 3-18: Subcutaneous tumours of PC9 and HCC827 cells are viable after long-term treatment with gefitinib and AZD9291 and might be enriched for EGFR-TKI resistant cells.

H&E and pHH3 staining performed on subcutaneously grown tumours of PC9 (A) and HCC827 (B) cells at the end of experiment. Nuclei are stained in blue with haematoxylin. C: Schematic about isolation of cells for *ex vivo* culture. HCC827 but not PC9 cells were depleted of mouse cells using a Miltenyi Biotech mouse cell depletion kit. D: IC_{50} values of ex vivo cultured PC9 cells as determined in 2D proliferation assays. Values represent the mean and SEM of one experiment performed in technical triplicates. Statistical significance of differences between mean IC50 values for cells from untreated and treated animals are indicated with * for p≤0.05, ** for p≤0.01, **** for p≤0.0001, ns for p>0.05. E: Crystal violet staining of ex vivo cultured HCC827 cells from an untreated (left) and a treated (right) animal after exposure to DMSO or AZD9291 for 14 days.

To further confirm the ability of EGFR M+ NSCLC cells to regrow *in vivo* under EGFR-TKI treatment, we used a potentially more relevant orthotopic lung cancer model. Orthototopic H1975 tumours were reduced in size under AZD9291 treatment though 1 out of 3 mice showed subsequent tumour regrowth during the 42-day treatment period (Figure 3-19 A/C). H&E staining confirmed the presence of proliferating tumour cells (mitotic figures on H&E sections) (Figure 3-19 B).

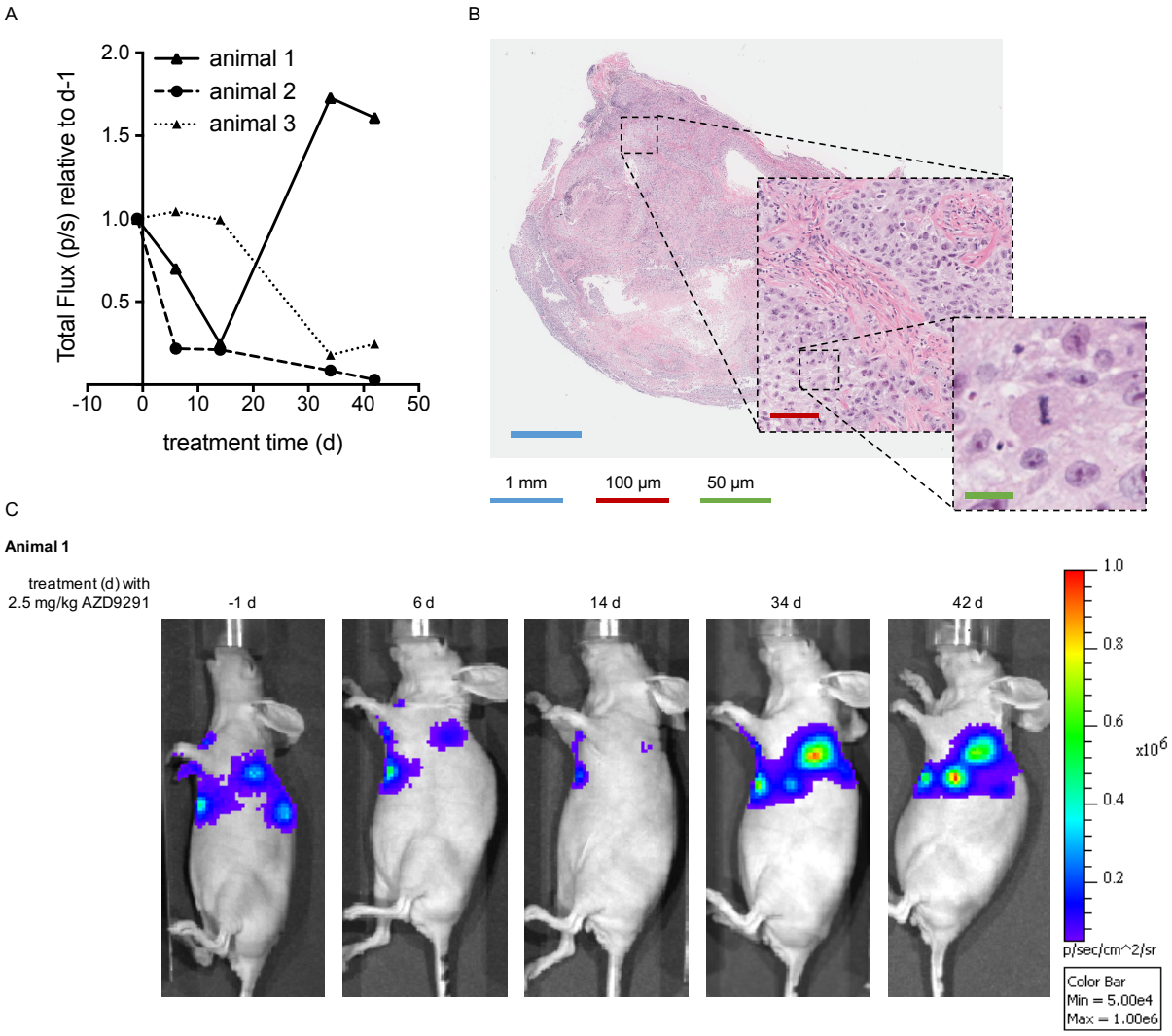


Figure 3-19: Orthotopic H1975 lung tumours can regrow under long-term treatment with AZD9291

Mice bearing luciferase expressing H1975 orthotopic lung tumours were treated with 2.5 mg/kg/d p.o. once daily for 6 cycles of 5 days, followed by 2 days treatment break. Tumour burden was assessed using luciferase activity of luciferase expression tumour cells as measured on the IVIS and the maximum total flux per animal per imaging session is reported in (A). Values are relative to d-1 for each animal. B: H&E staining of tumour from animal 1 on day 42 of treatment. C: Images of animal 1 at indicated days after treatment start, showing radiance at the time of maximum total flux. The scale bar indicates the radiance colour coding.

However, initial experiments do not indicate greater IC_{50} values for AZD9291 for *ex vivo* cultured cells from animal 1 (Figure 3-19) compared with parental H1975 cells when assessed in a standard 2D proliferation assay (data not shown).

3.6 Discussion response to EGFR-TKIs 3D/*in vivo*

To our knowledge, this is the first published study on long-term treatment of EGFR M+ NSCLC cell line spheroids with AZD9291. We show that this might be of some relevance, as we observe marked differences in signalling in 3D spheroids of H1975 cells compared to 2D, with lower levels of phosphorylated AKT and ERK but increased phosphorylation of EGFR and S6 rp in 3D compared to 2D, in line with findings by others (in a number of cell lines of different origins (Ekert, Johnson et al. 2014, Riedl, Schlederer et al. 2016)). Furthermore, we demonstrated that H1975 cells are more sensitive to induction of apoptosis under AZD9291 treatment in 3D compared to 2D. Treatment with doses as low as 10 nM led to a marked shrinkage in spheroid size as opposed to a response dominated by cell survival in 2D at doses as high as 1 μM. This initial sensitive phase was marked by reduction in signalling and induction of apoptosis as seen in 2D. However, a subset of spheroids showed re-engagement of signalling under sustained treatment, which in contrast to 2D experiments, included increased EGFR autophosphorylation. The heterogeneity in re-engagement of signalling was also reflected in spheroid regrowth, showing a distinct ‘regrowth’ and a ‘no regrowth’ population.

The differences in sensitivity might stem from model-specific signalling (e.g. differences in anti anoikis signalling of 2D vs 3D environment) (Paoli, Giannoni et al. 2013, Suzuki, Ito et al. 2017). It is unclear what role the re-engagement of EGFR signalling and up-regulation of EGFR protein levels has in resistance in 3D.

Published studies on response of spheroids of EGFR M+ NSCLC cells to EGFR inhibition show spheroid shrinkage upon treatment but do not document the emergence of resistance (Suzuki, Ito et al. 2017).

We also established subcutaneous and orthotopic xenograft resistance models. We observed initial tumour shrinkage and eventual regrowth under treatment with gefitinib or AZD9291, using PC9, HCC827 or H1975 cells, representing models of stable (PC9) or responsive (HCC827, H1975) disease. *Ex vivo* PC9 cells isolated from tumours of treated mice showed increased IC_{50}s for EGFR-TKIs compared to cells from untreated animals. Preliminary experiments further suggest increased potential for emergence of resistance in *ex vivo* cultured HCC827 cells from EGFR-TKI treated animals compared to those from untreated mice. To our knowledge there is no published study documenting the possible emergence of resistance in lung orthotopic models of established EGFR M+ NSCLC cell lines or on growing cells from comparable *in vivo* experiments *ex vivo* after emergence of resistance. Other groups have observed EGFR-TKI resistance *in vivo*, however mainly after significantly longer treatment times in xenograft tumours of cell lines (Cross, Ashton et al. 2014, Tricker, Xu et al. 2015, Chabon, Simmons et al. 2016, Emdal, Dittmann et al. 2017), patient derived xenograft models (McKenzie, Cranston et al. 2012, Mckenzie, Cranston et al. 2013) or in transgenic EGFR-induced lung adenocarcinoma mouse models (Politi, Fan et al. 2010, Ercan, Xu et al. 2012, Tricker, Xu et al. 2015).

Concluding, we document that responses to EGFR-TKI treatment in spheroids and *in vivo* are consistent with our findings in 2D but both models show a high degree of variability (Figure 3-20) and further experiments would be needed to characterise the more heterogeneous acquisition of resistance (Emdal, Dittmann et al. 2017).

Overall, our findings lend support to the hypothesis that there are distinct phases in the response of EGFR M+ NSCLC cells to EGFR-TKI treatment, as summarised in Figure 3-20. Therefore, we next used the 2D system to generate and characterise EGFR-TKI resistant cell lines.

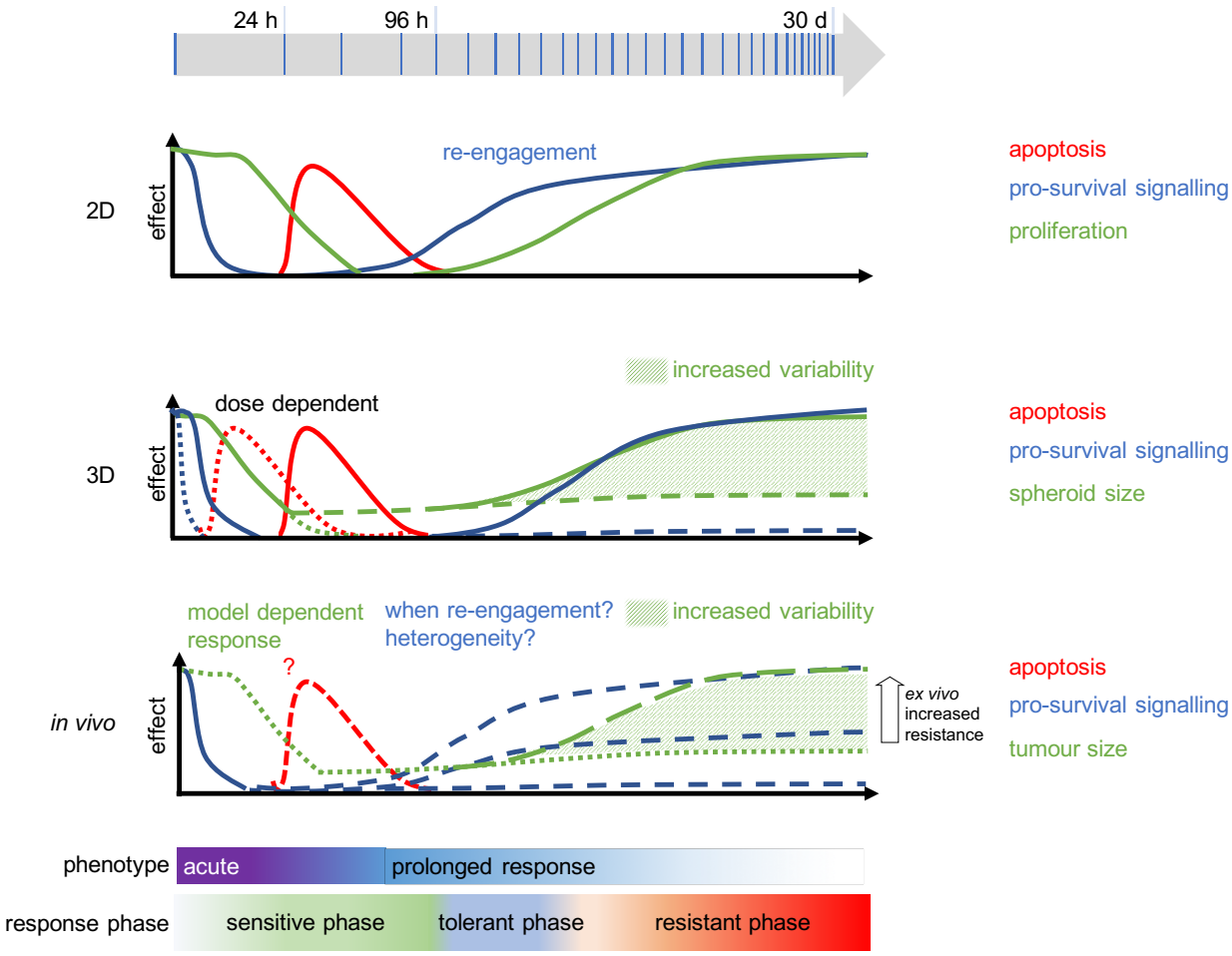


Figure 3-20: Comparison of findings on response and resistance to EGFR-TKIs in 2D, 3D and *in vivo*

Schematic summary of findings in the three model systems used in this study. Processes are colour-coded and indicated on the right. Responses in 3D are dose-dependent, as indicated by dotted lines for higher doses. Growth response *in vivo* is model-dependent and variable, as indicated with dotted lines and dashed lines, respectively. Increased variability between spheroids/animals in 3D/*in vivo* is indicated with green shading.

4 Generation and characterisation of EGFR-TKI resistant EGFR M+ NSCLC cells

Despite the marked responses to EGFR-TKI therapies in the clinic, few patients with metastatic disease are alive 5 years since tumours resume growth within 12-18 months of starting treatment as resistance emerges through secondary on-target EGFR mutations (e.g. T790M, C797S), or pathway activating mutations (e.g. NRAS Q61R). Secondary EGFR T790M mutations account for about 50% of cases of resistance to 1st generation EGFR-TKIs, and although it has not yet been accurately estimated, it seems likely that about 50% of the cases of resistance to 3rd generation EGFR-TKIs will be associated with secondary mutations in EGFR C797S or NRAS (Sequist, Waltman et al. 2011, Costa and Kobayashi 2015, Thress, Paweletz et al. 2015). Therapeutic options for these patients are either available (e.g. MEK inhibitors for NRAS mutant tumours, phase I clinical trial: NCT02143466), or under preclinical investigation (4th generation EGFR-TKIs, which overcome resistance due to EGFR C797S mutation (Jia, Yun et al. 2016)). It is to be expected, however, that with the introduction of 4th generation EGFR-TKIs, other mechanisms of resistance will dominate the picture. Even now, a large proportion of patients have tumours that become resistant to EGFR-TKI therapy without secondary activating mutations in either EGFR or downstream/parallel pathways, and no targeted therapeutic options are then available (Sequist, Waltman et al. 2011, Chabon, Simmons et al. 2016). Since a greater understanding of resistance mechanisms that overcome or bypass tumour cells' dependency on EGFR signalling may lead to the identification of novel therapeutic approaches, we considered the characterisation of such resistance mechanisms to be our priority.

Work presented in the previous chapter documented the major signalling changes which take place throughout the emergence of resistance to EGFR-TKIs. This chapter will discuss the generation of EGFR-TKI-resistant cell lines and their characterisation, aiming to identify mechanisms of resistance as well as common characteristics between different resistant lines. Subsequently a compound screen is performed to identify acquired targetable vulnerabilities and to select combination treatments for overcoming resistance.

4.1 Generation of EGFR-TKI resistant cell lines *in vitro*

Following experience from previous long-term treatment experiments, we knew that generation of resistant cells could be achieved by exposing EGFR-TKI-sensitive cell lines to high doses of EGFR-TKIs. PC9, HCC827 and H1975 were exposed to high concentrations (≥100x IC_{50}) of EGFR-TKIs for up to 2 weeks, until resistant clones or cell populations emerged (Figure 4-1 A, Table 4-1 for selection details).

In PC9 cells, gefitinib selection led to the emergence of resistant clones. On average, we detected 3 colonies per $1x10^8$ cells seeded. Pre-treatment of cells with 0.05 μM gefitinib for 16-20 h before seeding led to an increased frequency of formation of colonies at 116 prominent colonies per $1x10^8$ seeded cells. Colonies were formed were tightly packed, and consisted of highly proliferative cells, in contrast to single surviving enlarged cells on the remainder of the plate (Figure 4-1 B). Upcoming experiments are performed a representative colony from gefitinib pre-treated cells, here referred to as **$PC9^{GS}$** (PC9-gefitinib selected).

In contrast to treatment with gefitinib, colonies of proliferating cells were not observed when PC9 cells were treated with 1 μM AZD9291. However, cells survived and

proliferated once the drug was removed for a recovery period of 3 weeks, after which cells proliferated well under treatment with AZD9291. This resistant population is referred to as **PC9^{9291S}** (PC9-AZD9291 selected).

Exposure of HCC827 cells to 1 µM gefitinib led to the survival of a morphologically heterogeneous population of cells (Figure 4-1 B) and a subclone from this population was isolated for further analysis. These cells are referred to as **HCC827^{GS}**.

AZD9291 treatment of H1975 cells (gefitinib-resistant because of the pre-existing T790M mutation) led to the survival of a largely homogeneous population of cells. Compared to parental H1975 cells, these cells were larger, had markedly elongated nuclei and less evident cell protrusions (Figure 4-1 B). This population of AZD9291 selected cells is referred to as **H1975^{9291S}**.

After selection, resistant cells were maintained under continuous exposure to EGFR-TKIs. Inhibitors were added 1 day after plating, at doses indicated in Table 4-1.

Table 4-1: Selection conditions for resistant cell lines generated in this study

resistant cells	selection/maintenance conditions	clone/population
PC9^{GS}	2 µM gefitinib	clone
PC9^{9291S}	1 µM AZD9291 →break 1 µM AZD9291 after recovery	population
HCC827^{GS}	1 µM gefitinib	population, subcloned
H1975^{9291S}	1 µM AZD9291	population

Experiments for isolation of resistant cells were performed at least twice independently, showing the same cell line and compound-specific characteristics of emergence of resistance. Using the same approach, we were also able to generate cell lines from HCC2935 and HCC4006 that were resistant to AZD9291. Both cell

lines showed a pattern of emergence of resistance similar to HCC827 and H1975, where many cells survived drug exposure and reengaged in proliferation. Of note, HCC2935 was more sensitive than HCC4006 and only proliferated once AZD9291 had been removed but was subsequently resistant to AZD9291.

4.2 Characterisation of generated resistant cell lines: degree of resistance and known resistance-conferring mutations

In order to assess the degree of resistance in selected cells, proliferation assays were performed. Results confirmed a >100-fold increase in IC_{50} for compounds used for cell selection (Figure 4-1 C and Table 4-2), indicating robust resistance phenotypes of these cell lines. Additionally, we determined IC_{50}s for other EGFR-TKIs of the 1st, 2nd and 3rd generation. Compared to their corresponding parental lines, all resistant cell lines showed increased IC_{50}s for erlotinib and afatinib, a 1st and a 2nd generation EGFR-TKI, respectively. Resistance to 3rd generation inhibitors AZD9291 and CO-1686 could be observed in HCC827^{GS} but not PC9^{GS}. AZD9291 selected PC9^{9291S} and H1975^{9291S} were cross-resistant to CO-1686. Sensitivity of H1975^{9291S} and H1975 to the AZD9291 active metabolite AZ5104 was assessed and H1975^{9291S} were confirmed to be resistant (see Figure S 4 and Table S 2).

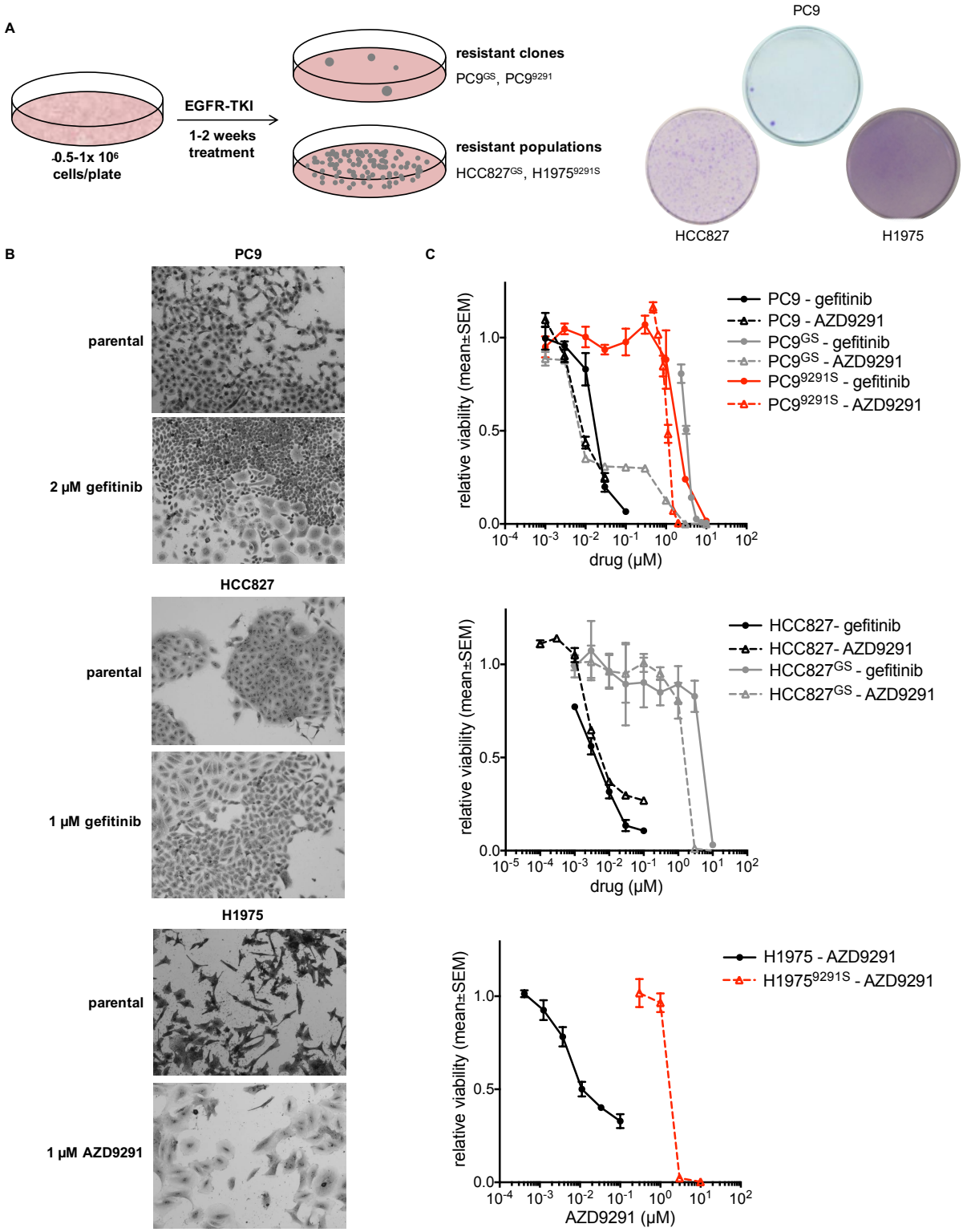


Figure 4-1: EGFR M+ NSCLC cell lines resistant to gefitinib and AZD9291 can be isolated and show a > 100x increase in IC_{50} for selection drugs.

A: Experimental setup for generation of resistant cell lines. Cells were treated with EGFR-TKIs under conditions indicated in Table 4-1 for up to two weeks. Pictures are of representative plates for gefitinib selected PC9 and HCC827 and AZD9291 selected H1975 cells at the end of the selection period. B: Example pictures of methanol fixed, crystal violet stained cells of parental and resistant cell lines from (A). C: Curves for viability of parental and resistant cell lines under gefitinib or AZD9291 treatment. Data are relative to viability of DMSO treated cells for each cell line and are from one representative experiment performed in technical triplicates.

To assess whether EGFR-TKI resistance was retained in the absence EGFR-TKIs, cells were cultured without selection and the IC_{50}s determined repeatedly. Data showed resistance to gefitinib and AZD9291 (IC_{50} > 100 nM) during and at the end of a culturing period of > 90 days. These data demonstrate that the resistance phenotypes are highly stable, and do not require the continued presence of selection.

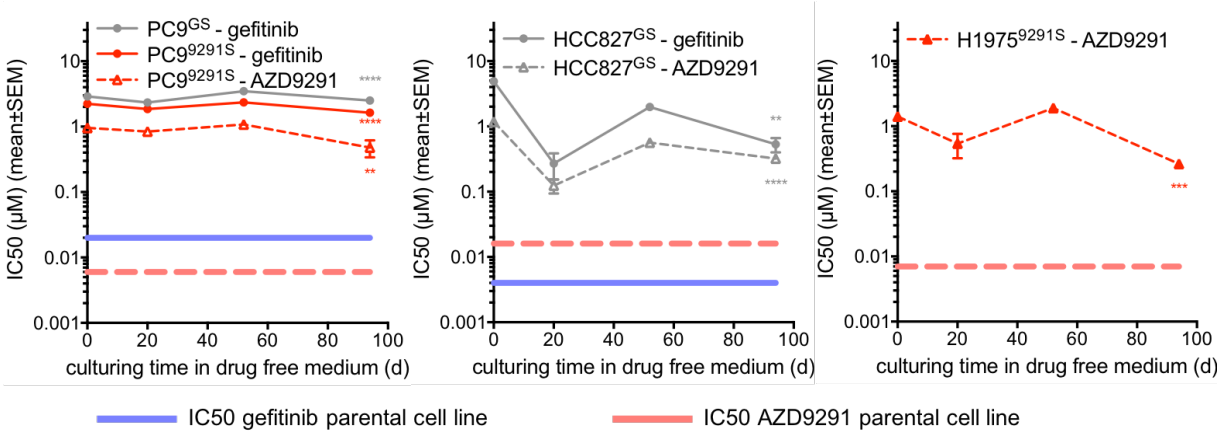


Figure 4-2: Resistance to EGFR-TKIs is maintained even after long-term culturing of cells in the absence of EGFR-TKIs

IC_{50}s for gefitinib and/or AZD9291 determined at various points after drug withdrawal from the culture stock. Data points in grey and red represent cell lines selected in gefitinib and AZD9291, respectively. Thick lines in faint blue and red represent the IC_{50} for parental cell lines as determined previously for gefitinib and AZD9291, respectively. A culturing time of 100 days is equivalent to 20 passages. Statistical significance of differences between mean IC50 values for parental and resistant cells at the last measured time point are indicated with ** for p≤0.01, *** for p≤0.001 and **** for p≤0.0001.

To investigate whether cells had become resistant due to secondary mutations in the EGFR or acquired resistance-conferring mutations in other genes, we performed RNA sequencing and identified variants in the resistant cells compared to the sensitive parental cell lines (Figure 4-6 A, full list in Table S 3). Analyses identified a heterozygous EGFR T790M mutation in $PC9^{GS}$ and a heterozygous NRAS Q61R mutation in $PC9^{9291S}$ (Figure 4-3 B and C). We were unable to detect mutations that are known to confer resistance to EGFR-TKIs (e.g. in EGFR, NRAS, BRAF, PIK3CA) in $HCC827^{GS}$ and $H1975^{9291S}$. Table 4-2 summarises the degree of resistance to the selection EGFR-TKI and other EGFR-TKIs compared to parental cell lines, detected resistance-conferring mutations and the origin for selected resistant cell lines.

Table 4-2: Characterisation of resistant cell lines.

IC_{50} values for EGFR-TKIS in parental and resistant cell lines were calculated from proliferation assays. Sensitivity to inhibitors of the 2nd generation was in line with response to 1st generation EGFR-TKIs. Cross resistance to other compounds of the same generation (erlotinib and CO-1686 for 1st and 3rd generation, respectively) is indicated. Known resistance-conferring mutations as detected by RNA sequencing as well as the origin of the resistant cell lines are also listed. n/d: not determined.

Cell line	IC_{50} gefitinib (µM) (±SEM)	cross resistance to 1st generation TKIs	IC_{50} AZD9291 (µM) (±SEM)	cross resistance to 3rd generation TKIs	resistance-conferring mutation	origin
PC9	*0.02 (0.001)*		*0.006 (0.0007)*			
$PC9^{GS}$	2.89 (0.27)	✓	*0.06 (0.03)*	✗	EGFR T790M	clonal
$PC9^{9291S}$	2.23 (0.25)	✓	0.98 (0.07)	✓	NRAS Q61R	clonal
HCC827	*0.004 (0.0007)*		*0.016 (0.009)*			
$HCC827^{GS}$	4.88 (0.24)	✓	1.21 (0.07)	✓	none	population
H1975	>3 µM		*0.007 (0.0009)*			
$H1975^{9291S}$	>3 µM	n/d	1.39 (0.08)	✓	none	population

To confirm that $PC9^{GS}$ and $PC9^{9291S}$ cells did not show a reduction in EGFR downstream signalling upon gefitinib and AZD9291 treatment, respectively, we performed western blotting experiments. Results confirmed no reduction of pEGFR, pAKT or pERK levels, nor detection of increased levels of cleaved PARP upon treatment with gefitinib. In contrast, and as expected, AZD9291 was able to inhibit EGFR signalling and induce apoptosis in $PC9^{GS}$ cells (which have an EGFR T790M mutation) since it is a 3rd generation EGFR-TKI. Neither gefitinib nor AZD9291 treatment led to a change in signalling or induction of apoptosis in $PC9^{9291S}$ cells.

Compared to untreated parental PC9, untreated PC9^{GS} and PC9^{9291S} cells showed higher and lower levels of pEGFR, respectively (Figure 4-3 A). Increased levels of pEGFR in EGFR T790M positive PC9^{GS} are in line with higher ATP affinity of T790M mutated EGFR, as discussed previously. Reduced levels of pEGFR in NRAS Q61R mutated PC9^{9291S} cells is in line with independence of EGFR signalling for proliferation and survival.

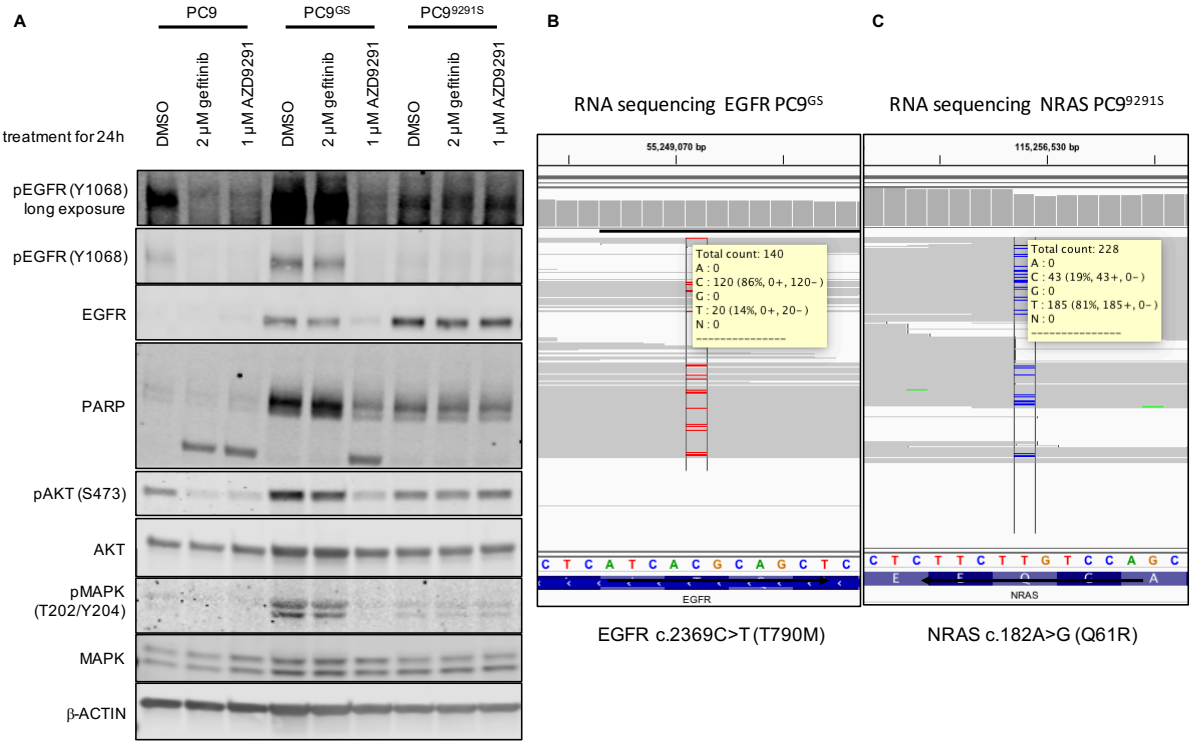


Figure 4-3: EGFR-TKI-resistant PC9 clones harbour resistance-conferring mutations in EGFR or NRAS, sustaining EGFR-signalling even in the presence of EGFR-TKI.

A: Western blot analysis of parental PC9, PC9^{GS} and PC9^{9291S} after exposure to DMSO, gefitinib or AZD9291. Compounds were added within 48 h after seeding of cells in drug free medium and cell lysates prepared 24 h thereafter. B: RNA sequencing based detection of EGFR T790M mutation in PC9^{GS}. 14 % of aligned reads show C>T mutation, encoding for threonine rather than methionine. C: RNA sequencing based detection of NRAS Q61R mutation in PC9^{9291S}. 19 % of aligned reads show A>G mutation, encoding for arginine rather than glutamine. Arrows indicated direction of transcription.

To investigate the potential importance of *de novo* mutations for the emergence of resistance to EGFR-TKIs in PC9, we exposed PC9 to S9-activated benzo[a]pyrene to increase the mutational burden of cells (Lindblad and Jackim 1982). Benzo[a]pyrene was selected as a mutagen, as it is known to cause transversions, as seen in

patients with EGFR C797S mutations. Surviving cells were expanded and are referred to as mutagenised PC9 from here on. Mutagenised PC9 cells were treated with 1 μM gefitinib and AZD9291 as described previously, to isolate resistant cells. With 800 colonies per $1x10^8$ seeded cells, mutagenised PC9 had a markedly increased frequency of resistant colonies compared to PC9 (3 colonies per $1x10^8$ cells, see chapter 4.1) under gefitinib selection. Furthermore, emergence of distinct resistant colonies was also evident with AZD9291 selection, which was not observed in previous experiments (see chapter 4.1). Sanger sequencing for detection of EGFR T790M or C797S and NRAS G12 or Q61 mutations was performed and results were taken as an indication of presence of mutations, due to the difficulty of detecting changes at low allelic frequencies (Engelman, Mukohara et al. 2006). We were unable to detect EGFR C797S or NRAS mutations in any of the 3 AZD9291 selected clones. Of 8 gefitinib selected EGFR-TKI resistant clones, all had resistance-conferring mutations; 7/8 had EGFR T790M mutations and 1/8 had an NRAS Q61H mutation.

To test whether resistance of generated AZD9291-resistant cell lines was also apparent in 3D models, cells were seeded for spheroid formation, treated with AZD9291 and spheroid size was measured regularly. Spheroids of $PC9^{9291S}$ and $H1975^{9291S}$ cells increased in size under AZD9291 treatment (Figure 4-4 A/B and D/E). Assessment of drug sensitivity of $HCC827^{GS}$ in 3D was not possible as these EGFR-TKI resistant cells did not form spheroids (Figure 4-4 C), unlike parental HCC827 cells.

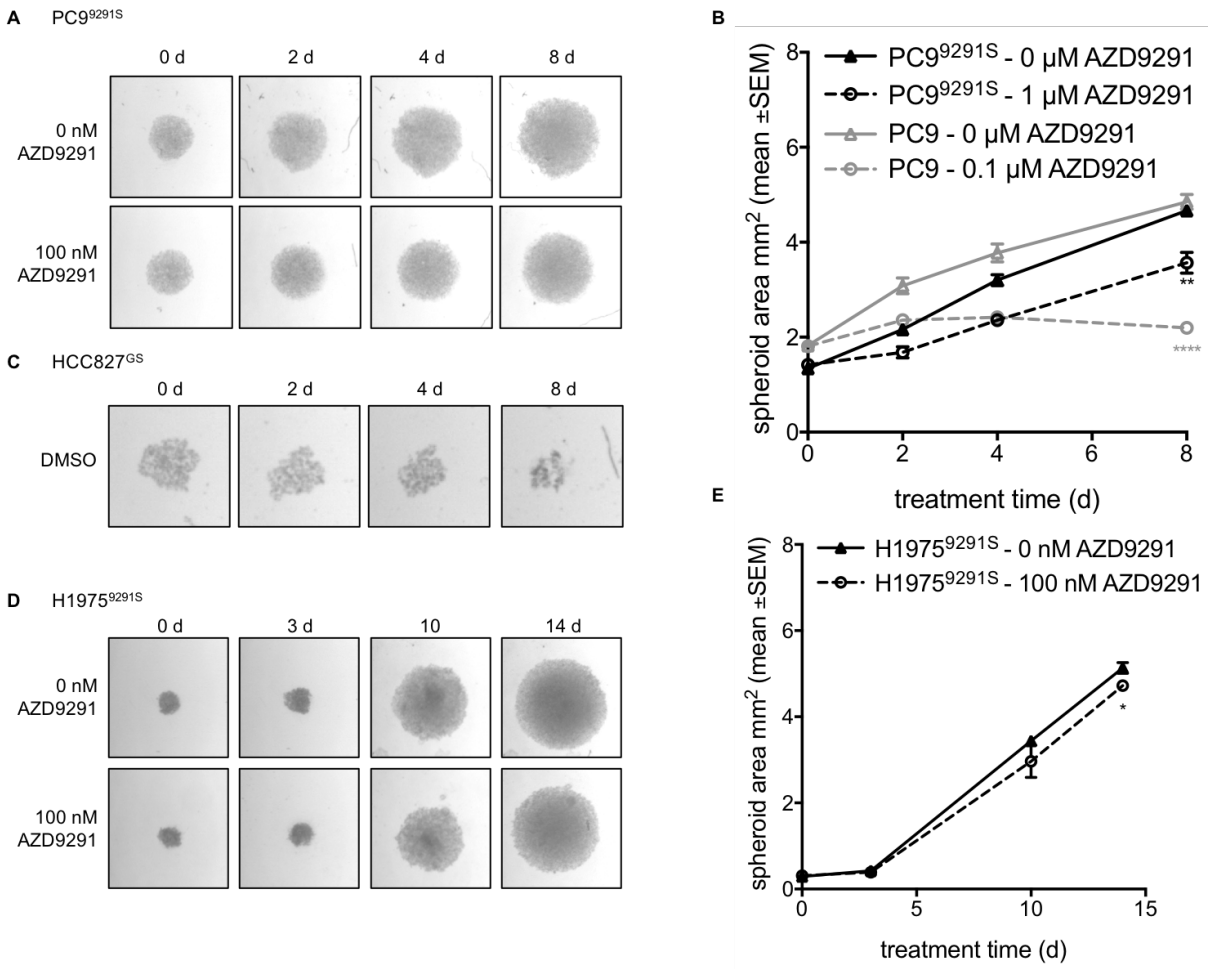


Figure 4-4: AZD9291 resistant PC9 and H1975 but not HCC827 form spheroids and are resistant to AZD9291 in 3D.

Images of representative spheroids under DMSO and AZD9291 treatment followed over time for $PC9^{9291S}$ (A), $HCC827^{GS}$ (C) and $H1975^{9291S}$ (D) cells. (B) and (E) show spheroid size over time for DMSO and AZD9291 treated spheroids of PC9/$PC9^{9291S}$ and $H1975^{9291S}$, respectively. Data are from one representative experiment performed in technical triplicates. Statistical significance of differences between mean spheroid sizes of untreated and treated spheroids are indicated with * for p≤0.05, ** for p≤0.01 and **** for p≤0.0001. Medium (and AZD9291) was changed every 96 h. Images were acquired on the Gelcount and spheroid size determined using the Gelcount software.

4.3 Discussion on generation of EGFR-TKI resistant cell lines

The first aim of this chapter was to generate cell lines with acquired resistance to EGFR-TKIs. In the past, *in vitro* studies using established cell lines have investigated mechanisms of resistance and the majority of these recapitulate the mechanisms of EGFR-TKI resistance observed in the clinic (Engelman, Zejnullahu et al. 2007, Ogino, Kitao et al. 2007, Avizienyte, Ward et al. 2008, Yoshida, Song et al. 2016). Some studies have identified resistance mechanisms (for example EGFR C797S)

before their identification in patients (Yu, Boggon et al. 2007, Avizienyte, Ward et al. 2008, Thress, Paweletz et al. 2015). The priority of this work was the generation of cell lines that were resistant by mechanisms other than well described genetic changes.

Methods for the generation of resistant cells differ between studies. A common approach is to expose cells to low doses of the drug and over several passages increase the dose in a stepwise manner, with or without pre-treatment using mutagens (Koizumi, Shimoyama et al. 2005, Ogino, Kitao et al. 2007). An alternative approach is to expose cells to concentrations of EGFR-TKIs in the 1-3 μM range immediately (Guix, Faber et al. 2008, Sharma, Lee et al. 2010).

Using the latter approach, we generated gefitinib and AZD9291 resistant cells of five AZD9291 sensitive NSCLC cell lines (PC9, HCC827, H1975, HCC2935 and HCC4006), showing a more than 100-fold increase in IC_{50} for proliferation for selection compounds. Gefitinib and AZD9291 selected PC9 cells showed known resistance mechanisms ($PC9^{GS}$: EGFR T790M and $PC9^{9291S}$: NRAS Q61R), which are observed in the clinic and in *in vitro* experiments by other groups, confirming the clinical relevance of our approach (Ogino, Kitao et al. 2007, Huang, Lee et al. 2013, Eberlein, Stetson et al. 2015). We did not identify EGFR C797S mutations, which have been observed *in vitro* and in patients (Ercan, Choi et al. 2015, Thress, Paweletz et al. 2015). We observed cross-resistance to other EGFR-TKIs of the 1st, 2nd and 3rd generation for all but the T790M mutated $PC9^{GS}$ cells, which were sensitive to 3rd generation inhibitors. Our data suggest that resistance to EGFR-TKIs is sustained even in absence of EGFR-TKI selection over >20 passages, in line with findings by (Koizumi, Shimoyama et al. 2005) and (Cortot, Repellin et al. 2013). This is in contrast to data published by other groups, showing loss of resistance after 16-

30 passages, in some instances accompanied by a reduction in T790M mutant alleles below detection levels (Sharma, Lee et al. 2010, Chmielecki, Foo et al. 2011).

We observed two distinct patterns of emergence of resistance. In PC9 cells, the process was dominated by apoptosis and survival of single cells that subsequently grew as individual clones. In HCC827 and H1975 cells, a larger proportion of cells survived and eventually proliferated under constant drug exposure. These results are supported by preliminary experiments in two further cell lines, HCC2935 and HCC4006. These patterns of emergence of resistance are in line with results from chapter 3.2.2, showing a more marked induction of apoptosis upon EGFR-TKI treatment in PC9 compared to other cell lines. The majority of published studies on generation of EGFR-mutated NSCLC cell lines with acquired resistance to EGFR-TKIs of the 1st or 3rd generation focus on PC9. Our data on increased emergence of resistant clones in benzo[a]pyrene treated PC9 cells suggest de novo mutagenesis can increase the frequency of resistance to AZD9291 and gefitinib, which is supported by work by other groups (Koizumi, Shimoyama et al. 2005, Ercan, Choi et al. 2015). The mechanism however is yet to be identified and future work will assess the mutational burden of benzo[a]pyrene treated PC9 cells. Notably, pre-treatment with low doses of gefitinib also increased the number of gefitinib resistant PC9 clones, possibly due to decreased cell death due to a less sudden inhibition of EGFR-activity or cell cycle arrest (Sharma, Gajowniczek et al. 2006).

We did not identify resistance-conferring mutations in EGFR-TKI resistant H1975 and HCC827 populations using RNAseq but this will need to be confirmed using whole genome or whole exome sequencing. Similarly, analysis of gene copy number, genetic rearrangements and epigenetic profiling is needed.

In contrast to mutation-associated changes, resistance driven by epigenetic changes and reactivation of signalling leading to resistance to EGFR-inhibition is less well understood (Eberlein, Stetson et al. 2015, Ichihara, Westover et al. 2017). We therefore focus on understanding the population-based resistance observed in HCC827^{GS} and H1975^{9291S}.

4.4 Signalling in EGFR-TKI resistant cell line (HCC827^{GS} and H1975^{9291S})

As previously discussed, EGFR-TKI resistance via mechanisms other than secondary EGFR mutations or activating mutations in EGFR downstream signalling pathways is likely to play a significant role in limiting the effectiveness of all generations of EGFR-TKIs in the clinic. In consequence, cell lines such as HCC827^{GS} and H1975^{9291S}, in which EGFR-TKI-resistance does not seem to be driven by EGFR signalling pathway mutations ('population-based resistance') are of primary interest in this project. In order to identify potential drivers of resistance and potential targetable weaknesses, we analysed signalling changes in HCC827^{GS} and H1975^{9291S}.

Western blotting analyses confirmed that gefitinib or AZD9291 treatment did not lead to changes in EGFR signalling. Resistant cell lines showed lower levels of pEGFR and pERK but not pAKT compared to parental cell lines, and these were unaffected by EGFR-TKI treatment (Figure 4-5 A and B).

To assess changes across a broader range of antigens, we compared RPPA analysis (117 antigens) of AZD9291-treated HCC827^{GS} and H1975^{9291S} cells with parental cell lines under DMSO treatment. There was a significant change in 40 and 37 antigens in HCC827^{GS} and H1975^{9291S}, respectively. Out of these, 21 antigens were changed in both cell lines (Figure 4-5 C). Significantly changed antigens in both

cell lines are listed in Figure 4-5 E. Perhaps surprisingly, compared with parental cell lines, EGFR-TKI resistant cells had reduced expression/phosphorylation levels of certain growth factor receptors (MET, HER2, IGF-1R) and signalling pathways (PI3-kinase, JAK/STAT) thought to be associated with EGFR-TKI resistance (Figure 4-5 D) (see reviews (Morgillo, Della Corte et al. 2016, Zulkifli, Tan et al. 2017)).

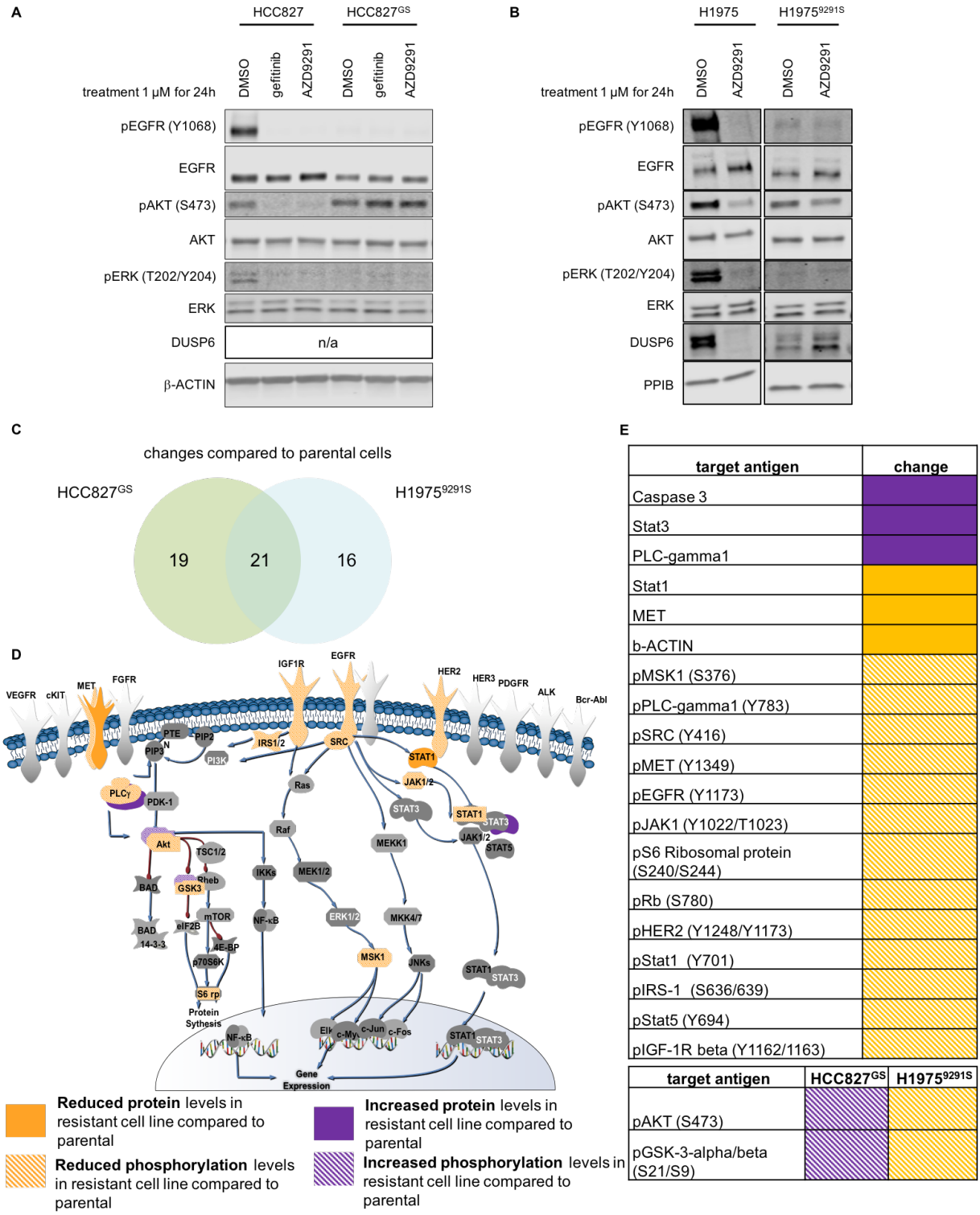


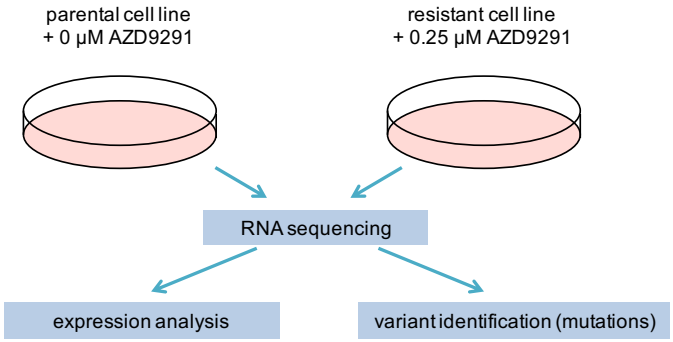
Figure 4-5: EGFR-TKI treatment does not reduce canonical EGFR-signalling in resistant cells

A/B: Western blot analysis of HCC827/HCC827^{GS} and H1975/H1975^{9291S} cells after indicated treatments. n/a: not available. C: Number of significant (p≤0.05) changes in protein levels in HCC827^{GS} and H1975^{9291S} compared to their parental cell lines, as detected by RPPA analysis. D/E: Significant changes in protein levels common to HCC827^{GS} and H1975^{9291S} compared to their parental cell lines, as detected by RPPA analysis. Parental cells were untreated, resistant cells were treated with 250 nM for 48 h. Data are from technical duplicates. Antigens changed in both resistant cell lines showed the same direction of change with the exception of pAKT (S473) and pGSK3-alpha/beta (S21/S9).

4.5 RNA expression changes EGFR-TKI resistant cell lines (HCC827^{GS} and H1975^{9291S})

To identify potential global changes in expression levels we performed RNA sequencing on parental and resistant cell lines (Figure 4-6 A). Analyses revealed a significant expression change in a higher number of transcripts comparing parental and resistant cells in HCC827^{GS} cells than H1975^{9291S} cells (Figure 4-6 B, Table S 4 and Table S 6). Compared with their respective parental cell lines, 91 transcripts were changed significantly in both HCC827^{GS} and H1975^{9291S} cells (Figure 4-6 C). The top 15 commonly up- or down-regulated transcripts are shown (data for H1975^{9291S}) in Figure 4-6 C. Amongst the most downregulated genes in both HCC827^{GS} and H1975^{9291S} was *DUSP6*. Detection of DUSP6 via western blotting was in agreement with the RNAseq results, showing lower levels of DUSP6 in H1975^{9291S} compared to H1975. The reduced expression of *DUSP6* RNA in H1975^{9291S} cells is consistent with the reduced levels of pERK, a known regulator of DUSP6 transcription, in H1975^{9291S} cells (Plotnikov, Zehorai et al. 2011). Furthermore, DUSP6 levels decreased under AZD9291 treatment of HCC827, H1975 and HCC4006 cells (see Figure 4-5 and Figure 3-7, respectively). In order identify changes relevant to resistance in both cell lines, we performed MetaCore pathway analysis on the 91 transcripts that were significantly different in both HCC827^{GS} and H1975^{9291S}. However, MetaCore analysis did not identify a common targetable biological process or pathway (Figure 4-6 C, list of top 10 identified pathways in Table S 5).

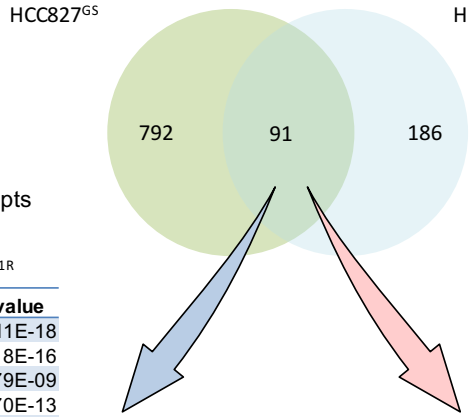
A



B

	number of differentially regulated transcripts (adjusted p-value ≤0.01)	
	up	down
HCC827^{GS}	438	445
H1975^{9291S}	64	213

C



downregulated transcripts

	H1975^{9291R}	
	log$_2$ FC	padj-value
SLCO2A1	-6.16	2.11E-18
IL1RL1	-5.67	7.18E-16
MIR205HG	-5.26	1.79E-09
FXYD3	-5.12	3.70E-13
TMPRSS11E	-4.94	9.57E-06
ST8SIA4	-4.80	1.94E-07
S100A14	-4.72	2.63E-16
CFH	-4.62	6.98E-15
CEACAM6	-4.30	3.88E-18
TMPRSS4	-4.20	1.28E-09
ABCA12	-4.11	6.65E-07
C1orf116	-4.02	6.13E-19
DUSP6	-4.02	6.47E-21
CNTN1	-4.01	1.21E-05
EGR1	-3.96	1.56E-07

Metacore enrichment analysis:

- blood vessel morphogenesis
- Cell-matrix interactions
- Chemotaxis

upregulated transcripts

	H1975^{9291R}	
	log$_2$ FC	padj-value
KRT17	5.30	5.78E-09
RETREG1	4.68	8.19E-10
ALPP	4.45	1.19E-23
GGT5	3.84	1.30E-03
SDC2	3.78	1.19E-09
ANKRD1	3.64	5.54E-11
IL32	3.53	2.49E-05
ABI3BP	3.46	1.51E-04
AMOT	3.40	9.92E-11
OLR1	3.08	9.89E-03
ZNF704	3.06	4.07E-11
HAVCR1	3.05	2.04E-04
PGBD5	2.58	5.10E-03
L1CAM	2.47	1.51E-06
GPC4	2.43	4.31E-06

Figure 4-6: RNA sequencing analysis of HCC827^{GS} and H1975^{9291S}

A: Setup for RNAseq analysis. Total mRNA of 48 h DMSO treated parental HCC827 and H1975 and 48 h 0.25 µM AZD9291 treated HCC827^{GS} and H1975^{9291S} cells were analysed using RNAseq. Variant calls were identified for detection of mutations and expression changes in resistant cells determined. The number of significant expression changes in resistant cell lines compared to parental cell lines is given in (B). (C) shows a Venn-diagram of significant changes for HCC827^{GS} and H1975^{9291S}. Tables show the top 15 up- and down-regulated genes amongst the 91 common changes as ranked in H1975^{9291S} based on fold change for genes with padj≤0.01 as well as the top three identified changed networks as determined by MetaCore enrichment analysis.

Taken together, the RPPA and RNAseq analyses did not identify clear targets for therapeutic interventions.

4.6 Compound screen for overcoming resistance to AZD9291 treatment in H1975^{9291R} cells

Data from RPPA and RNAseq analyses did not point clearly to a specific protein or signalling pathway that could be targeted to overcome or prevent resistance to EGFR-TKI treatment. Therefore, in addition, we perform a drug screen using a bioactive small molecule library to identify potential new sensitivities of H1975^{9291R} cells to compounds inhibiting a broad range of targets.

H1975^{9291S} and H1975 cells were treated with a compound library (Table S 7) in the presence or absence of AZD9291 (1 µM), respectively (Figure 4-7 A). The aim was to identify compounds, that inhibited proliferation of H1975^{9291S} to a greater extent than of H1975 cells. The 1902 compounds of the screening library (L1700, Selleck Chemicals) covered a set of 190 cellular targets (Figure 4-7 B and C). Compounds were aliquoted into six 384-well library master plates and tested at concentrations of 0.1 µM and 1 µM. Effects of compounds on cell viability were reproducible, showing a good correlation between the duplicate plates and the range of relative effectiveness of compounds was distributed broadly evenly over the six library plates (Figure 4-8).

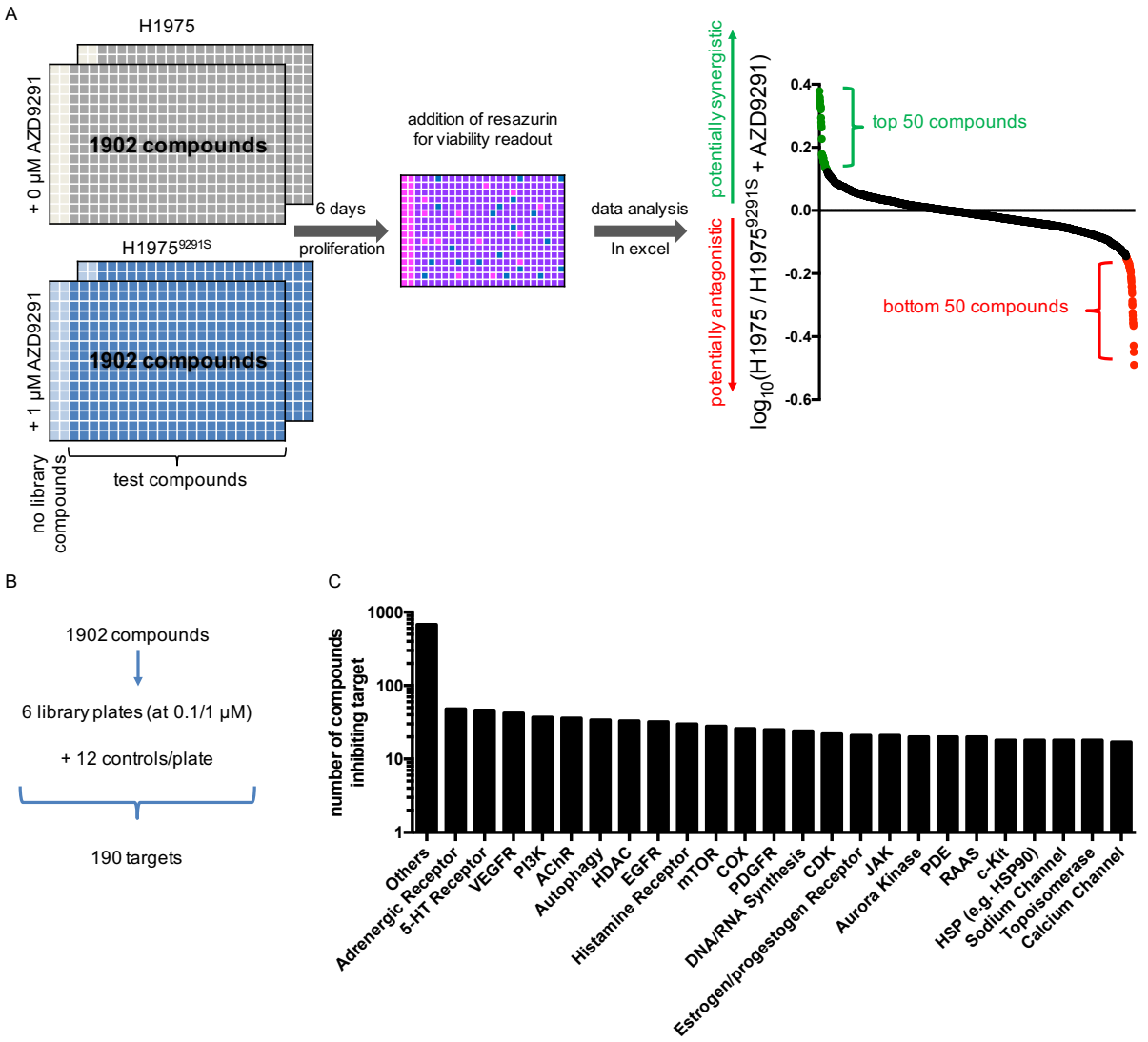


Figure 4-7: Proliferation based compound screen for L1700 library was performed in 384-well plates and covered 190 targets

A: Cells were seeded in 384-well plates and treated with the compound library at 0.1 µM and 1 µM in the absence or presence of 1 µM AZD9291 for H1975 and H1975^{9291S}, respectively. Viability was assessed on day 6 after treatment and compounds were ranked based on their differential ability to reduce proliferation in H1975^{9291S} compared to H1975. B: The L1700 library was redistributed onto six library plates, each including 12 control wells with DMSO. Compounds in the library inhibit a total of 190 targets. The top 25 most commonly inhibited targets are listed in (C).

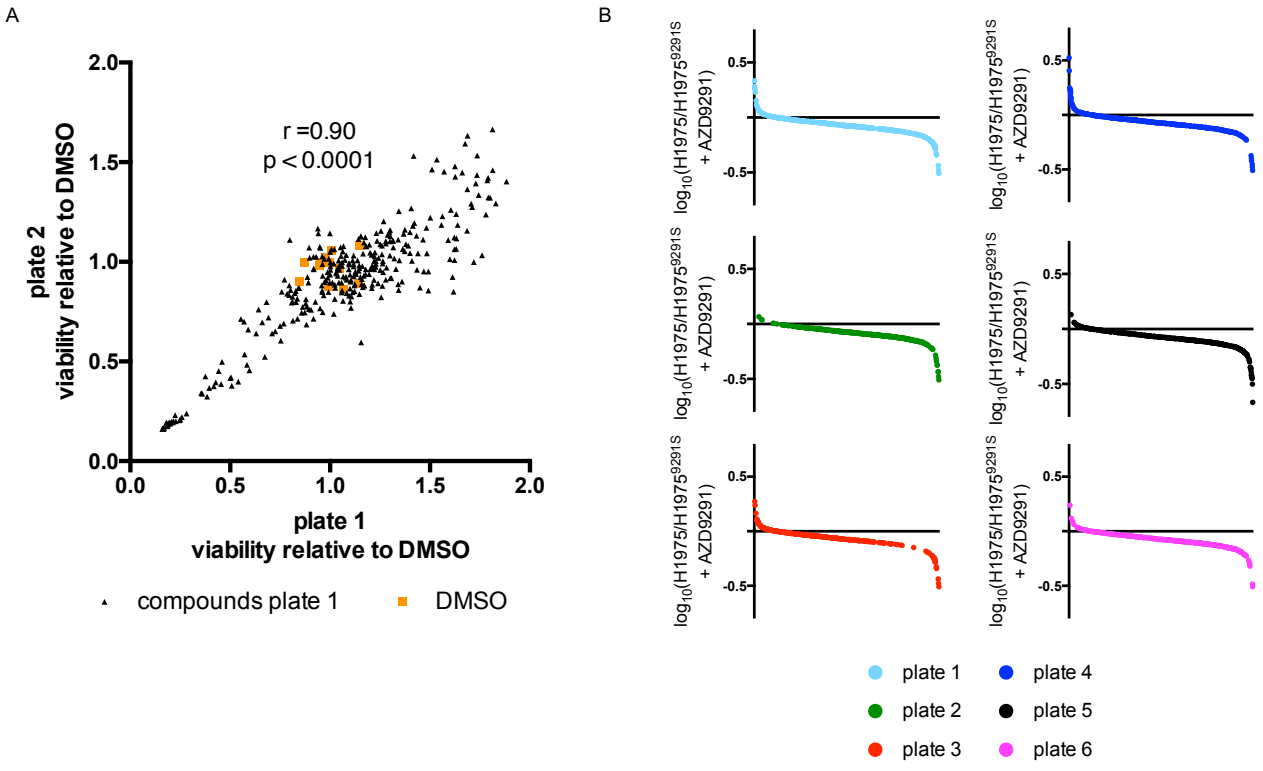


Figure 4-8: Effects of screen compounds were reproducible over two repeats and plates showed a similar range of effect sizes.

Comparison of drug (black triangles) and DMSO (orange squares) effects for duplicate plates is shown in (A) and the Pearson product-moment correlation coefficient r is reported. B: The observed values for effects of compounds on plates 1 to 6 in H1975^{9291S} compared to H1975 cells.

Out of the 1902 compounds, 129 compounds showed a positive z-score of 2 at either 0.1 µM or 1 µM for increased activity in AZD9291 treated H1975^{9291S} compared to H1975 (Table S 8, Figure 4-9). Hits targeted a number of proteins, including Aurora Kinase (AURK), HSPs, HDAC and IGF-1R. Analysis of individual values (Table S 8) revealed that the absolute differences in cell viability between H1975^{9291R} and H1975 cells were small in some instances, suggesting the cut-off for hit selection was insufficiently stringent to identify the most promising hits. This might be attributed to the relatively small standard deviation of plates, leading to a small difference between mean of the plate and hits with a z-score of 2. To identify those compounds with the largest biological effect, we selected those compounds with at least a two-fold difference in relative cell viability and/or an absolute difference in relative viability

of 0.4. Using these more stringent criteria identified 12 compounds that included inhibitors of AURK and IGF-1R (Figure 4-9, Table 4-3).

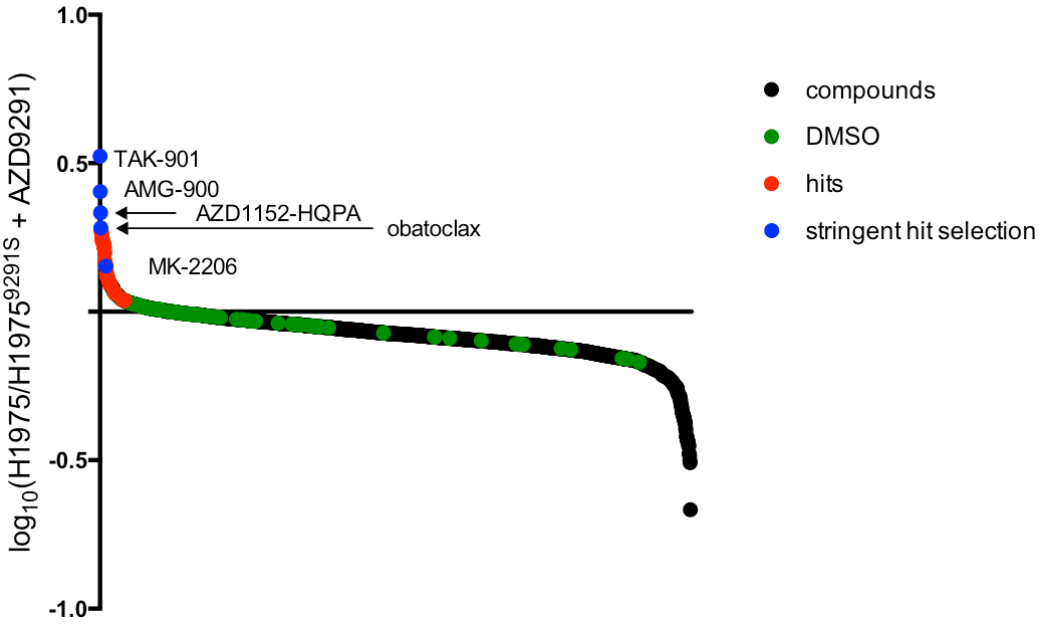


Figure 4-9: Distribution of hit compounds, other compounds and DMSO based on their anti-proliferative effect in AZD9291 treated H1975^{9291S} compared to H1975.

Compounds are plotted based on their differential inhibition of proliferation in H1975^{9291S} compared to H1975 at a dose of 0.1 µM. Hits identified via a z-score of 2 are marked in red, those identified using more stringent criteria of a 0.4 absolute or 2-fold relative difference in cell viability are marked in blue and named. DMSO controls are marked in green.

Table 4-3: Compounds that preferentially inhibit proliferation of H1975^{9291S} in compared to H1975 target proteins including AKT, Aurora Kinase and IGF-1R.

Relative viability for each cell line is reported for compounds at 0.1 µM or 1 µM ($^{\#}$). H1975^{9291S} but not H1975 cells were co-treated with 1 µM AZD9291. Compounds are listed in alphabetical order of their main target.

Compound	Listed targets	Relative viability of H1975	Relative viability of H1975^{9291S} + AZD9291	2-fold difference	0.4 absolute difference
MK-2206	AKT	1.52	1.07		✓
AZD1152-HQPA	Aurora Kinase	0.85	0.39	✓	✓
TAK-901	Aurora Kinase	0.47	0.14	✓	
AMG-900	Aurora Kinase	0.36	0.14	✓	
Obatoclax Mesylate	Bcl-2,Autophagy	0.89	0.46		✓
SU11274 $^{\#}$	c-MET	1.13	0.48	✓	✓
Quizartinib $^{\#}$	FLT3	0.95	0.46	✓	✓
PQ 401 $^{\#}$	IGF-1R	0.98	0.56		✓
GSK1904529A $^{\#}$	IGF-1R	1.09	0.54	✓	✓
CH5132799 $^{\#}$	mTOR,PI3K	0.55	0.24	✓	
Darapladib $^{\#}$	Phospholipase	0.97	0.23	✓	✓
SRT1720 $^{\#}$	Sirtuin	0.87	0.31	✓	✓

4.6.1 Drug target enrichment analysis

Our aim in the screen was not only to select the top compounds but also to identify drug targets that were enriched within the most selective compounds, we therefore performed a target enrichment analysis using the top and bottom 50 compounds (green and red in Figure 4-7 A). Analysis using Fisher's Exact test revealed significant enrichment of 10 targets in the top 50 compounds (Table 4-4). Targets for which compounds were more active against parental H1975 compared to resistant cell line were identified (ALK, ATPase, EGFR, kinesin, MEK, microtubule associated, PLK, proteasome and topoisomerase) but not analysed further in the context of this work.

Table 4-4: Significantly enriched targets within the 50 most selective compounds

Enriched targets identified via Fisher's exact test in the top 50 compounds for increased inhibition of proliferation in $H1975^{9291S}$ compared to H1975. Numbers indicate the fraction of compounds in the top 50 compounds in 0.1 µM library conditions or 1 µM library conditions ($^{\#}$). The p-value for the Fisher's exact test and the number of compounds per target in the entire library are listed.

Target	Fraction in top 50 compounds	p-value	Total count
IGF-1R$^{\#}$	0.44	<0.001	9
Aurora Kinase	0.30	<0.001	20
AKT$^{\#}$	0.25	0.003	12
mTOR$^{\#}$	0.25	<0.001	28
BCR-ABL	0.20	0.005	15
PI3K$^{\#}$	0.19	<0.001	37
FLT3$^{\#}$	0.18	0.029	11
HSP	0.17	0.009	18
HDAC	0.12	0.008	33

We generated a target set relative enrichment score based on the method suggested for gene set enrichment analysis by Subramanian et al. (Subramanian, Tamayo et al. 2005). The distributions of selected positively enriched targets is shown in Figure 4-10 A-C using their relative enrichment score across the library, ranked by effect size in $H1975^{9291S}$ compared to H1975. An increase in enrichment score indicates that the compound at this position inhibits the target of interest whereas a decrease indicates that the compound at this position does not inhibit the target of interest (see Figure 4-10 D). Details about the calculation of the enrichment score are described in chapter 2.18.

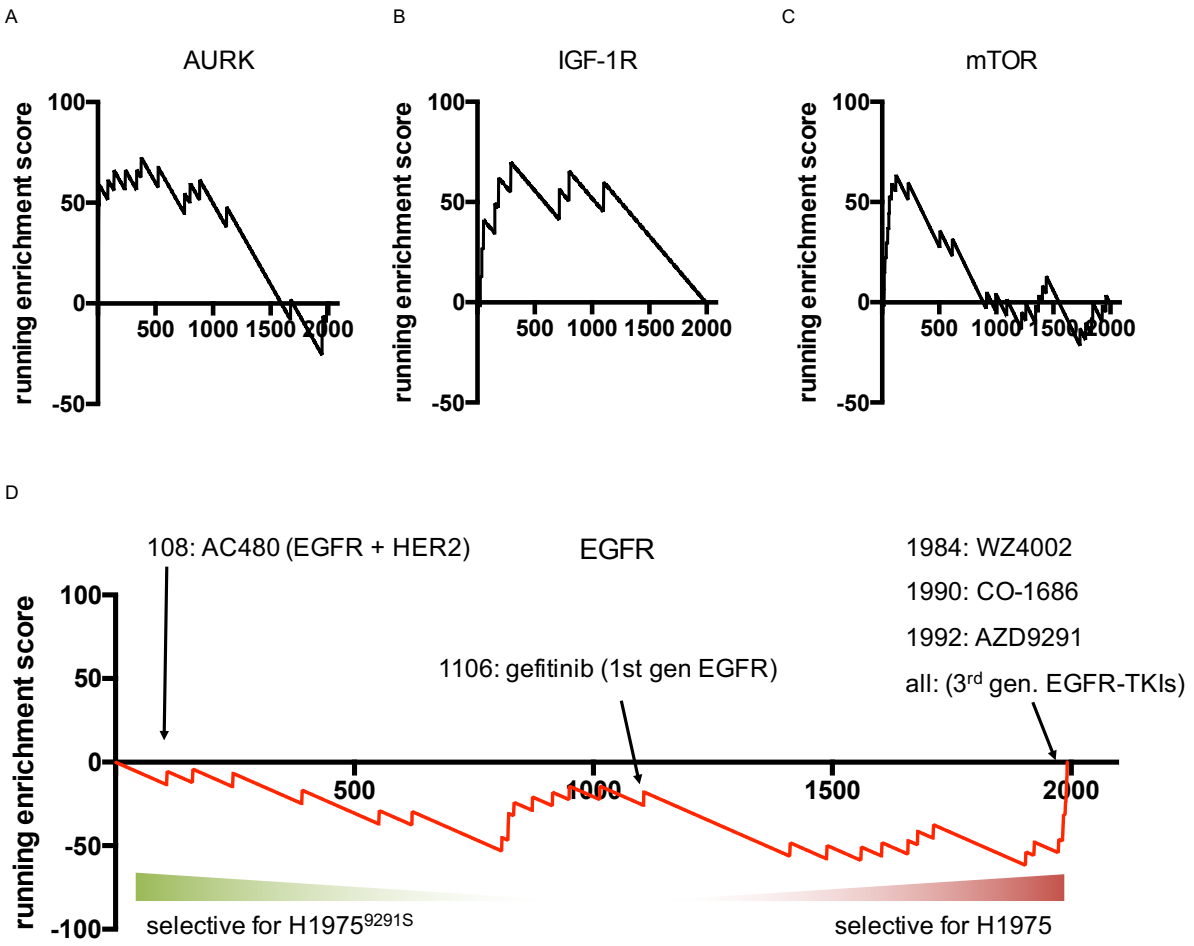


Figure 4-10: Aurora Kinase, IGF-1R and mTOR inhibitors are enriched among the compounds most active against H1975^{9291S}.

Graphs show the running enrichment score for compounds inhibiting the indicated targets, as calculated using gene set enrichment analysis. For the calculation and plotting of the running enrichment score, compounds are ranked (x-axis) in order of decreasing $\log_{10}$(H1975/H1975^{9291S}). The enrichment score is the sum of the enrichment score of the previous compound and a positive or negative factor for compounds that do or don't inhibit the examined target, respectively. A/B/C: "positively enriched" targets, D: "negatively enriched" target, arrows indicate the rank of EGFR-targeting compounds.

In this screen, 3rd generation EGFR-TKIs served as an internal control, showing enrichment amongst the compounds with greater effects in H1975 compared to H1975^{9291S} (right side in Figure 4-10 D, Table S 9). This is in line with resistance to 3rd generation EGFR-TKIs in H1975^{9291S} and sensitivity in H1975. Effects of other selective EGFR-TKIs were more similar in both cell lines, resulting in an intermediate rank (gefitinib: middle in Figure 4-10 D, Table S 9). Inhibitors that were not EGFR-selective were more H1975^{9291S} selective or had similar effects in both cell lines (left in Figure 4-10 D, Table S 9).

4.6.2 Confirmation of hits

Based on our analyses of the compound screen, inhibitors of IGF-1R and AURK, the target classes with the highest fraction of compounds in the top 50 compounds, were selected for further studies.

A panel of 15 Aurora Kinase inhibitors present in the compound library showed a broad range in their ability to selectively inhibit proliferation in H1975^{9291S} cells compared to H1975, but this was generally in agreement with the compound ranking observed in the screen (Table 4-5). In this 96-well format, 5 out of 6 AURK inhibitor hits from the 384-well assay confirmed selective inhibition of H1975^{9291S} over H1975 cells (Figure 4-11 A/B, Table 4-5). Additional experiments also demonstrated an increased sensitivity of H1975^{9291S} cells to the AURK inhibitors even in the absence of AZD9291 compared to H1975 cells (Figure 4-11 A and Table 4-5). Although numbers are limited, there is a suggestion of an overrepresentation of AURK B inhibitors within the confirmed most selective compounds (Table 4-5).

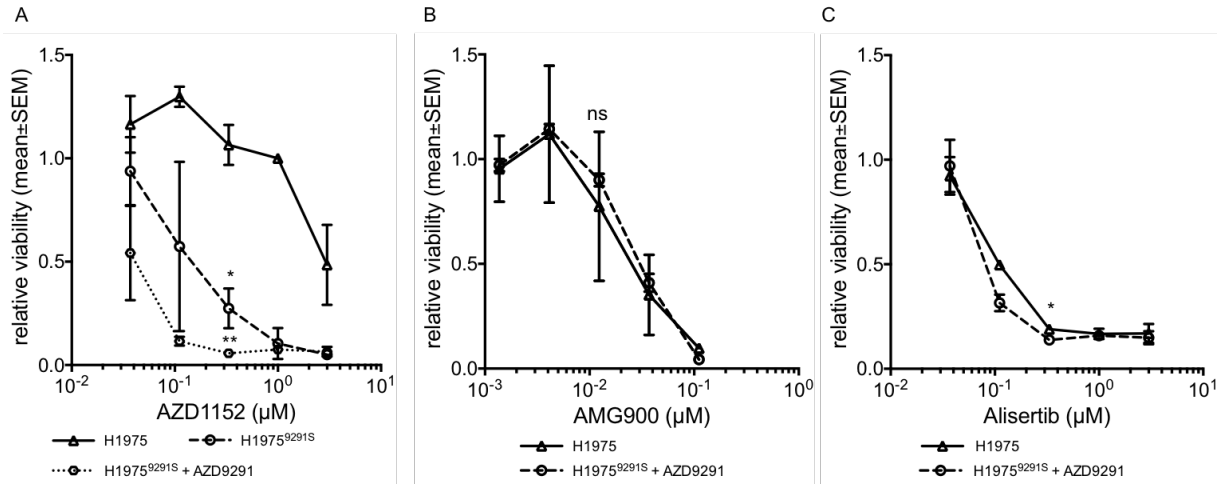


Figure 4-11: Some, but not all, AURK inhibitors selectively inhibit proliferation of H1975^{9291S} cells

Proliferation assays for a range of AURK inhibitors were performed in H1975 and H1975^{9291S} in the absence and presence of 1 μM AZD9291, as indicated. Graphs show the dose dependent decrease in cell viability of H1975 and H1975^{9291S} at increasing concentrations of AZD1152 (A), AMG900 (B) and Alisertib (C). Viability, as measured by resazurin fluorescence is relative to DMSO or 1 μM AZD9291 for H1975/H1975^{9291S} and AZD9291 treated H1975^{9291S}, respectively. Data are from one representative experiment, performed in technical duplicates. Statistical significance of differences between mean viability at the curve midpoint of H1975 cells and H1975^{9291S} are indicated with * for p≤0.05, ** for p≤0.01 and ns for p>0.05.

Table 4-5: Some but not all tested Aurora Kinase inhibitors show selectivity for H1975^{9291S} cells over H1975.

The table indicates the rank of all AURK inhibitors in the compound screen, information about inhibition of isoforms and IC_{50}s determined in validation experiments under indicated conditions. Data represent IC_{50} values determined based on one representative experiment performed in technical duplicates. n/d: not determined, compound was not used in validation experiments. Compounds marked in green were identified as hits in the compound screen. [1] as reported by Selleck Chemicals (www.selleckchem.com, accessed 24.08.2016) [2] bold numbers: ≥ 2 fold difference in IC_{50} for H1975 vs H1975^{9291S} + AZD9291 comparison [3] bold numbers: ≥ 2 fold difference in IC_{50} for H1975 vs H1975^{9291S} comparison

			IC_{50} (µM)		
Rank in screen	**compound**	**AURK selectivity[1]**	**H1975**	**H1975^{9291S} + AZD9291**	**H1975^{9291S}**
4	TAK-901	A/B	0.51	**0.12**[2]	**0.11**[3]
5	AMG-900	A	0.03	0.03	0.03
6	AZD1152	B	>3	**0.03**	**0.16**
9	VX-680	A/B/C	1.24	**0.20**	**0.33**
10	AT9283	A/B	1.38	**0.04**	**0.34**
16	Aurora A Inhibitor I	A	>3	**0.80**	2.14
90	JNJ-7706621	A/B	n/d	n/d	n/d
144	MK-8745	A	0.35	0.19	0.19
242	Danusertib	A>B/C	n/d	n/d	n/d
341	MK-5108	A	1.08	0.55	**0.46**
379	SNS-314	A/B/C	0.23	**<0.03**	**0.04**
527	ENMD-2076	A>B	n/d	n/d	n/d
756	Alisertib	A	0.14	0.10	**0.07**
804	KW-2449	A	n/d	n/d	n/d
888	CYC116	A/B	n/d	n/d	n/d
1121	PHA-680632	A>B/C	>3	**0.78**	>3
1678	MLN8054	A	n/d	n/d	n/d
1951	CCT129202	A>B/C	>3	>3	>3
1958	Hesperadin	B	0.08	0.04	0.05
1990	CCT137690	A/B/C	0.30	0.28	0.22

Validation of IGF-1R inhibitors showed good overlap with results from the compound screen, while also confirming compounds as hits that had ranked low in the initial screen, such as OSI906. In contrast to results obtained from AURK inhibitors, IC_{50}

values for IGF-1R inhibitors were only lower in H1975^{9291S} in the presence of AZD9291 compared with parental H1975 cells (Figure 4-12 and Table 4-6).

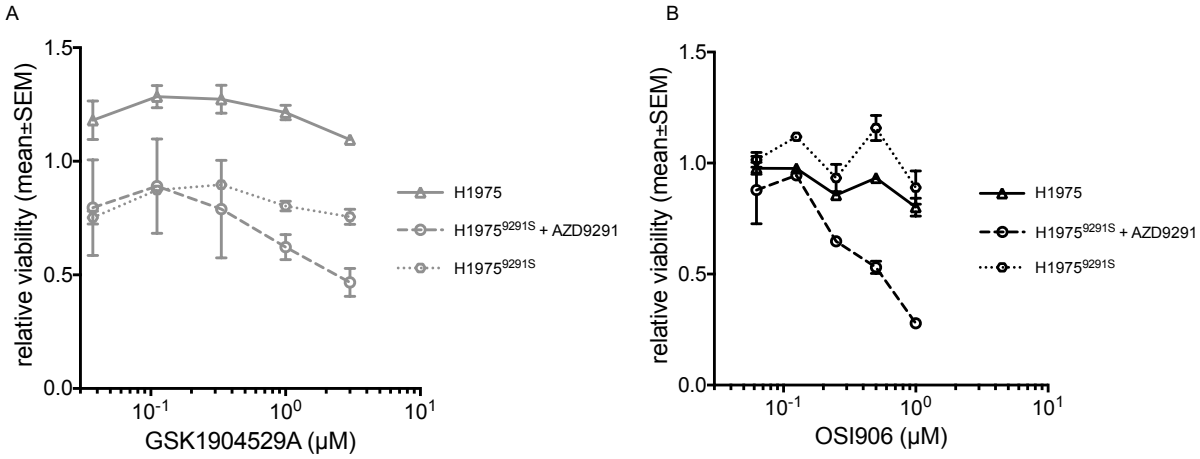


Figure 4-12: AZD9291 sensitises H1975^{9291S} cells to IGF-1R inhibitors.

H1975^{9291S} and H1975 cells were treated with IGF-1R inhibitors GSK1904529A (A) or OSI906 (B) in the absence of presence (not for H1975) of 1 μM AZD9291. Viability, as measured by resazurin fluorescence is relative to viability of cells in the absence of IGF-1R inhibitors for each condition. Data are from one representative experiment performed in technical duplicates.

Table 4-6: IGF-1R inhibitors showed increased inhibition of proliferation in AZD9291 treated H1975^{9291S} compared to untreated H1975 cells.

Ranking of IGF-1R inhibitors in compound screen and IC50s determined in validation experiments. Compounds marked in green were identified as hits in the compound screen. Data represent IC50 values determined based on one experiment performed in technical duplicates.

		IC50 (μM)		
Rank in screen	**compound**	**IC50 H1975**	**H1975^{9291S} + AZD9291**	**H1975^{9291S}**
6	GSK1904529A	>3	1.86	>3
14	PQ 401	>3	2.58	>3
17	NVP-ADW742	>3	1.95	>3
42	NVP-AEW541	n/d	n/d	n/d
91	GSK1838705A	n/d	n/d	n/d
327	BMS-536924	n/d	n/d	n/d
482	OSI-906	>1	0.53	>1
538	AG-1024	n/d	n/d	n/d
1382	BMS-754807	0.31	0.07	0.38

To gain further insight into effects of combination treatments with inhibitors of AURK or IGF-1R, we investigated signalling changes by western blot analysis. Data indicate an increase in apoptosis with combined treatment with AZD1152 and AZD9291, and a marked reduction in cell proliferation (as assessed by pHH3). This was less pronounced with OSI906 treatment. Interestingly, OSI906 treatment led to a transient reduction in pAKT levels, suggesting that AKT signalling was at least partly IGF-1R dependent in these cells, and this effect was more sustained with AZD9291 combination treatment (Figure 4-13 A).

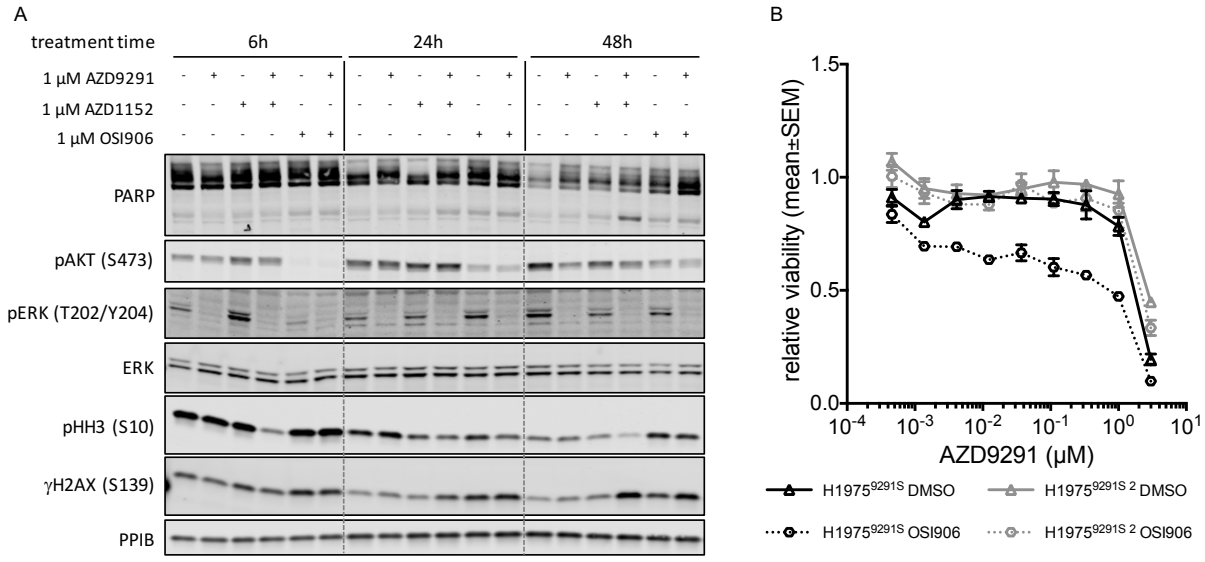


Figure 4-13: Combination treatment of H1975^{9291S} with AZD9291 and AZD1152 or OSI906 leads to induction of apoptosis and inhibition of signalling via AKT and ERK but not every AZD9291 selected cell line is sensitive to IGF-1R inhibitors.

A: Western blot analysis of H1975^{9291S} cells treated with AZD1152 or OSI906 in the presence or absence of AZD9291. B: Proliferation of H1975^{9291S} (black) and the independently generated H1975$^{9291S\ 2}$ (grey) cells was assessed under a range of AZD9291 concentrations in the presence or absence of 1 µM OSI906. Viability, as measured by resazurin fluorescence is relative to the viability in the absence of AZD9291 for each condition. Data represent one experiment performed in technical triplicates.

To investigate whether the increased dependency on IGF-1R with AZD9291 treatment was a mechanism of resistance dominating emergence of resistance in H1975 cells, we tested another AZD9291 resistant H1975 cell line (H1975^{9291S2}), that had been generated independently of H1975^{9291S}. Initial experiments indicate that

increased sensitivity to IGF-1R inhibitors is not a common feature of AZD9291 selected H1975 cells (Figure 4-13 B).

4.6.3 Expansion of potential targets and testing of other cell lines

To determine if the identified target(s) were cell line specific, we confirmed proliferation under single agent and combination treatments in other resistant cell lines. We also additionally investigated the AKT inhibitor MK-2206 and the MEK inhibitor AZD6244, as both had previously been reported as promising targets for combination approaches (Huang, Lee et al. 2013, Tricker, Xu et al. 2015).

Treatment of $PC9^{9291S}$ with AZD9291 led to a left shift in the dose response curve for the AURK inhibitor AZD1152, indicating a decrease in IC50 under combination treatment (Figure 4-14 A). Notably, the sensitising effect of the IGF-1R inhibitor OSI906 was selective to $H1975^{9291S}$ cells. In $PC9^{9291S}$ and $HCC827^{GS}$ cells, treatment with OSI906 only led to a mild or no sensitisation of cells to AZD9291, respectively (Figure 4-14 B). Inhibition of AKT using MK-2206 sensitised all cell lines to EGFR-TKIs, with the weakest and strongest shift in dose response curve for the EGFR-TKI being observed in $PC9^{GS}$ and $H1975^{9291S}$, respectively (Figure 4-14 C/D).

Sensitisation of cells to EGFR-TKIs by inhibition of MEK via treatment with AZD6244 was less pronounced with the exception of $PC9^{9291S}$, which harbours an NRAS Q61R mutation. Furthermore, $PC9^{9291S}$ were sensitive to AZD6244 (1 µM, monotherapy), showing a reduction of viability to 51 %.

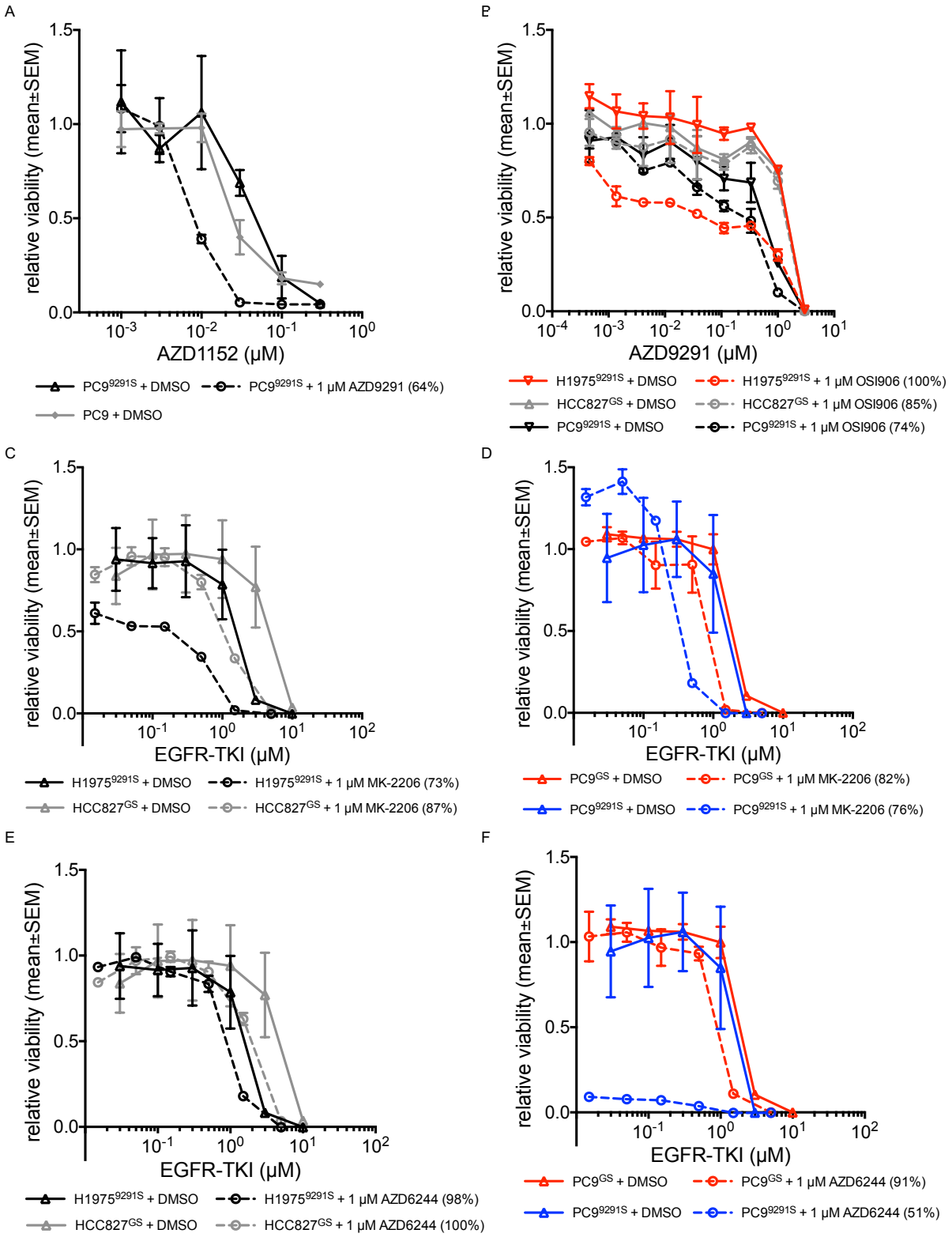


Figure 4-14: Different EGFR-TKI resistant cell lines are differentially sensitive to co-treatment with inhibitors of AURK, IGF-1R, AKT and MEK

Combination studies were performed with AZD9291 for H1975^{9291S}, HCC827^{GS} and PC9^{9291S} and with gefitinib for PC9^{GS}. Effects of combination compounds on their own are indicated in brackets. Viability, as measured by resazurin fluorescence is relative to viability of cells treated without AZD9291 for each condition. Data are from one representative experiment (total n=2), performed in technical triplicates (A) or duplicates (B-F).

4.6.4 Studies of combinations in H1975^{9291S} spheroids

To investigate the ability of these compounds to inhibit the growth of H1975^{9291S} in the more complex spheroid model, compounds were used as single agent and combination treatments. Spheroid size was assessed over time and signalling investigated using western blotting at the end of the experiment, and the studies included additional compounds targeting the MEK (trametinib) and AKT/mTOR (everolimus) pathways.

Compounds had different effects on spheroid growth. No delay of spheroid growth could be observed under treatment with the MEK inhibitor trametinib. Treatment with MK-2206 and everolimus however led to a reduction in spheroid growth. Inhibition of spheroid growth was even greater under treatment with AZD1152 and OSI906. Responses to the inhibitors in combination with AZD9291 were in line with observations from single treatments but the inhibition of spheroid growth by AZD1152 and OSI from the first to the last quantification after treatment addition was more marked than under single treatment. These experiments are however preliminary and statistical testing of significance of differences in spheroid size between the groups has not been performed. Western blotting analysis at the end of the experiment confirmed inhibition of targets and reduction of proliferation under AZD1152 combination treatment, as indicated by reduced levels of pHH3.

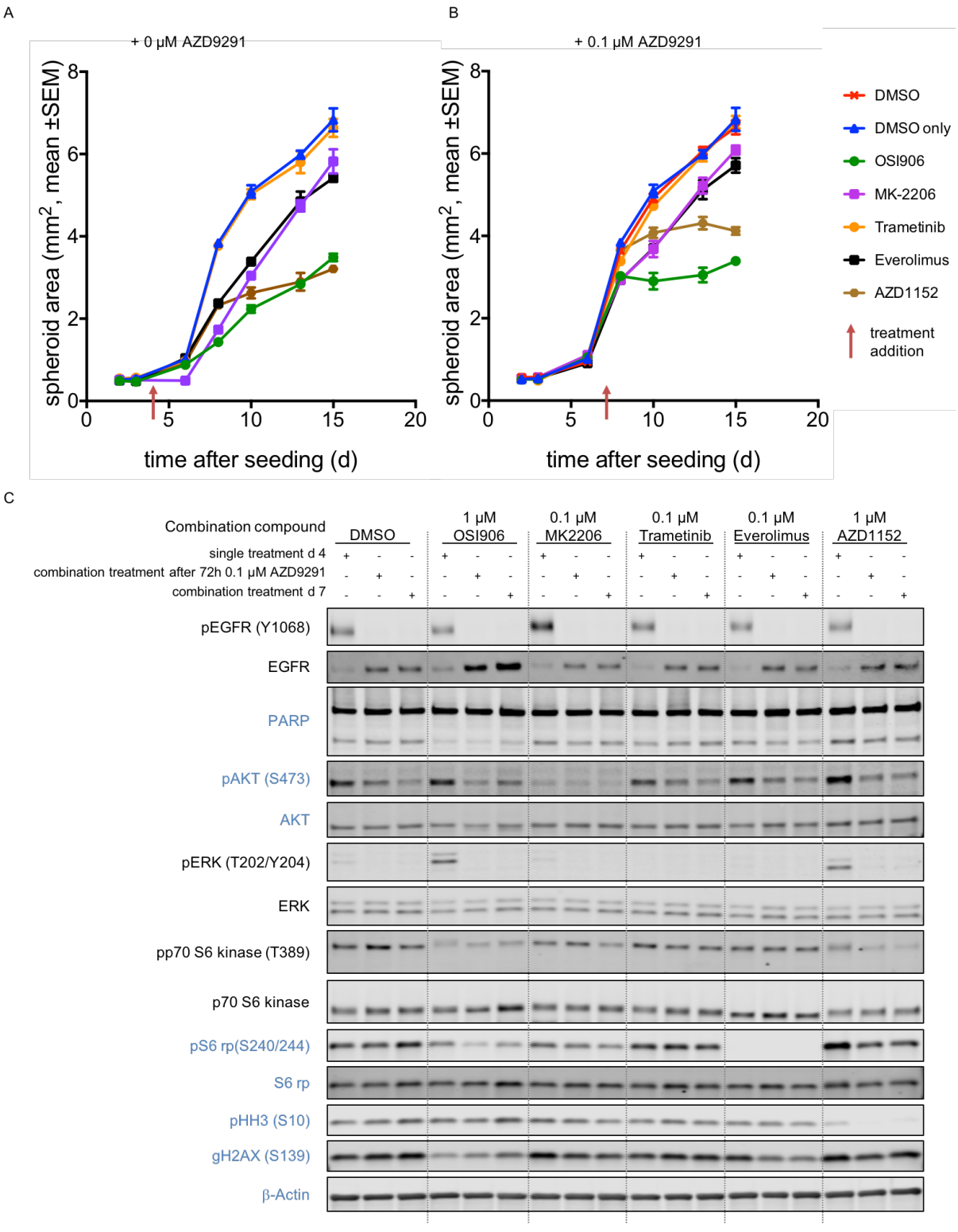


Figure 4-15: Growth of H1975^{9291S} spheroids is inhibited by AURK and IGF-1R inhibitors.

H1975^{9291S} cells were cultured as spheroids and treated with single compounds on day 4 after seeding (A) or compounds in combination with 0.1 µM AZD9291 on 7 after seeding (B). Spheroids were imaged on the Gelcount and spheroid size determined using the Gelcount software. OSI906 and AZD1152 treatment was at 1 µM, other treatments at 0.1 µM. Spheroids were lysed on day 16 after seeding and analysed via western blotting (C). β-actin was used as a loading control and antigens of the same colour writing were detected on the same membrane. Each treatment group consisted of 3 independent spheroids, treated identically.

4.7 Summary of characterisation and overcoming of population-based resistance to EGFR-TKIs

In summary we have shown, that HCC827^{GS} and H1975^{9291S} cells, which follow similar patterns of emergence of resistance EGFR-TKIs do not share a common mechanism of resistance apparent in our RPPA analyses. Changes were however in line with those observed by others in a similarly generated resistant H1975 cell line (Eberlein, Stetson et al. 2015). Surprisingly, RPPA analyses showed reduction in expression/phosphorylation of RTKs (HER2, MET, IGF-1R) and pathways (PI3K, JAK/STAT) thought to be involved in resistance to EGFR-TKIs but the relevance of this is unclear (Sequist, Waltman et al. 2011, Kim, Kwon et al. 2012, Planchard, Loriot et al. 2015, Ou, Wu et al. 2017, Zulkifli, Tan et al. 2017). Metacore pathway analysis of expression changes shared by the two resistant cell lines did not point to a targetable mechanism of resistance but *DUSP6* stood out among the commonly downregulated genes. DUSP6, a phosphatase that regulates cytoplasmic ERK1/2 has been described to impact survival of NSCLC patients (Diaz-Garcia, Agudo-Lopez et al. 2015) and shown to synergise with EGFR-TKIs when overexpressed in EGFR M+ NSCLC cells (Zhang, Kobayashi et al. 2010). As we were unable to identify potential therapeutic options from these analyses, we performed an unbiased compound screen using a bioactive small molecule library. To our knowledge this is the first published study to perform a compound screen of this size in combination with AZD9291, and our novel enrichment approach allowed us to identify key members of the PI3K-AKT-mTOR pathway as well as IGF-1R and AURK as promising targets. The sensitising effect of IGF-1R was cell line specific and dependent on the presence of the EGFR-TKI, whereas inhibition of AURK led to

reduced viability in all tested resistant cell lines in the presence but also absence of EGFR-TKIs compared to sensitive cells.

Expansion of our combination treatment experiments to the NRAS driven PC9^{9291S} cells, showed dramatically increased sensitivity to MEK inhibitors, in line with findings published while this work was ongoing (Eberlein, Stetson et al. 2015).

5 Prevention of emergence of resistance to EGFR-TKIs

In the previous chapter, we described a screen to identify compounds and targets that could be potential approaches to overcoming resistance of EGFR M+ tumours to EGFR-TKIs through mechanisms other than secondary mutations in either EGFR or downstream pathways. In this chapter, we have designed a screen to identify compounds that selectively increase the effectiveness of EGFR-TKIs in EGFR-TKI sensitive NSCLC cells. We reasoned that this alternative approach would identify compounds and targets that might prevent the emergence of resistance. Our research, and studies by other groups have shown, that a subset of cells survives initial drug exposure, which are generally referred to as drug-tolerant cells (Sharma, Lee et al. 2010). These might provide a reservoir of cells, from which acquired mechanisms of resistance (including mutations) can evolve (Sharma, Lee et al. 2010, Hata, Niederst et al. 2016, Ramirez, Rajaram et al. 2016). Considering, that initial survival of these cells may be facilitated by a number of features, including activation of alternative survival pathways, we hypothesised that a combination of EGFR-TKI with other compounds at treatment start could prevent or delay the emergence of EGFR-TKI resistance by increasing cell killing during the EGFR-TKI sensitive phase, thereby decreasing the pool of viable cells from which resistant cells could emerge (Figure 5-1). Furthermore, combination therapies may also have the potential to delay or prevent the entry into a drug tolerant or drug resistant phases.

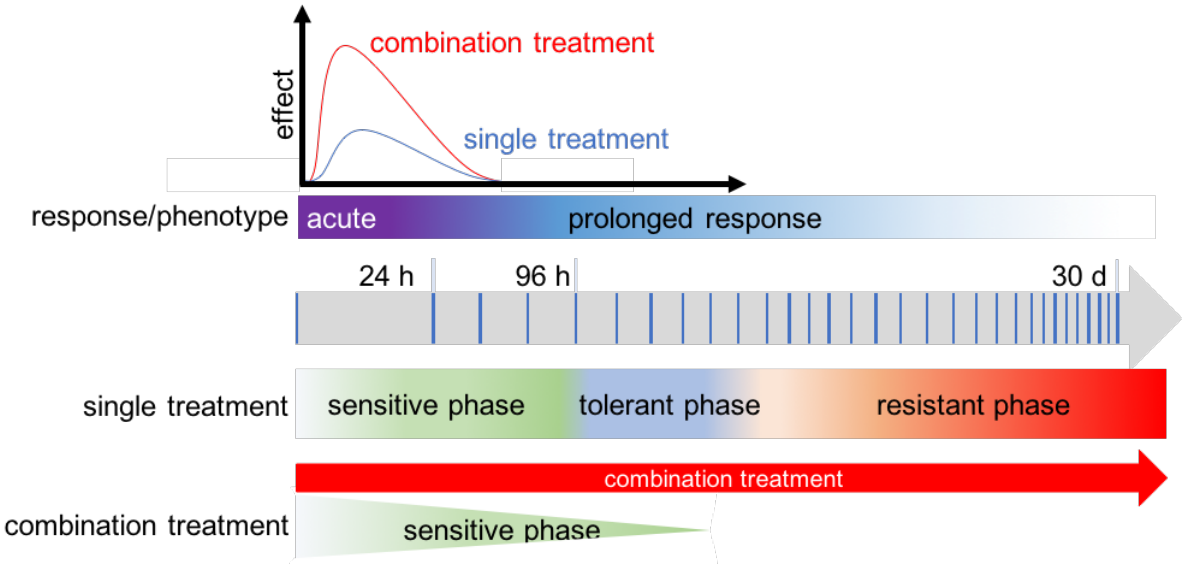


Figure 5-1: Combination treatments might prevent or delay the emergence of resistance by increasing the acute response and by delaying the entry of cells into tolerant and resistant phases.

Schematic of cellular response to EGFR-TKI treatment. EGFR TKI combination treatment has the potential to increase acute response processes in the EGFR-TKI sensitive phase, such as induction of apoptosis and reduction in signalling. This has the potential to reduce cell numbers and delay or prevent the emergence of resistance.

5.1 Compound screen for increased effectiveness of AZD9291 treatment in EGFR-TKI sensitive cells

To identify compounds that could prevent or delay the emergence of resistance, we performed a drug screen using the L1700 compound library (Chapter 4.6). As we had previously observed similar dynamics of response and resistance to AZD9291 in HCC827, H1975 and HCC4006 cell lines (see Figure 3-7 and Figure 3-8), we performed the screen on H1975 as a representative cell line.

A dose of 0.1 µM AZD9291 was chosen, as this dose inhibits cell proliferation but allows for detection of further decreases in proliferation under combination treatments. On average, proliferation was reduced to 32.4 % (± 0.8 %, SEM) on plates treated with 0.1 µM AZD9291 compared to plates treated with DMSO as a treatment control.

The results of the screen are outlined in Figure 3-36 (Table S 10) with the AKT inhibitor MK-2206, and the PI3K inhibitor PI-103 as highest-ranking hits.

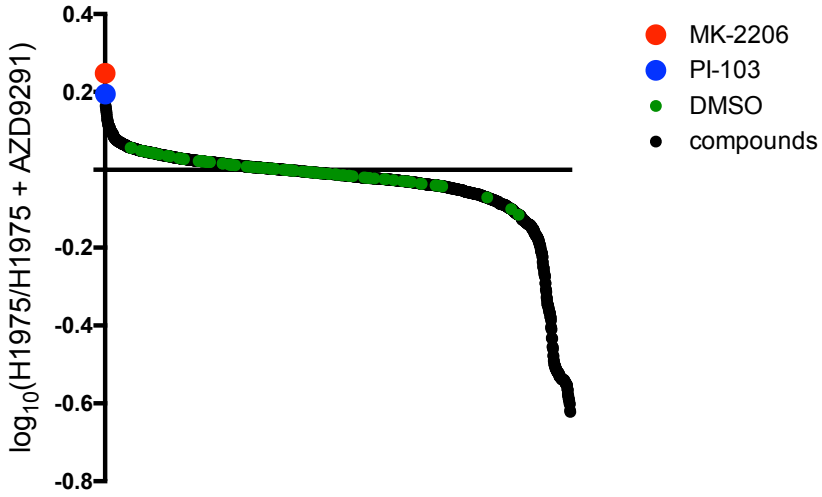


Figure 5-2: Compound ranking for screen for prevention of emergence of resistance.
Compounds of the screen are ranked in decreasing order of ability to sensitise H1975 cells to AZD9291 at a concentration of 0.1 µM. Hits are marked in red and blue, DMSO controls in green and other compounds in black.

5.1.1 Drug target enrichment analysis

As described previously, we wanted to use the screen primarily to identify the most promising targets rather than individual compounds. Therefore, we used drug target enrichment analysis to identify drug targets that were overrepresented in the top or bottom 50 compounds compared to the whole library. This analysis revealed enrichment of 8 targets in the top 50 compounds, with IGF1-R, AKT, mTOR, and PI3K being the most significant and all of which had also been identified as potential targets in EGFR TKI resistant cell lines in chapter 4.6.1. Notably, AURK was not identified as a hit target in this screen, in contrast to the screen in EGFR-TKI resistant cells. Negatively enriched targets (autophagy, CDK, EGFR, HDAC, HSP, kinesin, microtubule associated, PAK, proteasome, survivin and topoisomerase)

were identified but not analysed further in the context of this work (Table 5-1 and examples in Figure 5-3).

Table 5-1: Significantly enriched targets within the 50 most selective compounds

Enriched targets identified via Fisher's exact test in the top 50 compounds for increased inhibition of proliferation in AZD9291 co-treated H1975 compared to H1975. Numbers indicate the fraction of compounds in the top 50 compounds in 0.1 µM library conditions or 1 µM library conditions (#). The p-value for the Fisher's exact test and the number of compounds per target in the entire library are listed.

target	fraction in top 50 compounds	p-value	total count
IGF-1R	0.44	< 0.001	9
AKT #	0.33	< 0.001	12
SYK #	0.33	0.009	6
mTOR	0.21	< 0.001	28
Wnt/beta-catenin #	0.20	0.024	10
PI3K	0.16	< 0.001	37
AChR	0.11	0.011	36

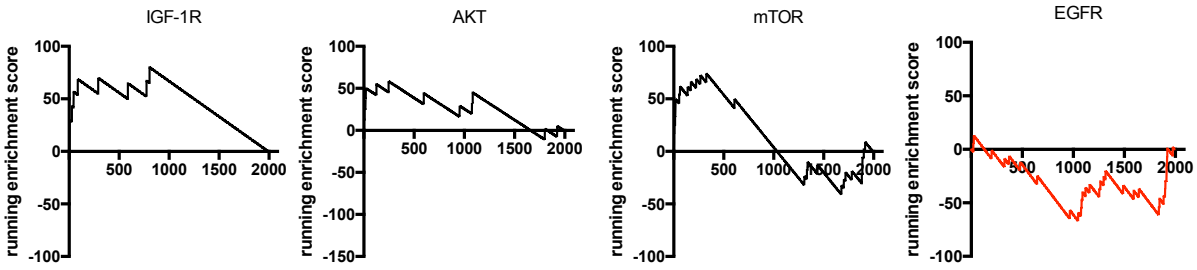


Figure 5-3: IGF-1R, AKT and mTOR inhibitors are positively enriched, as opposed to negatively enriched EGFR inhibitors.

Graphs show the running enrichment score for compounds inhibiting the indicated targets, as calculated using gene set enrichment analysis. Compounds are ranked in order of decreasing $\log_{10}(H1975/H1975^{9291S})$.

In conclusion, our combination screen demonstrated that the top 50 most active compounds were enriched for a number of targets. We focused on the most significantly enriched targets (p<0.001): AKT, mTOR and PI3K, known to play a role in response to EGFR-inhibition (see review by (Gadgeel and Wozniak 2013)) as well

as IGF-1R. As in the previous screen, 3rd generation EGFR-TKIs served as an internal control, showing enrichment amongst the compounds with greater effects under single treatment, compared to combination with AZD9291 (negatively enriched). This is expected, as H1975 cells are highly sensitive to these compounds but the effect of adding these compounds to a dose of 0.1 μM AZD9291 is relatively small.

5.1.2 Confirmation of IGF-1R as a hit target

All tested IGF-1R inhibitors showed greater reduction of H1975 cell viability when combined with AZD9291 treatment compared use as a single agent (Table 5-2 and examples in Figure 5-4).

Table 5-2: All tested IGF-1R inhibitors showed increased inhibition of proliferation in AZD9291 treated compared to untreated H1975 cells.

Ranking of IGF-1R inhibitors (at 0.1 μM) in compound screen and IC50s determined in validation experiments. If IC50 was > 3 μM, relative viability at 3 μM is given in brackets. Data represent IC50 values determined based on one experiment performed in technical duplicates. Compounds marked in green were also identified as hits in the compound screen.[1] numbers in brackets indicate relative viability (to DMSO/0.01 μM AZD9291) of cells at 3 μM IGF-1R inhibitor

		IC50 (μM)	
Rank in screen	**compound**	**IC50 H1975**	**IC50 H1975 + AZD9291**
7	NVP-AEW541	n/d	n/d
9	NVP-ADW742	>3	0.53
31	OSI-906	>1	0.46
48	BMS-754807	n/d	n/d
90	GSK1838705A	n/d	n/d
294	BMS-536924	0.31	0.07
591	AG-1024	n/d	n/d
778	PQ 401	>3 (94 %)[1]	>3 (77 %)
808	GSK1904529A	>3 (109 %)	>3 (54 %)

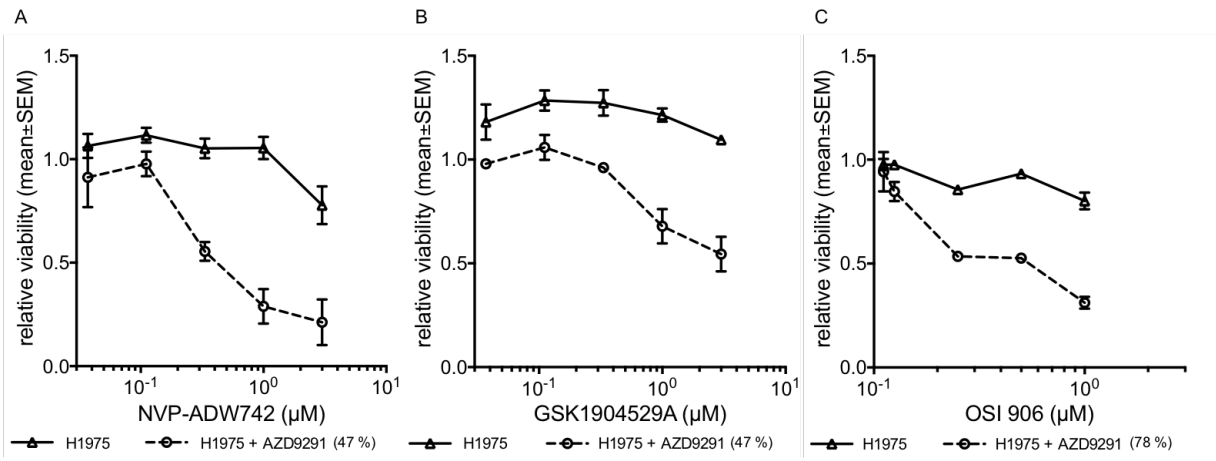


Figure 5-4: H1975 cells are sensitised to IGF-1R inhibitors by AZD9291.

H1975 cells were treated with increasing doses of NVP-ADW742 (A), GSK1904529A (B) or OSI906 (C) in the absence or presence of 0.01 μM (0.003 μM for (C)) AZD9291. Viability, as assessed using the resazurin assay, is relative to 0 μM IGF-1R inhibitor. The effect of AZD9291 treatment alone is indicated in brackets in the legend for each condition (A/B/C). Data are from one representative experiment (total n=2), performed in technical duplicates.

To test whether this was a cell line-specific effect, we assessed proliferation of PC9 and HCC827 under IGF-1R inhibitors in the presence and absence of low doses of AZD9291. PC9 but not HCC827 showed sensitivity to the combination (Figure 5-5).

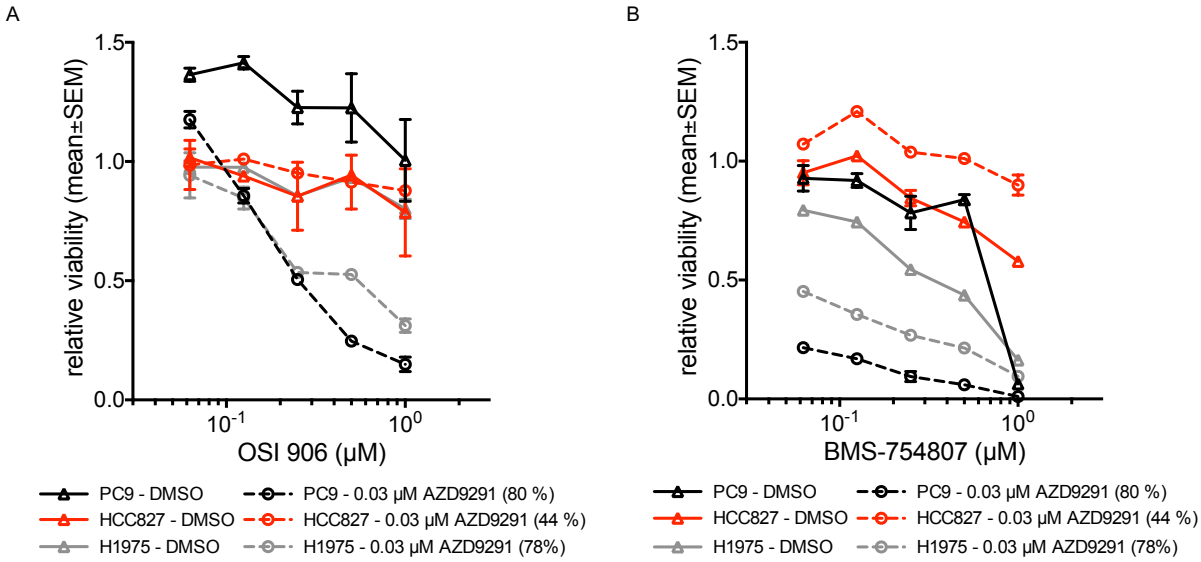


Figure 5-5: The sensitising effect of inhibitors of IGF-1R is cell line specific.

Viability of H1975, PC9 and HCC827 was assessed using resazurin under different doses of the IGF-1R inhibitors OSI906 (A) and BMS-754807 (B) in the presence of absence of 0.03 μM AZD9291. Effects of AZD9291 treatment on viability are indicated in brackets for each experiment. Data are from one representative experiment (total n=2) performed in technical duplicates.

As described previously, signalling is likely to be context specific and spheroids are

considered a valuable model in preclinical testing, bridging between 2D cell culture and in vivo experiments. We therefore assessed the ability of IGF-1R inhibitors to prevent the emergence of resistance in a 3D spheroid model of H1975 cells, as established and described in chapter 3.4 (Figure 5-7). The ability of IGF-1R inhibitors to delay or prevent the emergence of resistance to AZD9291 differed between compounds. NVP-ADW742 treatment led to a delay in spheroid regrowth whereas BMS754807 and OSI906 led to continued shrinkage and disintegration of spheroids over time (Figure 5-7 A-C, grey circles). While single treatment with BMS754807 led to a marked inhibition of spheroid growth, OSI906 only slowed down spheroid growth (Figure 5-7 B/C, grey triangle). This suggests a synergistic effect of AZD9291 and OSI906 on the prevention of emergence of resistance (Figure 5-7 C/D). Notably, addition of any of the IGF-1R inhibitors at the point of emergence of resistance to AZD9291, delayed growth but did not lead to spheroid shrinkage (Figure 5-7 A-C, grey squares).

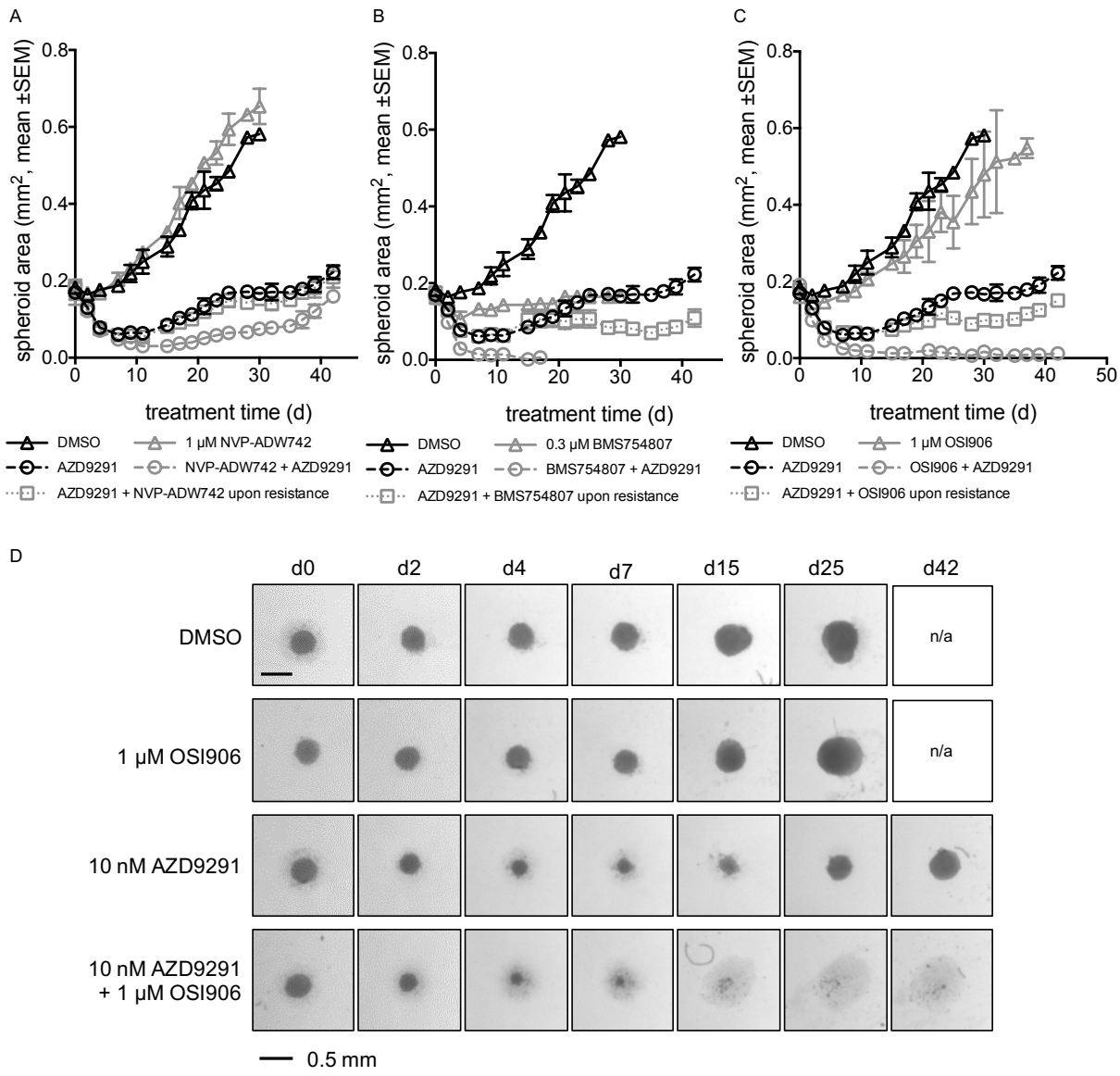


Figure 5-6: IGF-1R inhibitors prevent the emergence of resistance to AZD9291 in H1975 spheroids.

H1975 spheroids were treated with indicated compounds on day 3 after seeding and d15 for combination upon resistance. Quantification of spheroid size for treatment groups is shown in (A), (B), (C) and (D) for the AZD9291 withdrawal, IGF-1R inhibitors NVP-ADW742, BMS754807 and OSI906, respectively. Images of one representative spheroid per group for (D) over time are shown in (E). Images were acquired on the Gelcount ans analysed using the Gelcount software. Data are from one representative experiment (total n=2), performed in technical triplicates. n/a: not available.

5.1.3 AURK combined with EGFR as an approach to preventing the emergence of EGFR-TKI resistance

Surprisingly, in this screen AURK did not come up as a hit, in contrast to IGF-1R, AKT, PI3K and mTOR that had been identified in both screens, for overcoming resistance and preventing resistance. We therefore further investigated this

combination using an apoptosis endpoint. For validation, we also included compounds previously identified to increase apoptosis when combined with EGFR-TKIs, such as AKT, PI3K, BCL2, MEK and FAK as potential positive controls (unpublished data and (Cragg, Kuroda et al. 2007, Hirai, Sootome et al. 2010, Walter, Sjin et al. 2013, Tricker, Xu et al. 2015, Hata, Niederst et al. 2016, Ichihara, Westover et al. 2017)).

To assess whether combination treatments had the potential to accelerate and increase the induction of apoptosis in the acute response phase (chapter 3.1), we utilized the Hoechst apoptosis assay. To be able to distinguish between an increase in extent of apoptosis or an acceleration of apoptosis, we performed time-course experiments. In H1975 cells, AKT, AURK, BCL2, FAK and PI3K but not MEK inhibition increased both the speed and extent of induction of H1975 cell apoptosis when used in combination with AZD9291, compared to induction of apoptosis by AZD9291 alone (Figure 5-7). In contrast, in PC9 cells, BCL2 and PI3K inhibition did not augment AZD9291 induced apoptosis, although surprisingly, MEK inhibition strongly sensitised to AZD9291 treatment (Figure 5-8).

To confirm these results, we performed live cell imaging on CaspeR3-GR expressing PC9 cells using selected combinations treatments. The FAK inhibitor VS-6063 and the AURK inhibitor AZD1152 both led to increased induction of apoptosis when combined with AZD9291 (Figure 5-8 E). Increased apoptosis is less evident under AZD1152 treatment with the quantification method used for the live cell experiments because of the low cell number and apoptotic fraction, as seen in Figure 5-8 G.

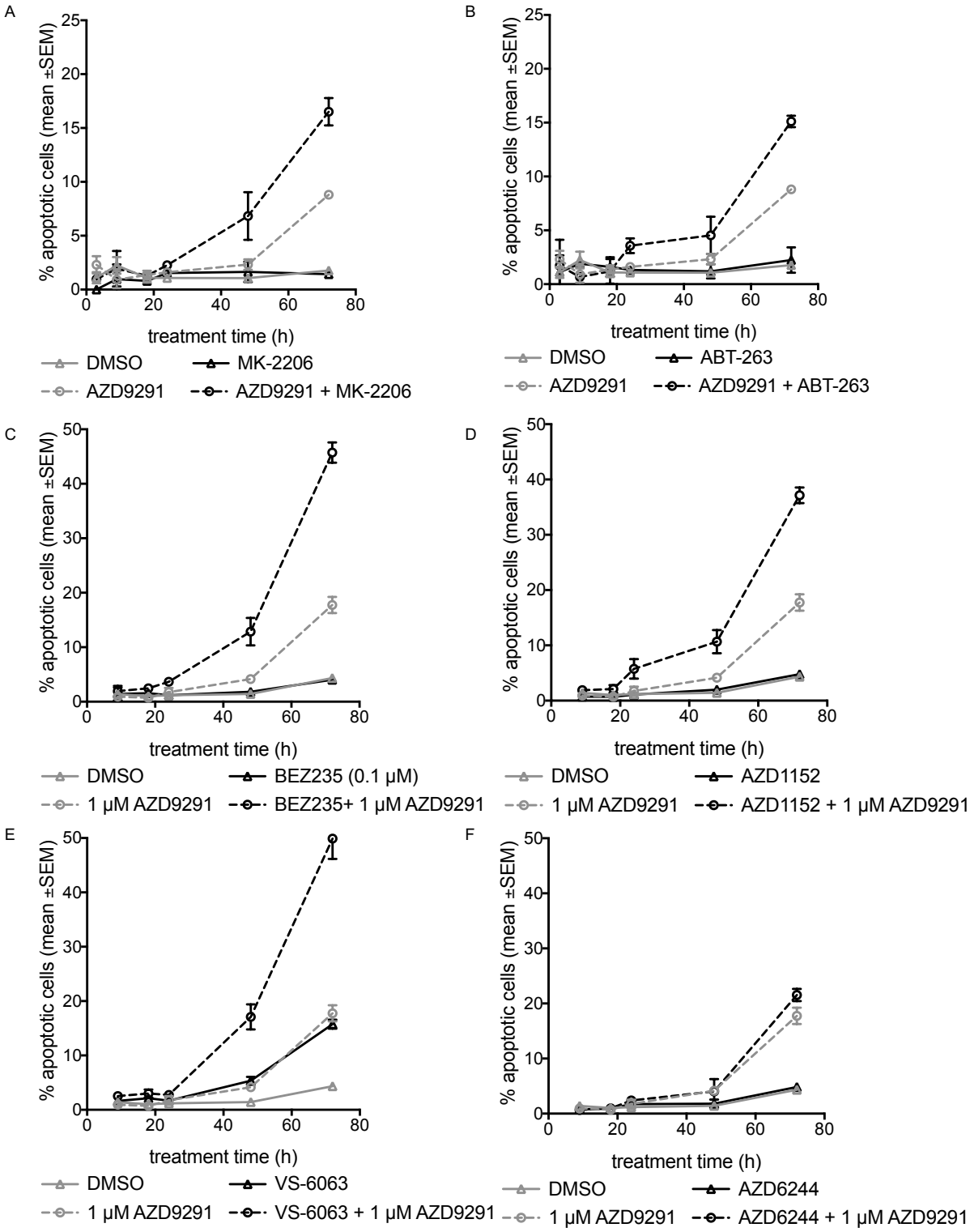


Figure 5-7: Inhibitors of AKT, Aurora Kinase, Bcl-2, FAK and PI3K but not MEK increase the extent and speed of induction of apoptosis under AZD9291 treatment in H1975 cells.

INCell analysis for induction of apoptosis based on the Hoechst assay in H1975 cells. Cells were treated with 0.1 μM AZD9291 (or 1 μM as indicated, C-F) or DMSO and indicated inhibitors were used at 0.1 μM (C), 1 μM (A, B, D, F) or 2 μM for VS-6063 (E). Data are from one representative experiment (total n=2), performed in technical triplicates.

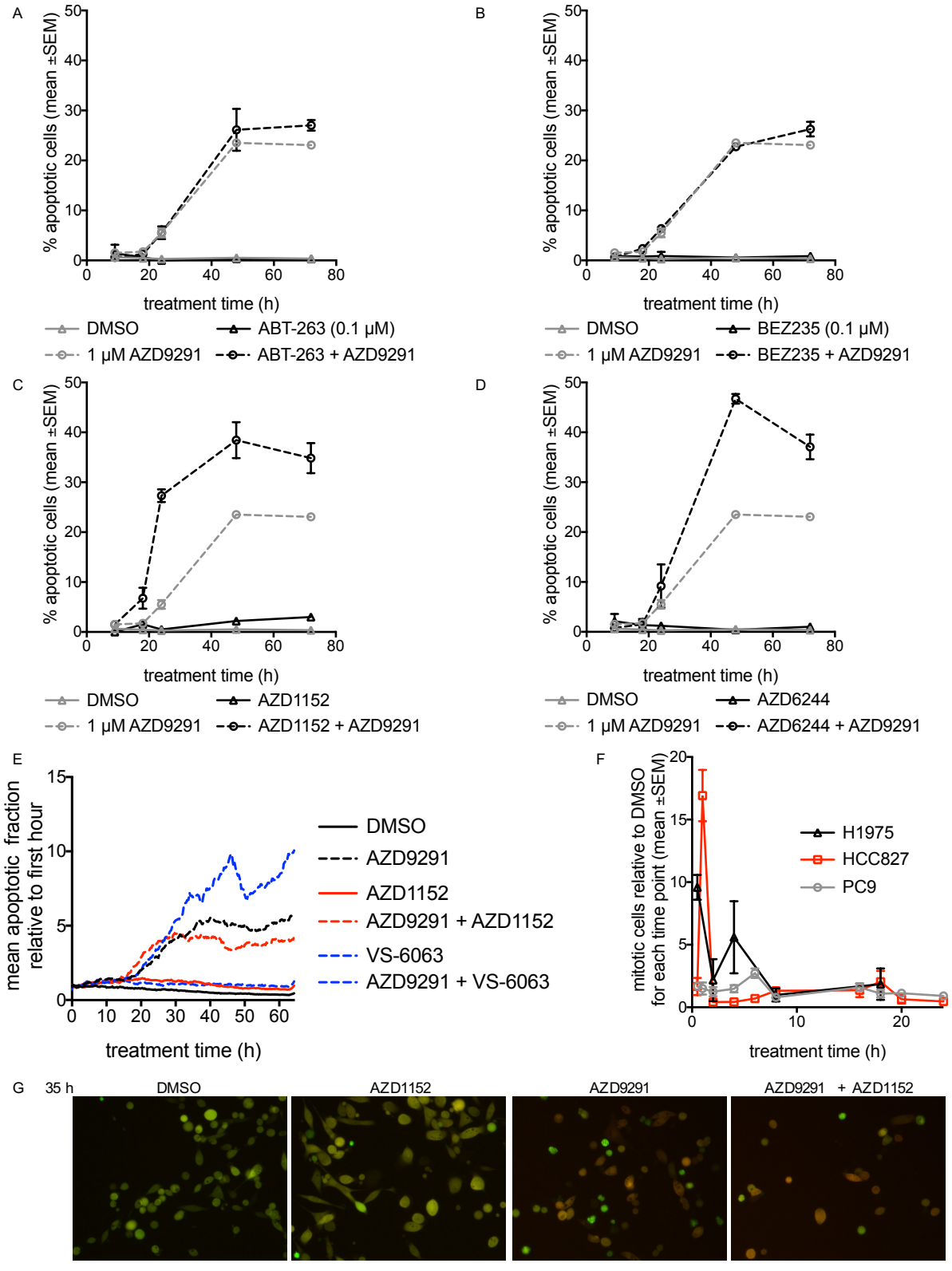


Figure 5-8: Inhibitors of Aurora Kinase, FAK and MEK increase both the extent and speed of induction of apoptosis under AZD9291 treatment in PC9 cells.

INCell analysis of induction of apoptosis based on the Hoechst assay in PC9 cells. Cells were treated with 1 µM AZD9291 or DMSO and indicated inhibitors were used at 0.1 µM (A/B) or 1 µM (C/D). Data are from one representative experiment, performed in technical triplicates. E: The apoptotic fraction per time point using PC9 CaspeR3-GR cells was determined on live cell imaging. Inhibitors were used at 1 µM (2 µM for VS-6063). Data represent the mean of 2 wells per condition. F: Quantification of mitotic cells under treatment with 1 µM AZD9291

over time using the INCell analyser Hoechst assay. Data are relative to the number of mitotic cells under DMSO treatment for each cell line at each time point. Data are from one representative experiment, performed in technical duplicates. G: Representative images of cells under indicated treatments from (E). Apoptotic cells are bright green.

Proliferation assays however only showed a moderate sensitisation to AURK inhibitors (AZD1152 and AT9283) by AZD9291 in H1975 and PC9 cells (Figure 5-9), which might explain why AURK inhibitors were not identified in our screen.

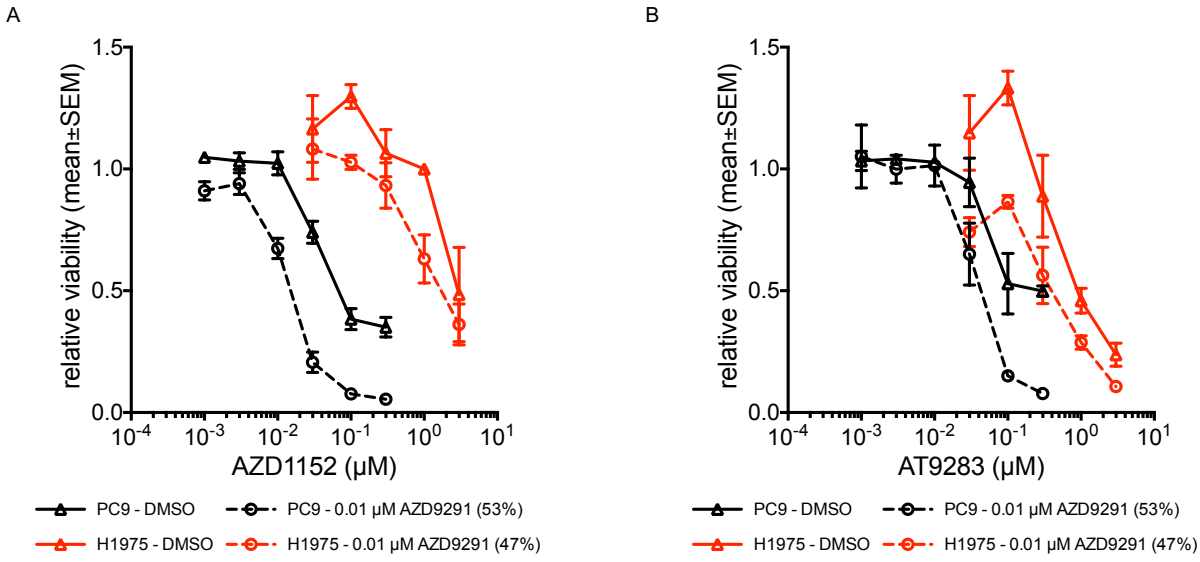


Figure 5-9: Combination effects of AURK and EGFR inhibitors are moderate in EGFR-TKI sensitive cells.
Viability of H1975 and PC9 cells was assessed under different doses of the indicated AURK inhibitors in the presence of absence of AZD9291. Effects of AZD9291 treatment on viability, as assessed using the resazurin assay, are indicated in brackets for each experiment. Data are from one representative experiment (total n=2) performed in technical triplicates.

5.2 Summary prevention of emergence of resistance

Using our unbiased 1902 small molecule screen, we identified compounds that sensitised H1975 cells to the anti-proliferative effects of the EGFR-TKI AZD9291. Our novel enrichment approach identified a number of targets of particular interest, including IGF-1R and the PI3K-AKT-mTOR pathway. As previously, 3rd generation EGFR-TKIs served as a negative control for the screen, as expected showing little additional effect in combination with AZD9291.

Our analyses further suggest, that the increased induction of apoptosis under combination treatments with inhibitors of AKT and PI3K might contribute to the

observed effect. Increased apoptosis under AZD9291 in combination with inhibitors of BCL-2, FAK and MEK was also observed, in line with findings by our group and others (Walter, Sjin et al. 2013, Tricker, Xu et al. 2015). AURK, in contrast, only led to a slight sensitisation to the anti-proliferative effects of AZD9291 treatment despite its ability to sensitise cells to AZD9291 induced apoptosis. Overall, there were differences between cell lines, which might be worthy of future investigation.

Using our assay of prevention of emergence of resistance in 3D spheroids, we showed that inhibition of IGF-1R can increase spheroid shrinkage. Importantly, in contrast to other identified targets (data not shown), we showed that IGF-1R inhibition can also fully prevent emergence of resistance at doses of inhibitors that did not lead to spheroid shrinkage as single treatment.

6 General discussion and conclusion

While KRAS is the most commonly identified oncogene in patients with smoking history, non-smokers most commonly present with activating mutations in EGFR. Standard of care therapy in patients with locally advanced, metastatic tumours are 1st generation EGFR-TKIs (gefitinib or erlotinib) and studies show that the 3rd generation EGFR-TKI AZD9291 prolongs tumour responses as first- and second-line therapy. The majority of patients with EGFR-M+ NSCLC respond well to treatment with EGFR-TKIs and experience marked tumour shrinkage (median tumour shrinkage: 50-60 %, partial response). Unfortunately, after a time of stable disease of 12-18 months, patients develop progressive disease under treatment as resistance to the drug emerges (Figure 6-1 A). A number of mechanisms of resistance have been identified, including secondary mutations in EGFR (e.g. T790M, C797S), activation of parallel or downstream pathways via mutations (e.g. NRAS, PIK3CA), increased protein expression (MET amplification) and histological transformation. However, the mechanism of resistance remains unknown in a substantial proportion of patients and there is a large unmet need for new treatment options.

The aim of this work was, to identify new mechanisms of resistance to EGFR-TKIs that are not related to mutations in EGFR or genetic changes leading to reactivation of downstream pathways, and to identify ways of overcoming and preventing resistance.

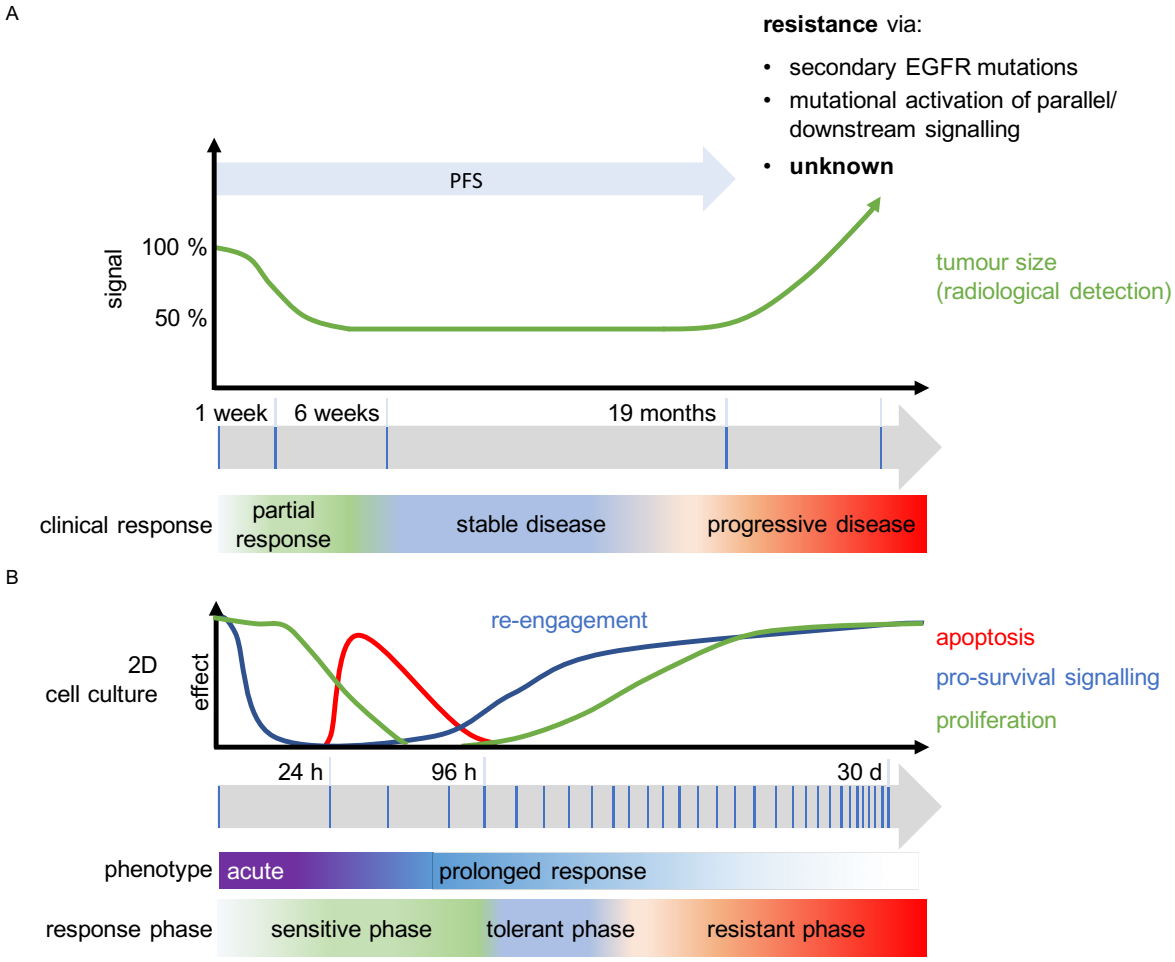


Figure 6-1: Response phases in cell culture models resemble treatment responses in patients under EGFR-TKI treatment

A: Schematic of changes in tumour size under AZD9291 treatment of EGFR M+ NSCLC patients. Illustrative data based on FLAURA trial (Astra Zeneca 2017). B: Schematic of cellular changes under sustained EGFR-TKI treatment in EGFR M+ NSCLC cell lines. Phases of clinical and cellular response as described in the literature and in our work, respectively are indicated below schematics.

We show that, analogous to the responses of patients in the clinic, EGFR M+ NSCLC cells under sustained EGFR-TKI treatment go through a drug sensitive phase, followed by a drug tolerant phase before entering a drug resistant phase, as outlined in comparison to a typical patient response in Figure 6-1.

The sensitive phase is marked by rapid reduction in signalling in all EGFR-dependent cell lines, showing marked reduction in signalling of two key pathways, AKT and ERK but also a number of other pathways, as identified by RPPA. This is in line with results from a number of published studies on 1st generation and 3rd generation

EGFR-TKIs (Sharma, Lee et al. 2010, Cross, Ashton et al. 2014, Yoshida, Zhang et al. 2014, Hirano, Yasuda et al. 2015, Zhang, Belkina et al. 2015, Zhang, Maity et al. 2017). Overall this shows that treatment with EGFR-TKIs leads to a disruption of the pro-proliferative and pro-survival EGFR signalling in cells with activating EGFR mutations.

We further showed that distinct biochemical changes are initiated at different time points even within 24 h of EGFR-TKI treatment, and are then followed by a number of phenotypic changes, including reduction in migration and proliferation and induction of apoptosis. Timing and extent of these changes were cell line dependent with early and extensive apoptosis dominating in PC9, but slower and less extensive apoptosis apparent in H1975 and HCC827. Our findings are consistent with those of other groups, despite variability in observed relative sensitivities to EGFR-TKIs between cell lines (Sharma, Lee et al. 2010, Eberlein, Stetson et al. 2015, Tricker, Xu et al. 2015, Ramirez, Rajaram et al. 2016). Differential responses between cell lines are in agreement with the oncogenic shock model, proposed by Sharma and colleagues and recently reviewed by other groups (Sharma, Fischbach et al. 2006, Sharma and Settleman 2006, Amin, Rajan et al. 2015, Pagliarini, Shao et al. 2015). In cells with constitutively active EGFR, pro-survival and pro-apoptotic signalling initiated by EGFR are in an equilibrium. Sharma and colleagues propose that the differential attenuation rates of pro-survival and pro-apoptotic signals following acute EGFR inhibition can lead to apoptotic death, as the balance between EGFR-mediated pro-survival and pro-apoptotic signalling is disrupted (i.e. pro-apoptotic signalling is reduced more slowly). Based on our results, we postulate that PC9 cells, compared with other cell lines (H1975, HCC827) do not regulate pro-apoptotic

signalling quickly enough to prevent apoptotic death in the majority of cells upon EGFR-TKI treatment (Figure 6-2 A; PC9: slow, H1975/HCC827: quick).

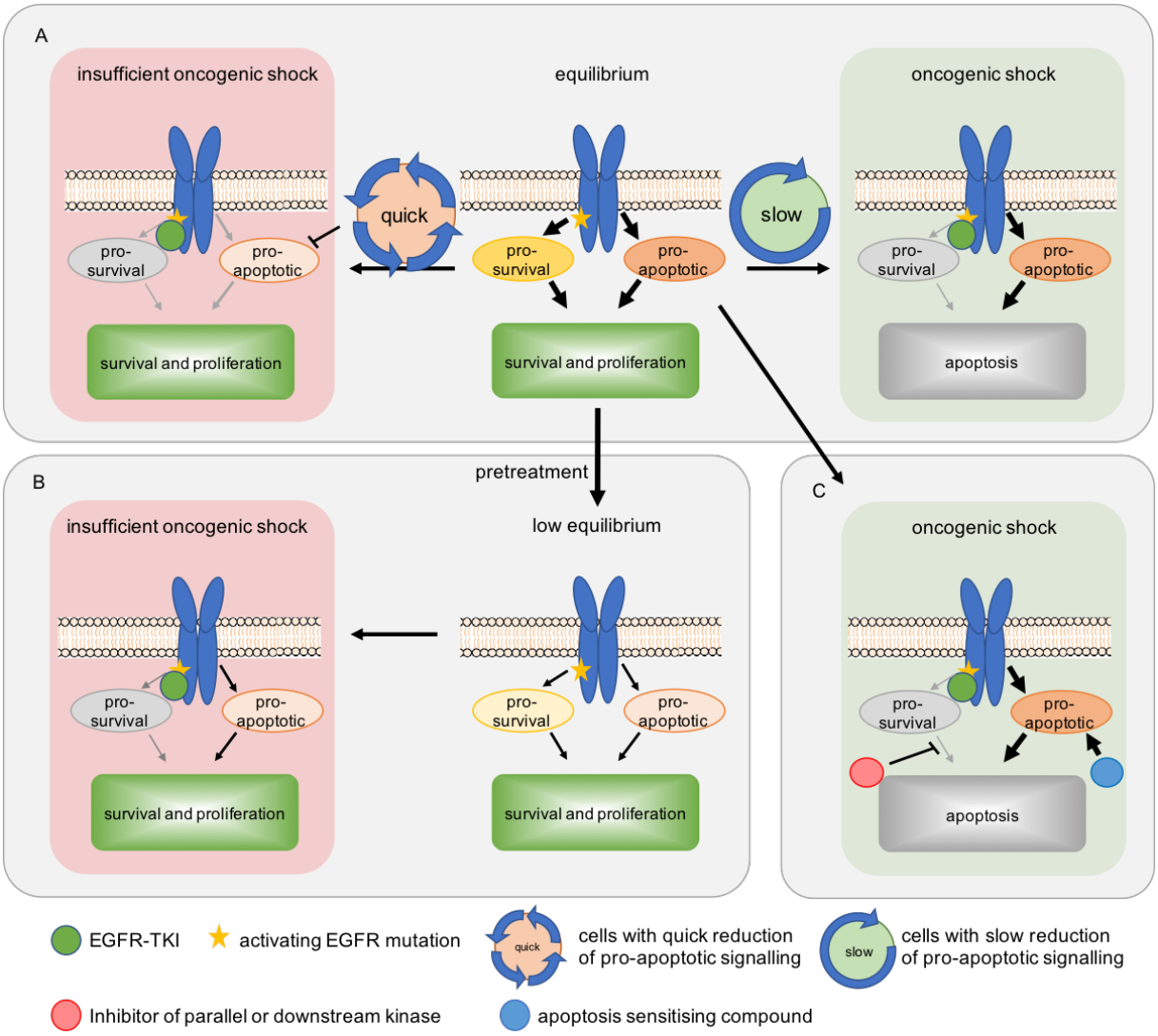


Figure 6-2: The extent of oncogenic shock upon inhibition of pro-survival signalling by EGFR-TKI treatment might influence the emergence of resistance.

Model of changes in pro-survival and pro-apoptotic signalling upon EGFR-TKI treatment based on oncogenic shock model proposed by (Sharma, Fischbach et al. 2006) A: Illustration of apoptosis upon oncogenic shock ()right, green box) and survival after insufficient oncogenic shock (left, red box), depending on the speed of regulation of pro-apoptotic signalling upon EGFR-TKI treatment. B: Pretreatment induced reduction in pro-survival and pro-apoptotic signalling reduces the potential for apoptotic shock induced apoptosis upon EGFR-TKI treatment. C: Concomitant inhibition of EGFR and pro-survival signalling (red circle) or increase of pro-apoptotic signalling (blue circle) increases the potential for oncogenic shock and apoptosis upon EGFR-TKI treatment.

For the less pro-apoptotic H1975 and HCC827 cell lines, the majority of cells survived and this population of cells entered a drug tolerant phase, marked by re-engagement of EGFR downstream signalling as early as 72-96 h after treatment start. This was followed by re-engagement of cell proliferation under EGFR-TKI

treatment, marking the resistant phase. This observation matches other studies, which report re-engagement of signalling as early as 16-96 h in a number of EGFR M+ NSCLC cell lines (Ercan, Xu et al. 2012, Eberlein, Stetson et al. 2015, Tricker, Xu et al. 2015, Ichihara, Westover et al. 2017). To our knowledge, however, ours is the first study documenting both the re-engagement of signalling and subsequent proliferation under continued EGFR-TKI treatment to this extent, and describing distinct phases of sensitivity, tolerance and resistance under 2D culture conditions. We were unable to identify the engagement of potential survival mechanisms common to PC9 and H1975 occurring in the time frame up to 24 h in our RPPA analyses. Considering the differences in fate after EGFR-TKI treatment however, future work will need to perform cell-line-specific analyses and include additional time points, to account for differences in timing of phenotypic responses.

Spheroid models are considered an important intermediate step to increase translatability of results from 2D *in vitro* studies into *in vivo* studies. We therefore performed some parallel experiments in 3D spheroid models of H1975 cells to confirm our 2D findings. To our knowledge, this is the first study looking at effects of sustained EGFR-inhibition in 3D models of EGFR M+ NSCLC cells. This might however be of relevance, as we show that there are marked differences in EGFR downstream signalling in 3D spheroids compared to 2D, in line with observations by other groups (Ekert, Johnson et al. 2014, Riedl, Schlederer et al. 2016). Our time course experiments show increased sensitivity in 3D compared to 2D, as well as an increased dynamic range for the reduction of cell numbers. Treatment with doses as low as 10 nM AZD9291 led to a marked shrinkage in spheroid size as opposed to a response dominated by cell survival in 2D under treatment with 1 μM AZD9291. The time to re-engagement of signalling and mean spheroid growth was longer in 3D

compared to 2D and marked by inter-spheroid heterogeneity that increased over time under sustained EGFR-TKI treatment. Though our 3D work so far is exploratory, it may have potential to identify resistance mechanisms not identifiable by 2D approaches, but clinical relevance or mechanism of 3D resistance has yet to be determined.

Our *in vivo* data from experiments using subcutaneous xenografts are further in line with these observations. Treatment with EGFR-TKIs led to initial tumour shrinkage, followed by stabilisation of tumour size. Even under long-term treatment tumours remained viable, showed growth under drug withdrawal and suggestions of increased resistance when cultured *ex vivo*. Preliminary experiments using a potentially more relevant orthotopic model however shows more marked regrowth and increased heterogeneity in tumour responses. In line with data published by a number of groups, this might be due to the slower process of emergence of resistance *in vivo*. A number of groups observed emergence of resistance in subcutaneous xenograft and transgenic *in vivo* models (Politi, Fan et al. 2010, Ercan, Xu et al. 2012, Cross, Ashton et al. 2014, Tricker, Xu et al. 2015, Chabon, Simmons et al. 2016, Emdal, Dittmann et al. 2017). Reported mechanisms of resistance in these studies include EGFR T790M mutations and reactivation of ERK (in some cases through MET amplification) (Politi, Fan et al. 2010, Tricker, Xu et al. 2015, Chabon, Simmons et al. 2016). Overall our 3D and *in vivo* data show effects consistent with drug sensitive, tolerant and resistant phases observed in 2D. Observations suggest, that a population-based change allows emergence of resistance in all models, rather than resistance being driven by a small subpopulation with a resistance-conferring mutation. Our 3D and *in vivo* data are however more limited, as we have not assessed changes in signalling as frequently over the course of treatment.

Sharma et al. first described a drug tolerant population in EGFR-TKI treated PC9 cells upon treatment with EGFR-TKIs that showed little-to-no growth under treatment but eventually became resistant and proliferated in the presence of EGFR-TKIs. These cells are referred to as drug tolerant persisters (Sharma, Lee et al. 2010). Further studies by Sharma and other groups showed, that these drug tolerant cells might form a reservoir of cells, from which acquired mechanisms of resistance (including mutations) can evolve (Hata, Niederst et al. 2016, Ramirez, Rajaram et al. 2016). This might be equivalent to our observations of the survival of a substantial population of the less pro-apoptotic H1975 and HCC827 cells during EGFR-TKI treatment.

In order to characterise resistance mechanisms, we generated EGFR-TKI resistant cell lines. In line with observations from experiments on cellular response to EGFR-TKI treatment in the first chapter, emergence of resistance in pro-apoptotic PC9 cells was dominated by the formation of resistant clones, while other cell lines survived as resistant populations. Cells were able to grow in doses of EGFR-TKIs >100 x IC50 and showed cross-resistance to other EGFR-TKIs of the 1st, 2nd and 3rd generation (except for gefitinib selected PC9). Resistance to EGFR-TKIs was maintained even after long-term culturing of resistant cells in the absence of EGFR-TKIs, suggesting a stable change in our cell lines, whereas observations in the literature are varied, with some studies similar to ours, whereas resistance is lost over time in others (Koizumi, Shimoyama et al. 2005, Sharma, Lee et al. 2010, Chmielecki, Foo et al. 2011, Cortot, Repellin et al. 2013). We showed that pre-treatment with low doses of EGFR-TKIs could increase the number of resistant clones. A potentially interesting observation from the clinic in this context is the lack of benefit of combined EGFR-TKI and chemotherapy treatment (Faehling, Eckert et al. 2013, Goldberg, Oxnard et al. 2013,

Halmos, Pennell et al. 2015, Soria, Kim et al. 2016). Returning to the oncogenic shock model, pre-treatment with low doses of EGFR-TKIs or chemotherapy would reduce cell proliferation and reduce the potential for a sufficient oncogenic shock upon EGFR-inhibition (Figure 6-2 B) (Sharma, Fischbach et al. 2006, Sharma, Gajowniczek et al. 2006).

A number of mechanisms are known to confer resistance to 1st and 3rd generation EGFR-TKIs in the clinic and are commonly detected in *in vitro* experiments, including EMT, re-activation of signalling via diverse mechanisms, on-target mutations and mutations in kinases affecting downstream signalling, which can confer similar levels of resistance as we observed in our cell lines (Koizumi, Shimoyama et al. 2005, Engelman, Zejnullahu et al. 2007, Ercan, Choi et al. 2015, Yoshida, Song et al. 2016). We showed that resistance in PC9 clones was driven by mutations in EGFR T790M and NRAS Q61R after gefitinib and AZD9291 selection, respectively, resulting in AZD9291 sensitivity of T790M positive gefitinib-resistant cells. In line with activation of NRAS by the Q61R mutation, these cells showed hypersensitivity to MEK inhibition, as also described in a study by Eberlein et al., published while this work was ongoing (Eberlein, Stetson et al. 2015). Findings by us and other groups demonstrate that pre-treatment of cells with mutagens increased the number of resistant PC9 clones, stressing the importance of mutations in the emergence of resistance to EGFR-TKIs (Koizumi, Shimoyama et al. 2005, Ercan, Choi et al. 2015). Recent work by a number of groups shows, that such mutations can pre-exist but can also be acquired under long-term EGFR-TKI treatment (Bhang, Ruddy et al. 2015, Hata, Niederst et al. 2016, Ramirez, Rajaram et al. 2016).

We were unable to identify known resistance-conferring mutations in resistant H1975 and HCC827 populations using RNAseq and analyses of expression using RPPA

and RNAseq did clearly identify EMT or any other mechanism of resistance common to the two cell populations. Overall, our findings are in line with those of other groups, showing generation of cell lines with marked resistance in a number of cell lines (Eberlein, Stetson et al. 2015, Hata, Niederst et al. 2016).

Though we have not characterised the mechanisms of resistance in resistant cells from our 3D or *in vivo* long-term experiments for mechanisms of resistance, we believe that they are likely to represent a population-based emergence of resistance rather than a process driven by resistance-conferring mutations. More work would be needed to compare 2D, 3D and *in vivo* models to observations in the clinic to determine whether 3D models of established cell lines or patient derived cell lines (spheroids, PDX, CDX) or transgenic models are able to identify mechanisms of resistance that are not observed in 2D but potentially clinically relevant.

Though we were unable to identify a clear biological process suitable for therapeutic targeting via RPPA and RNAseq in resistant populations, these data suggested significant differences in global transcription and signalling. This is in agreement with other studies, which find that drug resistant cells that are not associated with resistance-conferring mutations show expression profiles that differ from both parental cells and cells with mutation-driven resistance, suggesting a fundamental change and not only selection of a pre-existing population (Sharma, Lee et al. 2010, Hata, Niederst et al. 2016).

In order to identify therapeutic options for overcoming and preventing resistance to EGFR-TKIs, we performed a compound screen. Multiple studies have identified newly arisen sensitivities to combination treatments in resistant cell lines (e.g. sensitivity to MEK inhibitors upon ERK-reactivation or MET inhibitors upon MET

driven resistance) (Ercan, Xu et al. 2012, Nakagawa, Takeuchi et al. 2012, Eberlein, Stetson et al. 2015). Similarly, it has been described that combination therapies can prevent or delay the emergence of resistance (e.g. MEK or BCL-2 inhibitors) (Cragg, Kuroda et al. 2007, Eberlein, Stetson et al. 2015). Considering the oncogenic shock model in the context of EGFR-TKI treatment, a possible mechanism for combination therapies becomes apparent. Research by our group and others supports the hypothesis, that a number of alterations in the cell (e.g. signalling changes, (epi)genetic changes) might render cells capable of surviving during the time window between the decay of survival signals and pro-apoptotic signals after EGFR-TKI treatment. This allows cells to survive and become resistant. Inhibition of targets like MEK might lead to faster and more complete reduction of pro-survival signalling. Alternatively, inhibition of BCL-2 has increased pro-apoptotic signalling, thus increasing cell killing and decreasing the size of the reservoir of drug tolerant cells (Figure 6-2 C)(Sharma and Settleman 2006).

To our knowledge, this is the first study using a compound screen of this size to investigate the potential of combination therapies with AZD9291 to overcome and prevent resistance. Selection of the nearly 2000 bioactive compounds was unbiased - not driven by known mechanisms of resistance - and covered a broad range of nearly 200 targets. Our screen was performed at compound concentrations of 1 µM and 100 nM. This was a practical compromise due to the size of the library and the screening protocol but would likely lead to false negative hits compared to screening approaches covering more compound concentrations e.g. from 10 µM to 10 nM. Using selected compounds, other groups have performed compound screens for the identification of combination therapies (Crystal, Shaw et al. 2014, Eberlein, Stetson et al. 2015, Hata, Niederst et al. 2016, Ramirez, Rajaram et al. 2016) as well as

screens for synthetic lethal interactions to characterise EGFR inhibitor resistance as well as signalling dependencies in sensitive cells and thereby identify suitable combination approaches (reviewed by (Vyse, Howitt et al. 2017)). We utilised our more comprehensive screening approach (1902 compounds) for the identification of compounds for overcoming and for preventing resistance in combination with AZD9291 in EGFR-TKI resistant H1975^{9291S} and EGFR-TKI sensitive H1975 cells, respectively. Our novel enrichment approach identified overrepresentation of a number of targets in the compounds that were most effective in both combination settings. The strongest enrichments were seen for the PI3K-AKT-mTOR pathway, IGF-1R and AURK. Most targets were present in both screen settings. A number of studies have investigated the role of the PI3K-AKT-mTOR pathway in resistance to EGFR-TKIs as well as therapeutic options, and therefore our work focused on IGF-1R and AURK (Puglisi, Thavasu et al. 2014, Jacobsen, Bertran-Alamillo et al. 2017).

The Insulin-like growth factor 1 receptor (IGF-1R) is a RTK that is activated by binding of its ligands (IGF-1/2) and it plays a role in both cell growth and survival control, mainly signalling through the PI3K-AKT-mTOR and RAS-MAPK pathways (reviewed by (Pollak 2008, Pollak 2012)). A number of IGF-1R targeting therapies have been developed, including small molecule inhibitors (reviewed by (Arcaro 2013)).

We showed that inhibition of IGF-1R led to marked sensitisation of EGFR-TKI resistant H1975^{9291S} cells in combination with EGFR-TKIs. However sensitivity of EGFR-TKI resistant H1975^{9291S} cells to IGF-1R inhibitors was not generally increased. This supports the notion that IGF-1R signalling acts as bypass mechanism in this context (as described for other RTKs, including HER2 and MET (Engelman, Zejnullahu et al. 2007, Sequist, Waltman et al. 2011, Yu, Arcila et al.

2013)). This bypass mechanism is not crucial for survival in the absence of EGFR inhibition but potentially sufficient to sustain cell survival and proliferation under EGFR-TKI treatment. Importantly, this was not a feature common to all EGFR-TKI resistant cells. In fact, this feature was not even shared by a different, independently generated EGFR-TKI resistant H1975 population. This is in line with observations by Ramirez et al., showing that cells from the same original cell population develop different mechanisms of resistance, even when under the same culture conditions (Ramirez, Rajaram et al. 2016). This is further reflected in results published by other groups, identifying IGF-1R signalling as a mechanism of resistance and showing sensitivity to IGF-1R combinations in some but not all cell lines generated within one experiment or isolated from different patients (Morgillo, Woo et al. 2006, Cortot, Repellin et al. 2013, Crystal, Shaw et al. 2014, Eberlein, Stetson et al. 2015).

The ability of IGF-1R inhibitors to increase sensitivity of EGFR-TKI sensitive cells to AZD9291 was however apparent in the majority of tested cell lines and inhibition of IGF-1R and EGFR was the most effective combination in spheroids, leading not only to a delay in emergence of resistance as observed for other combinations, but disintegration of treated spheroids and prevention of emergence of resistance. Despite our promising results and positive data from a number of groups (Sharma, Lee et al. 2010, Hata, Niederst et al. 2016) and positive patient responses in a small phase I study, combining a 1st generation EGFR-TKI with an IGF-1R inhibitor (Macaulay, Middleton et al. 2016), phase II studies showed no clinical benefit as first line therapy in patients with EGFR M+ NSCLC or as second line therapy in EGFR M+ or EGFR WT NSCLC (Leighl, Rizvi et al. 2016, Ciuleanu, Ahmed et al. 2017). Despite the possibility that effects observed in established cell lines and patient-derived cells in preclinical experiments are due to culturing conditions, we

hypothesise that IGF-1R might play a role in resistance in some but not all patients. Considering that clinical studies have been performed without patient selection, future work will have to focus on the identification of biomarkers that could identify the patients with tumours most likely to respond to combination therapy with IGF-1R and EGFR inhibitors. Potential biomarkers might include levels of IGF-1R (high levels linked to progressive disease and shorter PFS (Peled, Wynes et al. 2013, Yeo, Park et al. 2015)), circulating IGF-1 or IGF-2 (Pollak 2012).

As illustrated by the lack of clinical benefit in IGF-1R-/EGFR-TKI combinations and postulated by a number of researchers, targeting of one specific bypass mechanism might allow for treatment of a resistant subclone of tumours but might not eliminate the tumour, due to intra-tumour heterogeneity observed in patients and associated multiple potential bypass mechanisms (Burrell and Swanton 2014, Zhao, Hemann et al. 2014, McGranahan and Swanton 2015, Schmitt, Loeb et al. 2016, Suda, Murakami et al. 2016).

Clinical benefit might be more readily achievable by targeting sensitivities that have the potential to be universal, as for example sensitivity to AURK inhibition. Aurora kinases (AURK) are a family of kinases (A, B & C) that are involved in multiple mitotic events. AURK A and B have been described to have functions in somatic cell division, while AURK C is thought to play a role in the meiotic cell cycle (Quartuccio and Schindler 2015). Functions of AURK A/B have been reviewed extensively (Andrews, Knatko et al. 2003, Hochegger, Hegarat et al. 2013). In short, although they have some overlapping functions, AURK A is essential for centrosome separation, duplication and maturation as well as in bipolar spindle assembly and stability. AURK B, which localises to centromeres is required for chromosome condensation and alignment and cytokinesis. A number of AURK inhibitors have

been developed which differ in their selectivity for AURK A/B/C, as reviewed by others (Gautschi, Heighway et al. 2008, Dar, Goff et al. 2010, Falchook, Bastida et al. 2015). A clinical trial in NSCLC patients (with WT EGFR) of the AURK A inhibitor alisertib with erlotinib was initiated but has currently paused recruitment for protocol amendment ((Godwin, Mehra et al. 2016), NCT01471964: accessed 03.10.2017)

We showed that a subset of tested AURK inhibitors sensitised all tested EGFR-TKI resistant cells to EGFR-TKI treatment. In contrast to findings with IGF-1R inhibitors, $H1975^{9291S}$ cells were sensitive to single agent treatment even in the absence of AZD9291 with a number of AURK inhibitors, compared to responses observed in EGFR-TKI sensitive H1975 cells. Our findings are in line with observations published by others while this work was ongoing, showing sensitivity to the AURK B inhibitor AZD1152 in a subset of tested EGFR-TKI resistant patient-derived and established cell lines (Crystal, Shaw et al. 2014) and in several EGFR-TKI resistant H1975 and PC9 cells (Eberlein, Stetson et al. 2015). Investigations into the effects of AURK inhibition on further sensitisation of EGFR-TKI sensitive cells to EGFR inhibition, showed a marked induction of apoptosis (similar to BCL-2, MEK, FAK, which have been shown to delay or prevent the emergence of resistance (Cragg, Kuroda et al. 2007, Eberlein, Stetson et al. 2015, Ichihara, Westover et al. 2017)), but only a moderate effect on proliferation, explaining why AURK was not identified in our screen in EGFR-TKI sensitive H1975 cells.

To prioritise the combination of AURK inhibitors and EGFR-TKIs in EGFR M+ NSCLC in the clinic, future work will have to expand the *in vitro* findings and confirm effects on the potential for prevention and overcoming of resistance *in vivo*. Furthermore, identification of the mechanism of interaction will have to be a focus of future work. One study proposes a functional link between EGFR and AURK A in

lung cancer cells involving phosphorylation by AURK A at EGFR-T654 and S1046, which still occurs in the EGFR M+ NSCLC cell line H1975 (Chen, Liu et al. 2013). However, little has been published in terms of follow-up work and this putative functional interaction remains poorly characterised. Nonetheless, this observation when considered alongside our data may make AURK A and B worthy of future investigation in the context of EGFR M+ lung cancer. As with IGF-1R, it will however be crucial to identify biomarkers for patient selection for AURK combination in the clinic.

In conclusion, our work shows that sustained exposure of EGFR M+ NSCLC cells *in vitro* to high concentrations of EGFR-TKIs identifies three phases of drug response; sensitive, tolerant and resistant, associated with distinct phenotypic responses, culminating in the emergence of a highly EGFR-TKI resistant population of cells. Using these resistant cells and sensitive cells, we show that combination treatment of EGFR-TKIs with IGF-1R inhibitors might be an attractive approach to prevent or overcome resistance to EGFR-TKIs, if suitable biomarkers for patient selection are identified. Similarly, targeting of AURK might be a novel and potentially more broadly applicable approach to overcoming and maybe preventing EGFR-TKI resistance.

Bibliography

Abdel-Rahman, M., D. Stockton, B. Rachet, T. Hakulinen and M. P. Coleman (2009). "What if cancer survival in Britain were the same as in Europe: how many deaths are avoidable?" Br J Cancer **101 Suppl 2**: S115-124.

Alvarez, J. V., H. Greulich, W. R. Sellers, M. Meyerson and D. A. Frank (2006). "Signal transducer and activator of transcription 3 is required for the oncogenic effects of non-small-cell lung cancer-associated mutations of the epidermal growth factor receptor." Cancer Res **66**(6): 3162-3168.

Amann, A., G. Gamerith, J. M. Huber, M. Zwierzina, W. Hilbe and H. Zwierzina (2015). "Predicting drug sensitivity by 3D cell culture models." memo - Magazine of European Medical Oncology **8**(1): 77-80.

American Cancer Society (2017). "Cancer Facts & Figures 2017.".

Amin, A. D., S. S. Rajan, M. J. Groysman, P. Pongtornpipat and J. H. Schatz (2015). "Oncogene Overdose: Too Much of a Bad Thing for Oncogene-Addicted Cancer Cells." Biomark Cancer **7**(Suppl 2): 25-32.

Andrews, P. D., E. Knatko, W. J. Moore and J. R. Swedlow (2003). "Mitotic mechanics: the auroras come into view." Curr Opin Cell Biol **15**(6): 672-683.

Arcaro, A. (2013). "Targeting the insulin-like growth factor-1 receptor in human cancer." Front Pharmacol **4**: 30.

Arkhipov, A., Y. Shan, R. Das, N. F. Endres, M. P. Eastwood, D. E. Wemmer, J. Kuriyan and D. E. Shaw (2013). "Architecture and membrane interactions of the EGF receptor." Cell **152**(3): 557-569.

Artal Cortes, A., L. Calera Urquizu and J. Hernando Cubero (2015). "Adjuvant chemotherapy in non-small cell lung cancer: state-of-the-art." Transl Lung Cancer Res **4**(2): 191-197.

Astra Zeneca. (2017). "AstraZeneca's TAGRISSO® (osimertinib) shows potential as a new standard of care in 1st-line EGFR-mutated non-small cell lung cancer at ESMO 2017 Congress." Retrieved 13.09.2017, from https://www.astrazeneca-us.com/media/press-releases/2017/astrazenecas-tagrisso-osimertinib-shows-potential-as-a-new-standard-of-care-in-1st-line-egfr-mutated-non-small-cell-lung-cancer-at-esmo-2017-congress-09082017.html.

Avizienyte, E., R. A. Ward and A. P. Garner (2008). "Comparison of the EGFR resistance mutation profiles generated by EGFR-targeted tyrosine kinase inhibitors and the impact of drug combinations." Biochem J **415**(2): 197-206.

Awad, M. M., G. R. Oxnard, D. M. Jackman, D. O. Savukoski, D. Hall, P. Shivdasani, J. C. Heng, S. E. Dahlberg, P. A. Janne, S. Verma, J. Christensen, P. S. Hammerman and L. M. Sholl (2016). "MET Exon 14 Mutations in Non-Small-Cell Lung Cancer Are Associated With Advanced Age and Stage-Dependent MET Genomic Amplification and c-Met Overexpression." J Clin Oncol **34**(7): 721-730.

Bailey, R., M. Kris, M. Wolf, A. Kay, S. Averbuch, J. Askaa, M. Janas, K. Schmidt and M. Fukuoka (2003). "O-242 Gefitinib ('Iressa', ZD1839) monotherapy for pretreated advanced non-small-cell lung cancer in IDEAL 1 and 2: tumor response is not clinically relevantly predictable from tumor EGFR membrane staining alone." Lung Cancer **41**: S71.

Barker, A. J., K. H. Gibson, W. Grundy, A. A. Godfrey, J. J. Barlow, M. P. Healy, J. R. Woodburn, S. E. Ashton, B. J. Curry, L. Scarlett, L. Henthorn and L. Richards (2001). "Studies leading to the identification of ZD1839 (IRESSA): an orally active, selective epidermal growth factor receptor tyrosine kinase inhibitor targeted to the treatment of cancer." Bioorg Med Chem Lett **11**(14): 1911-1914.

Bhang, H. E., D. A. Ruddy, V. Krishnamurthy Radhakrishna, J. X. Caushi, R. Zhao, M. M. Hims, A. P. Singh, I. Kao, D. Rakiec, P. Shaw, M. Balak, A. Raza, E. Ackley, N. Keen, M. R. Schlabach, M. Palmer, R. J. Leary, D. Y. Chiang, W. R. Sellers, F. Michor, V. G. Cooke, J. M. Korn and F. Stegmeier (2015). "Studying clonal dynamics in response to cancer therapy using high-complexity barcoding." Nat Med **21**(5): 440-448.

Bokobza, S. M., Y. Jiang, A. M. Weber, A. M. Devery and A. J. Ryan (2014). "Combining AKT inhibition with chloroquine and gefitinib prevents compensatory autophagy and induces cell death in EGFR mutated NSCLC cells." Oncotarget **5**(13): 4765-4778.

Burrell, R. A. and C. Swanton (2014). "Tumour heterogeneity and the evolution of polyclonal drug resistance." Mol Oncol **8**(6): 1095-1111.

Camidge, D. R., W. Pao and L. V. Sequist (2014). "Acquired resistance to TKIs in solid tumours: learning from lung cancer." Nat Rev Clin Oncol **11**(8): 473-481.

Cancer Genome Atlas Research, N. (2014). "Comprehensive molecular profiling of lung adenocarcinoma." Nature **511**(7511): 543-550.

Carpenter, G., L. King, Jr. and S. Cohen (1978). "Epidermal growth factor stimulates phosphorylation in membrane preparations in vitro." Nature **276**(5686): 409-410.

Chabon, J. J., A. D. Simmons, A. F. Lovejoy, M. S. Esfahani, A. M. Newman, H. J. Haringsma, D. M. Kurtz, H. Stehr, F. Scherer, C. A. Karlovich, T. C. Harding, K. A. Durkin, G. A. Otterson, W. T. Purcell, D. R. Camidge, J. W. Goldman, L. V. Sequist, Z. Piotrowska, H. A. Wakelee, J. W. Neal, A. A. Alizadeh and M. Diehn (2016). "Circulating tumour DNA profiling reveals heterogeneity of EGFR inhibitor resistance mechanisms in lung cancer patients." Nat Commun **7**: 11815.

Chaft, J. E., G. R. Oxnard, C. S. Sima, M. G. Kris, V. A. Miller and G. J. Riely (2011). "Disease flare after tyrosine kinase inhibitor discontinuation in patients with EGFR-mutant lung cancer and acquired resistance to erlotinib or gefitinib: implications for clinical trial design." Clin Cancer Res **17**(19): 6298-6303.

Chan, S. K., W. J. Gullick and M. E. Hill (2006). "Mutations of the epidermal growth factor receptor in non-small cell lung cancer -- search and destroy." Eur J Cancer **42**(1): 17-23.

Chang, L. and M. Karin (2001). "Mammalian MAP kinase signalling cascades." Nature **410**(6824): 37-40.

Chen, J., F. Zeng, S. J. Forrester, S. Eguchi, M.-Z. Zhang and R. C. Harris (2016). "Expression and Function of the Epidermal Growth Factor Receptor in Physiology and Disease." Physiological Reviews **96**(3): 1025-1069.

Chen, T. C., Y. W. Liu, Y. H. Huang, Y. C. Yeh, T. Y. Chou, Y. C. Wu, C. C. Wu, Y. R. Chen, H. C. Cheng, P. J. Lu, J. M. Lai and C. Y. Huang (2013). "Protein phosphorylation profiling using an in situ proximity ligation assay: phosphorylation of AURKA-elicited EGFR-Thr654 and EGFR-Ser1046 in lung cancer cells." PLoS One **8**(3): e55657.

Chmielecki, J., J. Foo, G. R. Oxnard, K. Hutchinson, K. Ohashi, R. Somwar, L. Wang, K. R. Amato, M. Arcila, M. L. Sos, N. D. Socci, A. Viale, E. de Stanchina, M. S. Ginsberg, R. K. Thomas, M. G. Kris, A. Inoue, M. Ladanyi, V. A. Miller, F. Michor and W. Pao (2011). "Optimization of dosing for EGFR-mutant non-small cell lung cancer with evolutionary cancer modeling." Sci Transl Med **3**(90): 90ra59.

Chou, T. Y., C. H. Chiu, L. H. Li, C. Y. Hsiao, C. Y. Tzen, K. T. Chang, Y. M. Chen, R. P. Perng, S. F. Tsai and C. M. Tsai (2005). "Mutation in the tyrosine kinase domain of epidermal growth factor receptor is a predictive and prognostic factor for gefitinib treatment in patients with non-small cell lung cancer." Clin Cancer Res **11**(10): 3750-3757.

Chuang, J. C., H. Stehr, Y. Liang, M. Das, J. Huang, M. Diehn, H. A. Wakelee and J. W. Neal (2017). "ERBB2-Mutated Metastatic Non-Small Cell Lung Cancer: Response and Resistance to Targeted Therapies." J Thorac Oncol **12**(5): 833-842.

Ciuleanu, T. E., S. Ahmed, J. H. Kim, J. Mezger, K. Park, M. Thomas, J. Chen, S. Poondru, J. M. VanTornout, D. Whitcomb and F. Blackhall (2017). "Randomised Phase 2 study of maintenance linsitinib (OSI-906) in combination with erlotinib compared with placebo plus erlotinib after platinum-based chemotherapy in patients with advanced non-small cell lung cancer." Br J Cancer **117**(6): 757-766.

Clayton, A. H., S. G. Orchard, E. C. Nice, R. G. Posner and A. W. Burgess (2008). "Predominance of activated EGFR higher-order oligomers on the cell surface." Growth Factors **26**(6): 316-324.

Clayton, A. H., F. Walker, S. G. Orchard, C. Henderson, D. Fuchs, J. Rothacker, E. C. Nice and A. W. Burgess (2005). "Ligand-induced dimer-tetramer transition during the activation of the cell surface epidermal growth factor receptor-A multidimensional microscopy analysis." J Biol Chem **280**(34): 30392-30399.

Cogliano, V. J., R. Baan, K. Straif, Y. Grosse, B. Lauby-Secretan, F. El Ghissassi, V. Bouvard, L. Benbrahim-Tallaa, N. Guha, C. Freeman, L. Galichet and C. P. Wild (2011). "Preventable exposures associated with human cancers." J Natl Cancer Inst **103**(24): 1827-1839.

Cohen, S. (1983). "The epidermal growth factor (EGF)." Cancer **51**(10): 1787-1791.

Cohen, S., H. Ushiro, C. Stoscheck and M. Chinkers (1982). "A native 170,000 epidermal growth factor receptor-kinase complex from shed plasma membrane vesicles." J Biol Chem **257**(3): 1523-1531.

Cortot, A. B., C. E. Repellin, T. Shimamura, M. Capelletti, K. Zejnullahu, D. Ercan, J. G. Christensen, K. K. Wong, N. S. Gray and P. A. Janne (2013). "Resistance to irreversible EGF receptor tyrosine kinase inhibitors through a multistep mechanism involving the IGF1R pathway." Cancer Res **73**(2): 834-843.

Costa, D. B. and S. S. Kobayashi (2015). "Whacking a mole-cule: clinical activity and mechanisms of resistance to third generation EGFR inhibitors in EGFR mutated lung cancers with EGFR-T790M." Transl Lung Cancer Res **4**(6): 809-815.

Cragg, M. S., J. Kuroda, H. Puthalakath, D. C. Huang and A. Strasser (2007). "Gefitinib-induced killing of NSCLC cell lines expressing mutant EGFR requires BIM and can be enhanced by BH3 mimetics." PLoS Med **4**(10): 1681-1689; discussion 1690.

Cross, D. A., S. E. Ashton, S. Ghiorghiu, C. Eberlein, C. A. Nebhan, P. J. Spitzler, J. P. Orme, M. R. Finlay, R. A. Ward, M. J. Mellor, G. Hughes, A. Rahi, V. N. Jacobs, M. Red Brewer, E. Ichihara, J. Sun, H. Jin, P. Ballard, K. Al-Kadhimi, R. Rowlinson, T. Klinowska, G. H. Richmond, M. Cantarini, D. W. Kim, M. R. Ranson and W. Pao (2014). "AZD9291, an Irreversible EGFR TKI, Overcomes T790M-Mediated Resistance to EGFR Inhibitors in Lung Cancer." Cancer Discov **4**(9): 1046-1061.

Crystal, A. S., A. T. Shaw, L. V. Sequist, L. Friboulet, M. J. Niederst, E. L. Lockerman, R. L. Frias, J. F. Gainor, A. Amzallag, P. Greninger, D. Lee, A. Kalsy, M. Gomez-Caraballo, L. Elamine, E. Howe, W. Hur, E. Lifshits, H. E. Robinson, R. Katayama, A. C. Faber, M. M. Awad, S. Ramaswamy, M. Mino-Kenudson, A. J. Iafrate, C. H. Benes and J. A. Engelman (2014). "Patient-derived models of acquired resistance can identify effective drug combinations for cancer." Science **346**(6216): 1480-1486.

Dar, A. A., L. W. Goff, S. Majid, J. Berlin and W. El-Rifai (2010). "Aurora kinase inhibitors--rising stars in cancer therapeutics?" Mol Cancer Ther **9**(2): 268-278.

Davies, R. L., V. A. Grosse, R. Kucherlapati and M. Bothwell (1980). "Genetic analysis of epidermal growth factor action: assignment of human epidermal growth factor receptor gene to chromosome 7." Proc Natl Acad Sci U S A **77**(7): 4188-4192.

Devesa, S. S., F. Bray, A. P. Vizcaino and D. M. Parkin (2005). "International lung cancer trends by histologic type: male:female differences diminishing and adenocarcinoma rates rising." Int J Cancer **117**(2): 294-299.

Diaz-Garcia, C. V., A. Agudo-Lopez, C. Perez, E. Prieto-Garcia, L. Iglesias, S. Ponce, A. Rodriguez Garzotto, J. L. Rodriguez-Peralto, H. Cortes-Funes, J. A. Lopez-Martin and M. T. Agullo-Ortuno (2015). "Prognostic value of dual-specificity phosphatase 6 expression in non-small cell lung cancer." Tumour Biol **36**(2): 1199-1206.

Dingemans, A.-M. C., M. Reck and V. Westeel (2015). Lung Cancer.

Dong, Y. U., W. Ren, J. Qi, B. O. Jin, Y. Li, H. Tao, R. Xu, Y. Li, Q. Zhang and B. Han (2016). "EGFR, ALK, RET, KRAS and BRAF alterations in never-smokers with non-small cell lung cancer." Oncol Lett **11**(4): 2371-2378.

Downward, J., P. Parker and M. D. Waterfield (1984). "Autophosphorylation sites on the epidermal growth factor receptor." Nature **311**(5985): 483-485.

Eberlein, C. A., D. Stetson, A. A. Markovets, K. J. Al-Kadhimi, Z. Lai, P. R. Fisher, C. B. Meador, P. Spitzler, E. Ichihara, S. J. Ross, M. J. Ahdesmaki, A. Ahmed, L. E. Ratcliffe, E. L. O'Brien, C. H. Barnes, H. Brown, P. D. Smith, J. R. Dry, G. Beran, K. S. Thress, B. Dougherty, W. Pao and D. A. Cross (2015). "Acquired Resistance to the Mutant-Selective EGFR Inhibitor AZD9291 Is Associated with Increased Dependence on RAS Signaling in Preclinical Models." Cancer Res **75**(12): 2489-2500.

Ekert, J. E., K. Johnson, B. Strake, J. Pardinas, S. Jarantow, R. Perkinson and D. C. Colter (2014). "Three-dimensional lung tumor microenvironment modulates therapeutic compound responsiveness in vitro--implication for drug development." PLoS One **9**(3): e92248.

Emdal, K. B., A. Dittmann, R. J. Reddy, R. S. Lescarbeau, S. L. Moores, S. Laquerre and F. M. White (2017). "Characterization of in vivo resistance to osimertinib and JNJ-61186372, an EGFR/Met bi-specific antibody, reveals unique and consensus mechanisms of resistance." Mol Cancer Ther.

Endres, N. F., R. Das, A. W. Smith, A. Arkhipov, E. Kovacs, Y. Huang, J. G. Pelton, Y. Shan, D. E. Shaw, D. E. Wemmer, J. T. Groves and J. Kuriyan (2013). "Conformational coupling across the plasma membrane in activation of the EGF receptor." Cell **152**(3): 543-556.

Engelman, J. A. and P. A. Janne (2008). "Mechanisms of acquired resistance to epidermal growth factor receptor tyrosine kinase inhibitors in non-small cell lung cancer." Clin Cancer Res **14**(10): 2895-2899.

Engelman, J. A., P. A. Janne, C. Mermel, J. Pearlberg, T. Mukohara, C. Fleet, K. Cichowski, B. E. Johnson and L. C. Cantley (2005). "ErbB-3 mediates phosphoinositide 3-kinase activity in gefitinib-sensitive non-small cell lung cancer cell lines." Proc Natl Acad Sci U S A **102**(10): 3788-3793.

Engelman, J. A., J. Luo and L. C. Cantley (2006). "The evolution of phosphatidylinositol 3-kinases as regulators of growth and metabolism." Nat Rev Genet **7**(8): 606-619.

Engelman, J. A., T. Mukohara, K. Zejnullahu, E. Lifshits, A. M. Borras, C. M. Gale, G. N. Naumov, B. Y. Yeap, E. Jarrell, J. Sun, S. Tracy, X. Zhao, J. V. Heymach, B. E. Johnson, L. C. Cantley and P. A. Janne (2006). "Allelic dilution obscures detection of a biologically significant resistance mutation in EGFR-amplified lung cancer." J Clin Invest **116**(10): 2695-2706.

Engelman, J. A., K. Zejnullahu, T. Mitsudomi, Y. Song, C. Hyland, J. O. Park, N. Lindeman, C. M. Gale, X. Zhao, J. Christensen, T. Kosaka, A. J. Holmes, A. M. Rogers, F. Cappuzzo, T. Mok, C. Lee, B. E. Johnson, L. C. Cantley and P. A. Janne (2007). "MET amplification leads to gefitinib resistance in lung cancer by activating ERBB3 signaling." Science **316**(5827): 1039-1043.

Ercan, D., H. G. Choi, C. H. Yun, M. Capelletti, T. Xie, M. J. Eck, N. S. Gray and P. A. Janne (2015). "EGFR Mutations and Resistance to Irreversible Pyrimidine-Based EGFR Inhibitors." Clin Cancer Res **21**(17): 3913-3923.

Ercan, D., C. Xu, M. Yanagita, C. S. Monast, C. A. Pratilas, J. Montero, M. Butaney, T. Shimamura, L. Sholl, E. V. Ivanova, M. Tadi, A. Rogers, C. Repellin, M. Capelletti, O. Maertens, E. M. Goetz, A. Letai, L. A. Garraway, M. J. Lazzara, N. Rosen, N. S. Gray, K. K. Wong and P. A. Janne (2012). "Reactivation of ERK signaling causes resistance to EGFR kinase inhibitors." Cancer Discov **2**(10): 934-947.

Faber, A. C., R. B. Corcoran, H. Ebi, L. V. Sequist, B. A. Waltman, E. Chung, J. Incio, S. R. Digumarthy, S. F. Pollack, Y. Song, A. Muzikansky, E. Lifshits, S. Roberge, E. J. Coffman, C. H. Benes, H. L. Gomez, J. Baselga, C. L. Arteaga, M. N. Rivera, D. Dias-Santagata, R. K. Jain and J. A. Engelman (2011). "BIM expression in treatment-naive cancers predicts responsiveness to kinase inhibitors." Cancer Discov **1**(4): 352-365.

Faehling, M., R. Eckert, T. Kamp, S. Kuom, U. Griese, J. Strater, G. Ott and W. Spengler (2013). "EGFR-tyrosine kinase inhibitor treatment beyond progression in long-term Caucasian responders to erlotinib in advanced non-small cell lung cancer: a case-control study of overall survival." Lung Cancer **80**(3): 306-312.

Falchook, G. S., C. C. Bastida and R. Kurzrock (2015). "Aurora Kinase Inhibitors in Oncology Clinical Trials: Current State of the Progress." Semin Oncol **42**(6): 832-848.

FDA, U. S. Food and Drug A. (2003). "IRESSA." from https://www.accessdata.fda.gov/drugsatfda_docs/label/2003/021399lbl.pdf.

FDA, U. S. Food and Drug A. (2017). "Osimertinib - approved drug database." Retrieved 06.09.2017, from https://www.fda.gov/drugs/informationondrugs/approveddrugs/ucm549683.htm.

Ferlay, J., I. Soerjomataram, M. Ervik, R. Dikshit, S. Eser, C. Mathers, M. Rebelo, D. Parkin, D. Forman and F. Bray (2013). "GLOBOCAN 2012 v1.0, Cancer Incidence and Mortality Worldwide: IARC CancerBase No. 11 [Internet]." Lyon, France: International Agency for Research on Cancer.

Fleishman, S. J., J. Schlessinger and N. Ben-Tal (2002). "A putative molecular-activation switch in the transmembrane domain of erbB2." Proc Natl Acad Sci U S A **99**(25): 15937-15940.

Fukuoka, M., S. Yano, G. Giaccone, T. Tamura, K. Nakagawa, J. Y. Douillard, Y. Nishiwaki, J. Vansteenkiste, S. Kudoh, D. Rischin, R. Eek, T. Horai, K. Noda, I. Takata, E. Smit, S. Averbuch, A. Macleod, A. Feyereislova, R. P. Dong and J. Baselga (2003). "Multi-institutional randomized phase II trial of gefitinib for previously treated patients with advanced non-small-cell lung cancer (The IDEAL 1 Trial) [corrected]." J Clin Oncol **21**(12): 2237-2246.

Gadgeel, S. M. and A. Wozniak (2013). "Preclinical rationale for PI3K/Akt/mTOR pathway inhibitors as therapy for epidermal growth factor receptor inhibitor-resistant non-small-cell lung cancer." Clin Lung Cancer **14**(4): 322-332.

Gainor, J. F., A. M. Varghese, S. H. Ou, S. Kabraji, M. M. Awad, R. Katayama, A. Pawlak, M. Mino-Kenudson, B. Y. Yeap, G. J. Riely, A. J. Iafrate, M. E. Arcila, M. Ladanyi, J. A. Engelman, D. Dias-Santagata and A. T. Shaw (2013). "ALK rearrangements are mutually exclusive with mutations in EGFR or KRAS: an analysis of 1,683 patients with non-small cell lung cancer." Clin Cancer Res **19**(15): 4273-4281.

Gajiwala, K. S. (2013). "EGFR: tale of the C-terminal tail." Protein Sci **22**(7): 995-999.

Garrido-Castro, A. C. and E. Felip (2013). "HER2 driven non-small cell lung cancer (NSCLC): potential therapeutic approaches." Transl Lung Cancer Res **2**(2): 122-127.

Gautschi, O., J. Heighway, P. C. Mack, P. R. Purnell, P. N. Lara, Jr. and D. R. Gandara (2008). "Aurora kinases as anticancer drug targets." Clin Cancer Res **14**(6): 1639-1648.

Gazdar, A., L. Robinson, D. Oliver, C. Xing, W. D. Travis, J. Soh, S. Toyooka, L. Watumull, Y. Xie, K. Kernstine and J. H. Schiller (2014). "Hereditary lung cancer syndrome targets never smokers with germline EGFR gene T790M mutations." J Thorac Oncol **9**(4): 456-463.

Gazdar, A. F., H. Shigematsu, J. Herz and J. D. Minna (2004). "Mutations and addiction to EGFR: the Achilles 'heal' of lung cancers?" Trends Mol Med **10**(10): 481-486.

Godwin, J. L., R. Mehra, S. Litwin, A. J. Olszanski, J. R. Bauman and H. Borghaei (2016). "A phase I/II study of MLN-8237 (alisertib), an oral aurora kinase inhibitor, in combination with erlotinib in patients with recurrent or metastatic EGFR wild-type non-small cell lung cancer." Journal of Clinical Oncology **34**(15_suppl): e20588-e20588.

Goldberg, S. B., G. R. Oxnard, S. Digumarthy, A. Muzikansky, D. M. Jackman, I. T. Lennes and L. V. Sequist (2013). "Chemotherapy with Erlotinib or chemotherapy alone in advanced non-small cell lung cancer with acquired resistance to EGFR tyrosine kinase inhibitors." Oncologist **18**(11): 1214-1220.

Greig, S. L. (2016). "Osimertinib: First Global Approval." Drugs **76**(2): 263-273.

Greulich, H., T. H. Chen, W. Feng, P. A. Janne, J. V. Alvarez, M. Zappaterra, S. E. Bulmer, D. A. Frank, W. C. Hahn, W. R. Sellers and M. Meyerson (2005). "Oncogenic transformation by inhibitor-sensitive and -resistant EGFR mutants." PLoS Med **2**(11): e313.

Guix, M., A. C. Faber, S. E. Wang, M. G. Olivares, Y. Song, S. Qu, C. Rinehart, B. Seidel, D. Yee, C. L. Arteaga and J. A. Engelman (2008). "Acquired resistance to EGFR tyrosine kinase inhibitors in cancer cells is mediated by loss of IGF-binding proteins." J Clin Invest **118**(7): 2609-2619.

Halmos, B., N. A. Pennell, P. Fu, S. Saad, S. Gadgeel, G. A. Otterson, T. Mekhail, M. Snell, J. P. Kuebler, N. Sharma and A. Dowlati (2015). "Randomized Phase II Trial of Erlotinib Beyond Progression in Advanced Erlotinib-Responsive Non-Small Cell Lung Cancer." Oncologist **20**(11): 1298-1303.

Ham, J. S., S. Kim, H. K. Kim, S. Byeon, J. M. Sun, S. H. Lee, J. S. Ahn, K. Park, Y. L. Choi, J. Han, W. Park and M. J. Ahn (2016). "Two Cases of Small Cell Lung Cancer Transformation from EGFR Mutant Adenocarcinoma During AZD9291 Treatment." J Thorac Oncol **11**(1): e1-4.

Hamilton, W., T. J. Peters, A. Round and D. Sharp (2005). "What are the clinical features of lung cancer before the diagnosis is made? A population based case-control study." Thorax **60**(12): 1059-1065.

Hata, A., N. Katakami, R. Kaji, S. Fujita and Y. Imai (2013). "Does T790M disappear? Successful gefitinib rechallenge after T790M disappearance in a patient with EGFR-mutant non-small-cell lung cancer." J Thorac Oncol **8**(3): e27-29.

Hata, A. N., M. J. Niederst, H. L. Archibald, M. Gomez-Caraballo, F. M. Siddiqui, H. E. Mulvey, Y. E. Maruvka, F. Ji, H.-e. C. Bhang, V. Krishnamurthy Radhakrishna, G. Siravegna, H. Hu, S. Raoof, E. Lockerman, A. Kalsy, D. Lee, C. L. Keating, D. A. Ruddy, L. J. Damon, A. S. Crystal, C. Costa, Z. Piotrowska, A. Bardelli, A. J. Iafrate, R. I. Sadreyev, F. Stegmeier, G. Getz, L. V. Sequist, A. C. Faber and J. A. Engelman (2016). "Tumor cells can follow distinct evolutionary paths to become resistant to epidermal growth factor receptor inhibition." Nat Med **22**(3): 262-269.

He, L. and K. Hristova (2012). "Consequences of replacing EGFR juxtamembrane domain with an unstructured sequence." Sci Rep **2**: 854.

Heberle, H., G. V. Meirelles, F. R. da Silva, G. P. Telles and R. Minghim (2015). "InteractiVenn: a web-based tool for the analysis of sets through Venn diagrams." BMC Bioinformatics **16**: 169.

Hellyer, N. J., K. Cheng and J. G. Koland (1998). "ErbB3 (HER3) interaction with the p85 regulatory subunit of phosphoinositide 3-kinase." Biochem J **333 (Pt 3)**: 757-763.

Hirai, H., H. Sootome, Y. Nakatsuru, K. Miyama, S. Taguchi, K. Tsujioka, Y. Ueno, H. Hatch, P. K. Majumder, B. S. Pan and H. Kotani (2010). "MK-2206, an allosteric Akt inhibitor, enhances antitumor efficacy by standard chemotherapeutic agents or molecular targeted drugs in vitro and in vivo." Molecular cancer therapeutics **9**(7): 1956-1967.

Hirano, T., H. Yasuda, T. Tani, J. Hamamoto, A. Oashi, K. Ishioka, D. Arai, S. Nukaga, M. Miyawaki, I. Kawada, K. Naoki, D. B. Costa, S. S. Kobayashi, T. Betsuyaku and K. Soejima (2015). "In vitro modeling to determine mutation specificity of EGFR tyrosine kinase inhibitors against clinically relevant EGFR mutants in non-small-cell lung cancer." Oncotarget **6**(36): 38789-38803.

Hirschhaeuser, F., H. Menne, C. Dittfeld, J. West, W. Mueller-Klieser and L. A. Kunz-Schughart (2010). "Multicellular tumor spheroids: an underestimated tool is catching up again." J Biotechnol **148**(1): 3-15.

Ho, C. C., W. Y. Liao, C. A. Lin, J. Y. Shih, C. J. Yu and J. Chih-Hsin Yang (2017). "Acquired BRAF V600E Mutation as Resistant Mechanism after Treatment with Osimertinib." J Thorac Oncol **12**(3): 567-572.

Hochegger, H., N. Hegarat and J. B. Pereira-Leal (2013). "Aurora at the pole and equator: overlapping functions of Aurora kinases in the mitotic spindle." Open Biol **3**(3): 120185.

Hossam, M., D. S. Lasheen and K. A. Abouzid (2016). "Covalent EGFR Inhibitors: Binding Mechanisms, Synthetic Approaches, and Clinical Profiles." Arch Pharm (Weinheim) **349**(8): 573-593.

Howlader N, N. A., Krapcho M, Miller D, Bishop K, Kosary CL, Yu M, Ruhl J, Tatalovich Z, Mariotto A, Lewis DR, Chen HS, Feuer EJ, Cronin KA (eds). (2015). "SEER Cancer Statistics Review, 1975-2012." from seer. cancer. gov/csr. 1975_2012/.

Huang, M. H., J. H. Lee, Y. J. Chang, H. H. Tsai, Y. L. Lin, A. M. Lin and J. C. Yang (2013). "MEK inhibitors reverse resistance in epidermal growth factor receptor mutation lung cancer cells with acquired resistance to gefitinib." Mol Oncol **7**(1): 112-120.

Huang, Q., J. Li, Y. Sun, R. Wang, X. Cheng and H. Chen (2016). "Efficacy of EGFR Tyrosine Kinase Inhibitors in the Adjuvant Treatment for Operable Non-small Cell Lung Cancer by a Meta-Analysis." Chest **149**(6): 1384-1392.

Hutter, G., C. Nickenig, H. Garritsen, F. Hellenkamp, A. Hoerning, W. Hiddemann and M. Dreyling (2004). "Use of polymorphisms in the noncoding region of the human mitochondrial genome to identify potential contamination of human leukemia-lymphoma cell lines." Hematol J **5**(1): 61-68.

Ichihara, E., D. Westover, C. B. Meador, Y. Yan, J. A. Bauer, P. Lu, F. Ye, A. Kulick, E. de Stanchina, R. McEwen, M. Ladanyi, D. Cross, W. Pao and C. M. Lovly (2017). "SFK/FAK Signaling Attenuates Osimertinib Efficacy in Both Drug-Sensitive and Drug-Resistant Models of EGFR-Mutant Lung Cancer." Cancer Res **77**(11): 2990-3000.

Inoue, A., K. Kobayashi, M. Maemondo, S. Sugawara, S. Oizumi, H. Isobe, A. Gemma, M. Harada, H. Yoshizawa, I. Kinoshita, Y. Fujita, S. Okinaga, H. Hirano, K. Yoshimori, T. Harada, Y. Saijo, K. Hagiwara, S. Morita and T. Nukiwa (2013). "Updated overall survival results from a randomized phase III trial comparing gefitinib with carboplatin–paclitaxel for chemo-naïve non-small cell lung cancer with sensitive EGFR gene mutations (NEJ002)." Annals of Oncology **24**(1): 54-59.

Ishikawa, Y., T. Kozakai, H. Morita, K. Saida, S. Oka and Y. Masuo (2006). "Rapid detection of mycoplasma contamination in cell cultures using SYBR Green-based real-time polymerase chain reaction." In Vitro Cell Dev Biol Anim **42**(3-4): 63-69.

Jacobsen, K., J. Bertran-Alamillo, M. A. Molina, C. Teixido, N. Karachaliou, M. H. Pedersen, J. Castellvi, M. Garzon, C. Codony-Servat, J. Codony-Servat, A. Gimenez-Capitan, A. Drozdowskyj, S. Viteri, M. R. Larsen, U. Lassen, E. Felip, T. G. Bivona, H. J. Ditzel and R. Rosell (2017). "Convergent Akt activation drives acquired EGFR inhibitor resistance in lung cancer." Nat Commun **8**(1): 410.

Janne, P. A., J. A. Engelman and B. E. Johnson (2005). "Epidermal growth factor receptor mutations in non-small-cell lung cancer: implications for treatment and tumor biology." J Clin Oncol **23**(14): 3227-3234.

Janne, P. A., S. Gurubhagavatula, B. Y. Yeap, J. Lucca, P. Ostler, A. T. Skarin, P. Fidias, T. J. Lynch and B. E. Johnson (2004). "Outcomes of patients with advanced non-small cell lung cancer treated with gefitinib (ZD1839, "Iressa") on an expanded access study." Lung Cancer **44**(2): 221-230.

Janne, P. A., S. S. Ramalingam, J. C.-H. Yang, M.-J. Ahn, D.-W. Kim, S.-W. Kim, D. Planchard, Y. Ohe, E. Felip, C. Watkins, M. Cantarini, S. Ghiorghiu and M. Ranson (2014). "Clinical activity of the mutant-selective EGFR inhibitor AZD9291 in patients (pts) with EGFR inhibitor–resistant non-small cell lung cancer (NSCLC)." Journal of Clinical Oncology **32**(15_suppl): 8009-8009.

Janne, P. A., J. C. Yang, D. W. Kim, D. Planchard, Y. Ohe, S. S. Ramalingam, M. J. Ahn, S. W. Kim, W. C. Su, L. Horn, D. Haggstrom, E. Felip, J. H. Kim, P. Frewer, M.

Cantarini, K. H. Brown, P. A. Dickinson, S. Ghiorghiu and M. Ranson (2015). "AZD9291 in EGFR inhibitor-resistant non-small-cell lung cancer." N Engl J Med **372**(18): 1689-1699.

Jeffrey, K. L., M. Camps, C. Rommel and C. R. Mackay (2007). "Targeting dual-specificity phosphatases: manipulating MAP kinase signalling and immune responses." Nat Rev Drug Discov **6**(5): 391-403.

Jia, Y., C. H. Yun, E. Park, D. Ercan, M. Manuia, J. Juarez, C. Xu, K. Rhee, T. Chen, H. Zhang, S. Palakurthi, J. Jang, G. Lelais, M. DiDonato, B. Bursulaya, P. Y. Michellys, R. Epple, T. H. Marsilje, M. McNeill, W. Lu, J. Harris, S. Bender, K. K. Wong, P. A. Janne and M. J. Eck (2016). "Overcoming EGFR(T790M) and EGFR(C797S) resistance with mutant-selective allosteric inhibitors." Nature **534**(7605): 129-132.

Jiang, J., H. Greulich, P. A. Janne, W. R. Sellers, M. Meyerson and J. D. Griffin (2005). "Epidermal growth factor-independent transformation of Ba/F3 cells with cancer-derived epidermal growth factor receptor mutants induces gefitinib-sensitive cell cycle progression." Cancer Res **65**(19): 8968-8974.

Jura, N., N. F. Endres, K. Engel, S. Deindl, R. Das, M. H. Lamers, D. E. Wemmer, X. Zhang and J. Kuriyan (2009). "Mechanism for activation of the EGF receptor catalytic domain by the juxtamembrane segment." Cell **137**(7): 1293-1307.

Jura, N., X. Zhang, N. F. Endres, M. A. Seeliger, T. Schindler and J. Kuriyan (2011). "Catalytic control in the EGF receptor and its connection to general kinase regulatory mechanisms." Mol Cell **42**(1): 9-22.

Kang, J., D. W. Lee, H. J. Hwang, S. E. Yeon, M. Y. Lee and H. J. Kuh (2016). "Mini-pillar array for hydrogel-supported 3D culture and high-content histologic analysis of human tumor spheroids." Lab Chip **16**(12): 2265-2276.

Kaplan, M., S. Narasimhan, C. de Heus, D. Mance, S. van Doorn, K. Houben, D. Popov-Celeketic, R. Damman, E. A. Katrukha, P. Jain, W. J. Geerts, A. J. Heck, G. E. Folkers, L. C. Kapitein, S. Lemeer, P. M. van Bergen En Henegouwen and M. Baldus (2016). "EGFR Dynamics Change during Activation in Native Membranes as Revealed by NMR." Cell **167**(5): 1241-1251 e1211.

Katakami, N., S. Atagi, K. Goto, T. Hida, T. Horai, A. Inoue, Y. Ichinose, K. Koboyashi, K. Takeda, K. Kiura, K. Nishio, Y. Seki, R. Ebisawa, M. Shahidi and N. Yamamoto (2013). "LUX-Lung 4: a phase II trial of afatinib in patients with advanced non-small-cell lung cancer who progressed during prior treatment with erlotinib, gefitinib, or both." J Clin Oncol **31**(27): 3335-3341.

Kaufman, J. and T. E. Stinchcombe (2017). "Treatment of KRAS-Mutant Non-Small Cell Lung Cancer: The End of the Beginning for Targeted Therapies." JAMA **317**(18): 1835-1837.

Keppel, T. R., K. Sarpong, E. M. Murray, J. Monsey, J. Zhu and R. Bose (2017). "Biophysical Evidence for Intrinsic Disorder in the C-terminal Tails of the Epidermal Growth Factor Receptor (EGFR) and HER3 Receptor Tyrosine Kinases." J Biol Chem **292**(2): 597-610.

Killion, J. J., R. Radinsky and I. J. Fidler (1998). "Orthotopic models are necessary to predict therapy of transplantable tumors in mice." Cancer Metastasis Rev **17**(3): 279-284.

Kim, S. M., O. J. Kwon, Y. K. Hong, J. H. Kim, F. Solca, S. J. Ha, R. A. Soo, J. G. Christensen, J. H. Lee and B. C. Cho (2012). "Activation of IL-6R/JAK1/STAT3 signaling induces de novo resistance to irreversible EGFR inhibitors in non-small cell lung cancer with T790M resistance mutation." Mol Cancer Ther **11**(10): 2254-2264.

Kim, T. M., A. Song, D. W. Kim, S. Kim, Y. O. Ahn, B. Keam, Y. K. Jeon, S. H. Lee, D. H. Chung and D. S. Heo (2015). "Mechanisms of Acquired Resistance to AZD9291: A Mutation-Selective, Irreversible EGFR Inhibitor." J Thorac Oncol **10**(12): 1736-1744.

Kobayashi, S., T. J. Boggon, T. Dayaram, P. A. Janne, O. Kocher, M. Meyerson, B. E. Johnson, M. J. Eck, D. G. Tenen and B. Halmos (2005). "EGFR mutation and resistance of non-small-cell lung cancer to gefitinib." N Engl J Med **352**(8): 786-792.

Koizumi, F., T. Shimoyama, F. Taguchi, N. Saijo and K. Nishio (2005). "Establishment of a human non-small cell lung cancer cell line resistant to gefitinib." Int J Cancer **116**(1): 36-44.

Kondo, I. and N. Shimizu (1983). "Mapping of the human gene for epidermal growth factor receptor (EGFR) on the p13 leads to q22 region of chromosome 7." Cytogenet Cell Genet **35**(1): 9-14.

Kovacs, E., J. A. Zorn, Y. Huang, T. Barros and J. Kuriyan (2015). "A structural perspective on the regulation of the epidermal growth factor receptor." Annu Rev Biochem **84**: 739-764.

Kozer, N., D. Barua, C. Henderson, E. C. Nice, A. W. Burgess, W. S. Hlavacek and A. H. Clayton (2014). "Recruitment of the adaptor protein Grb2 to EGFR tetramers." Biochemistry **53**(16): 2594-2604.

Lallo, A., M. W. Schenk, K. K. Frese, F. Blackhall and C. Dive (2017). "Circulating tumor cells and CDX models as a tool for preclinical drug development." Transl Lung Cancer Res **6**(4): 397-408.

Leahy, D. J. (2004). "Structure and function of the epidermal growth factor (EGF/ErbB) family of receptors." Adv Protein Chem **68**: 1-27.

Lee, C. K., C. Brown, R. J. Gralla, V. Hirsh, S. Thongprasert, C. M. Tsai, E. H. Tan, J. C. Ho, T. Chu da, A. Zaatar, J. A. Osorio Sanchez, V. V. Vu, J. S. Au, A. Inoue, S. M. Lee, V. Gebski and J. C. Yang (2013). "Impact of EGFR inhibitor in non-small cell

lung cancer on progression-free and overall survival: a meta-analysis." J Natl Cancer Inst **105**(9): 595-605.

Leighl, N. B., N. A. Rizvi, L. G. de Lima, Jr., W. Arpornwirat, C. M. Rudin, A. A. Chiappori, M. J. Ahn, L. Q. Chow, L. Bazhenova, A. Dechaphunkul, P. Sunpaweravong, K. Eaton, J. Chen, S. Medley, S. Poondru, M. Singh, J. Steinberg, R. A. Juergens and S. M. Gadgeel (2016). "Phase 2 Study of Erlotinib in Combination With Linsitinib (OSI-906) or Placebo in Chemotherapy-Naive Patients With Non-Small-Cell Lung Cancer and Activating Epidermal Growth Factor Receptor Mutations." Clin Lung Cancer.

Li, Y., Z. Song, Y. Jin, Z. Tang, J. Kang and X. Ma (2016). "Novel Selective and Potent EGFR Inhibitor that Overcomes T790M-Mediated Resistance in Non-Small Cell Lung Cancer." Molecules **21**(11).

Liao, S., T. Davoli, Y. Leng, M. Z. Li, Q. Xu and S. J. Elledge (2017). "A genetic interaction analysis identifies cancer drivers that modify EGFR dependency." Genes Dev **31**(2): 184-196.

Lindblad, W. J. and E. Jackim (1982). "Mechanism for the differential induction of mutation by S9 activated benzo[a]pyrene employing either a glucose-6-phosphate-dependent NADPH-regenerating system or an isocitrate-dependent system." Mutat Res **96**(1): 109-118.

Liu, W., Z. Ju, Y. Lu, G. B. Mills and R. Akbani (2014). "A comprehensive comparison of normalization methods for loading control and variance stabilization of reverse-phase protein array data." Cancer Inform **13**: 109-117.

Lynch, T. J., D. W. Bell, R. Sordella, S. Gurubhagavatula, R. A. Okimoto, B. W. Brannigan, P. L. Harris, S. M. Haserlat, J. G. Supko, F. G. Haluska, D. N. Louis, D. C. Christiani, J. Settleman and D. A. Haber (2004). "Activating mutations in the epidermal growth factor receptor underlying responsiveness of non-small-cell lung cancer to gefitinib." N Engl J Med **350**(21): 2129-2139.

Macaulay, V. M., M. R. Middleton, S. G. Eckhardt, C. M. Rudin, R. A. Juergens, R. Gedrich, S. Gogov, S. McCarthy, S. Poondru, A. Stephens and S. M. Gadgeel (2016). "Phase I Dose Escalation Study of Linsitinib (OSI-906) and Erlotinib in Patients with Advanced Solid Tumors." Clin Cancer Res.

Maemondo, M., A. Inoue, K. Kobayashi, S. Sugawara, S. Oizumi, H. Isobe, A. Gemma, M. Harada, H. Yoshizawa, I. Kinoshita, Y. Fujita, S. Okinaga, H. Hirano, K. Yoshimori, T. Harada, T. Ogura, M. Ando, H. Miyazawa, T. Tanaka, Y. Saijo, K. Hagiwara, S. Morita, T. Nukiwa and G. North-East Japan Study (2010). "Gefitinib or chemotherapy for non-small-cell lung cancer with mutated EGFR." N Engl J Med **362**(25): 2380-2388.

Maruyama, R., H. Wataya, T. Seto and Y. Ichinose (2009). "Treatment after the failure of gefitinib in patients with advanced or recurrent non-small cell lung cancer." Anticancer Res **29**(10): 4217-4221.

Mayo-de-Las-Casas, C., N. Jordana-Ariza, M. Garzon-Ibanez, A. Balada-Bel, J. Bertran-Alamillo, S. Viteri-Ramirez, N. Reguart, M. A. Munoz-Quintana, P. Lianes-Barragan, C. Camps, E. Jantus, J. Remon-Massip, S. Calabuig, D. Aguiar, M. L. Gil, N. Vinolas, A. K. Santos-Rodriguez, M. Majem, B. Garcia-Pelaez, S. Villatoro, A. Perez-Rosado, J. C. Monasterio, E. Ovalle, M. J. Catalan, R. Campos, D. Morales-Espinosa, A. Martinez-Bueno, M. Gonzalez-Cao, X. Gonzalez, I. Moya-Horno, A. E. Sosa, N. Karachaliou, R. Rosell and M. A. Molina-Vila (2017). "Large scale, prospective screening of EGFR mutations in the blood of advanced NSCLC patients to guide treatment decisions." Ann Oncol **28**(9): 2248-2255.

McGranahan, N. and C. Swanton (2015). "Biological and therapeutic impact of intratumor heterogeneity in cancer evolution." Cancer Cell **27**(1): 15-26.

McKenzie, A., A. Cranston, P. Mallinder, N. Papadopoulou, A. Reece-Smith, D. Onion, A. Grabowska, M. Page and R. Kumari (2012). "In Vivo Generation of EGFRi Resistance in a Proprietary Patient-derived Xenograft with an Activating EGFR Mutation (L858R); Subsequent Validation in an Orthotopic Lung Model with 3D Optical Tomographic MicroCT Imaging." European Journal of Cancer **48**: 51.

Mckenzie, A., A. Cranston, N. Papadopoulou, S. Jiang, J. Wrigley, Y. Yin, H. Li, M. Page and R. Kumari (2013). In vivo and in vitro generation and characterisation of EGFR TKI resistance in patient-derived and cell line-derived xenograft models of NSCLC with activating EGFR mutations, PRECOS Ltd., a Crown Bioscience Company.

Mendoza, M. C., E. E. Er and J. Blenis (2011). "The Ras-ERK and PI3K-mTOR pathways: cross-talk and compensation." Trends Biochem Sci **36**(6): 320-328.

Miettinen, P. J., J. E. Berger, J. Meneses, Y. Phung, R. A. Pedersen, Z. Werb and R. Derynck (1995). "Epithelial immaturity and multiorgan failure in mice lacking epidermal growth factor receptor." Nature **376**(6538): 337-341.

Miller, V. A., V. Hirsh, J. Cadranel, Y. M. Chen, K. Park, S. W. Kim, C. Zhou, W. C. Su, M. Wang, Y. Sun, D. S. Heo, L. Crino, E. H. Tan, T. Y. Chao, M. Shahidi, X. J. Cong, R. M. Lorence and J. C. Yang (2012). "Afatinib versus placebo for patients with advanced, metastatic non-small-cell lung cancer after failure of erlotinib, gefitinib, or both, and one or two lines of chemotherapy (LUX-Lung 1): a phase 2b/3 randomised trial." Lancet Oncol **13**(5): 528-538.

Mitsudomi, T., S. Morita, Y. Yatabe, S. Negoro, I. Okamoto, J. Tsurutani, T. Seto, M. Satouchi, H. Tada, T. Hirashima, K. Asami, N. Katakami, M. Takada, H. Yoshioka, K. Shibata, S. Kudoh, E. Shimizu, H. Saito, S. Toyooka, K. Nakagawa, M. Fukuoka and G. West Japan Oncology (2010). "Gefitinib versus cisplatin plus docetaxel in patients with non-small-cell lung cancer harbouring mutations of the epidermal growth factor receptor (WJTOG3405): an open label, randomised phase 3 trial." Lancet Oncol **11**(2): 121-128.

Mok, T. S., Y. L. Wu, M. J. Ahn, M. C. Garassino, H. R. Kim, S. S. Ramalingam, F. A. Shepherd, Y. He, H. Akamatsu, W. S. Theelen, C. K. Lee, M. Sebastian, A.

Templeton, H. Mann, M. Marotti, S. Ghiorghiu, V. A. Papadimitrakopoulou and A. Investigators (2017). "Osimertinib or Platinum-Pemetrexed in EGFR T790M-Positive Lung Cancer." N Engl J Med **376**(7): 629-640.

Mok, T. S., Y. L. Wu, S. Thongprasert, C. H. Yang, D. T. Chu, N. Saijo, P. Sunpaweravong, B. Han, B. Margono, Y. Ichinose, Y. Nishiwaki, Y. Ohe, J. J. Yang, B. Chewaskulyong, H. Jiang, E. L. Duffield, C. L. Watkins, A. A. Armour and M. Fukuoka (2009). "Gefitinib or carboplatin-paclitaxel in pulmonary adenocarcinoma." N Engl J Med **361**(10): 947-957.

Montagut, C. and J. Settleman (2009). "Targeting the RAF-MEK-ERK pathway in cancer therapy." Cancer Lett **283**(2): 125-134.

Morgillo, F., C. M. Della Corte, M. Fasano and F. Ciardiello (2016). "Mechanisms of resistance to EGFR-targeted drugs: lung cancer." ESMO Open **1**.

Morgillo, F., J. K. Woo, E. S. Kim, W. K. Hong and H. Y. Lee (2006). "Heterodimerization of insulin-like growth factor receptor/epidermal growth factor receptor and induction of survivin expression counteract the antitumor action of erlotinib." Cancer Res **66**(20): 10100-10111.

Mukohara, T., J. A. Engelman, N. H. Hanna, B. Y. Yeap, S. Kobayashi, N. Lindeman, B. Halmos, J. Pearlberg, Z. Tsuchihashi, L. C. Cantley, D. G. Tenen, B. E. Johnson and P. A. Janne (2005). "Differential effects of gefitinib and cetuximab on non-small-cell lung cancers bearing epidermal growth factor receptor mutations." J Natl Cancer Inst **97**(16): 1185-1194.

Nakagawa, T., S. Takeuchi, T. Yamada, S. Nanjo, D. Ishikawa, T. Sano, K. Kita, T. Nakamura, K. Matsumoto, K. Suda, T. Mitsudomi, Y. Sekido, T. Uenaka and S. Yano (2012). "Combined therapy with mutant-selective EGFR inhibitor and Met kinase inhibitor for overcoming erlotinib resistance in EGFR-mutant lung cancer." Mol Cancer Ther **11**(10): 2149-2157.

Nath, S. and G. R. Devi (2016). "Three-dimensional culture systems in cancer research: Focus on tumor spheroid model." Pharmacol Ther **163**: 94-108.

NCCN, National Comprehensive Care N. (2016). "Non-small Cell Lung Cancer - NCCN Guidelines for Patients." Version 1.2016. from https://www.nccn.org/patients/guidelines/quick_guides/lung-nsclc/treatment_options/files/assets/common/downloads/files/nccnquickguide-nsclcoptions.pdf.

Needham, S. R., S. K. Roberts, A. Arkhipov, V. P. Mysore, C. J. Tynan, L. C. Zanetti-Domingues, E. T. Kim, V. Losasso, D. Korovesis, M. Hirsch, D. J. Rolfe, D. T. Clarke, M. D. Winn, A. Lajevardipour, A. H. Clayton, L. J. Pike, M. Perani, P. J. Parker, Y. Shan, D. E. Shaw and M. L. Martin-Fernandez (2016). "EGFR oligomerization organizes kinase-active dimers into competent signalling platforms." Nat Commun **7**: 13307.

Neel, D. S. and T. G. Bivona (2017). "Resistance is futile: overcoming resistance to targeted therapies in lung adenocarcinoma." npj Precision Oncology **1**(1): 3.

Nishie, K., T. Kawaguchi, A. Tamiya, T. Mimori, N. Takeuchi, Y. Matsuda, N. Omachi, K. Asami, K. Okishio, S. Atagi, T. Okuma, A. Kubo, Y. Maruyama, S. Kudoh and M. Takada (2012). "Epidermal growth factor receptor tyrosine kinase inhibitors beyond progressive disease: a retrospective analysis for Japanese patients with activating EGFR mutations." J Thorac Oncol **7**(11): 1722-1727.

Ogino, A., H. Kitao, S. Hirano, A. Uchida, M. Ishiai, T. Kozuki, N. Takigawa, M. Takata, K. Kiura and M. Tanimoto (2007). "Emergence of epidermal growth factor receptor T790M mutation during chronic exposure to gefitinib in a non small cell lung cancer cell line." Cancer Res **67**(16): 7807-7814.

Onn, A., T. Isobe, S. Itasaka, W. Wu, M. S. O'Reilly, W. Ki Hong, I. J. Fidler and R. S. Herbst (2003). "Development of an orthotopic model to study the biology and therapy of primary human lung cancer in nude mice." Clin Cancer Res **9**(15): 5532-5539.

Ortiz-Zapater, E., R. W. Lee, W. Owen, G. Weitsman, G. Fruhwirth, R. G. Dunn, M. J. Neat, F. McCaughan, P. Parker, T. Ng and G. Santis (2017). "MET-EGFR dimerization in lung adenocarcinoma is dependent on EGFR mtations and altered by MET kinase inhibition." PLoS One **12**(1): e0170798.

Ou, Q., X. Wu, H. Bao, X. Tong, X. Wang, X. Zhang, Z. Chang, Y. Mao, Y. Shao and C. Zhou (2017). "Investigating novel resistance mechanisms to third generation EGFR TKI osimertinib in non-small cell lung cancer patients using next generation sequencing." Journal of Clinical Oncology **35**(15_suppl): 2572-2572.

Paez, J. G., P. A. Janne, J. C. Lee, S. Tracy, H. Greulich, S. Gabriel, P. Herman, F. J. Kaye, N. Lindeman, T. J. Boggon, K. Naoki, H. Sasaki, Y. Fujii, M. J. Eck, W. R. Sellers, B. E. Johnson and M. Meyerson (2004). "EGFR mutations in lung cancer: correlation with clinical response to gefitinib therapy." Science **304**(5676): 1497-1500.

Pagliarini, R., W. Shao and W. R. Sellers (2015). "Oncogene addiction: pathways of therapeutic response, resistance, and road maps toward a cure." EMBO Rep **16**(3): 280-296.

Pao, W., V. Miller, M. Zakowski, J. Doherty, K. Politi, I. Sarkaria, B. Singh, R. Heelan, V. Rusch, L. Fulton, E. Mardis, D. Kupfer, R. Wilson, M. Kris and H. Varmus (2004). "EGF receptor gene mutations are common in lung cancers from "never smokers" and are associated with sensitivity of tumors to gefitinib and erlotinib." Proc Natl Acad Sci U S A **101**(36): 13306-13311.

Pao, W., V. A. Miller, K. A. Politi, G. J. Riely, R. Somwar, M. F. Zakowski, M. G. Kris and H. Varmus (2005). "Acquired resistance of lung adenocarcinomas to gefitinib or erlotinib is associated with a second mutation in the EGFR kinase domain." PLoS Med **2**(3): e73.

Paoli, P., E. Giannoni and P. Chiarugi (2013). "Anoikis molecular pathways and its role in cancer progression." Biochim Biophys Acta **1833**(12): 3481-3498.

Park, K., C. J. Yu, S. W. Kim, M. C. Lin, V. Sriuranpong, C. M. Tsai, J. S. Lee, J. H. Kang, K. C. Chan, P. Perez-Moreno, P. Button, M. J. Ahn and T. Mok (2016). "First-Line Erlotinib Therapy Until and Beyond Response Evaluation Criteria in Solid Tumors Progression in Asian Patients With Epidermal Growth Factor Receptor Mutation-Positive Non-Small-Cell Lung Cancer: The ASPIRATION Study." JAMA Oncol **2**(3): 305-312.

Parkin, D. M., F. Bray, J. Ferlay and P. Pisani (2005). "Global cancer statistics, 2002." CA Cancer J Clin **55**(2): 74-108.

Peled, N., M. W. Wynes, N. Ikeda, T. Ohira, K. Yoshida, J. Qian, M. Ilouze, R. Brenner, Y. Kato, C. Mascaux and F. R. Hirsch (2013). "Insulin-like growth factor-1 receptor (IGF-1R) as a biomarker for resistance to the tyrosine kinase inhibitor gefitinib in non-small cell lung cancer." Cell Oncol (Dordr) **36**(4): 277-288.

Peters, S. and S. Zimmermann (2014). "Targeted therapy in NSCLC driven by HER2 insertions." Transl Lung Cancer Res **3**(2): 84-88.

Phuchareon, J., F. McCormick, D. W. Eisele and O. Tetsu (2015). "EGFR inhibition evokes innate drug resistance in lung cancer cells by preventing Akt activity and thus inactivating Ets-1 function." Proc Natl Acad Sci U S A **112**(29): E3855-3863.

Piotrowska, Z., M. J. Niederst, C. A. Karlovich, H. A. Wakelee, J. W. Neal, M. Mino-Kenudson, L. Fulton, A. N. Hata, E. L. Lockerman, A. Kalsy, S. Digumarthy, A. Muzikansky, M. Raponi, A. R. Garcia, H. E. Mulvey, M. K. Parks, R. H. DiCecca, D. Dias-Santagata, A. J. Iafrate, A. T. Shaw, A. R. Allen, J. A. Engelman and L. V. Sequist (2015). "Heterogeneity Underlies the Emergence of EGFRT790 Wild-Type Clones Following Treatment of T790M-Positive Cancers with a Third-Generation EGFR Inhibitor." Cancer Discov **5**(7): 713-722.

Piotrowska, Z., M. J. Niederst, M. Mino-Kenudson, V. Morales-Oyarvide, L. Fulton, E. L. Lockerman, E. Howe, J. F. Gainor, P. Fidias, S. Digumarthy, R. S. Heist, A. T. Shaw, J. A. Engelman and L. V. Sequist (2014). "Variation in mechanisms of acquired resistance (AR) among EGFR-mutant NSCLC patients with more than one post-resistant biopsy." J Clin Oncol **32:5s**: suppl; abstr 8053.

Pirker, R. and M. Filipits (2015). "Alectinib in RET-rearranged non-small cell lung cancer-Another progress in precision medicine?" Transl Lung Cancer Res **4**(6): 797-800.

Planchard, D., K. H. Brown, D. W. Kim, S. W. Kim, Y. Ohe, E. Felip, P. Leese, M. Cantarini, K. Vishwanathan, P. A. Janne, M. Ranson and P. A. Dickinson (2016). "Osimertinib Western and Asian clinical pharmacokinetics in patients and healthy volunteers: implications for formulation, dose, and dosing frequency in pivotal clinical studies." Cancer Chemother Pharmacol **77**(4): 767-776.

Planchard, D., Y. Loriot, F. Andre, A. Gobert, N. Auger, L. Lacroix and J. C. Soria (2015). "EGFR-independent mechanisms of acquired resistance to AZD9291 in EGFR T790M-positive NSCLC patients." Ann Oncol **26**(10): 2073-2078.

Plotnik, J. P., J. A. Budka, M. W. Ferris and P. C. Hollenhorst (2014). "ETS1 is a genome-wide effector of RAS/ERK signaling in epithelial cells." Nucleic Acids Res **42**(19): 11928-11940.

Plotnikov, A., E. Zehorai, S. Procaccia and R. Seger (2011). "The MAPK cascades: signaling components, nuclear roles and mechanisms of nuclear translocation." Biochim Biophys Acta **1813**(9): 1619-1633.

Politi, K., P. D. Fan, R. Shen, M. Zakowski and H. Varmus (2010). "Erlotinib resistance in mouse models of epidermal growth factor receptor-induced lung adenocarcinoma." Dis Model Mech **3**(1-2): 111-119.

Pollack, V. A., D. M. Savage, D. A. Baker, K. E. Tsaparikos, D. E. Sloan, J. D. Moyer, E. G. Barbacci, L. R. Pustilnik, T. A. Smolarek, J. A. Davis, M. P. Vaidya, L. D. Arnold, J. L. Doty, K. K. Iwata and M. J. Morin (1999). "Inhibition of epidermal growth factor receptor-associated tyrosine phosphorylation in human carcinomas with CP-358,774: dynamics of receptor inhibition in situ and antitumor effects in athymic mice." J Pharmacol Exp Ther **291**(2): 739-748.

Pollak, M. (2008). "Insulin and insulin-like growth factor signalling in neoplasia." Nat Rev Cancer **8**(12): 915-928.

Pollak, M. (2012). "The insulin and insulin-like growth factor receptor family in neoplasia: an update." Nat Rev Cancer **12**(3): 159-169.

Postmus, P. E., K. M. Kerr, M. Oudkerk, S. Senan, D. A. Waller, J. Vansteenkiste, C. Escriu and S. Peters (2017). "Early and locally advanced non-small-cell lung cancer (NSCLC): ESMO Clinical Practice Guidelines for diagnosis, treatment and follow-up†." Annals of Oncology **28**(suppl_4): iv1-iv21.

Puglisi, M., P. Thavasu, A. Stewart, J. S. de Bono, M. E. O'Brien, S. Popat, J. Bhosle and U. Banerji (2014). "AKT inhibition synergistically enhances growth-inhibitory effects of gefitinib and increases apoptosis in non-small cell lung cancer cell lines." Lung Cancer **85**(2): 141-146.

Quartuccio, S. M. and K. Schindler (2015). "Functions of Aurora kinase C in meiosis and cancer." Front Cell Dev Biol **3**: 50.

Quesnelle, K. M., A. L. Boehm and J. R. Grandis (2007). "STAT-mediated EGFR signaling in cancer." J Cell Biochem **102**(2): 311-319.

Ramirez, M., S. Rajaram, R. J. Steininger, D. Osipchuk, M. A. Roth, L. S. Morinishi, L. Evans, W. Ji, C. H. Hsu, K. Thurley, S. Wei, A. Zhou, P. R. Koduru, B. A. Posner, L. F. Wu and S. J. Altschuler (2016). "Diverse drug-resistance mechanisms can emerge from drug-tolerant cancer persister cells." Nat Commun **7**: 10690.

Red Brewer, M., S. H. Choi, D. Alvarado, K. Moravcevic, A. Pozzi, M. A. Lemmon and G. Carpenter (2009). "The juxtamembrane region of the EGF receptor functions as an activation domain." Mol Cell **34**(6): 641-651.

Reiter, J. L., D. W. Threadgill, G. D. Eley, K. E. Strunk, A. J. Danielsen, C. S. Sinclair, R. S. Pearsall, P. J. Green, D. Yee, A. L. Lampland, S. Balasubramaniam, T. D. Crossley, T. R. Magnuson, C. D. James and N. J. Maihle (2001). "Comparative genomic sequence analysis and isolation of human and mouse alternative EGFR transcripts encoding truncated receptor isoforms." Genomics **71**(1): 1-20.

Riedl, A., M. Schlederer, K. Pudelko, M. Stadler, S. Walter, D. Unterleuthner, C. Unger, N. Kramer, M. Hengstschlager, L. Kenner, D. Pfeiffer, G. Krupitza and H. Dolznig (2016). "Comparison of cancer cells cultured in 2D vs 3D reveals differences in AKT/mTOR/S6-kinase signaling and drug response." J Cell Sci.

Riely, G. J., M. G. Kris, B. Zhao, T. Akhurst, D. T. Milton, E. Moore, L. Tyson, W. Pao, N. A. Rizvi, L. H. Schwartz and V. A. Miller (2007). "Prospective assessment of discontinuation and reinitiation of erlotinib or gefitinib in patients with acquired resistance to erlotinib or gefitinib followed by the addition of everolimus." Clin Cancer Res **13**(17): 5150-5155.

Robinson, M. J. and M. H. Cobb (1997). "Mitogen-activated protein kinase pathways." Curr Opin Cell Biol **9**(2): 180-186.

Roskoski, R., Jr. (2014). "The ErbB/HER family of protein-tyrosine kinases and cancer." Pharmacol Res **79**: 34-74.

Rudin, C. M., E. Avila-Tang, C. C. Harris, J. G. Herman, F. R. Hirsch, W. Pao, A. G. Schwartz, K. H. Vahakangas and J. M. Samet (2009). "Lung cancer in never smokers: molecular profiles and therapeutic implications." Clin Cancer Res **15**(18): 5646-5661.

Rusch, V., J. Baselga, C. Cordon-Cardo, J. Orazem, M. Zaman, S. Hoda, J. McIntosh, J. Kurie and E. Dmitrovsky (1993). "Differential expression of the epidermal growth factor receptor and its ligands in primary non-small cell lung cancers and adjacent benign lung." Cancer Res **53**(10 Suppl): 2379-2385.

Rusnak, D. W., K. Lackey, K. Affleck, E. R. Wood, K. J. Alligood, N. Rhodes, B. R. Keith, D. M. Murray, W. B. Knight, R. J. Mullin and T. M. Gilmer (2001). "The effects of the novel, reversible epidermal growth factor receptor/ErbB-2 tyrosine kinase inhibitor, GW2016, on the growth of human normal and tumor-derived cell lines in vitro and in vivo." Mol Cancer Ther **1**(2): 85-94.

Scheck, R. A., M. A. Lowder, J. S. Appelbaum and A. Schepartz (2012). "Bipartite tetracysteine display reveals allosteric control of ligand-specific EGFR activation." ACS Chem Biol **7**(8): 1367-1376.

Schmitt, M. W., L. A. Loeb and J. J. Salk (2016). "The influence of subclonal resistance mutations on targeted cancer therapy." Nat Rev Clin Oncol **13**(6): 335-347.

Sequist, L. V., B. Besse, T. J. Lynch, V. A. Miller, K. K. Wong, B. Gitlitz, K. Eaton, C. Zacharchuk, A. Freyman, C. Powell, R. Ananthakrishnan, S. Quinn and J. C. Soria (2010). "Neratinib, an irreversible pan-ErbB receptor tyrosine kinase inhibitor: results of a phase II trial in patients with advanced non-small-cell lung cancer." J Clin Oncol **28**(18): 3076-3083.

Sequist, L. V., J. C. Soria, J. W. Goldman, H. A. Wakelee, S. M. Gadgeel, A. Varga, V. Papadimitrakopoulou, B. J. Solomon, G. R. Oxnard, R. Dziadziuszko, D. L. Aisner, R. C. Doebele, C. Galasso, E. B. Garon, R. S. Heist, J. Logan, J. W. Neal, M. A. Mendenhall, S. Nichols, Z. Piotrowska, A. J. Wozniak, M. Raponi, C. A. Karlovich, S. Jaw-Tsai, J. Isaacson, D. Despain, S. L. Matheny, L. Rolfe, A. R. Allen and D. R. Camidge (2015). "Rociletinib in EGFR-mutated non-small-cell lung cancer." N Engl J Med **372**(18): 1700-1709.

Sequist, L. V., B. A. Waltman, D. Dias-Santagata, S. Digumarthy, A. B. Turke, P. Fidias, K. Bergethon, A. T. Shaw, S. Gettinger, A. K. Cosper, S. Akhavanfard, R. S. Heist, J. Temel, J. G. Christensen, J. C. Wain, T. J. Lynch, K. Vernovsky, E. J. Mark, M. Lanuti, A. J. Iafrate, M. Mino-Kenudson and J. A. Engelman (2011). "Genotypic and histological evolution of lung cancers acquiring resistance to EGFR inhibitors." Sci Transl Med **3**(75): 75ra26.

Shan, Y., M. P. Eastwood, X. Zhang, E. T. Kim, A. Arkhipov, R. O. Dror, J. Jumper, J. Kuriyan and D. E. Shaw (2012). "Oncogenic mutations counteract intrinsic disorder in the EGFR kinase and promote receptor dimerization." Cell **149**(4): 860-870.

Sharma, S. V., D. W. Bell, J. Settleman and D. A. Haber (2007). "Epidermal growth factor receptor mutations in lung cancer." Nat Rev Cancer **7**(3): 169-181.

Sharma, S. V., M. A. Fischbach, D. A. Haber and J. Settleman (2006). ""Oncogenic shock": explaining oncogene addiction through differential signal attenuation." Clin Cancer Res **12**(14 Pt 2): 4392s-4395s.

Sharma, S. V., P. Gajowniczek, I. P. Way, D. Y. Lee, J. Jiang, Y. Yuza, M. Classon, D. A. Haber and J. Settleman (2006). "A common signaling cascade may underlie "addiction" to the Src, BCR-ABL, and EGF receptor oncogenes." Cancer Cell **10**(5): 425-435.

Sharma, S. V., D. Y. Lee, B. Li, M. P. Quinlan, F. Takahashi, S. Maheswaran, U. McDermott, N. Azizian, L. Zou, M. A. Fischbach, K. K. Wong, K. Brandstetter, B. Wittner, S. Ramaswamy, M. Classon and J. Settleman (2010). "A chromatin-mediated reversible drug-tolerant state in cancer cell subpopulations." Cell **141**(1): 69-80.

Sharma, S. V. and J. Settleman (2006). "Oncogenic shock: turning an activated kinase against the tumor cell." Cell Cycle **5**(24): 2878-2880.

Shcherbo, D., E. A. Souslova, J. Goedhart, T. V. Chepurnykh, A. Gaintzeva, Shemiakina, II, T. W. Gadella, S. Lukyanov and D. M. Chudakov (2009). "Practical and reliable FRET/FLIM pair of fluorescent proteins." BMC Biotechnol **9**: 24.

Shimizu, N., M. A. Behzadian and Y. Shimizu (1980). "Genetics of cell surface receptors for bioactive polypeptides: binding of epidermal growth factor is associated with the presence of human chromosome 7 in human-mouse cell hybrids." Proc Natl Acad Sci U S A **77**(6): 3600-3604.

Shostak, K. and A. Chariot (2015). "EGFR and NF-kappaB: partners in cancer." Trends Mol Med **21**(6): 385-393.

Sinclair, J. K., E. V. Denton and A. Schepartz (2014). "Inhibiting epidermal growth factor receptor at a distance." J Am Chem Soc **136**(32): 11232-11235.

Solca, F., G. Dahl, A. Zoephel, G. Bader, M. Sanderson, C. Klein, O. Kraemer, F. Himmelsbach, E. Haaksma and G. R. Adolf (2012). "Target binding properties and cellular activity of afatinib (BIBW 2992), an irreversible ErbB family blocker." J Pharmacol Exp Ther **343**(2): 342-350.

Soltoff, S. P., K. L. Carraway, 3rd, S. A. Prigent, W. G. Gullick and L. C. Cantley (1994). "ErbB3 is involved in activation of phosphatidylinositol 3-kinase by epidermal growth factor." Mol Cell Biol **14**(6): 3550-3558.

Soria, J. C., S. W. Kim, Y. L. Wu, K. Nakagawa, J. J. Yang, M. J. Ahn, J. Wang, J. C. H. Yang, Y. Lu, S. Atagi, S. P. Aix, Y. Rukazenkov, R. Taylor and T. S. K. Mok (2016). "Gefitinib/chemotherapy vs chemotherapy in EGFR mutation-positive NSCLC after progression on 1st line gefitinib (IMPRESS study): Final overall survival (OS) analysis." Annals of Oncology **27**(suppl_6): 1201O-1201O.

Sos, M. L., M. Koker, B. A. Weir, S. Heynck, R. Rabinovsky, T. Zander, J. M. Seeger, J. Weiss, F. Fischer, P. Frommolt, K. Michel, M. Peifer, C. Mermel, L. Girard, M. Peyton, A. F. Gazdar, J. D. Minna, L. A. Garraway, H. Kashkar, W. Pao, M. Meyerson and R. K. Thomas (2009). "PTEN loss contributes to erlotinib resistance in EGFR-mutant lung cancer by activation of Akt and EGFR." Cancer Res **69**(8): 3256-3261.

Stella, G. M., R. Scabini, S. Inghilleri, F. Cemmi, S. Corso, E. Pozzi, P. Morbini, A. Valentini, R. Dore, S. Ferrari, M. Luisetti and M. Zorzetto (2013). "EGFR and KRAS mutational profiling in fresh non-small cell lung cancer (NSCLC) cells." J Cancer Res Clin Oncol **139**(8): 1327-1335.

Subramanian, A., P. Tamayo, V. K. Mootha, S. Mukherjee, B. L. Ebert, M. A. Gillette, A. Paulovich, S. L. Pomeroy, T. R. Golub, E. S. Lander and J. P. Mesirov (2005). "Gene set enrichment analysis: a knowledge-based approach for interpreting genome-wide expression profiles." Proc Natl Acad Sci U S A **102**(43): 15545-15550.

Suda, K., I. Murakami, K. Sakai, K. Tomizawa, H. Mizuuchi, K. Sato, K. Nishio and T. Mitsudomi (2016). "Heterogeneity in resistance mechanisms causes shorter duration

of epidermal growth factor receptor kinase inhibitor treatment in lung cancer." Lung Cancer **91**: 36-40.

Sun, S., J. H. Schiller and A. F. Gazdar (2007). "Lung cancer in never smokers--a different disease." Nat Rev Cancer **7**(10): 778-790.

Sutherland, R. M. (1988). "Cell and environment interactions in tumor microregions: the multicell spheroid model." Science **240**(4849): 177-184.

Sutherland, R. M., J. A. McCredie and W. R. Inch (1971). "Growth of multicell spheroids in tissue culture as a model of nodular carcinomas." J Natl Cancer Inst **46**(1): 113-120.

Sutto, L. and F. L. Gervasio (2013). "Effects of oncogenic mutations on the conformational free-energy landscape of EGFR kinase." Proc Natl Acad Sci U S A **110**(26): 10616-10621.

Suzuki, T., R. Ito, T. Yamaoka, T. Ohmori, K. Nishio and Y. Ogasawara (2017). "Abstract 4098: Tyrosine kinase inhibitor resistance were decreased in spheroid culture platform." Cancer Research **77**(13 Supplement): 4098-4098.

Takeda, M., I. Okamoto and K. Nakagawa (2014). "Survival outcome assessed according to tumor response and shrinkage pattern in patients with EGFR mutation-positive non-small-cell lung cancer treated with gefitinib or erlotinib." J Thorac Oncol **9**(2): 200-204.

Taniguchi, K., J. Uchida, K. Nishino, T. Kumagai, T. Okuyama, J. Okami, M. Higashiyama, K. Kodama, F. Imamura and K. Kato (2011). "Quantitative detection of EGFR mutations in circulating tumor DNA derived from lung adenocarcinomas." Clin Cancer Res **17**(24): 7808-7815.

Thongprasert, S., E. Duffield, N. Saijo, Y. L. Wu, J. C. Yang, D. T. Chu, M. Liao, Y. M. Chen, H. P. Kuo, S. Negoro, K. C. Lam, A. Armour, P. Magill and M. Fukuoka (2011). "Health-related quality-of-life in a randomized phase III first-line study of gefitinib versus carboplatin/paclitaxel in clinically selected patients from Asia with advanced NSCLC (IPASS)." J Thorac Oncol **6**(11): 1872-1880.

Thress, K. S., C. P. Paweletz, E. Felip, B. C. Cho, D. Stetson, B. Dougherty, Z. Lai, A. Markovets, A. Vivancos, Y. Kuang, D. Ercan, S. E. Matthews, M. Cantarini, J. C. Barrett, P. A. Janne and G. R. Oxnard (2015). "Acquired EGFR C797S mutation mediates resistance to AZD9291 in non-small cell lung cancer harboring EGFR T790M." Nat Med.

Tricker, E. M., C. Xu, S. Uddin, M. Capelletti, D. Ercan, A. Ogino, C. A. Pratilas, N. Rosen, N. S. Gray, K. K. Wong and P. A. Janne (2015). "Combined EGFR/MEK Inhibition Prevents the Emergence of Resistance in EGFR-Mutant Lung Cancer." Cancer Discov **5**(9): 960-971.

Uchibori, K., N. Inase, M. Araki, M. Kamada, S. Sato, Y. Okuno, N. Fujita and R. Katayama (2017). "Brigatinib combined with anti-EGFR antibody overcomes osimertinib resistance in EGFR-mutated non-small-cell lung cancer." Nat Commun **8**: 14768.

Ullrich, A., L. Coussens, J. S. Hayflick, T. J. Dull, A. Gray, A. W. Tam, J. Lee, Y. Yarden, T. A. Libermann, J. Schlessinger and et al. (1984). "Human epidermal growth factor receptor cDNA sequence and aberrant expression of the amplified gene in A431 epidermoid carcinoma cells." Nature **309**(5967): 418-425.

Vallee, A., C. Audigier-Valette, G. Herbreteau, J. Merrien, L. Tessonnier, S. Theoleyre and M. G. Denis (2016). "Rapid clearance of circulating tumor DNA during treatment with AZD9291 of a lung cancer patient presenting the resistance EGFR T790M mutation." Lung Cancer **91**: 73-74.

Van Assche, K., L. Ferdinande, Y. Lievens, K. Vandecasteele and V. Surmont (2014). "EGFR Mutation Positive Stage IV Non-Small-Cell Lung Cancer: Treatment Beyond Progression." Front Oncol **4**: 350.

van der Wekken, A. J., A. Saber, T. J. Hiltermann, K. Kok, A. van den Berg and H. J. Groen (2016). "Resistance mechanisms after tyrosine kinase inhibitors afatinib and crizotinib in non-small cell lung cancer, a review of the literature." Crit Rev Oncol Hematol.

Vyse, S., A. Howitt and P. H. Huang (2017). "Exploiting Synthetic Lethality and Network Biology to Overcome EGFR Inhibitor Resistance in Lung Cancer." J Mol Biol **429**(12): 1767-1786.

Wakeling, A. E., S. P. Guy, J. R. Woodburn, S. E. Ashton, B. J. Curry, A. J. Barker and K. H. Gibson (2002). "ZD1839 (Iressa): an orally active inhibitor of epidermal growth factor signaling with potential for cancer therapy." Cancer Res **62**(20): 5749-5754.

Walter, A. O., R. T. Sjin, H. J. Haringsma, K. Ohashi, J. Sun, K. Lee, A. Dubrovskiy, M. Labenski, Z. Zhu, Z. Wang, M. Sheets, T. St Martin, R. Karp, D. van Kalken, P. Chaturvedi, D. Niu, M. Nacht, R. C. Petter, W. Westlin, K. Lin, S. Jaw-Tsai, M. Raponi, T. Van Dyke, J. Etter, Z. Weaver, W. Pao, J. Singh, A. D. Simmons, T. C. Harding and A. Allen (2013). "Discovery of a mutant-selective covalent inhibitor of EGFR that overcomes T790M-mediated resistance in NSCLC." Cancer Discov **3**(12): 1404-1415.

Wang, D. D., L. Ma, M. P. Wong, V. H. Lee and H. Yan (2015). "Contribution of EGFR and ErbB-3 Heterodimerization to the EGFR Mutation-Induced Gefitinib- and Erlotinib-Resistance in Non-Small-Cell Lung Carcinoma Treatments." PLoS One **10**(5): e0128360.

Wang, S., S. Cang and D. Liu (2016). "Third-generation inhibitors targeting EGFR T790M mutation in advanced non-small cell lung cancer." J Hematol Oncol **9**: 34.

Ward, R. A., M. J. Anderton, S. Ashton, P. A. Bethel, M. Box, S. Butterworth, N. Colclough, C. G. Chorley, C. Chuaqui, D. A. Cross, L. A. Dakin, J. E. Debreczeni, C. Eberlein, M. R. Finlay, G. B. Hill, M. Grist, T. C. Klinowska, C. Lane, S. Martin, J. P. Orme, P. Smith, F. Wang and M. J. Waring (2013). "Structure- and reactivity-based development of covalent inhibitors of the activating and gatekeeper mutant forms of the epidermal growth factor receptor (EGFR)." J Med Chem **56**(17): 7025-7048.

Wistuba, II, D. Bryant, C. Behrens, S. Milchgrub, A. K. Virmani, R. Ashfaq, J. D. Minna and A. F. Gazdar (1999). "Comparison of features of human lung cancer cell lines and their corresponding tumors." Clin Cancer Res **5**(5): 991-1000.

Workman, P., E. O. Aboagye, F. Balkwill, A. Balmain, G. Bruder, D. J. Chaplin, J. A. Double, J. Everitt, D. A. H. Farningham, M. J. Glennie, L. R. Kelland, V. Robinson, I. J. Stratford, G. M. Tozer, S. Watson, S. R. Wedge and S. A. Eccles (2010). "Guidelines for the welfare and use of animals in cancer research." Br J Cancer **102**(11): 1555-1577.

Yamaguchi, T., S. Isogai, T. Okamura, S. Uozu, Y. Mieno, T. Hoshino, Y. Goto, M. Hayashi, T. Nakanishi and K. Imaizumi (2015). "Pharmacokinetics of gefitinib in a patient with non-small cell lung cancer undergoing continuous ambulatory peritoneal dialysis." Case Rep Oncol **8**(1): 78-82.

Yang, J. C., Y. L. Wu, M. Schuler, M. Sebastian, S. Popat, N. Yamamoto, C. Zhou, C. P. Hu, K. O'Byrne, J. Feng, S. Lu, Y. Huang, S. L. Geater, K. Y. Lee, C. M. Tsai, V. Gorbunova, V. Hirsh, J. Bennouna, S. Orlov, T. Mok, M. Boyer, W. C. Su, K. H. Lee, T. Kato, D. Massey, M. Shahidi, V. Zazulina and L. V. Sequist (2015). "Afatinib versus cisplatin-based chemotherapy for EGFR mutation-positive lung adenocarcinoma (LUX-Lung 3 and LUX-Lung 6): analysis of overall survival data from two randomised, phase 3 trials." Lancet Oncol **16**(2): 141-151.

Yeo, C. D., K. H. Park, C. K. Park, S. H. Lee, S. J. Kim, H. K. Yoon, Y. S. Lee, E. J. Lee, K. Y. Lee and T. J. Kim (2015). "Expression of insulin-like growth factor 1 receptor (IGF-1R) predicts poor responses to epidermal growth factor receptor (EGFR) tyrosine kinase inhibitors in non-small cell lung cancer patients harboring activating EGFR mutations." Lung Cancer **87**(3): 311-317.

Yoshida, T., L. Song, Y. Bai, F. Kinose, J. Li, K. C. Ohaegbulam, T. Munoz-Antonia, X. Qu, S. Eschrich, H. Uramoto, F. Tanaka, P. Nasarre, R. M. Gemmill, J. Roche, H. A. Drabkin and E. B. Haura (2016). "ZEB1 Mediates Acquired Resistance to the Epidermal Growth Factor Receptor-Tyrosine Kinase Inhibitors in Non-Small Cell Lung Cancer." PLoS One **11**(1): e0147344.

Yoshida, T., G. Zhang, M. A. Smith, A. S. Lopez, Y. Bai, J. Li, B. Fang, J. Koomen, B. Rawal, K. J. Fisher, A. Y. Chen, M. Kitano, Y. Morita, H. Yamaguchi, K. Shibata, T. Okabe, I. Okamoto, K. Nakagawa and E. B. Haura (2014). "Tyrosine Phosphoproteomics Identifies Both Codrivers and Cotargeting Strategies for T790M-Related EGFR-TKI Resistance in Non-Small Cell Lung Cancer." Clin Cancer Res **20**(15): 4059-4074.

Yoshioka, H., T. Mitsudomi, S. Morita, Y. Yatabe, S. Negoro, I. Okamoto, T. Seto, M. Satouchi, H. Tada, T. Hirashima, K. Asami, N. Katakami, M. Takada, K. Shibata, S. Kudoh, E. Shimizu, H. Saito, S. Toyooka, K. Nakagawa and M. Fukuoka (2014). "Final overall survival results of WJTOG 3405, a randomized phase 3 trial comparing gefitinib (G) with cisplatin plus docetaxel (CD) as the first-line treatment for patients with non-small cell lung cancer (NSCLC) harboring mutations of the epidermal growth factor receptor (EGFR)." Journal of Clinical Oncology **32**(15_suppl): 8117-8117.

Yu, H. A., M. E. Arcila, M. D. Hellmann, M. G. Kris, M. Ladanyi and G. J. Riely (2014). "Poor response to erlotinib in patients with tumors containing baseline EGFR T790M mutations found by routine clinical molecular testing." Ann Oncol **25**(2): 423-428.

Yu, H. A., M. E. Arcila, N. Rekhtman, C. S. Sima, M. F. Zakowski, W. Pao, M. G. Kris, V. A. Miller, M. Ladanyi and G. J. Riely (2013). "Analysis of tumor specimens at the time of acquired resistance to EGFR-TKI therapy in 155 patients with EGFR-mutant lung cancers." Clin Cancer Res **19**(8): 2240-2247.

Yu, Z., T. J. Boggon, S. Kobayashi, C. Jin, P. C. Ma, A. Dowlati, J. A. Kern, D. G. Tenen and B. Halmos (2007). "Resistance to an irreversible epidermal growth factor receptor (EGFR) inhibitor in EGFR-mutant lung cancer reveals novel treatment strategies." Cancer Res **67**(21): 10417-10427.

Yun, C. H., T. J. Boggon, Y. Li, M. S. Woo, H. Greulich, M. Meyerson and M. J. Eck (2007). "Structures of lung cancer-derived EGFR mutants and inhibitor complexes: mechanism of activation and insights into differential inhibitor sensitivity." Cancer Cell **11**(3): 217-227.

Yun, C. H., K. E. Mengwasser, A. V. Toms, M. S. Woo, H. Greulich, K. K. Wong, M. Meyerson and M. J. Eck (2008). "The T790M mutation in EGFR kinase causes drug resistance by increasing the affinity for ATP." Proc Natl Acad Sci U S A **105**(6): 2070-2075.

Zaiontz, C. (2015). "Real Statistics Using Excel." Retrieved 07.08.2017, 2017, from http://www.real-statistics.com/.

Zhang, X., N. Belkina, H. K. Jacob, T. Maity, R. Biswas, A. Venugopalan, P. G. Shaw, M. S. Kim, R. Chaerkady, A. Pandey and U. Guha (2015). "Identifying novel targets of oncogenic EGF receptor signaling in lung cancer through global phosphoproteomics." Proteomics **15**(2-3): 340-355.

Zhang, X., J. Gureasko, K. Shen, P. A. Cole and J. Kuriyan (2006). "An allosteric mechanism for activation of the kinase domain of epidermal growth factor receptor." Cell **125**(6): 1137-1149.

Zhang, X., T. Maity, M. K. Kashyap, M. Bansal, A. Venugopalan, S. Singh, S. Awasthi, A. Marimuthu, H. K. Charles Jacob, N. Belkina, S. Pitts, C. M. Cultraro, S. Gao, G. Kirkali, R. Biswas, R. Chaerkady, A. Califano, A. Pandey and U. Guha

(2017). "Quantitative Tyrosine Phosphoproteomics of Epidermal Growth Factor Receptor (EGFR) Tyrosine Kinase Inhibitor-treated Lung Adenocarcinoma Cells Reveals Potential Novel Biomarkers of Therapeutic Response." Mol Cell Proteomics **16**(5): 891-910.

Zhang, Z., S. Kobayashi, A. C. Borczuk, R. S. Leidner, T. Laframboise, A. D. Levine and B. Halmos (2010). "Dual specificity phosphatase 6 (DUSP6) is an ETS-regulated negative feedback mediator of oncogenic ERK signaling in lung cancer cells." Carcinogenesis **31**(4): 577-586.

Zhao, B., M. T. Hemann and D. A. Lauffenburger (2014). "Intratumor heterogeneity alters most effective drugs in designed combinations." Proc Natl Acad Sci U S A **111**(29): 10773-10778.

Zhao, D., X. Chen, N. Qin, D. Su, L. Zhou, Q. Zhang, X. Li, X. Zhang, M. Jin and J. Wang (2017). "The prognostic role of EGFR-TKIs for patients with advanced non-small cell lung cancer." Sci Rep **7**: 40374.

Zhou, C., Y. L. Wu, G. Chen, J. Feng, X. Q. Liu, C. Wang, S. Zhang, J. Wang, S. Zhou, S. Ren, S. Lu, L. Zhang, C. Hu, C. Hu, Y. Luo, L. Chen, M. Ye, J. Huang, X. Zhi, Y. Zhang, Q. Xiu, J. Ma, L. Zhang and C. You (2011). "Erlotinib versus chemotherapy as first-line treatment for patients with advanced EGFR mutation-positive non-small-cell lung cancer (OPTIMAL, CTONG-0802): a multicentre, open-label, randomised, phase 3 study." Lancet Oncol **12**(8): 735-742.

Zulkifli, A. A., F. H. Tan, T. L. Putoczki, S. S. Stylli and R. B. Luwor (2017). "STAT3 signaling mediates tumour resistance to EGFR targeted therapeutics." Mol Cell Endocrinol **451**: 15-23.

Supplementary figures

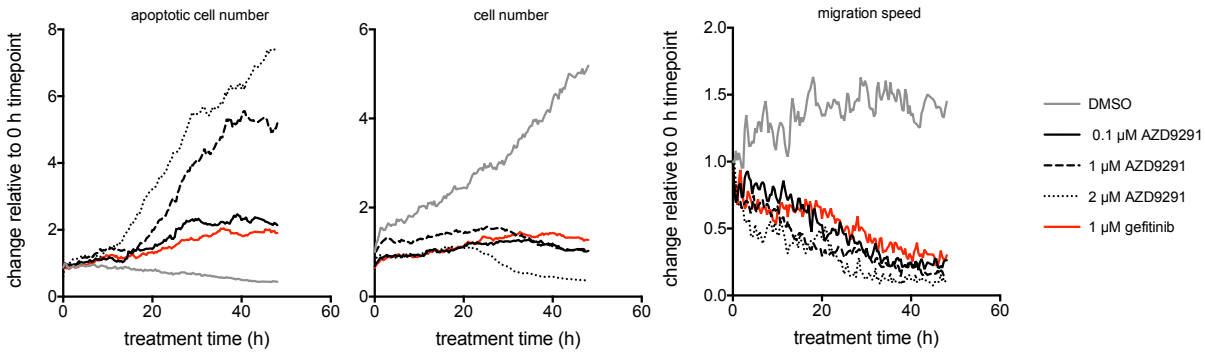


Figure S 1: Changes in apoptotic cell number, total cell number and migration speed of PC9 under AZD9291 or gefitinib treatment

Quantification of live cell imaging over 48 h. Cell number, number of apoptotic cells and migration speed as calculated by IMARIS software are relative to the highest measurement within the first hour. Data represents the mean of 2 wells/condition.

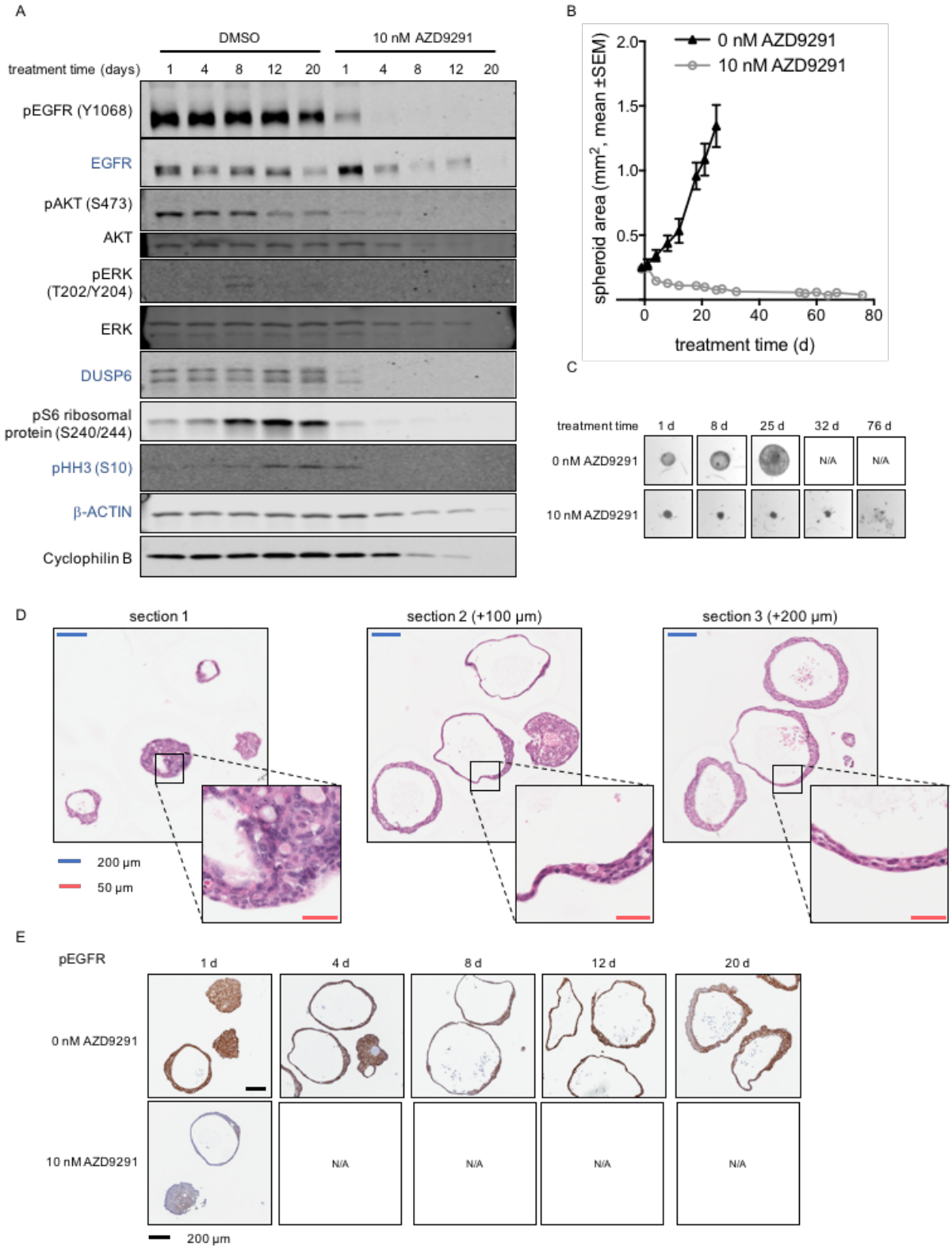


Figure S 2: HCC827 spheroids form hollow spheroids and are hypersensitive to AZD9291 treatment

A: Western blot analysis of HCC827 spheroids under AZD9291/DMSO treatment. It was not possible to extract sufficient protein from AZD9291 treated spheroids from day 8 onwards. B: Quantification of spheroid size over time for HCC827 spheroids treated with AZD9291/DMSO. C: Pictures of one representative spheroid over time for each treatment group. D: H&E staining of consecutive sections of 4 untreated HCC827 spheroids, showing thin layer of cells around a hollow spheroid centre. E: IHC staining for pEGFR on untreated HCC827 spheroid and spheroids treated for 24 h. Brown staining indicates presence of the antibody, showing reduction of pEGFR levels upon AZD9291 treatment. Analysis of spheroids treated for more than 24 h was not possible as we were unable to process those disintegrating spheroids.

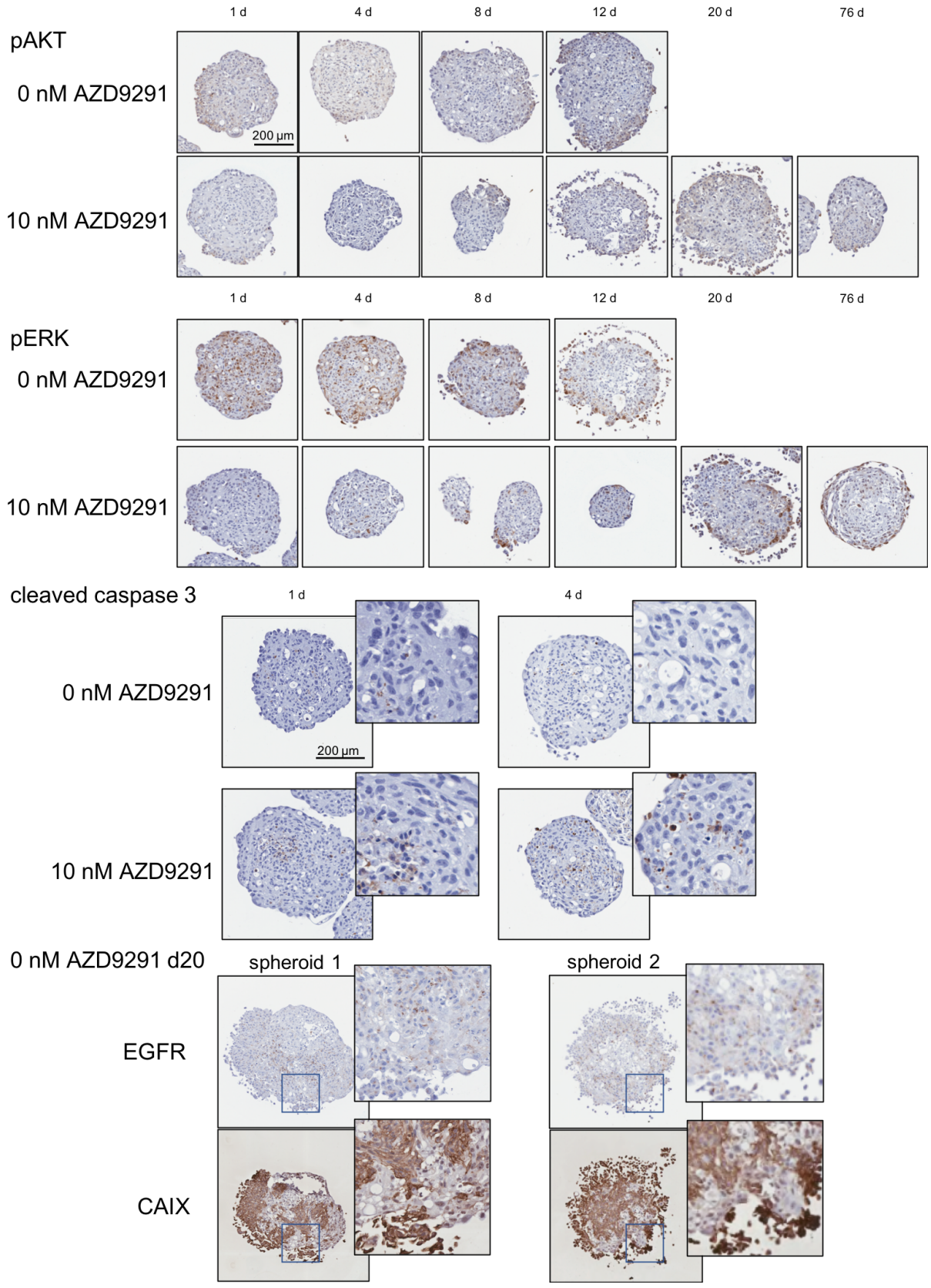


Figure S 3: AZD9291 treatment leads to transient reduction of pAKT and pERK as well as increase in cleaved caspase in H1975 spheroids

Images of representative H1975 spheroids under indicated treatments, stained for pAKT, pERK, cleaved caspase 3, EGFR and CAIX, brown colour indicates antibody reactivity. Spheroids were treated for indicated times, fixed in 10 % neutral buffered formalin and processed for paraffin embedding. All Spheroids are stained on one slide. Sections for EGFR and CAIX staining are serial sections.

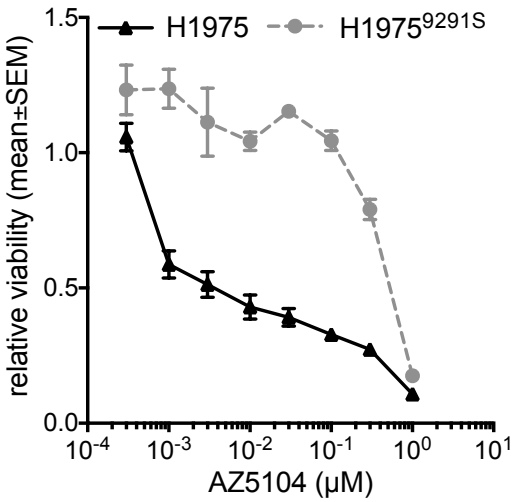


Figure S 4: H1975^{9291S} cells are resistant to the AZD9291 active metabolite AZ5104

Viability of H1975 and H1975^{9291S} cells was assessed under increasing concentrations of AZ5104. Data are from one experiment performed in technical triplicates.

Appendix

Table S 1: Antibodies used for RPPA analysis

Bad P Ser136	Stat5 P Tyr694	GSK-3-beta P Ser9	Raf1 (C-12)
IKK alpha/beta P Ser176/Ser177	Akt P Thr308	GSK-3-beta	p21 CIP/WAF1 p Thr145
MSK1 P Ser376	Met	Tuberin P S1387	mTOR P Ser2481
ErbB-2/Her2/EGFR P Tyr1248/Tyr1173	IkB-alpha P Ser32	PLC-gamma1	IRS-1 P S636/639
NFkB p65 Ser536	p44/42 MAPK (ERK1/2)	VEGFR P Tyr951	p70 S6 Kinase P Thr421,Ser424
E-Cadherin	p44/42 MAPK (ERK1/2) P Thr202/Thr185,Tyr204/Tyr187	Bcl-2 P Ser70	EGFR P Tyr1086
4E-BP1 P Thr37,Thr46	Src	ErbB-2/Her2/EGFR	Stat5
PTEN P Ser380,Thr382,Thr383	Akt	IGF-1R beta P Tyr1162,Tyr1163	Stat1 P Ser727
mTOR P Ser2448	Akt P Ser473	SAPK/JNK	JAK1 P Tyr1022,Thr1023
mTOR	c-Myc	GSK-3-alpha/beta P Ser21/Ser9	beta-Tubulin
PLC-gamma1 P Tyr783	4E-BP1 P Ser65	Stat6	Prohibitin
PDK-1 P Ser241	PTEN	MAPKAPK-2	p90 S6 kinase (Rsk1-3)
p90 S6 kinase (Rsk1-3) P Thr359,Ser363	Tsc-2 (Tuberin) P Thr1462	Stat3	p53
p70 S6 Kinase	p70 S6 Kinase P Thr389	VEGFR P Tyr1059	Histone H2A.X P Ser139
c-Myc P Thr58,Ser62	p53 P Ser15	IkB-alpha	CrkL
S6 Ribosomal protein p Ser240,Ser244	p38 MAPK PThr180,Tyr182	MEK1/2	Ki-67 (Annexin II, p36)
S6 Ribosomal Protein	p38 MAPK	MEK1/2 P Ser217/221	Cyclin D1
c-Jun N-term	Raf P Ser259	Met P Tyr1234	Stat1
Stat6 P Tyr641	PDK-1	Met P Tyr1349	Stat3 P Tyr705
PDGFR P Tyr1021	SAPK/JNK P Thr183,Tyr185	ErbB-1/EGFR	Ras
PDGFR P Tyr751	Rb P Ser807,Ser811	EGFR P Tyr1173	p21 CIP/WAF1
FAK1	Rb P Ser780	S6 Ribosomal protein P Ser235,Ser236	PKC-alpha
FAK1 P Y397	Raf P Ser338	beta-actin	Bak
CrkL P Tyr207	MAPKAPK-2 P Thr334	c-Jun P Ser73	Bim
Bad P Ser112	Stat1 P Tyr701	Rb	Bid
JAK1	Src (family) P Tyr416	VEGFR P Tyr1175	Bim P Ser69
MNK1 (MKNK) P Thr197,Thr202	Cyclin D1 P Thr286	Tsc-2 (Tuberin)	Bcl-x
PI3 Kinase p110-alpha	Bcl-2	IRS-1	Plk1 P
ErbB-3/Her3/EGFR	Caspase 3	NFkB p105/p50	
ErbB-3/Her3/EGFR P Tyr1289	Caspase 3 cleaved	PKC-alpha P Thr638	

Table S 2: IC50 values for selected EGFR M+ NSCLC cell lines and derived resistant cell lines for a number of EGFR-TKIs

Data represent mean IC50 (SEM) of at least 2 independent experiments performed in technical triplicates.

Cell line	gefitinib	erlotinib	afatinib	AZD9291	CO-1686
HCC827	0.004 (0.0007)	0.01 (0.003)	0.001 (0.00002)	0.016 (0.009)	0.05 (0.01)
PC9	0.02 (0.001)	0.04 (0.004)	0.00002 (0.00001)	0.006 (0.0007)	0.07 (0.01)
H1975	9.31 (0.29)	n/d	0.54 (0.05)	0.007 (0.0009)	0.23 (0.02)
$PC9^{GS}$	2.89 (0.27)	5.69 (0.12)	0.89 (0.11)	0.06 (0.03)	0.13 (0.01)
$PC9^{9291S}$	2.23 (0.25)	10.75 (2.09)	1.22 (0.1)	0.96 (0.05)	1.69 (0.27)
$HCC827^{GS}$	4.88 (0.24)	10.04 (1.27)	1.02 (0.11)	1.18 (0.05)	12.35 (1.37)
$H1975^{9291S}$	n/d	n/d	1 (0.05)	1.41 (0.06)	2.28 (0.11)

Table S 3: List of variant calls in resistant cells detected via RNAseq

Variant calls present in resistant but not parental cells with an allele frequency > 10 % are listed below, including gene name, amino acid position, reference and variant amino acid as well as allele frequency.

	AA position	AA ref/alt	allele frequency
PC9^{GS}			
CHCHD4	111/124	D/N	0.24
MCAT	240	G/V	0.21
YAP1	188/312/350/366	S/C	0.21
EGFR	790	T/M	0.16
MAP2K7	369	P/A	0.14
PC9^{9291S}			
PDS5A	839	I/M	0.41
PLXNA1	1364	K/Q	0.29
JUN	126	T/S	0.35
ASNA1	191	M/T	0.20
CTR9	1131	D/N	0.32
POLD1	417	T/I	0.26
HEATR1	1654	R/H	0.20
RPL3	334/383	E/*	0.15
NRAS	61	Q/R	0.16
IGSF3	1175/1195	N/K	0.12
HCC827^{GS}			
CCNYL1	31/101	E/D	0.27
APBB2	179	R/Q	0.33
GGCX	268/325	R/Q	0.48
SPTAN1	64	Q/K	0.23
TNRC18	27	P/H	0.37
ARHGAP23	630	T/P	0.11
EDN2	103	D/A	0.20
H1975^{9291S}			
PDE4DIP	77/109/112/175	I/M	0.69
TBC1D23	39	I/R	0.26
PEMT	86/101/123	T/P	0.15
MARCKSL1	153	E/D	0.10

Table S 4: Significant expression changes in HCC827^{GS} and H1975^{9291S} compared to their parental cell lines

	HCC827^{GS}			H1975^{9291S}	
transcript	log_2 FC	padj-value	transcript	log_2 FC	padj-value
PTH1R	8.83	1.34E-27	SELENOP	4.75	3.20E-06
ALDH1A1	8.36	1.62E-36	LINC01133	4.64	5.08E-05
TTC21B-AS1	8.26	2.38E-15	TAGLN	3.61	3.85E-17
SEMA6A	8.19	8.94E-37	AL590004.4	2.92	1.12E-05
MACROD2	8.07	3.84E-74	COL4A5	2.81	1.26E-08
TMEM52B	7.97	1.06E-17	CYBRD1	2.73	1.99E-07
PDZK1	7.76	6.84E-33	TMPRSS3	2.72	9.54E-03
DCDC2	7.66	5.66E-28	INHBB	2.71	1.52E-08
CRCT1	7.58	1.09E-11	PLSCR4	2.61	6.40E-04
FOLR3	7.50	1.26E-12	S1PR1	2.48	7.30E-03
AC013275.1	7.33	8.21E-13	C1orf115	2.46	3.17E-04
CHST9	7.31	4.11E-17	CTGF	2.40	2.77E-06
CXCL14	7.16	4.76E-11	PXYLP1	2.34	1.76E-04
CYS1	6.99	2.54E-13	PPM1L	2.29	2.06E-04
PSG8	6.98	1.72E-10	RFLNB	2.29	9.94E-03
ADGRL2	6.92	5.82E-62	ACKR3	2.26	2.02E-03
AL080314.2	6.86	4.44E-13	KRT16	2.14	1.51E-04
NCKAP5	6.70	8.85E-13	KLK5	2.11	4.41E-06
GJB1	6.67	1.61E-20	WFDC21P	2.08	6.18E-03
EDNRB	6.61	2.21E-08	PALMD	2.02	8.13E-03
IGFBP7	6.54	2.17E-23	CPA4	1.74	2.06E-04
RNA5-8SP6	6.48	3.34E-18	PVT1	1.74	1.40E-04
GSG1	6.26	7.14E-31	MEGF6	1.65	2.13E-03
BCL2	6.25	2.57E-15	NEDD9	1.64	7.24E-04
PSG5	6.18	1.72E-18	AQP3	1.61	6.36E-04
SPP1	6.13	7.70E-50	PTPRG	1.60	2.66E-03
MDGA1	6.07	1.53E-20	HS6ST2	1.51	4.25E-04
TNFAIP6	5.91	2.95E-07	CYP1B1	1.45	1.24E-03
NPNT	5.83	1.67E-09	NADK2	1.36	9.13E-03
MME	5.70	1.08E-19	AKR1C1	1.33	9.76E-03
SEMA5A	5.63	3.54E-17	PTGFRN	1.32	5.44E-03
DIRAS2	5.55	3.02E-07	AKR1B1	-1.17	6.92E-03
HOGA1	5.51	2.68E-12	PLAU	-1.27	5.61E-03
AQP4	5.40	1.87E-05	AMIGO2	-1.32	6.12E-03
UGT2B7	5.33	1.94E-06	ACSL5	-1.33	8.29E-03
KCTD12	5.29	2.10E-27	NPC2	-1.36	1.92E-03
EPDR1	5.03	1.08E-36	FHL2	-1.36	7.92E-03
Y_RNA	4.99	5.41E-05	ITGA5	-1.37	2.70E-03
EMX1	4.94	8.54E-05	ARHGDIB	-1.40	5.44E-03

ABCB1	4.91	2.51E-19	VEGFA	-1.41	1.65E-03
FLJ22447	4.89	3.06E-12	H1F0	-1.41	1.78E-03
RMRP	4.88	2.01E-07	CDS1	-1.42	5.59E-03
EFHB	4.86	1.03E-09	NRP1	-1.44	1.78E-03
CFAP221	4.80	2.69E-06	LIPH	-1.46	3.77E-03
PCSK5	4.77	4.06E-13	LAMB3	-1.47	6.13E-03
XK	4.74	4.11E-08	DCBLD2	-1.47	2.07E-04
VGLL1	4.69	1.87E-22	CRYBG1	-1.51	9.09E-04
7SK	4.67	1.30E-08	PLAUR	-1.52	8.57E-03
AL355075.4	4.66	2.49E-06	MYO1D	-1.52	3.77E-03
EDN2	4.62	5.01E-17	LAMC2	-1.53	1.08E-03
TMEM213	4.58	5.59E-04	IRS1	-1.55	2.17E-03
LINC01638	4.57	3.21E-05	LIMK1	-1.55	1.05E-03
HBEGF	4.50	3.08E-17	SMAGP	-1.58	4.40E-03
RFTN1	4.29	1.07E-06	TGM2	-1.59	3.84E-05
CLVS1	4.24	1.66E-03	IQANK1	-1.59	5.44E-03
SIRPA	4.20	1.41E-19	ENO2	-1.62	1.89E-03
AGT	4.16	2.54E-08	SCD	-1.67	7.67E-06
RNF182	4.16	6.33E-05	JADE2	-1.68	2.71E-04
SLC6A3	4.11	1.04E-03	ITGA3	-1.69	1.67E-04
ADAMTSL4	4.10	3.09E-16	LIPG	-1.72	4.90E-05
ATP6V0A4	4.03	1.40E-05	RARG	-1.75	2.03E-04
CSNK1A1P1	3.90	3.89E-03	GRHL1	-1.75	2.33E-03
USH1C	3.86	3.91E-03	PMEPA1	-1.77	2.07E-04
TNFRSF19	3.84	1.07E-08	SRCIN1	-1.77	8.42E-03
SLITRK5	3.84	2.62E-04	FAM129A	-1.82	9.45E-04
MATN2	3.83	2.75E-19	B3GNT3	-1.82	6.53E-05
CYFIP2	3.83	2.07E-08	OLMALINC	-1.84	6.18E-03
VNN2	3.82	7.84E-04	LTBP2	-1.85	4.49E-05
FGFR1	3.82	3.82E-20	PRKCH	-1.85	4.78E-04
PPP2R2C	3.81	4.28E-16	MYO5C	-1.87	1.31E-03
PLEKHA2	3.80	2.80E-24	PLEK2	-1.87	3.33E-04
ADAMTS1	3.80	4.67E-06	CCBE1	-1.87	1.62E-04
NPY4R	3.78	3.79E-03	MRC2	-1.89	1.52E-03
SERPINE1	3.78	1.36E-14	ANPEP	-1.89	1.12E-05
KCNS1	3.77	1.48E-04	SERPINA1	-1.92	2.15E-04
SLC38A4	3.76	8.89E-05	COL17A1	-1.92	2.06E-04
UPK3B	3.76	1.35E-05	PKIB	-1.95	1.71E-04
TFPI2	3.73	1.13E-19	PLEKHG6	-1.96	7.63E-03
LRRN2	3.72	1.36E-03	AC093840.1	-1.98	1.33E-03
AC097059.2	3.69	5.39E-07	TMC6	-1.98	7.45E-04
FILIP1L	3.69	6.88E-21	CLDN3	-2.00	7.52E-03

WISP2	3.67	3.01E-14	ARNTL2	-2.02	3.54E-05
PSG9	3.65	3.98E-03	TTC9	-2.02	1.52E-03
MED12L	3.63	8.91E-04	IFI27	-2.03	9.13E-05
ANKRD2	3.60	3.73E-05	TBC1D30	-2.03	1.85E-04
PDE1C	3.60	8.36E-04	GATM	-2.07	3.49E-03
SYT14	3.59	1.89E-09	DGKA	-2.08	2.82E-05
LINC00284	3.59	7.10E-03	BICDL1	-2.08	3.82E-03
DPF3	3.58	1.37E-03	FER1L4	-2.08	2.77E-06
PARD3B	3.58	5.13E-04	JCAD	-2.09	4.74E-06
OLFML3	3.56	8.01E-07	PHLDA1	-2.09	7.34E-08
VAV3	3.53	9.89E-13	KCNN4	-2.10	1.52E-06
THBS1	3.52	8.70E-22	CACNG6	-2.12	8.40E-03
NEURL1	3.50	1.06E-07	PPP1R9A	-2.12	1.73E-03
lnc-NEMF-1:7	3.50	9.46E-04	OAS1	-2.14	4.50E-03
RIPOR3	3.47	3.65E-05	PROM2	-2.15	3.82E-09
KRT5	3.47	2.30E-05	CLDN7	-2.16	2.93E-08
RP11-115K3.1	3.46	1.91E-03	ADAM8	-2.17	1.75E-04
PAPPA	3.45	1.17E-04	FAM83F	-2.20	6.37E-03
CLIC3	3.41	3.65E-08	SORCS2	-2.22	6.90E-05
ACTR3C	3.40	8.87E-08	MYO5B	-2.22	3.44E-07
NPR1	3.39	3.56E-03	HID1	-2.23	5.41E-05
CLDN2	3.38	3.40E-03	FN1	-2.25	2.64E-09
CA2	3.38	2.49E-03	EPCAM	-2.27	2.04E-10
LRRN4	3.37	1.60E-06	LCP1	-2.33	4.23E-06
ADAMTS10	3.36	1.04E-04	PDGFA	-2.38	1.47E-03
LINC01111	3.34	4.60E-04	ADGRF4	-2.38	1.11E-04
DLX3	3.31	8.00E-06	DKK3	-2.40	9.56E-03
LNC-LRR1-1:1	3.30	2.39E-03	TMSB4XP4	-2.40	1.19E-04
QPRT	3.28	1.14E-12	EREG	-2.41	1.89E-08
ADAMTS15	3.27	5.48E-12	PCED1B	-2.42	5.91E-07
AC016717.2	3.27	2.27E-04	PHLDA3	-2.43	1.61E-06
ERO1B	3.23	4.48E-03	EPHB6	-2.43	9.27E-06
DYSF	3.22	1.03E-13	LAMB1	-2.46	3.24E-10
LINC02015	3.22	5.13E-04	RAPGEF5	-2.48	1.71E-03
LINC01833	3.21	2.35E-04	FUT3	-2.49	3.58E-04
PDZD2	3.16	4.67E-03	SLC40A1	-2.49	2.57E-03
SLC25A30	3.15	7.06E-11	HSH2D	-2.50	1.68E-04
IGFL2-AS1	3.12	3.42E-05	NAALADL2	-2.52	3.00E-03
ANXA9	3.09	1.91E-09	GUCY1B3	-2.54	7.70E-04
DLC1	3.08	6.89E-11	RAB38	-2.67	9.25E-05
SECTM1	3.06	1.93E-07	CARD11	-2.70	6.04E-10
RHOB	3.06	9.84E-16	HOOK1	-2.72	1.58E-07

P3H2	3.05	5.92E-12	39873	-2.74	2.60E-06
MRAS	3.02	1.29E-06	GRHL3	-2.84	6.73E-03
HNF1B	3.00	2.01E-13	OVOL1	-2.91	1.78E-03
COL7A1	3.00	3.65E-13	OVOL2	-2.93	6.95E-03
MUC22	2.98	5.96E-03	ARAP2	-2.97	2.93E-08
SPNS3	2.95	3.97E-03	TMEM154	-2.98	7.21E-10
BPGM	2.95	2.43E-11	PLEKHG1	-2.99	6.67E-05
AC108062.1	2.94	6.70E-03	LINC00973	-2.99	2.33E-03
ZNF114	2.92	1.57E-11	ATP2C2	-2.99	8.08E-04
DOCK8	2.90	3.30E-03	SHROOM2	-2.99	7.45E-04
MAMDC2	2.88	3.86E-03	NECTIN4	-3.00	1.68E-05
MFAP3L	2.84	9.83E-03	CBLC	-3.02	6.91E-09
AL021392.1	2.83	8.68E-03	MAPK13	-3.02	4.90E-15
SNHG12	2.83	8.35E-08	ABCC3	-3.03	8.77E-17
OXTR	2.81	3.32E-05	TMC4	-3.09	4.24E-10
SNX10	2.77	5.90E-09	KIAA0040	-3.12	6.75E-04
ADM	2.77	3.61E-08	ST14	-3.14	1.36E-16
APCDD1L-AS1	2.76	9.40E-03	GALNT3	-3.20	7.18E-16
C15orf52	2.75	3.88E-13	SPINT1-AS1	-3.22	7.79E-03
TUBA1A	2.73	4.37E-13	C1orf210	-3.23	1.34E-04
TPM1	2.69	1.16E-14	BICDL2	-3.25	4.25E-04
EVI2A	2.68	9.91E-03	GJB3	-3.27	3.16E-08
DOCK11	2.66	1.62E-09	C6orf223	-3.28	5.70E-05
AXL	2.65	6.57E-09	SLC16A4	-3.29	7.24E-08
LRRC37A3	2.65	2.32E-03	HAS2	-3.30	4.14E-03
PAX6	2.64	6.21E-07	TMEM117	-3.30	7.79E-03
CHN1	2.63	4.41E-03	LRRC8C	-3.44	1.79E-09
GPRC5B	2.63	4.16E-12	NOTCH3	-3.49	2.63E-16
SLC28A1	2.63	7.59E-03	TMPRSS13	-3.53	4.62E-08
HLA-DMB	2.61	7.91E-03	PRR15	-3.68	5.91E-07
GABARAPL1	2.58	2.41E-11	ANGPTL4	-3.80	4.57E-08
TMEM86A	2.57	2.76E-04	CDH1	-3.82	8.43E-24
FSTL3	2.56	7.67E-09	VGF	-3.88	1.96E-08
LNC-C17ORF103-1	2.56	3.92E-04	KDF1	-3.91	2.48E-07
GPRIN2	2.55	9.56E-05	RBBP8NL	-3.96	2.36E-05
FAM46B	2.54	1.63E-03	SLC22A3	-3.98	1.69E-03
ZBED6CL	2.53	2.02E-06	BSPRY	-4.03	5.78E-09
GLP2R	2.50	7.77E-04	SYK	-4.07	1.14E-09
PRRG1	2.48	4.25E-08	MYEF2	-4.07	2.51E-03
STEAP4	2.47	4.22E-06	EPN3	-4.07	1.57E-11
EDN1	2.46	8.89E-05	MARVELD3	-4.12	1.79E-09

PPM1D	2.46	1.63E-07
MFNG	2.46	2.79E-03
GAS6	2.44	1.12E-05
NEURL3	2.44	5.07E-03
GPR160	2.43	1.82E-07
ANXA4	2.42	6.67E-11
KIRREL1	2.42	1.54E-10
RNASET2	2.40	8.53E-05
FBXO2	2.40	3.68E-05
TRIM9	2.39	3.69E-04
THBS2	2.38	9.89E-03
BIVM	2.36	2.25E-04
B3GALT5	2.36	2.36E-03
NPAS2	2.35	2.41E-08
SNAI2	2.35	5.39E-04
CD24P4	2.33	1.89E-09
KRT8P36	2.33	2.73E-05
C3	2.33	4.34E-11
PADI2	2.33	8.73E-06
F2R	2.32	2.06E-08
BNIP3P1	2.30	4.91E-04
LASP1	2.29	4.06E-09
FRMD3	2.29	4.58E-04
FAM110C	2.28	1.90E-05
ARHGAP23	2.27	1.18E-08
CREB5	2.27	8.44E-06
APH1B	2.26	5.93E-03
NUAK2	2.26	3.15E-05
CASZ1	2.26	6.63E-03
IFITM10	2.25	7.32E-03
TNFSF10	2.25	1.85E-03
HFE	2.24	8.38E-06
GALNT9	2.22	6.52E-03
DUSP14	2.21	9.35E-08
TMEM45A	2.19	3.40E-03
ADAMTS9	2.19	8.53E-05
FBN1	2.19	2.43E-03
RBKS	2.18	5.34E-04
DUSP1	2.18	2.75E-05
NR2F2	2.18	3.68E-07
GSTM4	2.17	9.21E-05
ID3	2.16	2.37E-05

ERBB3	-4.12	8.68E-23
SPINT1	-4.13	7.16E-29
EPHA1	-4.17	6.31E-16
PALM3	-4.22	1.51E-06
MAP7	-4.26	2.39E-17
PRSS8	-4.37	1.37E-16
LAD1	-4.46	3.54E-23
AP1M2	-4.50	2.16E-23
MACC1	-4.51	1.68E-15
MCTP2	-4.51	2.08E-07
C2orf54	-4.55	4.42E-13
GRHL2	-4.59	5.97E-24
GABRE	-4.63	3.89E-11
PRSS22	-4.66	7.61E-19
RAB25	-4.77	3.88E-16
GUCY1A3	-4.94	7.31E-07
ALDH3B2	-5.12	2.96E-13
ITGB6	-5.43	2.82E-39
ERP27	-5.64	4.56E-13
ESRP1	-6.24	7.80E-46
TMEM30B	-6.30	4.12E-29
UGT8	-6.36	2.72E-19

CACNB1	2.16	7.72E-04
LOXL4	2.16	3.32E-05
PRSS23	2.15	5.99E-10
SPOCK1	2.14	2.86E-06
NEXN	2.14	9.34E-06
APPBP2	2.14	3.31E-08
PPP1R3B	2.12	1.00E-06
PLK2	2.12	7.66E-08
PDGFB	2.12	2.26E-06
TRAM1	2.11	5.26E-08
KDELC1	2.10	2.41E-03
TIMP2	2.10	6.78E-09
RGS4	2.09	2.39E-03
STC1	2.08	2.58E-06
LEPROT	2.07	2.82E-08
HIP1R	2.07	2.52E-07
ZBTB47	2.05	6.63E-03
TNS2	2.05	4.56E-04
COL18A1	2.05	3.39E-06
RASD2	2.03	2.46E-03
AGAP2-AS1	2.03	9.00E-03
AMOTL2	2.02	1.33E-07
CREB3L1	2.02	3.88E-04
CTD-2328D6.1	2.02	8.14E-09
VLDLR	2.01	5.03E-05
B4GALT1	2.00	4.45E-08
SH3D21	1.99	1.82E-03
MMP24-AS1	1.99	1.17E-04
CRYBG2	1.99	2.42E-04
DKK1	1.98	7.62E-05
MYL9	1.97	4.86E-04
ARHGAP29	1.97	7.00E-08
PPFIA4	1.97	9.73E-03
OLFML2A	1.97	3.71E-05
ITGB8	1.95	3.90E-05
TLR3	1.94	5.86E-03
NR5A2	1.94	2.52E-05
KLF8	1.93	2.31E-03
SLC4A3	1.93	3.91E-03
AKT3	1.92	5.47E-06
RCAN1	1.91	5.54E-05
TMEM139	1.90	4.05E-03

NNMT	1.90	9.91E-07
F3	1.89	1.62E-07
ELFN2	1.89	9.74E-06
LINC02474	1.88	1.47E-05
FOLR1	1.87	4.94E-04
MYLK	1.87	2.48E-05
DUSP10	1.87	2.11E-04
CACHD1	1.86	2.81E-03
NDRG1	1.83	1.68E-04
SERPINE2	1.82	1.34E-06
FUT4	1.82	9.52E-03
TLN2	1.82	5.73E-03
PPP2R3A	1.82	5.67E-05
LMCD1	1.81	6.73E-03
MPC2	1.79	6.51E-05
BNIP3	1.79	3.72E-04
DNAJC6	1.79	1.37E-03
NBEA	1.78	1.48E-03
BCAM	1.77	1.50E-05
SLC44A2	1.77	1.18E-06
FTLP3	1.75	1.41E-05
EME2	1.75	5.02E-03
HIST1H2BD	1.74	5.93E-03
PLCB4	1.74	2.70E-03
AL161626.1	1.73	2.89E-04
SLC44A3	1.73	8.21E-04
SLC16A7	1.72	7.89E-03
MLLT6	1.71	4.27E-06
KRT8P3	1.71	2.72E-05
RIMS3	1.71	7.32E-03
NFIX	1.70	2.24E-03
HIST1H2AC	1.70	5.13E-04
ERO1A	1.70	3.14E-06
CTIF	1.70	1.05E-03
SLC2A1	1.69	1.60E-04
CCDC49	1.68	3.26E-04
PFKFB4	1.67	1.33E-03
PLXNB1	1.67	4.66E-04
LATS2	1.66	2.32E-03
HS3ST1	1.66	4.01E-03
PDGFD	1.66	3.67E-03
CA12	1.65	4.82E-03

P2RY6	1.65	1.60E-03
CGN	1.64	2.32E-04
EPS8L2	1.64	8.52E-05
RAB9A	1.63	1.08E-03
VGLL3	1.63	3.27E-03
CAV2	1.63	2.77E-05
CXXC5	1.63	4.37E-04
PPARD	1.63	1.41E-03
FERMT2	1.61	1.66E-04
LIMCH1	1.61	7.41E-05
CST6	1.60	4.07E-03
WWC1	1.59	1.00E-04
KRT8P45	1.59	5.27E-04
VASN	1.58	3.33E-03
STYX	1.58	4.45E-04
RNF19A	1.58	1.02E-03
BBS10	1.58	4.62E-03
TLE1	1.58	3.73E-04
ALS2CL	1.57	1.37E-03
DDHD1	1.57	4.36E-03
NDFIP2	1.57	1.85E-03
KRT80	1.56	4.86E-04
HMOX1	1.55	1.36E-03
TBC1D9	1.55	1.19E-03
SIK1	1.55	4.84E-03
KLF6	1.55	1.74E-04
APOL1	1.55	1.77E-04
APOL2	1.54	6.29E-04
RAD9A	1.54	4.78E-03
TMEM56	1.54	3.60E-03
PIP5K2B	1.54	1.21E-04
RIT1	1.53	1.50E-03
ORMDL3	1.53	7.43E-04
CAT	1.53	3.05E-04
CTSD	1.52	5.20E-05
FOSL2	1.52	1.94E-04
38961	1.51	8.25E-04
RASSF7	1.51	6.77E-03
GULP1	1.51	1.16E-03
CITED2	1.50	8.66E-04
FTL	1.50	7.78E-05
LIMS1	1.50	8.80E-04

IFIT2	1.50	8.41E-03
VARS2	1.49	2.25E-03
TACC1	1.49	1.42E-03
NECTIN3	1.49	7.93E-03
TGFB2	1.47	4.95E-04
TMEM132A	1.47	4.64E-04
MCAM	1.45	7.42E-04
DDX52	1.45	6.99E-04
PHLDB2	1.45	1.26E-03
ARMC9	1.45	5.97E-03
JUN	1.44	3.66E-03
PDE5A	1.44	7.71E-03
RAB11FIP1	1.44	4.86E-04
AP1GBP1	1.43	9.66E-04
IFFO2	1.43	3.56E-03
CHST11	1.42	6.21E-04
HCFC1R1	1.42	2.75E-03
ERBB2	1.41	1.52E-03
COL6A2	1.40	2.39E-03
TMX1	1.40	1.26E-03
SH3BP4	1.40	2.42E-03
PCGF2	1.40	4.75E-03
PICALM	1.39	2.93E-04
DYRK2	1.39	1.52E-03
CAVIN1	1.38	5.05E-03
RASSF8	1.38	8.77E-03
ADCY6	1.38	3.80E-03
GCC2	1.37	3.35E-03
AK4	1.36	1.47E-03
CERS2	1.36	3.47E-03
PDZK1IP1	1.35	2.61E-03
MIGA1	1.34	6.73E-03
INSIG2	1.34	7.19E-03
CISD3	1.33	8.06E-03
MRPL45	1.33	1.47E-03
MYL6	1.32	7.84E-04
PLXNA3	1.32	4.04E-03
SLC45A3	1.31	5.16E-03
BTG1	1.31	2.49E-03
STARD3	1.31	5.07E-03
MAPK8IP3	1.31	6.91E-03
PSMB3	1.30	1.38E-03

KRT8	1.29	1.15E-03
PODXL	1.28	2.30E-03
EPB41L2	1.28	5.17E-03
FRMD6	1.28	7.93E-03
SERPINH1	1.27	1.82E-03
JPT2	1.25	2.05E-03
CDC42EP3	1.25	4.16E-03
AGRN	1.24	4.25E-03
PBXIP1	1.24	9.78E-03
RALA	1.24	9.57E-03
ABHD12	1.24	6.93E-03
SLC12A7	1.22	6.93E-03
F2RL1	1.22	4.77E-03
DSE	1.21	9.01E-03
KRT18	1.21	2.00E-03
ADAM9	1.19	3.04E-03
RPL19	1.19	2.42E-03
OSBPL8	1.19	9.22E-03
PDXK	1.18	4.79E-03
ACACA	1.16	4.37E-03
ANO6	1.14	7.89E-03
MBOAT7	1.14	6.93E-03
PGK1	1.09	7.32E-03
NAP1L1	1.08	8.79E-03
CCT6A	-1.07	8.92E-03
IGFBP3	-1.11	7.80E-03
PPP2R5C	-1.11	8.96E-03
DPY19L1	-1.15	8.96E-03
UBR5	-1.17	5.93E-03
NEK9	-1.17	6.76E-03
RPS29	-1.18	4.41E-03
CCNA2	-1.19	7.78E-03
MYBBP1A	-1.20	8.70E-03
ELK3	-1.20	9.34E-03
RAB31	-1.21	6.12E-03
NUP210	-1.21	6.23E-03
DDX24	-1.22	5.29E-03
TKT	-1.23	3.03E-03
CSF1	-1.23	4.88E-03
DLST	-1.23	2.67E-03
SUPT16H	-1.24	6.07E-03
CENPE	-1.25	8.10E-03

MTRR	-1.25	7.48E-03
NUP93	-1.25	3.81E-03
SLC7A11	-1.26	4.52E-03
ITPK1	-1.27	8.37E-03
FARSB	-1.27	2.18E-03
SLFN5	-1.28	3.80E-03
LANCL2	-1.29	6.72E-03
PEG10	-1.29	2.55E-03
TUBGCP3	-1.29	9.53E-03
FKBP10	-1.30	2.17E-03
ASPH	-1.30	1.50E-03
RPS6KA3	-1.30	1.34E-03
AURKB	-1.30	5.77E-03
PIK3R3	-1.30	3.37E-03
LYN	-1.30	4.24E-03
MEGF9	-1.31	6.24E-03
XRCC3	-1.31	6.93E-03
DHX33	-1.32	3.98E-03
FKBP3	-1.32	7.93E-03
NIPSNAP2	-1.32	1.54E-03
MTHFD2	-1.33	1.37E-03
FAM49B	-1.34	1.82E-03
ARFGEF1	-1.34	1.35E-03
DTL	-1.35	9.53E-03
RPL7P9	-1.36	4.50E-04
KLHL5	-1.36	1.22E-03
AREL1	-1.37	2.12E-03
FNIP2	-1.38	9.00E-03
RAI14	-1.39	3.75E-04
JAG1	-1.40	6.07E-03
AHSA1	-1.40	6.96E-04
SLC39A11	-1.40	2.69E-03
E2F4	-1.40	1.51E-03
CKAP2L	-1.41	4.61E-03
E2F1	-1.41	4.09E-03
TDP1	-1.41	6.94E-03
AHNAK2	-1.41	1.82E-03
ALDH3A2	-1.42	6.08E-04
CHD1L	-1.42	1.46E-03
STRA6	-1.42	9.02E-03
CPD	-1.42	2.42E-04
FAM174B	-1.42	7.80E-03

DNMBP	-1.42	5.75E-03
MTHFD1	-1.42	3.35E-04
SREBF1	-1.43	1.71E-03
FBXO34	-1.43	3.03E-03
PLCE1	-1.43	8.88E-03
NSMAF	-1.43	3.80E-03
PTK2B	-1.44	5.92E-03
CDKN3	-1.46	4.02E-03
TTC8	-1.46	4.33E-03
MET	-1.46	1.93E-04
CINP	-1.47	2.22E-03
CPSF2	-1.47	4.31E-04
NCOA7	-1.47	1.51E-03
PTTG1	-1.48	4.11E-04
HEATR5A	-1.49	8.25E-03
CHURC1	-1.49	1.52E-03
TNFAIP3	-1.49	4.36E-03
ARRB2	-1.49	9.30E-03
PNP	-1.49	1.72E-03
MRPS28	-1.50	9.97E-03
ABCC2	-1.50	4.55E-03
RPL7	-1.51	5.26E-04
CCDC88C	-1.51	8.37E-03
SRPX2	-1.52	2.14E-03
IPO5	-1.53	5.56E-05
RRS1	-1.53	3.81E-03
SLCO4A1	-1.54	2.21E-04
GINS3	-1.55	2.56E-03
PCDH7	-1.56	3.57E-04
EFNB2	-1.56	2.60E-03
BTG3	-1.56	7.69E-03
CENPV	-1.56	7.30E-03
TMC5	-1.56	3.69E-04
PARP2	-1.56	2.41E-03
PPP1R13B	-1.57	5.36E-03
FOSL1	-1.57	1.91E-03
SIPA1L1	-1.58	2.23E-04
ORC6	-1.59	3.44E-03
SPTSSA	-1.60	1.07E-03
SEMA4B	-1.60	1.98E-04
LTBP3	-1.60	8.77E-05
OXA1L	-1.61	1.06E-04

WDR62	-1.61	3.71E-03
SPRY1	-1.62	4.21E-03
BARD1	-1.62	1.99E-03
CCNB1IP1	-1.63	1.90E-03
MCM10	-1.63	4.78E-03
DLGAP5	-1.64	7.67E-05
RAP1GAP2	-1.65	7.58E-04
TMEM64	-1.65	9.49E-04
ID1	-1.66	1.37E-03
DHRS3	-1.67	2.18E-04
FOXA1	-1.68	1.68E-04
ZGRF1	-1.70	7.89E-03
SCFD2	-1.70	4.33E-03
VDR	-1.70	6.30E-04
CYB5A	-1.71	9.13E-05
MT2A	-1.72	1.90E-04
MPRIP	-1.72	1.42E-04
CDC6	-1.72	4.51E-05
BMF	-1.72	6.62E-04
DNAH5	-1.73	6.12E-03
ZC3H12A	-1.73	2.70E-03
TK2	-1.73	2.86E-03
ABHD17C	-1.75	9.92E-05
CDCA7	-1.75	3.78E-05
MBIP	-1.76	3.19E-03
PLA2G16	-1.77	5.03E-05
ARSJ	-1.77	4.61E-03
TMEM173	-1.77	5.51E-04
FAM111B	-1.78	1.34E-03
GJA1	-1.78	2.81E-04
RGMB	-1.78	1.94E-03
TIAM1	-1.79	8.30E-04
TMEM70	-1.80	1.61E-04
CLSPN	-1.82	5.32E-03
FUT8	-1.82	6.39E-06
TOP2A	-1.82	7.22E-07
NETO2	-1.83	5.75E-06
CAMK2D	-1.83	3.01E-04
SGK1	-1.84	9.56E-05
KLF13	-1.86	6.92E-03
ANO1	-1.87	1.04E-03
VRK1	-1.87	8.80E-04

KIAA0586	-1.88	6.10E-05
AHCYL2	-1.88	3.96E-05
FAM84B	-1.89	8.93E-07
FAM241A	-1.89	1.37E-03
FAM83A	-1.89	1.04E-04
LONRF3	-1.90	3.80E-03
CR2	-1.90	9.00E-03
SERTAD4	-1.91	2.42E-03
PAX9	-1.92	7.10E-03
RAMP1	-1.92	4.33E-06
SEMA3A	-1.94	5.02E-05
BAHC1	-1.94	2.15E-04
PCSK6	-1.95	3.46E-04
NRIP1	-1.95	3.71E-07
FA2H	-1.95	4.53E-04
AEN	-1.96	2.28E-04
LRP8	-1.96	1.77E-06
NR2F1	-1.96	3.12E-04
NFKBIA	-1.98	1.42E-06
GALNT12	-1.98	2.30E-05
POLE2	-2.02	1.82E-03
ALOX5	-2.02	7.18E-06
OAT	-2.03	1.22E-08
FAM3C	-2.03	1.16E-06
NRP2	-2.04	1.51E-05
ANKRD50	-2.05	2.66E-06
STON2	-2.05	4.10E-03
RASGEF1A	-2.05	4.29E-04
CXCL5	-2.06	5.19E-07
NAT8L	-2.07	8.66E-03
GPC6	-2.07	3.36E-04
SLAIN1	-2.09	7.89E-03
TLE2	-2.10	8.54E-04
DUSP4	-2.10	1.71E-07
CDKN1A	-2.12	6.39E-04
SESTD1	-2.13	4.45E-08
TRIM31	-2.14	2.11E-05
HOXC13	-2.15	6.07E-03
ZCCHC24	-2.16	1.82E-04
OTUB2	-2.16	1.80E-03
TOX3	-2.17	6.49E-04
FAM3C2	-2.17	1.76E-07

PTGER4	-2.19	1.50E-03
HYDIN	-2.19	4.78E-03
HPDL	-2.20	3.26E-04
HES1	-2.22	3.08E-06
STMN3	-2.26	1.13E-05
TRABD2A	-2.27	9.19E-04
LTBP1	-2.28	1.26E-06
CDCA4	-2.28	1.56E-06
NCR3LG1	-2.29	4.63E-03
PLXND1	-2.30	4.76E-08
EMP2	-2.30	7.66E-08
CCND1	-2.31	5.17E-10
NRARP	-2.33	7.13E-03
NRCAM	-2.34	2.77E-05
RARRES3	-2.36	1.42E-04
AC068724.1	-2.38	2.67E-03
NMNAT2	-2.38	7.67E-09
CNTNAP3	-2.38	9.96E-03
HAS3	-2.39	7.78E-05
ASS1	-2.39	1.48E-10
TMEM156	-2.40	3.11E-05
PRSS3	-2.40	1.33E-04
YBX2	-2.40	4.76E-03
ANGEL1	-2.40	1.34E-08
PTPRU	-2.41	5.37E-06
KLK6	-2.42	3.92E-08
RASAL1	-2.42	4.38E-03
LCN2	-2.43	1.14E-12
KIF21B	-2.43	2.06E-03
WDHD1	-2.44	8.14E-09
RDH10	-2.45	4.15E-10
HMGA1P2	-2.45	3.92E-07
GPAT3	-2.49	2.22E-08
KLF9	-2.51	9.43E-04
CHST4	-2.51	2.42E-03
MCF2L	-2.52	3.49E-05
ABCG2	-2.53	1.05E-07
WARS	-2.56	3.56E-09
LRP4	-2.56	2.57E-03
IFITM2	-2.56	9.66E-05
DYRK1B	-2.56	5.32E-03
CASP14	-2.59	3.48E-03

PLXNA2	-2.60	2.96E-05
SLC2A12	-2.61	1.36E-04
COL4A1	-2.62	3.19E-04
ZNF655	-2.62	3.32E-05
S1PR3	-2.62	2.57E-03
CASC8	-2.63	1.73E-04
ICOSLG	-2.63	1.42E-06
SGPP2	-2.63	2.01E-08
NRK	-2.64	5.17E-04
FIBCD1	-2.64	1.77E-04
CX3CL1	-2.65	3.08E-07
E2F2	-2.70	2.08E-04
LYNX1	-2.72	7.14E-03
CHI3L1	-2.75	6.78E-03
NRP2	-2.75	2.89E-04
NKX2-1	-2.76	7.22E-07
FBLN2	-2.77	6.42E-08
SLC27A2	-2.79	6.55E-06
UPP1	-2.79	3.34E-11
TOX2	-2.80	5.90E-05
DNER	-2.82	2.47E-07
KLK10	-2.84	1.91E-03
AL512488.1	-2.85	1.64E-07
FBP1	-2.85	1.03E-09
KIAA1644	-2.88	5.07E-06
CPT1A	-2.89	5.76E-11
NPR3	-2.90	2.01E-03
HMGA1	-2.92	4.89E-03
ADAM19	-2.92	3.33E-07
VSTM2L	-2.93	1.21E-04
AKAP6	-2.93	3.02E-06
EVA1A	-2.94	2.53E-07
SLPI	-2.97	3.73E-11
SPTB	-2.99	4.01E-07
ASS1P1	-3.03	2.18E-07
FOS	-3.06	2.23E-04
AIM2	-3.08	6.07E-03
BEAN1	-3.09	9.52E-03
DGLUCY	-3.13	2.06E-05
ITGB2	-3.14	2.76E-06
SLC26A9	-3.14	8.41E-03
GFPT2	-3.15	5.92E-12

AC104024.2	-3.15	7.33E-04
PLLP	-3.17	7.42E-04
ETV5	-3.17	1.03E-14
IFITM1	-3.18	3.74E-06
TP53I11	-3.19	4.29E-11
S100A9	-3.22	1.29E-06
CCAT1	-3.26	5.21E-03
IL1B	-3.27	3.13E-03
LAPTM5	-3.30	1.57E-04
DEPTOR	-3.30	9.55E-08
SFTA1P	-3.31	4.41E-05
BTBD11	-3.38	6.73E-09
SLC16A9	-3.39	5.11E-07
AC005077.4	-3.40	5.76E-03
DMBX1	-3.40	3.83E-03
COLCA2	-3.41	4.75E-03
ACP5	-3.42	8.54E-05
FAM167A	-3.43	2.77E-05
AC144548.1	-3.46	1.34E-06
LRCH2	-3.46	5.76E-04
MAML3	-3.47	1.36E-09
SLITRK6	-3.49	2.33E-08
AC091173.1	-3.49	3.48E-03
MMP28	-3.51	7.06E-04
ATP8A1	-3.52	8.87E-08
SLC2A3	-3.53	1.50E-10
ETV4	-3.53	2.80E-17
PARP11	-3.53	4.69E-03
FRY	-3.54	1.93E-04
KRT6A	-3.55	4.22E-03
TNC	-3.55	5.37E-03
SLCO5A1	-3.55	1.59E-04
ADAM28	-3.59	1.34E-03
TLE3	-3.60	5.50E-17
RNF128	-3.60	3.57E-03
THBD	-3.60	3.87E-09
RASD1	-3.60	1.02E-03
IL1A	-3.64	2.28E-03
EPHA7	-3.65	9.97E-03
CLDN11	-3.67	1.41E-03
DNAH2	-3.71	6.77E-15
RASGRF2	-3.72	1.96E-06

LPCAT2	-3.72	1.71E-07
BCL11A	-3.72	4.23E-03
SESN3	-3.74	2.12E-09
TP63	-3.76	4.66E-06
MFSD4A	-3.78	5.62E-06
PID1	-3.78	1.19E-03
DUSP5	-3.80	4.24E-20
LRRC6	-3.81	3.09E-11
ETV1	-3.84	2.20E-12
WDR13	-3.87	5.47E-10
KCNQ3	-3.88	1.57E-11
GSDMC	-3.88	1.66E-04
STEAP1	-3.88	5.46E-14
FMO5	-3.89	2.29E-05
SHC3	-3.91	5.23E-05
LYPD6B	-3.95	2.25E-05
SEMA4A	-3.95	6.91E-07
IL7R	-3.97	5.72E-13
RNF43	-4.03	1.67E-09
MIR100HG	-4.08	4.99E-10
ACOX2	-4.10	5.26E-09
AC079062.1	-4.10	2.05E-07
HAGLR	-4.14	6.33E-04
PTGS2	-4.17	3.58E-15
CD70	-4.19	8.76E-09
GLI3	-4.24	2.51E-05
NKX1-2	-4.27	9.82E-07
IGFBP4	-4.30	4.67E-17
PELI2	-4.30	2.25E-07
ADORA1	-4.34	3.40E-14
DIRAS1	-4.35	3.71E-06
ROS1	-4.40	4.33E-06
MYB	-4.41	1.14E-05
SERPINB3	-4.49	4.43E-06
SLC28A3	-4.50	9.32E-06
HGD	-4.51	3.56E-05
CYP24A1	-4.51	1.08E-16
BMP3	-4.61	5.34E-06
S100P	-4.65	1.69E-13
IGFBP2	-4.76	1.04E-15
COL4A2	-4.84	2.68E-16
KRT16P2	-4.86	7.24E-07

AOAH	-4.86	1.25E-09
RP13-238F13.5	-4.87	1.63E-10
CHI3L2	-4.88	9.79E-13
KRT16P3	-4.99	8.16E-05
RGCC	-5.00	7.69E-05
LINC01446	-5.03	2.58E-06
TSPAN8	-5.04	2.03E-06
PLEKHS1	-5.11	8.70E-10
SERPINB4	-5.17	3.92E-09
SLC34A2	-5.21	1.33E-06
PPP1R14D	-5.22	2.82E-05
SDR16C5	-5.23	4.21E-05
CPHL1P	-5.25	1.55E-13
CELF2	-5.37	4.25E-06
SIPA1L2	-5.47	4.35E-19
TCIM	-5.60	9.56E-15
SPDEF	-5.62	2.50E-14
MUC5AC	-5.68	5.23E-08
PIGR	-5.74	7.34E-21
SOX21	-5.78	3.28E-06
KRT4	-5.80	1.68E-07
EDNRA	-6.00	5.39E-10
KDR	-6.27	7.48E-08
SOX21-AS1	-6.54	5.58E-08
B4GALNT3	-6.57	7.31E-26
IGF1	-6.58	1.07E-08
C4BPA	-6.65	1.36E-09
KRT20	-6.79	9.09E-09
MUC4	-6.79	9.33E-30
CHIA	-6.86	8.76E-09
FAM20A	-6.98	2.29E-11
CP	-7.29	5.98E-22
F5	-7.31	2.89E-13
DEFB4A	-7.52	7.47E-11
KRT16P1	-7.57	7.78E-26
TNIP3	-7.91	3.98E-14
ST6GALNAC1	-9.24	6.22E-19
CEACAM5	-9.61	1.45E-32
MUC5B	-10.00	9.20E-52
TRPC6	-10.08	4.50E-30

Table S 5: Pathway associated with common expression changes of HCC827^{GS} and H1975^{9291S}

Top 10 enriched process networks identified using MetaCore analysis.

Enrichment by Process Networks			common between H1975^{9291S} and HCC827^{GS}			
#	Networks	Total	p-value	FDR	In Data	Network Objects from overlap
1	Development_Blood vessel morphogenesis	228	0.002	0.128	6	PDE, PDE9A, PD-ECGF (TdRPase), L1CAM, TGF-alpha, Cyr61
2	Cell adhesion_Cell-matrix interactions	211	0.035	0.756	4	MMP-24, Collagen XII, ITGA2, Fibulin-1
3	Chemotaxis	137	0.046	0.756	3	PD-ECGF (TdRPase), Cyr61, GCP2
4	Response to hypoxia and oxidative stress	161	0.068	0.756	3	Gamma-glutamyltranspeptidase, Xanthine oxidase, GPX2
5	Cell adhesion_Platelet-endothelium-leucocyte interactions	174	0.082	0.756	3	OLR1, Cyr61, ITGA2
6	Cell adhesion_Attractive and repulsive receptors	175	0.083	0.756	3	Collagen XII, L1CAM, ITGA2
7	Cell adhesion_Synaptic contact	177	0.085	0.756	3	CNTN1 (F3), Syndecan-2, L1CAM
8	Development_EMT_ Regulation of epithelial-to-mesenchymal transition	224	0.144	0.756	3	EGR1, microRNA 205, HMGA2
9	Reproduction_Spermatogenesis, motility and copulation	228	0.150	0.756	3	Gamma-glutamyltranspeptidase, TGF-alpha, SPRY4
10	Development_Neurogenesis_Axonal guidance	230	0.153	0.756	3	Syndecan-2, L1CAM, SIAT8D

Table S 6: transcripts significantly changed in both HCC827^{GS} and H1975^{9291S}

	HCC827^{GS}		H1975^{9291S}	
transcript	**log_2 FC**	**padj-value**	**log_2 FC**	**padj-value**
KRT17	3.43	4.17E-03	5.30	5.78E-09
RETREG1	4.23	1.56E-06	4.68	8.19E-10
ALPP	2.62	9.57E-09	4.45	1.19E-23
GGT5	-3.57	5.06E-03	3.84	1.30E-03
SDC2	2.22	1.11E-03	3.78	1.19E-09

ANKRD1	1.76	6.97E-03	3.64	5.54E-11
IL32	4.40	8.70E-10	3.53	2.49E-05
ABI3BP	3.12	3.73E-04	3.46	1.51E-04
AMOT	1.79	7.09E-05	3.40	9.92E-11
OLR1	7.13	1.45E-16	3.08	9.89E-03
ZNF704	-1.60	6.74E-04	3.06	4.07E-11
HAVCR1	2.98	2.92E-14	3.05	2.04E-04
PGBD5	2.85	7.10E-05	2.58	5.10E-03
L1CAM	2.08	4.96E-04	2.47	1.51E-06
GPC4	4.73	2.66E-18	2.43	4.31E-06
BICC1	2.13	9.36E-07	2.40	1.94E-07
ANTXR1	3.65	1.74E-14	2.36	3.96E-07
MMP24	1.54	6.57E-04	2.28	1.08E-07
TMOD1	-2.05	7.89E-03	2.24	8.93E-04
JPH2	5.18	1.08E-19	2.20	2.36E-05
COL8A1	1.96	8.55E-05	2.08	2.26E-05
FSTL1	2.81	1.41E-14	1.89	2.58E-06
UGCG	2.19	1.67E-09	1.85	1.84E-06
CYR61	2.88	2.03E-16	1.68	3.22E-05
COL12A1	5.25	2.34E-49	1.62	7.13E-05
BCAT1	1.23	7.68E-03	1.58	4.78E-04
FADS3	1.42	4.01E-03	1.58	1.96E-03
NABP1	1.99	1.55E-06	1.47	2.38E-03
RAB32	1.69	5.51E-04	1.45	9.96E-03
FBLN1	2.89	2.45E-15	1.45	2.13E-03
TUFT1	1.73	4.43E-05	1.34	8.13E-03
GPRC5A	1.62	2.28E-05	1.30	3.27E-03
DAPK1	2.58	7.35E-14	1.27	3.94E-03
HMGB3	-2.21	1.45E-08	-1.49	1.27E-03
SCNN1A	-1.68	1.04E-05	-1.52	2.95E-04
MLPH	-1.45	1.10E-03	-1.53	8.44E-04
CELSR1	1.55	4.86E-04	-1.53	1.62E-03
ACP6	-1.99	1.43E-06	-1.54	8.93E-04
RAB15	-2.30	9.33E-10	-1.61	3.13E-04
GALNT10	-1.46	2.34E-04	-1.68	2.95E-05
ITGA2	-2.05	2.47E-07	-1.68	1.30E-04
SPNS2	4.92	9.28E-33	-1.70	2.20E-03
GALNT6	-1.31	2.59E-03	-1.70	5.08E-05
PHLDA2	-1.87	1.15E-03	-1.75	5.07E-03
PCDH1	-3.07	2.66E-14	-1.76	9.37E-05
CLDN4	1.14	6.63E-03	-1.80	2.19E-06
CAPS	1.82	2.42E-03	-1.88	2.33E-03

HMGA2	-1.67	8.62E-04	-1.99	1.12E-04
TYMP	2.04	2.54E-03	-1.99	9.46E-03
AC064799.1	-2.03	2.06E-05	-2.03	7.47E-05
SPRY4	-3.65	1.05E-10	-2.06	2.07E-04
TGFA	1.52	3.69E-04	-2.16	1.94E-07
TCN1	-5.69	4.41E-24	-2.21	2.23E-05
PDE9A	-3.40	8.16E-07	-2.25	9.96E-03
FOXQ1	-3.25	2.60E-05	-2.28	1.89E-03
CALB1	-1.29	7.83E-03	-2.39	1.29E-04
FLRT3	3.51	5.80E-15	-2.48	5.43E-05
MAL2	1.18	7.83E-03	-2.48	1.26E-10
GPX2	-5.19	9.09E-32	-2.55	4.39E-05
SOX2	-8.49	2.78E-29	-2.60	9.65E-04
FGFBP1	-1.75	3.15E-03	-2.61	1.80E-05
SERPINB5	-2.22	4.52E-08	-2.61	1.03E-10
MYEOV	-1.86	1.21E-04	-2.61	1.62E-10
JPH1	-2.16	2.42E-03	-2.63	7.51E-04
PRODH	-6.42	9.11E-49	-2.86	1.52E-06
SCEL	-2.81	4.32E-08	-2.92	1.87E-07
AGR2	-6.98	1.85E-62	-3.03	1.07E-13
TNS4	-4.39	4.54E-08	-3.23	3.56E-06
XDH	-2.02	9.66E-04	-3.50	1.26E-10
CAPN8	-4.58	1.71E-14	-3.67	8.21E-11
CXCL6	-2.84	5.24E-05	-3.68	5.24E-06
PTHLH	-3.99	8.86E-07	-3.75	4.84E-05
NT5E	-5.45	1.70E-48	-3.82	2.92E-24
SULT1B1	4.17	6.17E-08	-3.90	7.03E-04
SFTPB	-7.60	3.32E-16	-3.90	8.16E-05
ANKRD22	-3.26	5.26E-09	-3.95	3.98E-10
EGR1	-3.92	2.21E-08	-3.96	1.56E-07
CNTN1	-7.04	3.07E-32	-4.01	1.21E-05
DUSP6	-7.14	1.14E-45	-4.02	6.47E-21
C1orf116	1.67	1.84E-04	-4.02	6.13E-19
ABCA12	-1.86	5.83E-03	-4.11	6.65E-07
TMPRSS4	-6.87	3.84E-27	-4.20	1.28E-09
CEACAM6	-7.45	2.22E-89	-4.30	3.88E-18
CFH	-2.10	8.11E-04	-4.62	6.98E-15
S100A14	-1.77	3.94E-05	-4.72	2.63E-16
ST8SIA4	-4.88	3.43E-12	-4.80	1.94E-07
TMPRSS11E	-3.36	2.83E-04	-4.94	9.57E-06
FXYD3	-2.08	1.13E-04	-5.12	3.70E-13
MIR205HG	-3.74	5.39E-07	-5.26	1.79E-09

IL1RL1	-4.01	6.42E-11	-5.67	7.18E-16
SLCO2A1	-6.08	5.85E-19	-6.16	2.11E-18

Table S 7: Compounds in L1700 compound library used for screen

(-)-Blebbistatin	A66	Albendazole	Amiodarone HCl
(-)-Epigallocatechin Gallate	A922500	Albendazole Oxide	Amisulpride
(-)-MK 801 Maleate	ABT-199 (GDC-0199)	Alfacalcidol	Amitriptyline HCl
(-)-p-Bromotetramisole Oxalate	ABT-263 (Navitoclax)	Alfuzosin HCl	Amlodipine
(-)-Parthenolide	ABT-737	Alibendol	Ammonium Glycyrrhizinate
(+,-)-Octopamine HCl	ABT-751 (E7010)	Alisertib (MLN8237)	Amonafide
(+)-Bicuculline	AC480 (BMS-599626)	Aliskiren Hemifumarate	Amorolfine HCl
(+)-JQ1	Acadesine	Alizapride HCl	Amoxicillin
(+)-Matrine	Acarbose	Alizarin	Amoxicillin Sodium
(+)-Usniacin	Acebutolol HCl	Allopurinol	Amphotericin B
（6-）ε-Aminocaproic acid	Acemetacin	Allopurinol Sodium	Ampicillin sodium
(R)-Nepicastat HCl	Acesulfame Potassium	Allylthiourea	Ampicillin Trihydrate
(S)-crizotinib	Acetanilide	Almorexant HCl	Ampiroxicam
1-Azakenpaullone	Acetylcholine Chloride	Almotriptan Malate	Amprenavir
1-Hexadecanol	Acetylcysteine	Aloe-emodin	Amprolium HCl
10-Deacetylbaccatin-III	Aciclovir	Alogliptin	Amuvatinib (MP-470)
10058-F4	Acipimox	Aloin	Anacetrapib (MK-0859)
17-AAG (Tanespimycin)	Acitretin	Aloperine	Anagrelide HCl
17-DMAG (Alvespimycin) HCl	Aclidinium Bromide	Aloxistatin	Anastrozole
2-Methoxyestradiol (2-MeOE2)	Adapalene	Alprostadil	Andarine
2-Thiouracil	Adefovir Dipivoxil	Altrenogest	Andrographolide
20-Hydroxyecdysone	Adenine HCl	Altretamine	Anidulafungin (LY303366)
3-Aminobenzamide	Adenosine	Alvelestat (AZD9668)	Aniracetam
3-Deazaneplanocin A (DZNeP)	Adiphenine HCl	Alverine Citrate	Antazoline HCl
3-Indolebutyric acid (IBA)	AdipoRon	AM1241	Antipyrine
3-Methyladenine	ADL5859 HCl	AM251	AP26113
4-Aminohippuric Acid	Adrenalone HCl	Amantadine HCl	Apatinib
4-Methylumbelliferone (4-MU)	ADX-47273	Ambrisentan	Apigenin
4E1RCat	AEBSF HCl	Ambroxol HCl	Apixaban
4EGI-1	AEE788 (NVP-AEE788)	Amfebutamone HCl	Apocynin
4μ8C	Afatinib (BIBW2992)	Amfenac Sodium Monohydrate	Apoptosis Activator 2
5-Aminolevulinic acid HCl	AG-1024	AMG-458	Apremilast (CC-10004)
5-hydroxymethyl Tolterodine (PNU 200577, 5-HMT, 5-HM)	AG-14361	AMG-517	Aprepitant
5-hydroxytryptophan (5-HTP)	AG-1478 (Tyrphostin AG-1478)	AR-42	AT7867
6H05	AG-18	Amidopyrine	AR-A014418
A-205804	AG-490 (Tyrphostin B42)	Amiloride HCl	Arbidol HCl
A-674563	AGI-5198	Aminoglutethimide	Arbutin
A-769662	AGI-6780	Aminophylline	Arecoline
A-803467	Agomelatine	Aminothiazole	Argatroban

Aripiprazole
ARN-509
ARQ 621
Artemether
Artemisinin
Artesunate
Articaine HCl
AS-252424
AS-604850
Asaraldehyde
Asenapine
Asiatic Acid
Aspartame
Aspirin
AST-1306
Astragaloside A
AT101
AT13387
AT7519
AZD8055
AZD8330
Ataluren (PTC124)
Atazanavir Sulfate
Atglistatin
Atomoxetine HCl
Atorvastatin Calcium
Atovaquone
Atracurium Besylate
Atropine
AZD9291
AUY922 (NVP-AUY922)
Avagacestat (BMS-708163)
Avanafil
Avasimibe
AVL-292
Avobenzone
Axitinib
AZ 3146
AZ 628
AZ 960
AZ191
AZ20
Azacitidine
Azacyclonol
Azaguanine-8
Azaperone
Azatadine dimaleate
Azathioprine
AZD1080
AZD1208
AZD1480
AZD1981
AZD2014
AZD2461
AZD2858
BI 2536
AZD3514
AZD4547
AZD5363
AZD5438
AZD6482
AZD7545
AZD7762
Brefeldin A
Camptothecin
AZD8931 (Sapitinib)
CCT129202
Azelastine HCl
Azelnidipine
Azilsartan
Azilsartan Medoxomil
Azithromycin
Azlocillin sodium salt
Azomycin
Aztreonam
Bacitracin
Baicalein
Baicalin
Balofloxacin
Bambuterol HCl
BAPTA-AM
CCT137690
Bardoxolone Methyl
Baricitinib (LY3009104, INCB028050)
Batimastat (BB-94)
BAY 11-7082
Bazedoxifene HCl
Beclomethasone dipropionate
Belinostat (PXD101)
Bemegride
Benazepril HCl
Bendamustine HCl
Benidipine HCl
Benserazide HCl
Benzbromarone
Benzethonium Chloride
Benzocaine
Benzoic Acid
Benztropine mesylate
Benzydamine HCl
Bepotastine Besilate
Cephalomannine
Bergapten
Bergenin
Beta Carotene
Beta-Lapachone
Betahistine 2HCl
Betamethasone
Betamipron
Betaxolol
Bethanechol chloride
Betulinic acid
Bexarotene
Bezafibrate
CHIR-124
CNX-2006
BI-D1870
BIBR 1532
Bicalutamide
Bifonazole
BIIB021
Bilobalide
Bimatoprost
Bindarit
BIO
Biochanin A
Biotin (Vitamin B7)
Biperiden HCl
BIRB 796 (Doramapimod)
Birinapant
Bisacodyl
Bisoprolol fumarate
BIX 01294
BIX 02188
BIX 02189
BKM120 (NVP-BKM120, Buparlisib)
Bleomycin Sulfate
BML-190
BMN 673
BMS-265246
BMS-345541
BMS-378806
BMS-536924
BMS-707035
BMS-754807
BMS-777607
BMS-794833
BMS-833923
BMY 7378
Bortezomib (PS-341)
Bosentan
Bosentan Hydrate
Bosutinib (SKI-606)
CO-1686 (AVL-301)
Brimonidine Tartrate
Brinzolamide
Brivanib (BMS-540215)
Brivanib Alaninate (BMS-582664)
BRL-15572
BRL-54443
Bromfenac Sodium
Bromhexine HCl
Bromosporine
Brompheniramine hydrogen maleate
Broxyquinoline
BS-181 HCl
BTB06584
BTZ043 Racemate
Budesonide
Bufexamac
Buflomedil HCl
Bumetanide
Bupivacaine HCl
Buspirone HCl
Busulfan
Butein
Butenafine HCl
Butoconazole nitrate
Butylscopolamine Bromide
Crystal Violet
BX-795
BX-912
BYL719
C646
CX-6258 HCl

Cabozantinib (XL184, BMS-907351)
Cabozantinib malate (XL184)
Caffeic Acid
Caffeic Acid Phenethyl Ester
CAL-101 (Idelalisib, GS-1101)
Calcifediol
Calcitriol
Camostat Mesilate
CYT997 (Lexibulin)
Canagliflozin
Candesartan
Candesartan Cilexetil
Capecitabine
Captopril
Carbamazepine
Carbazochrome sodium sulfonate (AC-17)
Carbenicillin disodium
Carbidopa
Carbimazole
Dacomitinib (PF299804, PF299)
Carmofur
Carprofen
Carteolol HCl
Carvedilol
Caspofungin Acetate
Catharanthine
Cathepsin Inhibitor 1
CAY10505
CCG 50014
CCT128930
Decitabine
Deflazacort
Cediranib (AZD2171)
Cefdinir
Cefditoren Pivoxil
Cefoperazone
Ceftiofur HCl
Celecoxib
CEP-18770 (Delanzomib)
CEP-32496
CEP-33779
Cephalexin
Digoxin
Cepharanthine
Cetirizine DiHCl
Cetrimonium Bromide (CTAB)
Cetylpyridinium Chloride
CFTRinh-172
CGI1746
CGK 733
CGP 57380
CGS 21680 HCl
CH5132799
CH5138303
Chenodeoxycholic Acid
Disulfiram
CHIR-99021 (CT99021) HCl
Chloramphenicol
Chlorhexidine HCl
Chlormezanone
Chloroambucil
Chlorocresol
Chlorogenic Acid
Chloroprocaine HCl
Chlorothiazide
Chloroxine
Chlorpheniramine Maleate
Chlorpromazine HCl
Chlorpropamide
Chlorprothixene
Chlorquinaldol
Chlorzoxazone
Choline Chloride
Chromocarb
Chrysin
Chrysophanic Acid
CI994 (Tacedinaline)
Ciclopirox
Ciclopirox ethanolamine
Cilazapril Monohydrate
Cilengitide
Cilnidipine
Cilomilast
Cilostazol
Cimetidine
Cinacalcet HCl
Cinchonidine
Cinchophen
Cinepazide maleate
Ciprofibrate
Ciproxifan
Cisatracurium Besylate
Cisplatin
CK-636
Cladribine
Clarithromycin
Clemastine Fumarate
Clevidipine Butyrate
Clevudine
Climbazole
Clindamycin
Clindamycin HCl
Clindamycin palmitate HCl
Clinofibrate
Clobetasol propionate
Clofarabine
Clofazimine
Clofibric Acid
Clomifene citrate
Clomipramine HCl
Clonidine HCl
Clopidogrel
Clorprenaline HCl
Clorsulon
Closantel
Closantel Sodium
Clotrimazole
Cloxacillin Sodium
Clozapine
Docetaxel
CNX-774
Dovitinib (TKI-258) Dilactic Acid
Cobicistat (GS-9350)
Conivaptan HCl
CORM-3
Cortisone acetate
Costunolide
Coumarin
CP-673451
CP-724714
CP-91149
CPI-203
CPI-613
Crenolanib (CP-868596)
Crizotinib (PF-02341066)
CRT0044876
Cryptotanshinone
Epirubicin HCl
CTEP (RO4956371)
CUDC-101
GSK461364
Curcumin
Curcumol
CW069
CX-4945 (Silmitasertib)
GSK923295
CYC116
Cyclamic acid
Cyclandelate
Cyclizine 2HCl
Cyclobenzaprine HCl
Cyclocytidine HCl
Cyclosporin A
Cyclosporine
Cyproheptadine HCl
Cyproterone Acetate
Cyromazine
Cysteamine HCl
CYT387
Hesperadin
Cytidine
Cytisine
CZC24832
D-Mannitol
D-Pantothenic acid
Dabigatran Etexilate
Dabrafenib (GSK2118436)
Dacarbazine
Daclatasvir (BMS-790052)
HSP990 (NVP-HSP990)
Daidzein
Dalcetrapib (JTT-705, RO4607381)
Danoprevir (ITMN-191)
Danusertib (PHA-739358)
Dapagliflozin
Daphnetin
Dapivirine (TMC120)
Dapoxetine HCl
DAPT (GSI-IX)
Darapladib (SB-480848)
Darifenacin HBr
Darunavir Ethanolate
Dasatinib
Daunorubicin HCl
DBeQ

Idarubicin HCl
Decamethonium Bromide
KPT-185
Deferasirox
KPT-276
Degrasyn (WP1130)
Dehydroepiandrosterone (DHEA)
Deltarasin
Demeclocycline HCl
Deoxyarbutin
Desloratadine
Desonide
Desvenlafaxine
Desvenlafaxine Succinate
Detomidine HCl
Dexamethasone (DHAP)
Dexlansoprazole
Dexmedetomidine
Dexrazoxane HCl (ICRF-187, ADR-529)
Dextrose
Diacerein
Dibenzothiophene
Dibucaine HCl
Dichlorphenamide
Diclazuril
Diclofenac Diethylamine
Diclofenac Potassium
Diclofenac Sodium
Dicloxacillin Sodium
Dicoumarol
Didanosine
Dienogest
Diethylstilbestrol
Difluprednate
KPT-330
Dihydroartemisinin (DHA)
Dihydromyricetin
Diltiazem HCl
Dimesna
Dimethyl Fumarate
Diminazene Aceturate
MG-132
Dinitolmide
Dioscin
Diosmetin
Diosmin
Diphemanil Methylsulfate
Diphenhydramine HCl
Diphenidol HCl
Dipyridamole
Dirithromycin
Mitoxantrone
Divalproex Sodium
DL-Carnitine HCl
DMH1
DMXAA (Vadimezan)
Mitoxantrone HCl
Dofetilide
Dolutegravir (GSK1349572)
Domiphen Bromide
Domperidone
Dopamine HCl
Doripenem Hydrate
Dovitinib (TKI-258, CHIR-258)
MLN2238
Doxapram HCl
Doxazosin Mesylate
Doxercalciferol
Doxifluridine
Doxofylline
Doxorubicin (Adriamycin)
Doxycycline HCl
Doxycycline Hyclate
Doxylamine Succinate
Dronedarone HCl
Droperidol
Dropropizine
Drospirenone
Droxinostat
Duloxetine HCl
Dutasteride
Dyclonine HCl
Dydrogesterone
Dynasore
Dyphylline
E-64
Econazole nitrate
Edaravone
Edoxaban
Efaproxiral Sodium
EHop-016
EHT 1864
Elesclomol (STA-4783)
Eletriptan HBr
Eltrombopag
Elvitegravir (GS-9137, JTK-303)
Embelin
Emodin
Empagliflozin (BI 10773)
MLN9708
MPI-0479605
NSC 319726
Oprozomib (ONX 0912)
Emtricitabine
Enalapril Maleate
Enalaprilat Dihydrate
ENMD-2076
Enoxacin
Enoxolone
Entacapone
Entecavir Hydrate
Entinostat (MS-275)
Enzalutamide (MDV3100)
Enzastaurin (LY317615)
Epalrestat
Epiandrosterone
Epinastine HCl
Epinephrine Bitartrate
Epinephrine HCl
Paclitaxel
Epothilone A
Epothilone B (EPO906, Patupilone)
Eprosartan Mesylate
EPZ-6438
EPZ004777
EPZ5676
Equol
Erastin
Erdosteine
Erlotinib HCl (OSI-744)
Erythritol
Erythromycin
Escitalopram Oxalate
Esculin
ESI-09
Esmolol HCl
Esomeprazole Sodium
Estradiol
Estradiol Benzoate
Estradiol Cypionate
Estradiol valerate
Estriol
Estrone
Ethacridine lactate monohydrate
Ethambutol HCl
Ethamsylate
Ethinyl Estradiol
Ethionamide
Ethynodiol diacetate
Etizolam
Etodolac
Etofibrate
Etomidate
Etoposide
ETP-46464
Etravirine (TMC125)
EUK 134
Evacetrapib (LY2484595)
Everolimus (RAD001)
EX 527 (Selisistat)
Exemestane
Ezetimibe
Famciclovir
Famotidine
Fasudil (HA-1077) HCl
Febuxostat
Felbamate
Felodipine
Fenbendazole
Fenofibrate
Fenoprofen Calcium
Fenspiride HCl
Fenticonazole Nitrate
Ferrostatin-1 (Fer-1)
Ferulic Acid
Fesoterodine Fumarate
Fexofenadine HCl
FG-4592
FH1(BRD-K4477)
FH535
Fidaxomicin
Filgotinib (GLPG0634)
Finasteride
Fingolimod (FTY720) HCl
Fisetin

Flavopiridol HCl
Flavoxate HCl
FLI-06
Flopropione
Florfenicol
Floxuridine
Fluconazole
Flucytosine
Fludarabine Phosphate
Flufenamic acid
Flumazenil
Flumequine
Flumethasone
Flunarizine 2HCl
Flunixin Meglumin
Fluocinolone Acetonide
Fluocinonide
Fluorometholone Acetate
Fluorouracil (5-Fluoracil, 5-FU)
Fluoxetine HCl
Flupirtine maleate
Flurbiprofen
Flutamide
Fluticasone propionate
Fluvastatin Sodium
Fluvoxamine maleate
Foretinib (GSK1363089)
Formestane
Formononetin
Formoterol Hemifumarate
Forskolin
Fosaprepitant dimeglumine salt
Foscarnet Sodium
Fostamatinib (R788)
FPH1 (BRD-6125)
FPH2 (BRD-9424)
FT-207 (NSC 148958)
Fulvestrant
Furaltadone HCl
Furosemide
Gabexate Mesylate
Galeterone
Gallamine Triethiodide
Ganciclovir
Ganetespib (STA-9090)
Gastrodin
GDC-0068
GDC-0152
GDC-0349
GDC-0879
GDC-0941
GDC-0980 (RG7422)
Gefitinib (ZD1839)
PF-3758309
Gemcitabine
Gemfibrozil
Genipin
Geniposide
Geniposidic acid
Genistein
Gestodene
GF109203X
Gimeracil
Ginkgolide A
Ginkgolide B
Givinostat (ITF2357)
Gliclazide
Glimepiride
Glipizide
Gliquidone
Glyburide
Glycyrrhizic Acid
GNE-0877
GNE-7915
GNE-9605
GNF-2
GNF-5
Go 6983
Golgicide A
Golvatinib (E7050)
Gossypol
Gramine
Griseofulvin
GS-9973
GSK J4 HCl
GSK1059615
GSK1292263
GSK1838705A
GSK1904529A
GSK2126458 (GSK458)
GSK2334470
GSK256066
GSK2606414
GSK2636771
GSK2656157
GSK3787
GSK429286A
Pirarubicin
GSK650394
GSK690693
Piroxicam
Guaifenesin
Guanabenz Acetate
Guanidine HCl
Guanosine
GW0742
GW2580
GW3965 HCl
GW4064
GW5074
GW788388
GW842166X
GW9508
GW9662
Gynostemma Extract
GZD824
H 89 2HCl
HA14-1
Halcinonide
Halobetasol Propionate
Haloperidol
HC-030031
Hematoxylin
HER2-Inhibitor-1
Ro3280
Hesperetin
Hesperidin
Hexestrol
Histamine 2HCl
HJC0350
HMN-214
HO-3867
Homatropine Bromide
Homatropine Methylbromide
Honokiol
Hordenine
HS-173
SB743921
Hydrochlorothiazide
Hydrocortisone
Hydroxyurea
Hydroxyzine 2HCl
Hyodeoxycholic acid (HDCA)
Hyoscyamine
I-BET-762
I-BET151 (GSK1210151A)
Ibrutinib (PCI-32765)
Ibuprofen
Ibutilide Fumarate
Icariin
ICG-001
Icotinib
ID-8
TAK-733
Idebenone
Idoxuridine
IEM 1754 dihydrobroMide
Ifenprodil Tartrate
Ifosfamide
IKK-16 (IKK Inhibitor VII)
Ilomastat (GM6001, Galardin)
Iloperidone
IM-12
Imatinib (STI571)
Imatinib Mesylate (STI571)
IMD 0354
Imidapril HCl
INCB024360
Indacaterol Maleate
Indapamide
Indirubin
Indole-3-carbinol
Indomethacin
INH1
INH6
Iniparib (BSI-201)
INK 128 (MLN0128)
INO-1001
Inosine
IOWH032
IOX1
IOX2
IPA-3
IPI-145 (INK1197)
Ipratropium Bromide
Ipriflavone (Osteofix)
Irinotecan
Irinotecan HCl Trihydrate

Irsogladine
Isoconazole nitrate
Isoliquiritigenin
Isoniazid
Isoprenaline HCl
Isosorbide
Isotretinoin
Isovaleramide
Ispinesib (SB-715992)
Isradipine
Istradefylline
Itraconazole
IU1
Ivabradine HCl
Ivacaftor (VX-770)
Ivermectin
IWP-2
IWP-L6
IWR-1-endo
JNJ-1661010
JNJ-26854165 (Serdemetan)
JNJ-38877605
JNJ-7706621
JNJ-7777120
JNK Inhibitor IX
JNK-IN-8
JSH-23
JTC-801
JZL184
K-Ras(G12C) inhibitor 6
K-Ras(G12C) inhibitor 9
K02288
Kaempferol
Ketanserin
Ketoconazole
Ketoprofen
Ketorolac
Ketotifen Fumarate
Ki16198
Ki16425
Ki8751
Kinetin
KN-62
KN-93 Phosphate
Tazarotene
Teniposide
Trametinib (GSK1120212)
KRN 633
KU-0063794
KU-55933 (ATM Kinase Inhibitor)
KU-60019
KW-2449
KW-2478
Vinblastine
KY02111
L-(+)-Rhamnose Monohydrate
L-Adrenaline
L-Ascorbyl 6-palmitate
L-Thyroxine
Labetalol HCl
Lacidipine
Laetrile
Lafutidine
Lamivudine
Lamotrigine
Lansoprazole
Lapatinib (GW-572016) Ditosylate
Lappaconite HBr
LAQ824 (Dacinostat)
Laquinimod
LB42708
LDC000067
LDE225 (NVP-LDE225,Erismodegib)
LDK378
LDN-212854
LDN-57444
LEE011
Leflunomide
Lenalidomide (CC-5013)
Lenvatinib (E7080)
Letrozole
Leupeptin Hemisulfate
Levetiracetam
Levobetaxolol HCl
Levodropropizine
Levofloxacin
Levonorgestrel
Levosimendan
Levosulpiride
LGK-974
LGX818
Licofelone
Lidocaine
Limonin
Linagliptin
Lincomycin HCl
Linezolid
Linifanib (ABT-869)
Liothyronine Sodium
Lithocholic acid
Lomeguatrib
Lomerizine HCl
Lomitapide
Lomustine
Lonafarnib
Lonidamine
Loperamide HCl
Lopinavir
Loratadine
Lorcaserin HCl
Lornoxicam
Losartan Potassium (DuP 753)
Losmapimod (GW856553X)
Loteprednol etabonate
Lovastatin
Loxapine Succinate
Loxistatin Acid (E-64C)
Lubiprostone
Luliconazole
Lumiracoxib
Luteolin
LY2157299
LY2228820
LY2603618
LY2608204
LY2784544
LY2811376
LY2835219
LY2886721
LY294002
LY411575
M344
Macitentan
Magnolol
Malotilate
Manidipine
Manidipine 2HCl
Maprotiline HCl
Maraviroc
Masitinib (AB1010)
MC1568
Mdivi-1
ME0328
Mecarbinate
Mechlorethamine HCl
Meclofenamate Sodium
Meclofenoxate (Centrophenoxine) HCl
Medetomidine HCl
Medroxyprogesterone acetate
Mefenamic Acid
Mefloquine HCl
Megestrol Acetate
Meglumine
MEK162 (ARRY-162, ARRY-438162)
Melatonin
Meloxicam
Memantine HCl
Menadione
Mepivacaine HCl
Meprednisone
Meptazinol HCl
Mequinol
Mercaptopurine (6-MP)
Meropenem
Mesalamine
Mesna
Mestranol
Methacycline HCl
Methazolamide
Methenamine
Methimazole
Methocarbamol
Methotrexate
Methoxsalen
Methscopolamine
Methyclothiazide
Methyl-Hesperidin
Methylprednisolone
Methylthiouracil
MetoclopraMide HCl
Metolazone
Metoprolol Tartrate
Metronidazole
Mevastatin
Mexiletine HCl

Mezlocillin Sodium
Vinorelbine Tartrate
MGCD-265
MI-2 (MALT1 inhibitor)
Mianserin HCl
Miconazole
Miconazole Nitrate
Mifepristone
Miglitol
Milciclib (PHA-848125)
Milnacipran HCl
Milrinone
Mirabegron
Mirtazapine
Mitotane
Volasertib (BI 6727)
WZ3146
MK-0752
MK-1775
MK-2048
WZ4002
MK-2461
MK-2866 (GTx-024)
MK-5108 (VX-689)
MK-801 (Dizocilpine)
MK-8245
MK-8745
MK-8776 (SCH 900776)
ML130 (Nodinitib-1)
ML133 HCl
ML161
ML167
ML323
ML347
WZ8040
MLN8054
XL888
MM-102
MNS (3,4-Methylenedioxy-β-nitrostyrene, MDBN)
Mocetinostat (MGCD0103)
Moclobemide (Ro 111163)
Moexipril HCl
Moguisteine
Mometasone furoate
Monobenzone
Montelukast Sodium
Morin Hydrate
Moroxydine HCl
Mosapride Citrate
Motesanib Diphosphate (AMG-706)
Moxifloxacin HCl
Moxonidine
MPEP
AMG-900
MRS 2578
Mubritinib (TAK 165)
Mupirocin
Mycophenolate Mofetil
Mycophenolic acid
Myricetin
Myricitrin
N6-methyladenosine (m6A)
N6022
Nabumetone
Nadifloxacin
Nafamostat Mesylate
Nafcillin Sodium
Naftopidil
Naftopidil DiHCl
Nalidixic acid
Naloxone HCl
Naltrexone HCl
Nanchangmycin
Naphazoline HCl
Naproxen
Naratriptan
Naringenin
Naringin
Naringin Dihydrochalcone
Natamycin
Nateglinide
Nebivolol
Necrostatin-1
Nefiracetam
Nelarabine
Nelfinavir Mesylate
Neohesperidin
Nepafenac
Nevirapine
Nexturastat A
NH125
Nicaraven
Nicardipine HCl
Nicorandil
Nicotinamide (Vitamin B3)
Nicotinic Acid
Nifedipine
Niflumic acid
Nifuroxazide
Nilotinib (AMN-107)
Nilvadipine
Nimesulide
Nimodipine
Nintedanib (BIBF 1120)
Nisoldipine
Nitazoxanide
Nithiamide
Nitrendipine
Nitrofural
Nizatidine
NLG919
NMDA (N-Methyl-D-aspartic acid)
NMS-873
NMS-E973
NMS-P937 (NMS1286937)
Nobiletin
Nocodazole
Noradrenaline bitartrate monohydrate
Norethindrone
Novobiocin Sodium
NPS-2143
NSC 23766
AT9283
NSC 405020
NSC697923
NU6027
NU7441 (KU-57788)
Nutlin-3
Nutlin-3a
Nutlin-3b
NVP-ADW742
NVP-AEW541
NVP-BHG712
NVP-BSK805 2HCl
NVP-BVU972
NXY-059
Nystatin (Fungicidin)
OAC1
Aurora A Inhibitor I
OC000459
Odanacatib (MK-0822)
OG-L002
Olanzapine
Olaparib (AZD2281, Ku-0059436)
Oleanolic Acid
Oligomycin A
Olmesartan Medoxomil
Olopatadine HCl
Olsalazine Sodium
Omecamtiv mecarbil (CK-1827452)
Omeprazole
Ondansetron HCl
ONX-0914 (PR-957)
AZD3463
Optovin
Org 27569
Oridonin
Orlistat
Ornidazole
Orotic acid (6-Carboxyuracil)
Orphenadrine Citrate
OSI-027
OSI-420
OSI-906 (Linsitinib)
OSI-930
Ospemifene
Osthole
OSU-03012 (AR-12)
Otilonium Bromide
OTX015
Ouabain
Oxaliplatin
Oxaprozin
Oxcarbazepine
Oxfendazole
Oxiracetam
Oxybuprocaine HCl
Oxybutynin chloride
Oxymatrine
Oxymetazoline HCl
Oxytetracycline (Terramycin)
Ozagrel
Ozagrel HCl
P22077

P276-00
P5091 (P005091)
PA-824
PAC-1
Barasertib (AZD1152-HQPA)
Pacritinib (SB1518)
Paeoniflorin
Paeonol
Palbociclib (PD-0332991) HCl
Palmatine chloride
Palomid 529 (P529)
Pancuronium dibromide
Panobinostat (LBH589)
Paroxetine HCl
Pazopanib
Pazopanib HCl (GW786034 HCl)
PCI-24781 (Abexinostat)
PCI-34051
PD 151746
PD0325901
PD123319
PD128907 HCl
PD168393
PD173074
PD173955
PD184352 (CI-1040)
PD318088
PD98059
Pefloxacin Mesylate
Pefloxacin Mesylate Dihydrate
Pelitinib (EKB-569)
Penciclovir
Penfluridol
Penicillin G Sodium
Pentamidine
Pentoxyverine Citrate
Pergolide mesylate
PF-00562271
PF-04217903
PF-04620110
PF-04691502
Berberine HCl
BGT226 (NVP-BGT226)
PF-3845
PF-4708671
PF-477736
PF-4981517
PF-5274857
PF-543
PF-562271
PF-562271 HCl
PF-573228
PFI-1 (PF-6405761)
PFK15
PH-797804
PHA-665752
PHA-680632
PHA-767491
PHA-793887
Phenacetin
Phenazopyridine HCl
Phenformin HCl
Phenindione
Pheniramine Maleate
Phenothiazine
Phenoxybenzamine HCl
Phentolamine Mesylate
Phenylbutazone
Phenylephrine HCl
Phenytoin
Phenytoin sodium
BV-6
Phlorizin
Phosphoramidon Disodium Salt
PHT-427
PI-103
PI-1840
Piceatannol
Pidotimod
Pifithrin-α (PFTα)
Pifithrin-μ
PIK-293
PIK-294
PIK-75
PIK-93
Pilocarpine HCl
Pimasertib (AS-703026)
Pimobendan
Pioglitazone
Pioglitazone HCl
Piperacillin Sodium
Piperine
Piracetam
Cabazitaxel
Pirfenidone
Carfilzomib (PR-171)
Pitavastatin Calcium
Pizotifen Malate
PJ34
PJ34 HCl
PluriSIn #1 (NSC 14613)
PLX-4720
PMSF
PNU-120596
Polydatin
Pomalidomide
Ponatinib (AP24534)
Posaconazole
Potassium Iodide
PP1
PP121
PP2
PP242
PQ 401
PR-619
Pracinostat (SB939)
Pralatrexate
Pramipexole
Pramiracetam
Pramoxine HCl
Pranlukast
Pranoprofen
Prasugrel
Pravastatin sodium
Praziquantel
Prednisolone
Prednisone
Pregnenolone
Prilocaine
Primaquine Diphosphate
Primidone
Pritelivir (BAY 57-1293)
Probenecid
Probucol
Procainamide HCl
Procaine HCl
Progesterone
Promethazine HCl
Propafenone HCl
Proparacaine HCl
Propranolol HCl
Propylthiouracil
Protionamide
PRT062607 (P505-15, BIIB057) HCl
Prucalopride
Prucalopride Succinat
PRX-08066 Maleic acid
PTC-209
PTC-209 HBr
PU-H71
Puerarin
Purmorphamine
CUDC-907
PYR-41
Pyrazinamide
Pyridostigmine Bromide
Pyridoxine HCl
Pyrimethamine
QNZ (EVP4593)
Quercetin
Quercetin Dihydrate
Quetiapine Fumarate
Quinacrine 2HCl
Quinapril HCl
Quinine HCl Dihydrate
Quisinostat (JNJ-26481585)
Quizartinib (AC220)
R406
R406 (free base)
R547
Racecadotril
RAF265 (CHIR-265)
Raloxifene HCl
Raltegravir (MK-0518)
Raltitrexed
Ramelteon
Ramipril
Ranitidine
Ranolazine
Ranolazine 2HCl
Rapamycin (Sirolimus)
Rasagiline Mesylate
Rebamipide
Reboxetine mesylate
Refametinib (RDEA119, Bay 86-9766)
Regorafenib (BAY 73-4506)

Repaglinide
RepSox
Reserpine
Resminostat
Resveratrol
Retapamulin
RG108
RG2833 (RGFP109)
RGFP966
Rheochrysidin
RI-1
Ribavirin
Ribitol
Ridaforolimus (Deforolimus, MK-8669)
Rifabutin
Rifampin
Rifapentine
Rifaximin
Rigosertib (ON-01910)
Rilpivirine
Riluzole
Rimantadine
Rimonabant
Risperidone
RITA (NSC 652287)
Ritodrine HCl
Ritonavir
Rivaroxaban
Rivastigmine Tartrate
Rizatriptan Benzoate
RKI-1447
Ro 31-8220 Mesylate
DCC-2036 (Rebastinib)
RO4929097
Rocilinostat (ACY-1215)
Rocuronium Bromide
Rofecoxib
Roflumilast
Rolipram
Dinaciclib (SCH727965)
Ronidazole
Ropinirole HCl
Ropivacaine HCl
Roscovitine (Seliciclib,CYC202)
Rosiglitazone
Rosuvastatin Calcium
Rotigotine
Rotundine
Roxatidine Acetate HCl
Roxithromycin
RS-127445
Rucaparib (AG-014699,PF-01367338)
Rufinamide
Rupatadine Fumarate
Rutaecarpine
Rutin
Ruxolitinib (INCB018424)
RVX-208
S- (+)-Rolipram
S-Ruxolitinib (INCB018424)
S3I-201
Sabutoclax
Safinamide Mesylate
Sal003
Salicylanilide
Salidroside
Salubrinal
SANT-1
Santacruzamate A (CAY10683)
SAR131675
SAR245409 (XL765)
Saracatinib (AZD0530)
Sasapyrine
Saxagliptin
SB-3CT
SB202190 (FHPI)
SB203580
SB216763
SB269970 HCl
SB271046
SB408124
SB415286
SB431542
SB505124
SB525334
SB590885
SB705498
SB742457
SC-514
SC144
SC75741
Schisandrin B (Sch B)
Sclareolide
Scopine
Scopine HCl
Scopolamine HBr
Scriptaid
Secnidazole
Selumetinib (AZD6244)
Semagacestat (LY450139)
Semaxanib (SU5416)
Serotonin HCl
Sertaconazole nitrate
Sertraline HCl
Sesamin
SF1670
SGC 0946
SGC-CBP30
SGI-1027
SGI-1776 free base
SGX-523
SH-4-54
Shikimic Acid
Sildenafil Citrate
Silibinin
Silodosin
Silymarin
Simvastatin
Sinomenine
Sirtinol
Sitagliptin phosphate monohydrate
Sitaxentan sodium
Skepinone-L
SKI II
SKLB1002
SL-327
SMI-4a
SNS-032 (BMS-387032)
SNS-314 Mesylate
Geldanamycin
Sodium 4-Aminosalicylate
Sodium ascorbate
Sodium Danshensu
Sodium Nitrite
Sodium Nitroprusside
Sodium Phenylbutyrate
Sodium Picosulfate
Sodium salicylate
Sofosbuvir (PSI-7977, GS-7977)
Solifenacin succinate
Sophocarpine
Sorafenib
Sorafenib Tosylate
Sorbitol
Sotalol
Sotrastaurin
SP600125
Sparfloxacin
Spectinomycin HCl
Spiramycin
Spironolactone
SRPIN340
SRT1720
SSR128129E
Stattic
Stavudine (d4T)
StemRegenin 1 (SR1)
STF-118804
STF-62247
Streptozotocin (STZ)
SU11274
Sucralose
Sulbactam
Sulbactam sodium
Sulconazole Nitrate
Sulfacetamide Sodium
Sulfadiazine
Sulfaguanidine
Sulfamerazine
Sulfameter
Sulfamethazine
Sulfamethizole
Sulfamethoxazole
Sulfamethoxypyridazine
Sulfanilamide
Sulfasalazine
Sulfathiazole
Sulfisoxazole
Sulindac
Sulphadimethoxine
Sumatriptan Succinate
Sunitinib Malate
Suplatast Tosylate
Suprofen

Suvorexant (MK-4305)
Synephrine
Synephrine HCl
T0070907
T0901317
Tacrolimus (FK506)
Tadalafil
TAE226 (NVP-TAE226)
TAK-285
TAK-438
TAK-632
TAK-700 (Orteronel)
TAK-715
KX2-391
TAK-875
MK-2206 2HCl
TAME
Tamibarotene
Tamoxifen Citrate
Tandutinib (MLN518)
Tangeretin
Tanshinone I
Tanshinone IIA
TAPI-1
Tariquidar
Tasisulam
Taxifolin (Dihydroquercetin)
Obatoclax Mesylate (GX15-070)
TCID
TCS 359
Tebipenem Pivoxil
Telaprevir (VX-950)
Telatinib
Telbivudine
Telmisartan
Telotristat Etiprate (LX 1606 Hippurate)
Temocapril HCl
Temozolomide
Tempol
Temsirolimus (CCI-779, NSC 683864)
PF-04929113 (SNX-5422)
Tenofovir Disoproxil Fumarate
Tenovin-1
Tenovin-6
Tenoxicam
Terazosin HCl
Terbinafine
Terbinafine HCl
Teriflunomide
Tetracaine HCl
Tetracycline HCl
Tetrahydropapaverine HCl
Tetrahydrozoline HCl
Tetrandrine
TG003
TG100-115
TG100713
TG101209
TG101348 (SAR302503)
TGX-221
Thalidomide
Thiabendazole
Thiamet G
Thiamphenicol
Thiazovivin
Tianeptine sodium
TIC10
Ticagrelor
Ticarcillin sodium
Tie2 kinase inhibitor
Tigecycline
Tilmicosin
Timolol Maleate
Tinidazole
Tioconazole
Tiopronin
Tiotropium Bromide hydrate
Tioxolone
Tipifarnib
Tiratricol
Tivozanib (AV-951)
Tizanidine HCl
TMP269
Tofacitinib (CP-690550,Tasocitinib)
Tofacitinib (CP-690550) Citrate
Tolazoline HCl
Tolbutamide
Tolcapone
Tolfenamic Acid
Tolnaftate
Tolperisone HCl
Tolterodine tartrate
Toltrazuril
Tolvaptan
Topiramate
Topotecan HCl
Torcetrapib
Toremifene Citrate
Phloretin
TPCA-1
Puromycin 2HCl
Tranilast
Tranylcypromine (2-PCPA) HCl
Trelagliptin
Tretinoin
Triamcinolone
Triamcinolone Acetonide
Triamterene
Triapine
Trichlormethiazide
Trichostatin A (TSA)
Triciribine
Triclabendazole
Trifluoperazine 2HCl
Trifluridine
Triflusal
Trilostane
Trimebutine
Trimethoprim
Tripelennamine HCl
Romidepsin (FK228, Depsipeptide)
Trometamol
Tropicamide
Tropisetron
Trospium chloride
Troxerutin
Troxipide
TSU-68 (SU6668, Orantinib)
TTNPB (Arotinoid Acid)
Salicin
Tubastatin A
Tubastatin A HCl
TW-37
TWS119
Tylosin tartrate
Tyrphostin 9
Tyrphostin AG 1296
Tyrphostin AG 879
U-104
U0126-EtOH
UK 383367
Ulipristal
UNC1215
UNC1999
UNC2881
UNC669
UPF 1069
Uracil
Urapidil HCl
URB597
Uridine
Ursodiol
Ursolic Acid
Valaciclovir HCl
Valdecoxib
Valganciclovir HCl
Valnemulin HCl
Valproic acid sodium salt (Sodium valproate)
Valsartan
Vandetanib (ZD6474)
Vanillin
Vanillylacetone
Vardenafil HCl Trihydrate
Varespladib (LY315920)
Varlitinib
Vatalanib (PTK787) 2HCl
VE-821
VE-822
Vecuronium Bromide
Veliparib (ABT-888)
Vemurafenib (PLX4032, RG7204)
Venlafaxine
VER-49009
VER-50589
Verapamil HCl
VGX-1027
Vidarabine
Vilazodone HCl
Vildagliptin (LAF-237)
Sclareol
Vincristine
SN-38
Vismodegib (GDC-0449)

Vitamin B12	VX-765	XL147	Zebularine
Vitamin C	VX-809 (Lumacaftor)	XL335	Zibotentan (ZD4054)
Vitamin D2	WAY-100635 Maleate	VX-680 (Tozasertib, MK-0457)	Zidovudine
Vitamin D3	WAY-600	XMD8-92	Zileuton
Voglibose	WH-4-023	Xylazine HCl	Zinc Pyrithione
SNX-2112 (PF-04928473)	WHI-P154	Xylometazoline HCl	Ziprasidone HCl
Voreloxin (SNS-595)	WIKI4	Xylose	ZLN005
Voriconazole	Wnt-C59 (C59)	Y-27632 2HCl	ZM 306416
Vorinostat (SAHA, MK0683)	Wortmannin	Y-320	ZM 323881 HCl
Vortioxetine (Lu AA21004) HBr	WP1066	YH239-EE	ZM 336372
VS-5584 (SB2343)	WY-14643 (Pirinixic Acid)	YM155 (Sepantronium Bromide)	ZM 39923 HCl
VU 0357121	WYE-125132 (WYE-132)	YM201636	ZM 447439
VU 0361737	WYE-354	YO-01027	Zolmitriptan
VU 0364439	Torin 2	Yohimbine HCl	Zonisamide
VU 0364770	Triptolide (PG490)	Z-FA-FMK	Zosuquidar (LY335979) 3HCl
VUF 10166	WZ4003	Z-VAD-FMK	Zotarolimus(ABT-578)
VX-222 (VCH-222, Lomibuvir)	Tubacin	Zafirlukast	Zoxazolamine
VX-661	WZ811	Zalcitabine	ZSTK47
TAK-901	Xanthone	Zaltoprofen	
VX-702	XAV-939	Zanamivir	
VX-745	XL019	ZCL278	

Table S 8: Screen hits for compound screen for acquired sensitivity of H1975^{9291S}

Compounds that showed a z-score ≥ 2 at either 0.1 µM or 1 µM for increased inhibition of proliferation in H1975^{9291S} compared to H1975. Compounds are sorted alphabetically based on their first reported target.

compound	listed targets	H1975 0.1 µM	H1975 1 µM	H1975^{9291S} 0.1 µM	H1975^{9291S} 1 µM
GDC-0068	Akt	1.11	0.79	1.40	0.51
MK-2206 2HCl	Akt	1.52	0.89	1.07	0.57
AZD3463	ALK	0.96	0.31	0.71	0.36
Torin 2	ATM/ATR,mTOR	0.23	0.19	0.16	0.12
AMG-900	Aurora Kinase	0.36	0.27	0.14	0.15
Aurora A Inhibitor I	Aurora Kinase	0.83	0.21	0.49	0.31
Barasertib (AZD1152-HQPA)	Aurora Kinase	0.85	0.32	0.39	0.39
MK-5108 (VX-689)	Aurora Kinase	1.13	0.28	1.16	0.18
PHA-680632	Aurora Kinase	1.23	0.81	1.49	0.41
TAK-901	Aurora Kinase	0.47	0.20	0.14	0.11
VX-680 (Tozasertib, MK-0457)	Aurora Kinase	0.69	0.29	0.37	0.39
ZM 447439	Aurora Kinase	0.87	0.68	1.05	0.44
KW-2449	Aurora Kinase,Bcr-Abl,FLT3	1.09	0.54	1.25	0.31
Obatoclax Mesylate (GX15-070)	Bcl-2,Autophagy	0.89	0.19	0.46	0.31
DCC-2036 (Rebastinib)	Bcr-Abl	1.13	0.88	0.90	0.62
SU11274	c-Met	1.39	1.13	1.44	0.48

Dinaciclib (SCH727965)	CDK	0.16	0.17	0.11	0.11
Milciclib (PHA-848125)	CDK	0.85	0.31	0.75	0.17
Bazedoxifene HCl	Estrogen/progestogen Receptor	0.96	0.95	1.24	0.64
Quizartinib (AC220)	FLT3	0.93	0.95	1.09	0.46
M344	HDAC	1.04	0.52	1.23	0.33
Romidepsin (FK228, Depsipeptide)	HDAC	0.15	0.15	0.09	0.09
Tubacin	HDAC	0.98	0.93	0.78	0.89
CUDC-101	HDAC,HER2,EGFR	1.04	0.64	1.23	0.43
KW-2478	HSP (e.g. HSP90)	0.98	0.25	1.10	0.13
PF-04929113 (SNX-5422)	HSP (e.g. HSP90)	0.51	0.17	0.27	0.28
SNX-2112 (PF-04928473)	HSP (e.g. HSP90)	0.47	0.16	0.27	0.27
Geldanamycin	HSP (e.g. HSP90), Autophagy	0.18	0.17	0.10	0.10
NMS-E973	HSP90	1.01	0.67	1.42	0.34
BV-6	IAP	0.90	0.66	0.74	0.72
GSK1904529A	IGF-1R	1.07	1.09	0.82	0.54
NVP-ADW742	IGF-1R	1.14	0.74	1.12	0.43
NVP-AEW541	IGF-1R	1.00	0.70	0.96	0.48
PQ 401	IGF-1R	0.95	0.98	0.96	0.56
AT9283	JAK,Aurora Kinase,Bcr-Abl	0.65	0.26	0.35	0.32
Nocodazole	Microtubule Associated,Autophagy	0.17	0.16	0.13	0.11
WAY-600	mTOR	1.05	0.80	1.12	0.50
CH5132799	mTOR,PI3K	1.12	0.55	0.96	0.24
GDC-0980 (RG7422)	mTOR,PI3K	0.97	0.22	0.79	0.14
Berberine HCl	Others	1.13	0.85	0.88	0.97
Cabazitaxel	Others	0.16	0.17	0.10	0.10
Cepharanthine	Others	0.89	0.81	0.94	0.52
Cyclosporin A	Others	1.04	0.80	1.04	0.62
Mometasone furoate	Others	1.04	1.08	1.30	0.79
Phloretin	Others	0.89	0.84	0.61	0.79
Pitavastatin Calcium	Others	0.95	0.75	1.06	0.55
Puromycin 2HCl	Others	0.80	0.11	0.61	0.21
Salicin	Others	1.01	1.00	0.81	0.99
SC144	Others	0.94	0.58	1.00	0.34
Sclareol	Others	0.92	0.93	0.73	0.95
Triptolide (PG490)	Others	0.16	0.16	0.10	0.10
Darapladib (SB-480848)	Phospholipase	0.96	0.97	0.95	0.23
HS-173	PI3K	0.98	0.54	1.22	0.37
YM201636	PI3K	0.99	1.09	1.03	0.77
CUDC-907	PI3K, HDAC	0.14	0.14	0.08	0.09
BGT226 (NVP-BGT226)	PI3K, mTOR	0.18	0.15	0.12	0.09
Ro 31-8220 Mesylate	PKC	0.91	0.65	0.94	0.38

Carfilzomib (PR-171)	Proteasome	0.14	0.15	0.08	0.09
Zinc Pyrithione	Proton Pump	0.93	0.15	1.14	0.09
SRT1720	Sirtuin	1.29	0.87	1.59	0.31
KX2-391	Src	0.17	0.17	0.10	0.10
Daunorubicin HCl	Telomerase	0.15	0.16	0.12	0.10
SN-38	Topoisomerase	0.49	0.13	0.28	0.21
Nintedanib (BIBF 1120)	VEGFR, PDGFR, FGFR	0.85	0.83	1.07	0.58

Table S 9: Ranking of EGFR-TKIs in screen for selectivity for H1975^{9291S} over H1975

Compouds are ranked by decreasing ability to selectively inhibit proliferation in H1975^{9291S} compared to H1975 when used at 0.1 μM. Green background indicates 3rd generation, mutant specific EGFR-TKIs.

Rank	Compound	Target
108	AC480 (BMS-599626)	HER2,EGFR
162	Varlitinib	EGFR
246	AST-1306	EGFR
391	Butein	EGFR
552	WHI-P154	JAK,EGFR
621	AG-490 (Tyrphostin B42)	JAK,EGFR
809	Lapatinib (GW-572016) Ditosylate	HER2,EGFR
822	PD168393	EGFR
823	CP-724714	EGFR,HER2
834	OSI-420	EGFR
873	AZD8931 (Sapitinib)	HER2,EGFR
915	Chrysophanic Acid	mTOR,EGFR
950	CUDC-101	HDAC,HER2,EGFR
1014	Genistein	Topoisomerase,EGFR
1106	Gefitinib (ZD1839)	EGFR
1412	Erlotinib HCl (OSI-744)	Autophagy,EGFR
1489	Tyrphostin 9	EGFR
1561	Pelitinib (EKB-569)	EGFR
1604	HER2-Inhibitor-1	HER2,EGFR
1659	TAK-285	EGFR,HER2
1679	AG-1478 (Tyrphostin AG-1478)	EGFR
1712	AG-18	EGFR
1905	Afatinib (BIBW2992)	EGFR,HER2
1923	Icotinib	EGFR
1974	Dacomitinib (PF299804, PF299)	EGFR
1983	CNX-2006	EGFR
1984	WZ4002	EGFR
1988	WZ3146	EGFR
1990	CO-1686 (AVL-301)	EGFR
1991	WZ8040	EGFR
1992	AZD9291	EGFR

Table S 10: Hit compounds identified in H1975 screen +/- AZD9291

Compounds that showed a z-score ≥ 2 at either 0.1 μM or 1 μM for increased inhibition of proliferation in H1975 in the presence of AZD9291 compared to the compound alone or a difference of 0.4 between conditions.

compound	listed targets	H1975 0.1 μM	H1975 1 μM	H1975 0.1 μM + AZD9291	H1975 1 μM + AZD9291
MK-2206 2HCl	Akt	1.52	0.89	0.86	0.67
PI-103	PI3K, Autophagy, DNA-PK, mTOR	1.25	0.36	0.80	0.63